# Investigating a role for CaMKIIδ in mediating the cardiotoxic effects of anti-cancer tyrosine kinase inhibitors

**A thesis presented by**

**Calum J. McMullen**

**In fulfilment of the requirements for the degree of Doctor of Philosophy**

**University of Strathclyde**
**Strathclyde Institute of Pharmacy and Biomedical Sciences**

**July 2021**

This thesis is the result of the author's original research. It has been composed by the author and has not been previously submitted for examination which has led to the award of degree. Part of the research has been published previously in peer-reviewed journals.

The copyright of this thesis belongs to the author under the terms of the United Kingdom Copyright Acts as qualified by the University of Strathclyde Regulations 3.50. Due acknowledgement must always be made of the use of any material contained in, or derived from, this thesis.

**Signed:**

**Date:**

**Acknowledgements:**

My sincerest thanks to Susan Currie for all your guidance throughout my studies. I have faced some challenging periods during my time at Strathclyde, and I am eternally grateful for your continuous and unwavering support throughout. My profound thanks also to Margaret Cunningham. I can honestly say I wouldn't be where I am now without you. You challenge me, allow me to make mistakes (and learn from them!) and allow me the freedom to develop and work things out on my own. I am forever grateful for your mentorship, for treating me like family, and for giving me a kick up the a**e when needed!

Thank you to Sandy MacMillan, my partner in crime. Your friendship means so much to me, and your constant willingness join me for coffee and cake at a moment's notice has got me through some awful days in the lab. To Rachel Wood, my eternal thanks for your patience, friendship and for making the lab such a fun place to be. I can't describe how big a role you have played in my PhD. You helped me settle in the lab, taught me to be confident in my own abilities and have driven me to constantly learn and do better. My thanks also to Mark Barbour for all your help and guidance, particularly since Rachel left (I was the step-student he never wanted).

Thank you to Linda Horan, Brian Lepes, Lee Wheeler and Peter Conte for all your help with animal husbandry. Thank you to Margaret MacDonald for all your assistance and training. To Graeme McKenzie, thank you for all your help and, more importantly, for being a really good mate. A special thanks also to Christine Fletcher Poland and Anne Cairney for your kindness, caring nature and for the warm welcome I receive from you both every day.

I have been incredibly fortunate to work with so many talented and immensely intelligent individuals. There are too many to mention individually, but I thank you all for your support and friendship. It is truly comforting to know that you are not alone in this

experience. A special thanks to Ryan Brown, Ben Veerman, Ashley McCulloch, Rachel Craig, Nick Klemm, Stuart McEwan, MoA Safar, Daniel Longhorn, Carolina Locatelli and Mirna Merkler. Our eccentric support group based on shared misery, imposter syndrome and trips to the pub, has gotten us through some difficult days and bonded us for life. I wouldn't have made it this far without you all and, even now as we begin to move on to pastures new, I am so thankful we went through this experience together and am so proud of you all.

Finally, thank you to my friends and family for your unfaltering encouragement and reassurance throughout my studies. To my Mum, Dad, Niall, Rachel and Ziva, your unconditional love and relentless belief in me has carried me through periods when I have doubted myself. I cannot put into word how grateful I am for all you have done and continue to do for me. I love you all.

**Publications:**

**Journal article:**

McMullen, C. J., Chalmers, S., Wood, R., Cunningham, M. R. & Currie, S. (2021). Sunitinib and imatinib display differential cardiotoxicity in adult rat cardiac fibroblasts that involves a role for calcium/calmodulin dependent protein kinase II. *Frontiers in Cardiovascular Medicine.* 1;7:630480. doi: 10.3389/fcvm.2020.630480

**Abstract Publications:**

McMullen, CJ., Chalmers, S., Cunningham, MR. & Currie, S. (2020). Sunitinib mediates mitochondrial ROS production in adult rat cardiac fibroblasts via CaMKII oxidation. *Heart*, 106, Suppl 1, 1 p., OP8. http://dx.doi.org/10.1136/heartjnl-2020-SCF.8

McMullen, C. J., Wood, R. A., Cunningham, M. R., & Currie, S. (2019). Assessment of adult rat cardiac fibroblast viability following chronic sunitinib treatment. *Heart*, 105 (suppl 4), A6-A7. https://doi.org/10.1136/heartjnl-2019-SCF.13

McMullen, CJ., McCluskey, C., Kim, SJ., Laovitthayanggoon, S., MacDonald, M., Safar, M., Cunningham. M.R. & Currie, S. (2018). Anti-cancer tyrosine kinase inhibitors increase oxidative stress in primary cardiac fibroblasts. *Heart*, 104(S4). https://doi.org/10.1136/heartintjnl-2018-SCF22

**Meeting Communication:**

McMullen, C. J., Veerman, B., Safar, M., Currie, S. & Cunningham, M. R. (2020). Pharmacology Matters Article - 'The 23rd annual meeting of the Scottish Cardiovascular Forum.

**Poster Communications:**

Physiology, Aberdeen (2019). McMullen, C. J., Chalmers, S., Cunningham, M. R., & Currie, S. Assessment of adult rat cardiac fibroblast viability following chronic sunitinib treatment.

Scottish Cardiovascular Forum Annual Meeting, Inverness (2019). McMullen, C. J., Wood, R. A., Cunningham, M. R., & Currie, S. Assessment of adult rat cardiac fibroblast viability following chronic sunitinib treatment.

British Pharmacology Society Annual Meeting, London (2018). McMullen, CJ., McCluskey, C., Kim, SJ., Laovitthayanggoon, S., MacDonald, M., Safar, M., Cunningham. M.R. & Currie, S. Anti-cancer tyrosine kinase inhibitors increase oxidative stress in primary cardiac fibroblasts.

Scottish Cardiovascular Forum Annual Meeting, Dublin (2018). McMullen, CJ., McCluskey, C., Kim, SJ., Laovitthayanggoon, S., MacDonald, M., Safar, M., Cunningham. M.R. & Currie, S. Anti-cancer tyrosine kinase inhibitors increase oxidative stress in primary cardiac fibroblasts.

**Oral Communications:**

Scottish Cardiovascular Forum Annual Meeting, Glasgow (2020). McMullen, CJ., Chalmers, S., Cunningham, MR. & Currie, S. Sunitinib mediates mitochondrial ROS production in adult rat cardiac fibroblasts via CaMKII oxidation.

Tenovus Scotland Researchers' Networking Symposium, Perth (2019). McMullen, CJ., Chalmers, S., Cunningham, MR. & Currie, S. Sunitinib mediates CF cell death via a mechanism involving mitochondrial ROS production and CaMKII oxidation.

# Table of Contents:


Acknowledgements I

Publications III

Poster Communications IV

Oral Communications V

Table of Contents VI

List of Figures XI

List of Tables XV

Abbreviations XVI

Abstract XX

## Chapter One: Introduction 1

1.1 Cardiac physiology 2

1.1.1 Structure and Function of the heart 2

1.1.2 Cardiac myocytes and excitation contraction coupling 5

1.1.3 Cardiac fibroblasts and their role in the heart 7

1.2 The pathophysiology of heart disease 9

1.2.1 Monitoring cardiac pathophysiology 13

1.2.2 The role of calcium dysregulation in cardiac myocyte dysfunction in heart failure 14

1.2.3 The role of oxidative stress in cardiac myocyte dysfunction in heart failure 15

1.2.4 The role of inflammation in cardiac myocyte dysfunction in heart failure 19

1.2.5 Cardiac fibroblast to myofibroblast differentiation 20

1.2.6 The role of calcium in cardiac fibroblast activation 21

1.2.7 The role of inflammation in cardiac fibroblast activation 22

1.2.8 The role of oxidative stress in cardiac fibroblast activation 23
1.3 Cardiovascular experimental models 24
1.3.1 Cardiac myocyte experimental models 25
1.3.2 Cardiac fibroblast experimental models 27
1.4 Cardiotoxicity 28
1.4.1 Anti-cancer drug induced cardiotoxicity 29
1.4.2 Anthracycline induced cardiotoxicity 30
1.5 Tyrosine kinase inhibitors 31
1.5.1 Imatinib mesylate 32
1.5.2 Sunitinib malate 33
1.5.3 Proposed cardiotoxic mechanism of tyrosine kinase inhibitors 34
1.6 Calcium/calmodulin-dependent protein kinase II (CaMKII) 36
1.6.1 The activation and autoregulation of CaMKII 39
1.6.2 CaMKIIδ regulates calcium handling in cardiac myocytes 42
1.6.3 CaMKIIδ influences mitochondrial function 43
1.6.4 CaMKIIδ regulates cardiac fibroblast activation 45
1.6.5 CaMKIIδ mediates altered calcium handling in cardiac myocytes 47
1.6.6 The possible role of CaMKIIδ in mitochondrial dysfunction 48
1.6.7 CaMKIIδ mediates cardiovascular remodelling 49
1.6.8 CaMKIIδ: A mediator of tyrosine kinase inhibitor-induced cardiotoxicity? 50
1.7 Hypothesis and aims 51

**Chapter Two: Materials and Methods 52**

2.1 Materials 53
2.2 Buffer/solution composition 56
2.3 Methods 58

2.3.1 Animal ethics 58
2.3.2 Adult primary cardiac fibroblast isolation 58
2.3.3 Cardiac myocyte isolation 59
2.3.4 Swiss 3T3 cell culture 59
2.3.5 Cardiac fibroblast cell culture 60
2.3.6 Progenitor cardiac myocyte cell culture 60
2.3.7 Cryopreservation 61
2.3.8 *In vitro* drug treatment 61
2.3.9 Brightfield imaging 61
2.3.10 MTT assays 62
2.3.11 Fluorescence-activated cell sorting 62
2.3.12 Immunofluorescence 63
2.3.13 Intracellular calcium release assay 65
2.3.14 SDS-PAGE Western blot 65
2.3.14.1 Cardiac fibroblast SDS-PAGE Western blot 66
2.3.14.2 Progenitor cardiac myocyte SDS-PAGE Western blot 68
2.3.15 DCFDA cellular reactive oxygen species detection assay 69
2.3.16 Live cell imaging of mitochondrial superoxide using MitoSOX red 70
2.3.17 Co-localisation 70
2.3.18 Measuring mitochondrial respiration 72
2.4 Data Analysis 75

**Chapter Three: Investigating the effect of tyrosine kinase inhibitor treatment on cardiac cells 76**

3.1 Introduction 77
3.2 Characterising healthy cardiac fibroblasts in culture 79

3.3 TKI treatment impacts cardiac fibroblast morphology 85

3.4 TKI treatment causes cardiac fibroblast cell death 93

3.5 TKI treatment impacts upon myofibroblast phenotype 103

3.6 TKI treatment impacts upon progenitor cardiac myocyte morphology 107

3.7 TKI treatment causes progenitor cardiac myocyte cell death 118

3.8 Discussion 123

3.9 Conclusion 128

**Chapter Four: Investigating the cardiotoxic mechanism of tyrosine kinase inhibitors 129**

4.1 Introduction 130

4.2 TKI treatment increases intracellular calcium mobilisation in cardiac cells 136

4.3 TKI treatment alters CaMKII activation in cardiac cells 143

4.4 The cardiotoxic mechanism of tyrosine kinase inhibitors involve mitochondrial dysfunction 156

4.5 KN-93 pre-treatment does not reduce TKI-induced cardiac cell death 182

4.6 CaMKII inhibition via KN-93 does not attenuate sunitinib-induced changes in intracellular calcium 195

4.7 Discussion 199

4.8 Conclusions 207

**Chapter Five: General Discussion 208**

5.0. General Discussion 209

5.1. Sunitinib displays greater cardiotoxic potential than imatinib 209

5.2. Unravelling the cardiotoxic mechanism of tyrosine kinase inhibitors 210

5.3 CaMKII inhibition attenuates cardiovascular pathophysiology 212

5.4 Future directions 214

**References 216**

# List of Figures:

## Chapter One:

Figure 1.1.1.1 Schematic representation of the organisation of the cellular components of the heart 4

Figure 1.1.2.1 Calcium transport and cardiac contraction in cardiac myocytes 6

Figure 1.2.1. An overview of the progression from left ventricular dysfunction to heart failure 12

Figure 1.2.3.1. An overview of the role of reactive oxygen species in the pathophysiology of heart failure 17

Figure 1.6.1. A schematic representation of the structure and activation of CaMKII 38

Figure 1.6.3.1. An overview of oxidative phosphorylation 44

Figure 1.6.4.1. A schematic representation of CaMKIIδ substrates 46

## Chapter Two:

Figure 2.3.18.1. An overview of the mitochondrial respiration protocol 74

## Chapter Three:

Figure 3.2.1. Brightfield imaging of cardiac fibroblast phenotype post-isolation and throughout culture until the first passage 80

Figure 3.2.2. Phenotypic characterization of cardiac fibroblasts and myofibroblasts in culture 82

Figure 3.2.3. Assessment of cardiac fibroblast and myofibroblast phenotype 84

Figure 3.3.1. Determining the effect of TKI treatment on cardiac fibroblast phenotype in the absence of serum 86

Figure 3.3.2. Determining the effect of TKI treatment on cardiac fibroblast phenotype in the presence of serum 88
Figure 3.3.3. Investigating the effect of TKI treatment on cardiac fibroblast marker expression via immunofluorescence 90
Figure 3.3.4. Investigating the effect of TKI treatment on cardiac fibroblast marker expression via western blot 92
Figure 3.4.1. MTT assay optimisation using hydrogen peroxide 94
Figure 3.4.2. Investigating the effect of sunitinib or imatinib treatment on cardiac fibroblast viability 96
Figure 3.4.3. The parameters used for flow cytometry 98
Figure 3.4.4. Optimisation of flow cytometry using cardiac fibroblasts treated with hydrogen peroxide 99
Figure 3.4.5. Investigating the effect of sunitinib treatment on cardiac fibroblast cell death parameters 101
Figure 3.4.6. Investigating the effect of imatinib treatment on cardiac fibroblast cell death parameters 102
Figure 3.5.1. Determining the effect of TKI treatment on myofibroblast phenotype in the presence of serum 104
Figure 3.5.2. Investigating the effect of TKI treatment on myofibroblast marker expression via immunofluorescence 106
Figure 3.6.1. Phenotypic characterization of progenitor cardiac myocyte and adult rat cardiac myocyte in culture 109
Figure 3.6.2. Assessment of progenitor cardiac myocyte marker expression 111
Figure 3.6.3. Investigating the effect of TKI treatment on progenitor cardiac myocyte phenotype in the presence of serum 113
Figure 3.6.4. Evaluating the effect of TKI treatment on progenitor cardiac myocyte marker expression 115

Figure 3.6.5. Determining the effect of TKI treatment on progenitor cardiac myocyte marker expression 117
Figure 3.7.1. Investigating the effect of sunitinib or imatinib treatment on progenitor cardiac myocyte viability 119
Figure 3.7.2. Investigating the effect of sunitinib treatment on progenitor cardiac myocyte cell death parameters 121
Figure 3.7.3. Investigating the effect of imatinib treatment on progenitor cardiac myocyte cell death parameters 122

## Chapter Four:

Figure 4.1.1. Comparing mitochondrial function in healthy and failing cardiac myocytes 134
Figure 4.2.1. Investigating the effect of sunitinib or imatinib stimulation on intracellular calcium mobilisation in cardiac fibroblasts 137
Figure 4.2.2. Determining whether TKI pre-treatment influences angiotensin II–induced intracellular calcium mobilisation in cardiac fibroblasts 139
Figure 4.2.3. Investigating the effect of angiotensin II stimulation on intracellular calcium mobilisation in progenitor cardiac myocytes 141
Figure 4.2.4. Determining whether TKI pre-treatment influences angiotensin II–induced intracellular calcium mobilisation in progenitor cardiac myocytes 142
Figure 4.3.1. Verification of CaMKII antibody conditions using untreated cardiac fibroblast lysates 144
Figure 4.3.2. Investigating the effect of sunitinib treatment on CaMKII activation and expression in cardiac fibroblasts 146
Figure 4.3.3. Investigating the effect of imatinib treatment on CaMKII activation and expression in cardiac fibroblasts 147
Figure 4.3.4. Comparing the effect of dithiothreitol inclusion in the expression of Ox-CaMKII in cardiac fibroblasts 149

Figure 4.3.5. Determining the effect of sunitinib or imatinib treatment on CaMKII activation and expression in cardiac fibroblasts 151
Figure 4.3.6. Optimisation of CaMKII antibodies using untreated progenitor cardiac myocytes 153
Figure 4.3.7. Investigating the effect of imatinib treatment on CaMKII activation and expression in progenitor cardiac myocytes 155
Figure 4.4.1. Optimisation of the DCFDA assay using hydrogen peroxide 158
Figure 4.4.2. Investigating the effect of sunitinib or imatinib treatment on intracellular reactive oxygen species production in cardiac fibroblasts 160
Figure 4.4.3. Investigating whether intrinsic drug fluorescence introduces bias to the DCFDA assay 162
Figure 4.4.4. Optimisation of MitoSOX Red using Swiss 3T3 cells 164
Figure 4.4.5. Optimising MitoSOX Red concentration in untreated cardiac fibroblasts 166
Figure 4.4.6. Investigating the effect of sunitinib or imatinib treatment on mitochondrial superoxide production in cardiac fibroblasts 168
Figure 4.4.7 Investigating the effect of CaMKII inhibition on mitochondrial superoxide production in sunitinib and imatinib treated cardiac fibroblasts 170
Figure 4.4.8. Optimisation of antibodies for cardiac fibroblast co-localisation experiments 172
Figure 4.4.9. Investigating whether TKI treatment influences CaMKII translocation to the mitochondria in cardiac fibroblasts 174
Figure 4.4.10. Optimisation of antibodies for progenitor cardiac myocyte co-localisation experiments 176
Figure 4.4.11. Investigating whether TKI treatment influences CaMKII translocation to the mitochondria in progenitor cardiac myocytes 178
Figure 4.4.12. Optimisation of the protocol for assessing mitochondrial bioenergetics in untreated cardiac fibroblasts 181
Figure 4.5.1. Investigating whether CaMKII inhibition has any effect on sunitinib-induced cell death parameters in cardiac fibroblasts 184

Figure 4.5.2. Investigating whether CaMKII inhibition has any effect on imatinib-induced cell death parameters in cardiac fibroblasts 185
Figure 4.5.3. A comparison of the effect of CaMKII inhibition via KN-93 on sunitinib induced cell death in cardiac fibroblasts 187
Figure 4.5.4. A comparison of the effect of CaMKII inhibition via KN-93 on imatinib induced cell death in cardiac fibroblasts 188
Figure 4.5.5. Investigating whether CaMKII inhibition has any effect on sunitinib-induced cell death parameters in progenitor cardiac myocytes 190
Figure 4.5.6. Investigating whether CaMKII inhibition has any effect on imatinib-induced cell death parameters in progenitor cardiac myocytes 191
Figure 4.5.7. A comparison of the effect of CaMKII inhibition via KN-93 on sunitinib induced cell death in progenitor cardiac myocytes 193
Figure 4.5.8. A comparison of the effect of CaMKII inhibition via KN-93 on imatinib induced cell death in progenitor cardiac myocytes 194
Figure 4.6.1. Determining the effect of CaMKII inhibition on angiotensin II–induced intracellular calcium mobilisation in cardiac fibroblasts 196
Figure 4.6.2. A comparison of the effect of CaMKII inhibition via KN-93 on angiotensin II-induced intracellular calcium release in cardiac fibroblasts pre-treated with sunitinib or imatinib 198

# List of Tables:

## Chapter Two:

Table 1. Antibodies and corresponding conditions optimised for immunofluorescence 64
Table 2. Antibodies and corresponding conditions optimised for immunoblotting 67
Table 3. Optimised antibody concentrations for co-localisation experiments 71

# Abbreviations:

| | |
|---|---|
| AF | Atrial fibrillation |
| AIP | Autocamtide-2 related inhibitor peptide |
| AnV | Annexin V |
| ARCC | Advanced renal cell carcinoma |
| ATP | Adenosine triphosphate |
| AVM | Adult ventricular myocyte |
| BNP | Brain natriuretic peptide |
| BP | Blood pressure |
| BSA | Bovine serum albumin |
| $Ca^{2+}$ | Calcium |
| $CaCl_2$ | Calcium chloride |
| CaM | Calmodulin |
| CaMKII | Calcium/calmodulin dependent protein kinase II |
| CaR | Calcium sensing receptor |
| CF | Cardiac fibroblast |
| CICR | Calcium-induced calcium release |
| CM | Cardiac myocyte |
| CO | Cardiac output |
| CRP | C-reactive protein |
| CVD | Cardiovascular disease |
| CXCL | C-X-C motif ligand |
| DAPI | 4′,6-diamidino-2-phenylindole |
| DCFDA | 2',7' –dichlorofluorescin diacetate |
| DHE | Dihydroethidium |
| DMEM | Dulbecco's modified eagle medium |
| DMSO | Dimethyl sulfoxide |

| | |
|---|---|
| DTT | Dithiothreitol |
| EC | Endothelial cell |
| ECC | Excitation-contraction coupling |
| ECL | Enhanced chemiluminescence |
| ECM | Extracellular matrix |
| EGTA | Ethylene glycol-bis(2-aminoethylether)-N N N′N′-tetraacetic acid |
| FCS | Foetal calf serum |
| GAPDH | Glyceraldehyde 3-phosphate dehydrogenase |
| GIST | Gastrointestinal stromal tumours |
| GlcNAc | N-acetylglucosamine |
| GNSO | S-Nitrosoglutathione |
| GPCR | G protein-coupled receptor |
| $H_2O_2$ | Hydrogen peroxide |
| HEPES | 4-(2-hydroxyethyl)-1-piperazineethanesulfonic acid |
| HES | Hypereosinophilic syndrome |
| HF | Heart failure |
| HUVEC | Human umbilical vein endothelial cell |
| IL | Interleukin |
| iPSC | Induced pluripotent stem cell |
| KCl | Potassium chloride |
| $KH_2PO_4$ | Potassium dihydrogen phosphate |
| KOH | Potassium hydroxide |
| LOX | Lysyl oxidase |
| LTCC | L-type calcium channel |
| LVEF | Left ventricular ejection fraction |
| MCU | Mitochondrial calcium uniporter |
| MF | Myofibroblast |
| $MgCl_2.6H_2O$ | Magnesium chloride hexahydrate |

| | |
|---|---|
| $MgSO_4 \cdot 7H_2O$ | Magnesium sulfate heptahydrate |
| MI | Myocardial infarction |
| MMP | Metalloproteinase |
| MOPS | 3-(N-morpholino)propanesulfonic acid |
| MPD | Myeloproliferative diseases |
| mPTP | Mitochondrial membrane transition pore |
| msrA | Methionine sulfoxide reductase A |
| MTT | Thiazolyl blue tetrazolium bromide |
| $Na^+$ | Sodium |
| $Na_2HPO_4.2H_2O$ | Sodium phosphate dibasic dihydrate |
| NaCl | Sodium chloride |
| NADPH | Nicotinamide adenine dinucleotide phosphate hydrogen |
| $NaH_2PO_4$ | Sodium dihydrogen orthophosphate |
| $NaHCO_3$ | Sodium bicarbonate |
| NCX | Sodium-calcium exchanger |
| NO | Nitric oxide |
| NRVM | Neonatal rat ventricular myocyte |
| O-GlcNAcylation | O-linked glycosylation |
| Ox | Oxidised |
| OXPHOS | Oxidative phosphorylation |
| PBS | Phosphate buffered saline |
| PCM | Progenitor cardiac myocyte |
| PDGFR | Platelet derived growth factor receptor |
| Ph+CML | Philadelphia chromosome positive chronic myeloid leukemia |
| Phos | Phosphorylated |
| PI | Propidium iodide |
| PLB | Phospholamban |
| PS | Phosphatidylserine |

| | |
|---|---|
| PTM | Post-translational modification |
| RAAS | Renin-angiotensin aldosterone system |
| ROS | Reactive oxygen species |
| RyR2 | Ryanodine receptor |
| S.E.M. | Standard error of the mean |
| S3T3 | Swiss 3T3 cell |
| SDS | Sodium dodecyl sulphate |
| SERCA | Sarcoplasmic-endoplasmic reticulum calcium-ATPase pump |
| SMCa | α-smooth muscle cell actin |
| SR | Sarcoplasmic reticulum |
| TAC | Transverse aortic constriction |
| TBHP | Tert-Butyl hydrogen peroxide |
| TBS-T | Tris-buffered saline + 0.1% Tween 20 |
| TGF-β | Transforming growth factor β |
| TGF-β R1 | Transforming growth factor β receptor 1 |
| TIMP | Tissue inhibitor of metalloproteinase |
| TKI | Tyrosine kinase inhibitor |
| TNFα | Tumour necrosis factor α |
| VEGFR | Vascular endothelial growth factor |
| VSMC | Vascular smooth muscle cell |
| vWF | Von Willebrand factor |

# Abstract:

**Introduction:** Tyrosine kinase inhibitors (TKIs) have dramatically improved cancer treatment but are known to cause cardiotoxicity. The pathophysiological consequences of TKI therapy are likely to manifest across different cell types of the heart, yet there is little understanding of the differential adverse cellular effects. Cardiac fibroblasts (CFs) play a pivotal role in the repair and remodelling of the heart following insult or injury, yet their involvement in anti-cancer drug induced cardiotoxicity has been largely overlooked. Here, we examine and compare the direct effects of two TKIs, sunitinib malate and imatinib mesylate, on CFs and progenitor cardiac myocytes (PCMs).

**Methodology:** CFs and PCMs were treated with sunitinib and imatinib (0.1-10μM) for 18 hours and then subject to *in vitro* analyses to determine the role of $Ca^{2+}$/calmodulin dependent protein kinase II (CaMKII) in the cardiotoxic mechanism of TKIs. Variations in cell phenotype were monitored via brightfield imaging. Changes in cell viability were determined via MTT assays and flow cytometry. Western blot and immunofluorescent imaging were utilised to investigate potential changes in protein expression. Changes in calcium mobility were investigated using a Fluo4-AM intracellular calcium release assay and mitochondrial function was explored using MitoSOX Red live cell imaging and an Oroborous oxygraph O2k respirometer.

**Results/Discussion:** In investigating the cardiotoxic mechanism of anti-cancer TKIs, this project has shown that (i) TKI treatment leads to contractile and non-contractile cellular dysfunction and death, (ii) TKI treatment, particularly sunitinib treatment, increases intracellular [$Ca^{2+}$] release and cellular oxidative stress in CFs by increasing reactive oxygen species (ROS) production via effects at the level of the mitochondria, correlating with increased oxidation and autonomous activation of CaMKII and (iii) CaMKII inhibition via KN-

93 reduces the detrimental effects of sunitinib and imatinib treatment at the level of the mitochondria, but this does not improve CF viability. Interestingly, the study found that TKI treatment had no effect on intracellular [$Ca^{2+}$] release in PCMs and actually reduced CaMKII phosphorylation, despite previous reports of pathophysiological changes in CMs that are similar to those obtained in CFs here. This study also established that the PCMs used here do not express key CM $Ca^{2+}$ handling proteins and this makes them unsuitable to investigate the cardiotoxic mechanism of TKIs.

**Conclusion:** These findings highlight a new role for CaMKII in TKI-induced cardiotoxicity, particularly at the level of the mitochondria, and confirm differential off-target toxicity in both contractile and non-contractile cardiac cells, consistent with the differential selectivity of sunitinib and imatinib.

# Chapter One: Introduction

*1.1 Cardiac physiology:*

The heart functions to supply the body's tissues and organs with oxygenated, nutrient rich blood, while simultaneously removing potentially harmful by-products and metabolites in the process (Goonasekera and Molkentin, 2012). The human heart is comprised of four chambers; two atria and two ventricles, separated by the septum. The right side of the heart serves to pump de-oxygenated blood to the lungs, while the left side pumps oxygenated blood throughout the body. Deoxygenated blood is returned to the right atrium via the venae cavae. Contraction of the right atria pumps the blood through the tricuspid valve into the right ventricle. The blood is then expelled from the right ventricle into the pulmonary artery via the pulmonary valve, where it travels to the lungs to be oxygenated. The oxygenated blood is then returned by the pulmonary vein to the left atria. From here, the blood is pumped through the mitral valve into the left ventricle. As the left ventricle contracts, the oxygenated blood is ejected from the heart into the aorta via the aortic valve, where it enters systemic circulation.

*1.1.1 Structure and function of the heart:*

The heart is comprised of cardiac myocytes (CMs), cardiac fibroblasts (CFs), vascular smooth muscle cells (VSMCs) and endothelial cells (ECs) and it is the dynamic interaction of these contractile and non-contractile cells that allow for proper form and function (Figure 1.1.1.1) (Souders *et al.,* 2009). The composition of the heart is still the subject of debate amongst cardiovascular researchers. Although CMs comprise the majority of the myocardial volume, previous work had estimated that these contractile cells constitute just 30% of the total cardiac cell number (Nag, 1980). The remaining 70% of cardiac cells are the non-contractile cells of the heart, predominantly CFs with a small proportion of ECs and VSMCs (Camelliti *et al.,* 2005). More recent publications have challenged this

estimation, suggesting that CFs may in fact not be the most abundant cell type within the heart (Pinto *et al.,* 2016). These inconsistencies are thought to be caused by the different methods and cell markers used to distinguish CFs, given that no specific cell marker exists for this cell type. It is also known that the composition of cardiac tissue varies across the different chambers of the heart (Litviňuková *et al.,* 2020). Litviňuková estimated that atrial tissue consists of approximately 30% CMs, 24% CFs, 17% VSMCs and 12% ECs, with immune cells comprising the remainder of the atrial tissue. In contrast, ventricular tissues contained 49% CMs, 16% CFs, 21% VSMCs, 8% ECs and 6% immune cells. This variation in the cellular composition reflects the functional differences in the different chambers of the heart, with ventricular tissue known to be thicker than atrial tissue to facilitate the ejection of blood from the heart throughout the body. Regardless, the literature is very much in agreement that CMs and CFs are the most prominent cell types within the heart (Souders *et al.,* 2009). ECs and VSMCs on the other hand form a much smaller part of the cardiac cellular network and are limited to the vasculature (Figure 1.1.1.1) (Baudino *et al.,* 2006). The distinct arrangement of these cardiac cells not only preserves cardiac structure, but also facilitates the biochemical, electrical and mechanical properties of the heart.

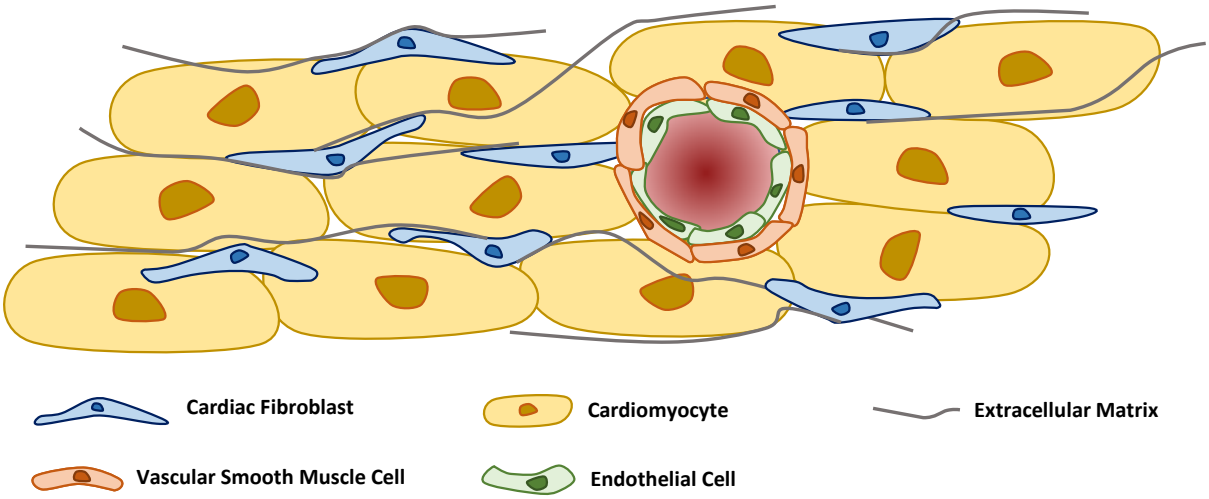


**Figure 1.1.1.1. Schematic representation of the organisation of the cellular components of the heart.** CMs are organised into laminae and are interspersed with CFs, allowing for homogeneous and heterogeneous cell signalling. Activated CFs regulate the ECM by secreting factors that synthesise and degrade the collagen framework. ECs and VSMCs make up a relatively small proportion of the heart and are restricted to the vasculature. This complex arrangement maintains proper cardiac structure and facilitates the dynamic interaction of these cells. This figure was adapted from Baudino *et al.,* 2006.

*1.1.2 Cardiomyocytes and excitation contraction coupling:*

CMs facilitate the coordinated contraction of the heart, derived primarily from oscillating $Ca^{2+}$ ion movements (Goonasekera and Molkentin, 2012). CM contraction is reliant upon $Ca^{2+}$ release, predominantly from the sarcoplasmic reticulum (SR), and is regulated via $Ca^{2+}$ handling proteins, $Ca^{2+}$ transporters and $Ca^{2+}$ channels such as the L-type $Ca^{2+}$ channel (LTCC), ryanodine receptor (RyR2), phospholamban (PLB), sodium-calcium exchanger (NCX) and sarcoplasmic-endoplasmic reticulum $Ca^{2+}$-ATPase pump (SERCA). All of these are subject to regulation by biochemical modification via kinases and phosphatases. These $Ca^{2+}$ handling proteins tightly regulate CM intracellular $Ca^{2+}$ channels, and in doing so, control intracellular $Ca^{2+}$ concentrations (Currie *et al.,* 2004). This in turn facilitates normal cardiac excitation-contraction coupling (ECC), the physiological process whereby an electrical signal is rendered into a contractile force (Figure 1.1.2.1) (Bers, 2002).

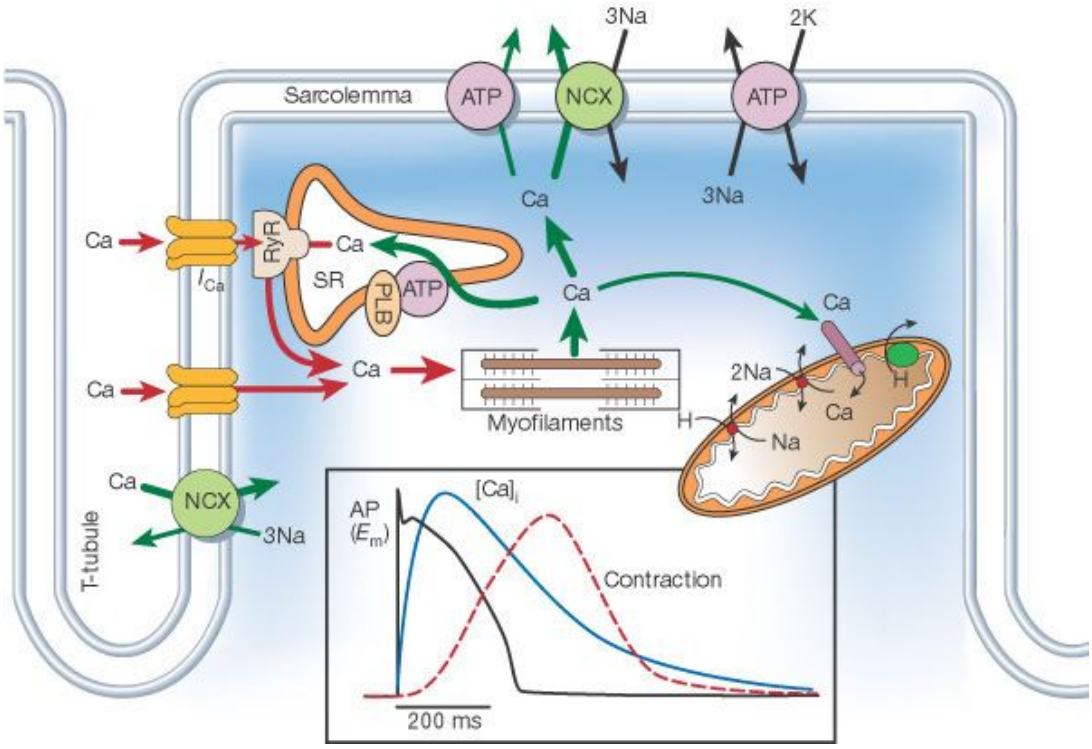


**Figure 1.1.2.1. Calcium transport and cardiac contraction in cardiac myocytes.** Membrane depolarisation facilitates an influx of $Ca^{2+}$ into the cytosol via the L-type $Ca^{2+}$ channels. The $Ca^{2+}$ influx triggers the release of stored $Ca^{2+}$ from the sarcoplasmic reticulum by phosphorylating the ryanodine receptor. This creates a $Ca^{2+}$ spark that facilitates cardiac contraction, allowing cross-bridge formation and contraction of the cardiac muscle (Bers, 2002).

Cardiac contraction originates with the opening of voltage gated $Na^+$ channels causing membrane depolarisation (Aronsen *et al.,* 2013). The resulting $Na^+$ influx triggers membrane depolarisation and generates electrical impulses which spread into contractile myocardial cells through gap junctions to facilitate synchronised cardiac contraction. The resultant depolarisation stimulates the opening of the LTCC within the T-tubules, allowing for an influx of $Ca^{2+}$ ions down the concentration gradient into the cytosol (Figure 1.1.2.1) (Ottolia *et al.,* 2013). The relatively small influx of $Ca^{2+}$ ions facilitate the release of large quantities of stored $Ca^{2+}$ from the SR via direct interaction with RyR2 in a phenomenon termed calcium-induced calcium release (CICR) (Figure 1.1.2.1) (Aronsen *et al.,* 2013). The $Ca^{2+}$ ions then diffuse through the cytosol where they bind to troponin C to shift the troponin-tropomyosin complex to expose the actin binding sites to facilitate cross-bridge formation and allow CM contraction. To allow cardiac relaxation, the transient increase in intracellular $Ca^{2+}$ must be restored to baseline, allowing the troponin-tropomyosin complex to return to its inhibitory position (Bers, 2002). In healthy myocytes, the restoration of $Ca^{2+}$ concentration occurs by four main mechanisms: (i) by extrusion from the cell in exchange for $Na^+$ via the NCX; (ii) by re-uptake into the SR by SERCA to replenish the SR $Ca^{2+}$ stores (iii) the uptake of $Ca^{2+}$ ions into the mitochondria via the mitochondrial $Ca^{2+}$ uniporter and (iv) by extrusion from the cell via the sarcolemmal $Ca^{2+}$-ATPase. This tight regulation of $Ca^{2+}$ movement is critical to the efficient and effective functioning of CMs. This, combined with the dynamic cell-cell interaction with CFs, is critical in regulating normal cardiac function (Porter and Turner, 2009).

### *1.1.3 Cardiac fibroblasts and their role in the heart:*

CFs are responsible for maintaining cardiac structure and function in both the healthy and diseased heart (Souders *et al.,* 2009). Although the source of CFs remains unclear, they are believed to be of mesenchymal origin and are critical to the development of the cardiac

skeleton due to their regulation of collagen deposition and degradation that forms the extracellular matrix (ECM). CF content, and thus secreted factors, varies with development stage and health. During embryonic development, collagen deposition from CFs forms the cardiac skeleton and valves (Camelliti *et al.,* 2005). During foetal development, collagen deposition increases, and formation of the ECM begins. This increase continues into neonatal development, concomitant with CF proliferation, until infancy where it subsides until stimulated by physiological signalling or disease.

In the healthy heart, CFs are quiescent cells whose primary function is to facilitate intercellular signalling. Although CFs are non-excitable cells, the cardiac cellular arrangement (Figure 1.1.1.1) and the high membrane resistance make CFs excellent conductors of hetero- and homogeneous cell signalling (Camelliti *et al.,* 2005; Souders *et al.,* 2009; Hall *et al.* 2021). This proximity of CFs to CMs allows the formation of functional gap junctions, connexins, to convey electrical excitation via heterogeneous signalling. This ability of CFs to convey electrical signalling between different cardiac cells make them central to cardiac contraction, relaying information to CMs that would otherwise be isolated by connective tissue (Camelliti *et al.,* 2005; Hall *et al.* 2021). CFs are also capable of homogeneous signalling, transmitting spontaneous electrical activity from CF to CF, as is the case in cardiac scars, in order to convey the signals to distant CMs to facilitate synchronized cardiac contraction.

CFs are sentinel cells that play a critical role in responding to biochemical and biomolecular signalling in order to preserve normal cardiac function (Díaz-Araya *et al.,* 2015). In addition to their role in cardiac cell signalling, CFs regulate the ECM structure through the secretion of factors that synthesise and degrade the collagen framework. This dynamic process is critical to both cardiac repair and cardiac pathology. CFs are a key source of factors that regulate ECM turnover, including interstitial collagen, metalloproteinases (MMPs), tissue inhibitors of metalloproteinases (TIMPs), cytokines and

growth factors (Porter and Turner, 2009; Hall *et al.* 2021). The collagen secreted by CFs provides the structural basis of the ECM and is responsible for maintaining cardiac structure. The collagen fibres distribute the contractile force across the cardiac muscle, facilitating synchronised cardiac contraction.

*1.2 The pathophysiology of heart disease:*

The distinct arrangement of cardiovascular cells is equally important to cardiac pathophysiology as it is to normal cardiac physiology. In response to stress or injury, the cardiovascular cells attempt to compensate for the disruption in normal function, preserving cardiac function via processes that involve both the contractile and non-contractile cells of the heart. These processes are induced by a variety of cell signalling pathways that contribute to altered cellular function, such as neurohormonal activation (Chaggar et al., 2009), inflammatory signalling (Squires et al., 2005; Suetomi et al., 2018), oxidative stress (O'Toole et al., 2009; Joiner et al., 2012), and irregular $Ca^{2+}$ handling, mediated by changes in the expression and activation of $Ca^{2+}$ handling proteins, such as calcium/calmodulin dependent protein kinase II (CaMKII), and their substrates (Sossalla et al., 2010; Martin et al., 2014). Although intent on preserving cardiac function, these compensatory mechanisms cannot be sustained, and eventually lead to worsening of cardiovascular pathophysiology.

Cardiovascular dysfunction is typically associated with a reduction in left ventricular function. The pathological changes that follow typically involve a reduction in cardiac output (CO) and arterial pressure, resulting in a failure to meet the body's metabolic demand (Figure 1.2.1). As a result, the failing heart attempts to compensate via coordinated structural changes and neurohormonal activation to mitigate the reduction in blood pressure (BP) and CO. The reduction in BP is detected by baroreceptors, resulting in activation of the renin-angiotensin aldosterone system (RAAS). RAAS activation increases blood volume by

increasing water reabsorption, thereby attenuating the reduction in BP. RAAS activation also augments BP via the secretion of angiotensin II, a potent vasoconstrictor that increases peripheral resistance, thereby inducing a prolonged increase in BP (Hartupee and Mann, 2017).

In addition to neurohormonal activation, the failing heart also undergoes structural changes that are aimed at increasing CO. The heart achieves this by increasing cardiac muscle mass, primarily in the ventricles. Predominantly, this is mediated by CF activation, a process whereby CFs differentiate into myofibroblasts (MFs), their active cell type which secretes factors that synthesise and degrade the ECM (Hall *et al.* 2021). This transition results in increased ECM deposits that promote ventricular remodelling that is aimed at increasing ventricular ejection (Figure 1.2.1). However, previous studies have also suggested a role for changes in CM $Ca^{2+}$ handling in this process. In the failing heart, changes in intracellular $Ca^{2+}$ cycling have been linked to changes in contractility (Nerheim et al., 2004; Curl et al., 2018), an adaptive mechanism to increase BP and CO. However, studies have also shown that these changes in intracellular $Ca^{2+}$ also cause the CMs to swell, and this has been suggested to contribute to the increase in ventricular mass alongside CF activation (Beuckelmann et al., 1992; Curl et al., 2018). However, other studies have reported finding to the contrary, showing no significant difference in intracellular $Ca^{2+}$ in ventricular CMs isolated from failing vs non-failing hearts at diastole (Kubo et al., 2001; Piacentino III et al., 2003). Taken together, these conflicting reports suggest that the role of $Ca^{2+}$-induced swelling of the CMs in the pathophysiology of HF may depend on the underlying index event, though the role of fibrotic remodelling in increasing ventricular mass is well established (Tham et al., 2015).

Although intent on preserving cardiac function, these compensatory mechanisms cannot be sustained, leading to an untenable, increased cardiac workload (Figure 1.2.1). The increased pressure and fibrotic remodelling create a negative loop which, over time,

drive further pathophysiological changes. Eventually, the cardiac muscle will hypertrophy – ultimately worsening the already impaired CO and BP, causing the heart to fail.

Recent evidence suggests that certain drug groups, for example anti-cancer agents, can contribute to cardiovascular dysfunction due to their off target, potentially toxic, side effects. The pathological consequences and progressive dysfunction are very similar to what is observed in heart disease, suggesting that the underlying pathophysiology of drug-induced cardiotoxicity is similar to that of cardiovascular disease (CVD). This will be described in more detail in section 1.4.

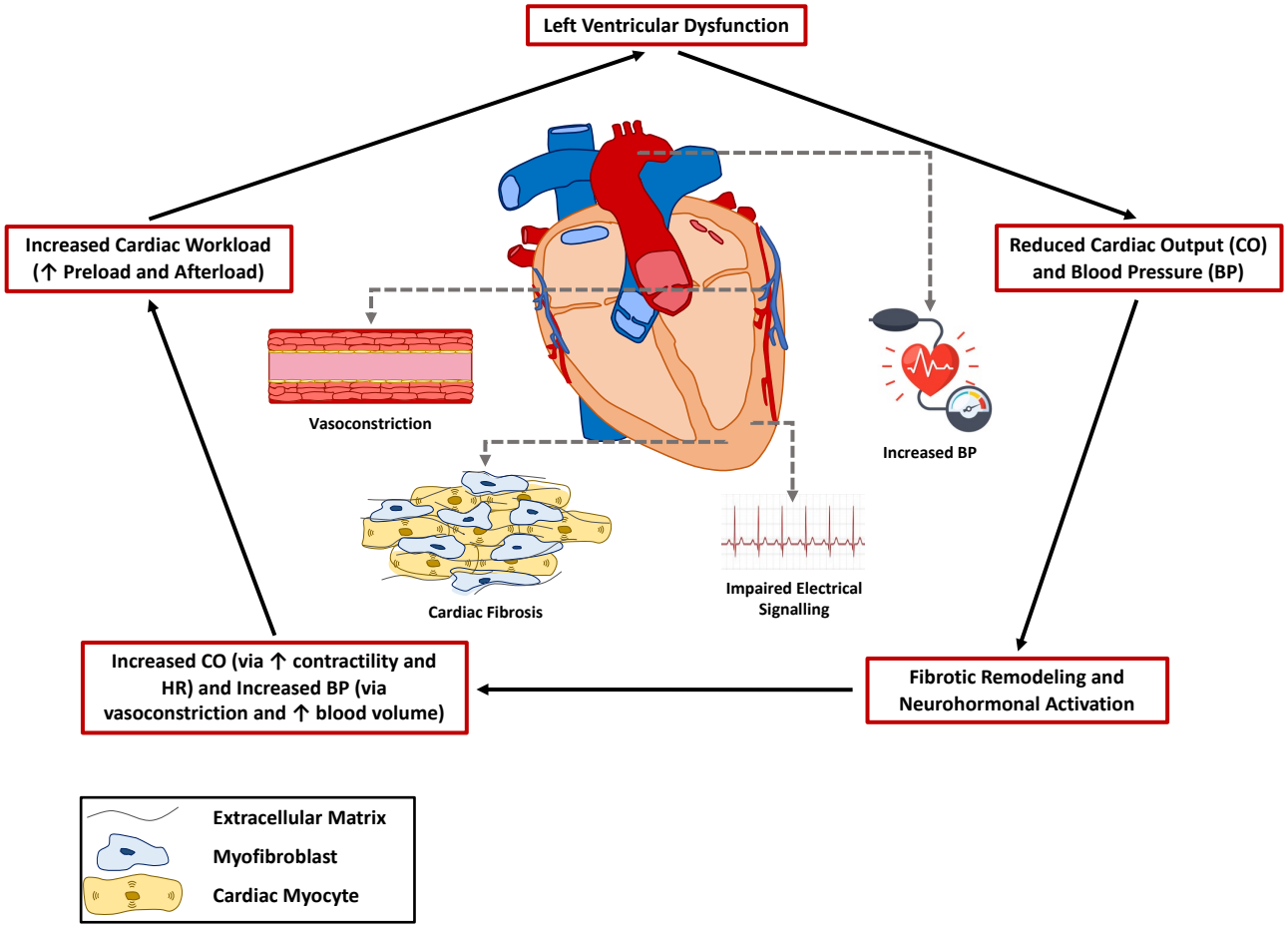


**Figure 1.2.1. An overview of the progression from left ventricular dysfunction to heart failure.** Left ventricular dysfunction in common in cardiovascular pathologies, including heart failure (HF), resulting in reduced cardiac output (CO) and blood pressure (BP). This results in a failure to meet the body's metabolic demand, causing the heart to undergo coordinated structural changes and neurohormonal activation in order to compensate for the shortfall in CO. The reduction in BP activates the renin-angiotensin aldosterone system, increasing water reabsorption to increase blood volume, and promoting vasoconstriction via the secretion of angiotensin II. The heart also undergoes structural changes to attenuate the reduction in CO. Specifically, the thickness of the myocardium, predominantly the ventricles, is increased in order to increase the ejection of blood from the heart via processes that involve both the contractile and non-contractile cells of the heart. This increase in ventricular mass is believed to be caused, in part, by $Ca^{2+}$-induced swelling of the CMs; though some publications have reported findings to the contrary, which suggests that the role of $Ca^{2+}$-induced swelling of the CMs in the pathophysiology of HF may depend on the underlying index event. Fibrotic remodelling is the primary mechanism mediating the increase in cardiac muscle mass. The activated cardiac fibroblasts, myofibroblasts (MFs), regulate ECM deposits. To compensate for the reduced CO, MFs increase ECM deposit to thicken the ventricular muscle to aid in the ejection of blood from the heart. Although these compensatory mechanisms are intent on preserving cardiac function, they cannot be sustained, leading to an untenable, increased cardiac workload. This results in negative loop which drives further pathophysiological changes, leading to hypertrophic remodelling, cardiomyopathy and, eventually, HF.

*1.2.1 Monitoring cardiac pathophysiology:*

Cardiac pathophysiology, driven by changes in the cardiac cells, can have a profound effect on the structure and function of the heart. As a result, it is possible to monitor these changes and use this to determine cardiovascular health and function. The two main methods used to determine this are cardiac imaging and the monitoring of cardiac biomarkers (Zamorano *et al.,* 2016; Modin *et al.,* 2018). Cardiac imaging is a frequently used, non-invasive technique that can identify changes in cardiac structure and blood flow (Esmaeilzadeh *et al.,* 2013). There is no gold standard for cardiac imaging and several different imaging techniques are used clinically, including echocardiography, magnetic resonance imaging, computed tomography and nuclear cardiac imaging (Foley *et al.,* 2012). The most common use of these imaging techniques is to assess left ventricular ejection fraction (LVEF). This calculates the amount of oxygenated blood that is leaving the heart and is something that is commonly reduced in cardiac pathologies due, in part, to the aforementioned changes in cardiac cell phenotype and function. This reduction in LVEF, and the use of cardiac imaging to assess it, can be seen across several different cardiac pathologies, including heart disease (Karaye and Sani, 2008) and drug induced cardiotoxicity (Kerkela *et al.,* 2006; Motzer *et al.,* 2007; Telli *et al.,* 2008). However, this reduction in LVEF does not manifest across all cardiovascular pathologies. Consequently, cardiac biomarkers also serve as a common and robust method of determining cardiovascular health (Liquori *et al.,* 2014). There is no single cardiac biomarker that is used to infer cardiovascular dysfunction. Instead, markers of inflammation (C-reactive protein (CRP) and tumour necrosis factor α (TNFα)), biochemical strain (brain natriuretic peptide (BNP)), cardiomyocyte injury (cardiac troponins) and fibrosis and ECM remodelling (procollagen, MMPs and TIMPs) can be used to assess cardiovascular dysfunction (Elster *et al.,* 1956; Liquori *et al.,* 2014; Suetomi *et al.,* 2018). Taken together, cardiac imaging and biomarkers can provide a comprehensive overview of cardiovascular function that can be

used to not only diagnose heart disease, but estimate prognosis, guide the treatment plan for mitigating cardiovascular dysfunction and assess the patient's response to intervention.

*1.2.2 The role of calcium dysregulation in cardiac myocyte dysfunction in heart failure:*

Drug induced cardiotoxicity and HF share many clinical features, suggesting that the pathophysiological changes that underlie both conditions may also be similar. As such, it is important to have an understanding of the cellular pathophysiology of HF in order to establish a framework for investigating the cardiotoxic mechanism of anti-cancer drugs. Altered $Ca^{2+}$ handling is a key feature of HF and it is clear that the pathophysiological changes that induce HF occur at a cellular level. Changes in $Ca^{2+}$ handling proteins, such as SERCA or RyR2, and the expression and activation of the proteins that regulate their activity, such as CaMKII, are partly responsible for the impaired CM contractility seen in HF (Sossalla *et al.,* 2010). Failing CMs exhibit impaired $Ca^{2+}$ cycling, with reduced peak $Ca^{2+}$ and prolonged decay of the $Ca^{2+}$ transients (Beuckelmann *et al.,* 1992; Kubo *et al.,* 2001; Piacentino *et al.,* 2003). Previous publications have postulated that this disruption of $Ca^{2+}$ cycling may be caused by reduced expression of the $Ca^{2+}$ pump, SERCA, and that this may be an underlying factor in the pathophysiology of HF (Arai *et al.,* 1993; Hasenfuss *et al.,* 1994; Kubo *et al.,* 2001). SERCA is the primary mechanism facilitating relaxation of CMs, reintegrating free $Ca^{2+}$ from the cytosol back into the SR. Reduced SERCA expression causes a disruption in $Ca^{2+}$ cycling, allowing for increased free cytosolic $Ca^{2+}$ concentration. This may account for the prolonged decay of the $Ca^{2+}$ transient that is seen in CMs in some patients with HF (Beuckelmann *et al.,* 1992). The reduction in $Ca^{2+}$ transport by SERCA places an increased burden on NCX to preserve intracellular $Ca^{2+}$ concentrations, as reported by Piacentino *et al.* (2003). However, several studies have reported no change in the expression or activity of the NCX (Beuckelmann *et al.,* 1992; Kubo *et al.,* 2001; Piacentino *et al.,* 2003). This may explain why the decay of $Ca^{2+}$ transients, and thus

contraction duration, is prolonged in HF. However, the changes in SERCA expression also have a profound influence on cardiac contraction. Reduced SERCA expression correlates with reduced $Ca^{2+}$ in the SR, a well-documented characteristic of HF (Piacentino *et al.,* 2003). The reduction in SR $Ca^{2+}$ content correlates with the hearts inability to function properly.

The cellular changes that seemingly underpin the HF mechanism can be alleviated via pharmacologic intervention using conventional cardiovascular drugs. β-blockers have been found to restore $Ca^{2+}$ handling protein expression known to be altered in failing hearts (Kubo *et al.,* 2001). Kubo *et al.* showed that β-blocker treatment increased SERCA expression in CMs to levels consistent with healthy hearts, thereby re-establishing regular $Ca^{2+}$ cycling. The study also found that the ratio of SERCA/PLB and SERCA/NCX was restored by β-blocker therapy, increasing the rate of $Ca^{2+}$ decay and subsequently reducing the duration of the $Ca^{2+}$ transient that is dysregulated in HF. Recent articles have highlighted the efficacy of β-blocker therapy in HF patients with preserved ejection fraction, decreasing mortality in comparison to patients not receiving β-blocker treatment (Stolfo *et al.,* 2020; Yang *et al.,* 2020). However, it should be noted that β-blocker therapy can be associated with an increased risk of rehospitalisation due to worsening HF (Yang *et al.,* 2020). These findings reaffirm the critical nature of maintaining regular $Ca^{2+}$ cycling in the heart and how chronic dysregulation of this intricate interplay of $Ca^{2+}$ handling proteins can have a devastating consequence on cardiac contraction.

*1.2.3 The role of oxidative stress in cardiac myocyte dysfunction in heart failure:*

In addition to altered $Ca^{2+}$ cycling, oxidative stress is also believed to play an important role in the pathophysiology of HF (Tsutsui *et al.,* 2011). Oxidative stress is a change in redox status caused by an increase in reactive oxygen species (ROS) production.

ROS are generated as a by-product of several physiological processes, such as the oxidation of hypoxanthine and xanthine by xanthine oxidase (Cappola *et al.,* 2001), the production of nitric oxide (NO) by nitric oxide synthase (Vasquez-Vivar *et al.,* 1998), the oxidation of nicotinamide adenine dinucleotide phosphate hydrogen (NADPH) by NADPH oxidase (Panday *et al.,* 2015) and, principally, via the mitochondrial electron transport chain (Zhao *et al.,* 2019). Low levels of ROS are perfectly normal and have been demonstrated to play a role in physiological processes such as immune cell activation, autophagy and cell differentiation (Sena and Chandel, 2012; Bardaweel *et al.,* 2018). However, when ROS production is increased and not mitigated by the innate antioxidant defence mechanisms, the resultant oxidative stress causes cellular dysfunction and death (Figure 1.2.3.1) (Tsutsui *et al.,* 2011, van der Pol *et al.,* 2019).

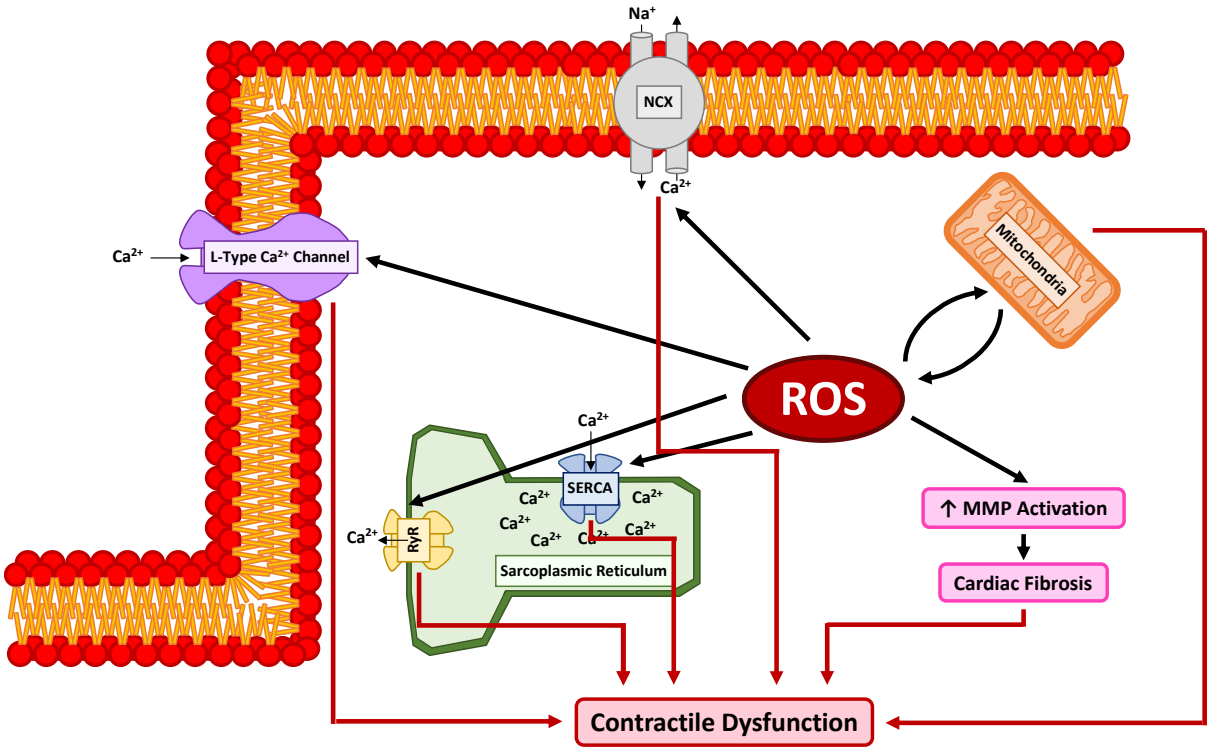


**Figure 1.2.3.1. An overview of the role of reactive oxygen species in the pathophysiology of heart failure.** ROS have been demonstrated to contribute towards the pathophysiology of HF via several mechanisms, including cardiac remodelling, impaired excitation-contraction coupling and mitochondrial dysfunction (Rajagoplan *et al.,* 1996; Xu *et al.,* 1997; Kawakami and Okabe, 1998; Spinale *et al.,* 1998; Fearon *et al.,* 1999; Eigel *et al.,* 2003; Gutierrez-Martin *et al.,* 2004; van der Pol *et al.,* 2019; Zhao *et al.,* 2019).

ROS contribute towards the pathophysiology of HF via impaired $Ca^{2+}$ cycling and mitochondrial dysfunction. The mechanisms underlying ROS-induced impaired ECC are complex and have been shown to involve several $Ca^{2+}$ handling proteins. ROS have been demonstrated to cause $Ca^{2+}$ influx via oxidation of the LTCC (Campbell *et al.,* 1996). ROS-induced $Ca^{2+}$ influx was also observed via NCX, with ROS enabling reverse-mode NCX activity (Eigel *et al.,* 2003). NCX operating in reverse mode facilitates $Ca^{2+}$ entry into the cytosol, increasing intracellular $Ca^{2+}$ concentration. ROS have also been shown to affect the function of SR $Ca^{2+}$ handling proteins, namely RyR2 (Kawakami and Okabe, 1998) and SERCA (Xu *et al.,* 1997; Gutierrez-Martin *et al.,* 2004). The effect of ROS on both of these proteins increases intracellular $Ca^{2+}$, by increasing the opening probability of RyR2, facilitating $Ca^{2+}$ release from the SR, and by inactivating SERCA, preventing SR re-uptake of intracellular $Ca^{2+}$. These changes in $Ca^{2+}$ mobility have a detrimental effect on cardiac contractility, which requires a cyclic movement of intracellular $Ca^{2+}$ for efficient contraction and relaxation of the myocardium.

ROS and their downstream effects on intracellular $Ca^{2+}$ are known to affect mitochondrial function. The role of mitochondria in the pathophysiology of HF is well documented (Joiner *et al.,* 2012; Luo and Anderson, 2013; Zhou and Tian, 2018). A previous study showed that in HF, mitochondrial dysfunction is mediated by increased $Ca^{2+}$ entry into the mitochondria and this uptake of $Ca^{2+}$ into the mitochondria is mediated by the $Ca^{2+}$ handling protein CaMKII (Joiner *et al.,* 2012). This interferes with the mitochondrial electron transport chain, resulting in increased ROS production and reduced ATP production caused by impaired oxidative phosphorylation. Such changes stimulate the opening of the mPTP, a high conductance channel which releases mitochondrial ROS and pro-apoptotic factors, such as cytochrome c, into the cytosol (Akopova *et al.,* 2011; Joiner *et al.,* 2012). This causes mitochondrial dysfunction and subsequent cell death, consistent with the decline in cardiac contractility seen in HF. These observations also highlight the reciprocal relationship between $Ca^{2+}$ and ROS in the pathophysiology of HF.

*1.2.4 The role of inflammation in cardiac myocyte dysfunction in heart failure:*

The role of inflammation in cardiovascular dysfunction was first discovered in 1956 when Elster *et al.* (1956) reported elevated concentrations of the systemic inflammatory marker, CRP, in the serum of patients with congestive HF. The study found that the severity of congestive HF correlated with CRP expression, highlighting the prominent role inflammation plays in the pathophysiology of the condition. Since then, the link between inflammation and the pathophysiology of cardiovascular dysfunction has grown considerably, with multiple research articles reporting an upregulation of inflammatory mediators in cardiac pathologies (Levine *et al.,* 1990; Matsumori *et al.,* 1994; Testa *et al.,* 1996; Torre-Amione *et al.,* 1996). In response to insult or injury, an acute inflammatory response is perfectly normal, acting as a protective mechanism to compensate for the decline in cardiac function in the immediate sense and preserve cardiac function in the long term (Dick and Epelman, 2016). However, when the inflammatory response becomes excessive or sustained, inflammation can cause adverse cardiac remodelling that can cause cardiac dysfunction and, eventually, HF.

Recently, a role for CMs in cardiac inflammation has been discovered (Suetomi *et al.,* 2018). CMs are now believed to be a key source of inflammatory mediators, initiating the immune response in the heart. Transverse aortic constriction (TAC) is an established model of cardiac pressure overload and has been used previously to investigate inflammatory and fibrotic responses in the heart (Ying *et al.,* 2009). A recent publication by Suetomi (2018) utilised TAC to investigate the role of CMs in cardiac inflammation and adverse cardiac remodelling. The study found that TAC increased the expression of several pro-inflammatory genes in CMs: monocyte chemoattractant protein 1, macrophage inflammatory protein 1α, C-X-C motif ligand 1 (CXCL1), CXCL2, interleukin 6 (IL-6), IL-1β, IL-18 and TNFα. This upregulation of pro-inflammatory mediators was accompanied by adverse cardiac remodelling. Interestingly, the study also found that this pro-inflammatory signalling in CMs

was regulated by the $Ca^{2+}$ handling protein, CaMKII. CaMKII inhibition not only ameliorated the increase in pro-inflammatory gene expression, but also reduced cardiac remodelling. These findings show that CM induced inflammatory signalling is regulated by CaMKII, which in turn, suggests a role for $Ca^{2+}$ dysregulation in this potentially pathological mechanism.

*1.2.5 Cardiac fibroblast to myofibroblast differentiation:*

Fibrotic remodelling is a well-known hallmark of cardiovascular disease and its role in the pathophysiology of many cardiovascular disorders is well established. Fibrotic remodelling is induced by CF activation. Activated CF undergo CF to MF differentiation, a biochemical process characterised by increased cell proliferation and ECM remodelling (Vasquez *et al.,* 2011). The purpose of CFs extends far beyond maintaining structural integrity and conveying electrical signalling, and their role in adverse cardiac remodelling, and in the aetiology of cardiovascular dysfunction, cannot be overlooked. The activated CFs facilitate ECM turnover, a tightly regulated process involving the synthesis and degradation of collagen, the primary structural element of the ECM (Vasquez *et al.,* 2011; Nagaraju *et al.,* 2019). The activated CF not only secrete collagen but also factors that regulate collagen metabolism, namely MMPs and TIMPs (Camelliti *et al.,* 2005; Souders *et al.,* 2009; Vasquez *et al.,* 2011). MMPs degrade collagen while TIMPs inhibit MMP activity.

MF transdifferentiation is a dynamic process that has been observed to be induced by several mechanisms, acting in both an independent and complementary manner. CF activation has been suggested to be caused by mechanical stretch of the myocardium (Takeda *et al.,* 2010) and via pro-fibrotic (Squires *et al.,* 2005; Khalil *et al.,* 2017; Bradley *et al.,* 2018) and pro-inflammatory (Bradham *et al.,* 2002; Bujak *et al.,* 2008; Sandstedt *et al.,* 2019) signalling, in both a paracrine and autocrine fashion. Ultimately, CF activation is intent on preserving cardiac function via structural remodelling to compensate for the damaged or

diseased cardiac tissue; however, prolonged excessive activity is associated with cardiovascular dysfunction.

*1.2.6 The role of calcium in cardiac fibroblast activation:*

It has been shown that activation of the calcium sensing receptor (CaR), a G protein-coupled receptor (GPCR) that responds to extracellular $Ca^{2+}$, is associated with cardiac remodelling (Lu *et al.,* 2013). More recently, CaR activation was found to induce CF activation and influence the activation of ECM remodelling enzymes that favour fibrosis (Zhang *et al.,* 2014). Specifically, CaR activation was found to significantly increase MMP activation and reduce that of TIMPs. This pro-fibrotic signalling, mediated by CaR activation, induced LV dysfunction and resulted in reduced CO. CaR inhibition meanwhile was found to attenuate fibrotic remodelling and restore normal cardiac function. These results highlight the synergy between CFs and CMs in mediating cardiovascular dysfunction. $Ca^{2+}$ dysregulation is well documented in CMs, and given that CaR responds to extracellular $Ca^{2+}$, it is entirely possible that the CaR mediated fibrotic remodelling may be driven, at least in part, by CM dysfunction in the failing heart.

A more recent study showed that CF proliferation, an indicator of CF activation (Vasquez *et al.,* 2011), is regulated by the $Ca^{2+}$ handling protein, CaMKII (Martin *et al.,* 2014). Martin *et al,* found that the expression and activation of CaMKII and CF proliferation were increased in a murine model of cardiac fibrosis and hypertrophy. Moreover, the study showed that CF proliferation can be reduced via CaMKII inhibition. These findings mirror those of Zhang *et al.* (2010), who showed that CaMKII inhibition attenuated CF proliferation and reduced the secretion of pro-fibrotic mediators from CFs. Although neither study assessed changes in intracellular $Ca^{2+}$ directly, both suggest a role for $Ca^{2+}$ in the activation of CFs. It is well documented that $Ca^{2+}$ flux is a rate limiting step for CaMKII activation

(Clapham, 2007, Erickson *et al.,* 2008; Erickson *et al.,* 2015), and from this it is possible to infer that the increase in CaMKII expression and activation likely occurs alongside an increase in the concentration of intracellular $Ca^{2+}$.

*1.2.7 The role of inflammation in cardiac fibroblast activation:*

The literature suggests that CF differentiation is mediated largely by the pro-fibrotic cytokine, transforming growth factor β 1 (TGF-β1). TGF-β1 has been found to be significantly upregulated in fibrotic remodelling and has been shown to mediate an increase in secreted factors from activated CF that regulate the ECM (Villarreal and Dillmann, 1992; Squires *et al.,* 2005, Khalil *et al.,* 2017; Nagaraju *et al.,* 2019). Squires and colleagues (2005) found that stimulation of CFs with TGF-β1 induced CF differentiation, adhesion and production of collagen type I, the main fibrillar collagen mediating ECM remodelling. A similar upregulation in the expression of pro-fibrotic mediators was also observed in CFs isolated from the LV of failing hearts. Nagaraju (2019) reported a significant increase in the expression of several profibrotic genes including collagen type I, collagen type III and lysyl oxidase (LOX), an enzyme that promotes collagen cross-linkage. The study also observed a significant increase in the gene expression of MMPs and TIMPs, factors that regulate collagen metabolism. Further analysis revealed that the increased gene expression of these ECM structural constituents and remodelling enzymes is mediated via TGF-β1 signalling. Inhibition of TGF-β receptor 1 (TGF-β R1) significantly reduced the increased gene expression driving the fibrotic remodelling seen in CFs isolated from failing hearts. These findings are largely consistent with those of Khalil (2017), who observed a similar reduction in pro-fibrotic gene expression that correlated with improved left ventricular function and reduced cardiac remodelling.

Several articles have highlighted the role of the Smad2/3 signalling pathway in mediating TGF-β induced fibrotic remodelling. Smad2 and Smad3 are transcription factors that, when activated by TGF-β, induce pro-fibrotic gene transcription (Khalil *et al.,* 2017). As has already been established, the TGF-β signalling pathway is activated in response to cardiovascular dysfunction (Nagaraju *et al.,* 2019). This causes increased activation of the Smad2/3 signalling pathway, inducing cardiac remodelling. This is highlighted by Khalil (2017), who observed that activation of the Smad2/3 signalling pathway induced CF differentiation and fibrosis in a model of pressure overload and in response to TGF-β. Genetically modified mice with Smad2/3 and Smad3 deletion alone reduced CF activation and subsequent fibrotic remodelling in response to TGF-β activation. Interestingly, Smad2 deletion alone had little effect on TGF-β induced fibrosis, suggesting that Smad3 is the primary mediator of this fibrotic mechanism. However, Smad deletion ultimately did not attenuate cardiac hypertrophy or left ventricular dysfunction.

### *1.2.8 The role of oxidative stress in cardiac fibroblast activation:*

It has long been established that ROS have a profound influence on the ECM (Takimoto and Kass, 2006). ROS are known to be one of several factors that regulate CF proliferation (Fujisaki *et al.,* 1995; Cheng *et al.,* 2003) and have also been observed to have a direct effect on ECM metabolism via the secretion and activation of MMPs (Zhang *et al.,* 2002; O'Toole *et al.,* 2009; Lin *et al.,* 2012; Mori *et al.,* 2019). More recent studies have provided deeper insight into this mechanism and have found that the ROS-induced secretion and activation of MMPs actually occurs downstream of inflammatory signalling and changes in intracellular $Ca^{2+}$ handling (O'Toole *et al.,* 2009; Lin *et al.,* 2012). O'Toole *et al.* (2009) reported that MMP-9 secretion is increased by ROS in a mechanism that involves changes in intracellular $Ca^{2+}$. Specifically, the increase in $Ca^{2+}$ was found to increase intracellular ROS production via xanthine oxidase activation, which in turn, stimulates MMP-9 secretion.

The same study also found that MMP-9 expression was increased by the inflammatory mediator TNFα. Although these findings were obtained in macrophages, a potent source of MMP-9 (Fang *et al.,* 2010), activated CFs have also been found to secrete MMP-9 (Siwik *et al.,* 2001; Brown *et al.,* 2007) and MMP-9 has been linked to cardiovascular remodelling associated with HF (Bradham *et al.,* 2002). Similar findings were reported by Lin *et al,* (2012), who also coupled inflammation and $Ca^{2+}$ dysregulation to intracellular ROS production as part of a mechanism that stimulates MMP-9 secretion in astrocytes. The similarity of these findings suggest that the mechanism of MMP-9 secretion may be conserved amongst cell types and could therefore explain the increase in MMP-9 secretion in activated CFs. These studies also highlight the interplay between the different mechanisms of CF activation, similar to what is seen in CMs (Suetomi *et al.,* 2018). It is important to acknowledge that these processes do not occur independently, and it is the culmination of the effect of inflammatory signalling, $Ca^{2+}$ dysregulation and oxidative stress on both cardiac cell types that mediates cardiovascular pathophysiology.

*1.3 Cardiovascular experimental models:*

It is very difficult to choose an appropriate experimental model, particularly in the cardiovascular field. Each experimental model has its own caveats, and the model itself can have a profound effect on the outcome of the study. Animal models, in particular rodent models, remain an important part of cardiovascular research. There are clear advantages towards the use of rodent models in cardiovascular research. They are relatively easy to manage, provide physiological relevance and can be used to study circulation (Jimenez-Tellez and Greenway, 2019). However, there are many limitations to the use of animal models. They are expensive, time-consuming and, in terms of cardiovascular research, it is very difficult to extrapolate findings obtained in animal models due to the differences in the cardiovascular systems of humans and rodents (Milani-Nejad and Janssen, 2014). Cellular

models offer a cost-effective alternative to animal models. Generally speaking, cellular models are easy to maintain, don't require a lot of time and the findings are able to be translated (Jimenez-Tellez and Greenway, 2019). However, cell models also come with limitations. Cell models can lack physiological relevance and, depending on the source from which the cells are isolated, may have altered ion channels and protein expression, which again complicates the extrapolation of findings obtained in these models (Mitcheson *et al.,* 1998).

### *1.3.1 Cardiac myocyte experimental models:*

Isolated CMs have been a mainstay of cardiovascular research for decades. There are several different CM cellular models that are used routinely in cardiovascular research. Again, each model has its own strengths and limitations, and these must be considered when selecting an appropriate experimental model for use. Neonatal rat ventricular myocytes (NRVMs) are commonly used in cardiovascular research (Barr *et al.,* 2014; Kerkela *et al.,* 2009). NRVMs are cost-effective cells that are relatively easy to isolate and yield a high number of cells (Peter *et al.,* 2016). Most importantly, these cells can be maintained in culture, even in serum free conditions, and can beat spontaneously. However, these cells do have an immature phenotype, meaning that they lack ion channels and proteins only expressed in the mature, adult cell (Mitcheson *et al.,* 1998). Primary adult ventricular myocytes (AVMs), isolated from adult rodents, can circumvent the immature phenotype and marker expression of NRVMs (Peter *et al.,* 2016). AVMs are again cost-effective and can be produced in high yields, though the isolation procedure is more difficult than that of NRVMs. They can, however, be isolated from disease models, making them versatile in terms of cardiovascular research. Unlike NVRMs, AVMs cannot be maintained in culture for prolonged periods of time and do not beat spontaneously (Mitcheson *et al.,* 1998; Abi-Gerges *et al.,* 2013). Immortalised cardiac cell lines, such as H9C2 cells, offer another

alternative for cardiovascular research. H9C2 cells are cardiomyoblasts, a precursor to CMs, that can be differentiated into adult-like CMs that have a genetic profile consistent with the mature cell type (Branco *et al.,* 2015). In the undifferentiated form, H9C2 cells are proliferative and can be maintained in culture, though they do not beat spontaneously (Peter *et al.,* 2016). Although NRVMs, AVMs and immortalised cardiac cell lines have all proven invaluable to cardiovascular research, they all share a common limitation – they are not of human origin, and therefore will not recapitulate the human cellular response to disease or toxicity. Cardiac progenitor cells, such as Promocell's human progenitor cardiac myocytes (PCMs), have also been used in cardiovascular research. PCMs can be maintained in culture, allowing for chronic pharmacologic treatment, and, importantly, are of human origin. However, these cells are phenotypically different from adult CMs and the protein expression of these progenitor cells is not yet known. More recently, human induced pluripotent stem cells (iPSCs) have offered a novel opportunity to study human cardiovascular physiology and disease at a cellular level (Musunuru *et al.,* 2018). In addition to being of human origin, these cells can be differentiated into any cardiac cell type, meaning they can be used in a wide variety of cardiovascular research. These cells can also be isolated from patients with underlying cardiovascular disease, which establishes an accurate phenotype of the diseased cell, or can be genetically manipulated to recapitulate a diseased cardiovascular cell (Peter *et al.,* 2016; Musunuru *et al.,* 2018). However, these cells are expensive, and it can be costly, both financially and in terms of time, to maintain and differentiate iPSCs into adult cardiovascular cells (Peter *et al.,* 2016). While iPSCs can be used to derive CMs, several studies have reported that iPSC-derived CMs do not recapitulate the structure and excitation-contraction coupling of mature CMs (Kamakura *et al.,* 2013; Lundy *et al.,* 2013; Parikh *et al.,* 2017). Ideally, research would be conducted using adult cells isolated from healthy or diseased human donors, depending on the research being carried out. This is the only way to ensure the structure and phenotype of the human cell in the desired setting, diseased or otherwise. However, this too is subject to similar limitations as AVMs. The cells cannot be maintained in culture for prolonged periods, the isolation process is difficult and,

unlike AVMs, the yield is often low. Moreover, human cardiac tissue is difficult to obtain, particularly young, healthy cardiac tissue, further limiting the use of primary adult human CMs in cardiovascular research. Ultimately, there are limitations with all of these models that cannot be mitigated. Researchers therefore need to consider the pros and cons of each of these models when designing their investigation.

*1.3.2 Cardiac fibroblast experimental models:*

Given the prominent role that they play in cardiovascular remodelling, CFs are becoming increasingly more recognised for the role they play in heart disease. Admittedly, CF experimental models are fewer in number than CM models. Primary, isolated CFs are the most commonly used CF cellular model (Bujak *et al.,* 2008; Takeda *et al.,* 2010; Khalil *et al.,* 2017, Burke *et al.,* 2019; Nagaraju *et al.,* 2019). There are two main ways to isolate primary CFs, the Langendorff perfusion method (Burke *et al.,* 2019) and the bulk, collagenase digestion method (Khalil *et al.,* 2017). The bulk collagenase digestion method is by far the simpler and least expensive of the two. The protocol allows for the isolation of CFs under sterile conditions, so the isolated cells can be cultured. The Langendorff perfusion method, on the other hand, is far more involved and requires the use of expensive, specialised perfusion apparatus. The size of the perfusion apparatus means that it is also difficult to conduct the isolation under sterile conditions. The benefit of primary CFs is that they can be isolated from both animal (Bujak *et al.,* 2008; Takeda *et al.,* 2010; Khalil *et al.,* 2017, Burke *et al.,* 2019) and human cardiac tissue (Nagaraju *et al.,* 2019; Sandstedt *et al.,* 2019); though, as with CMs, sourcing human cardiac tissue is difficult, particularly from non-diseased hearts. Adult CFs can be maintained in culture following isolation. However, the cells do tend to differentiate into MFs after multiple passages, an indicator of cellular stress. Recently, CFs have been differentiated from human iPSCs (Zhang *et al.,* 2019). These cells expressed proteins consistent with native CFs and responded appropriately to hypertrophic

stimuli. However, in comparison to adult CFs, the human iPSC-derived CFs were more aligned phenotypically and genetically with embryonic CFs. The limitations of primary, isolated CF cellular models are similar to that of CMs. As a cellular model, primary rodent CFs lack physiological relevance and, as human cardiac tissue is very difficult to obtain, results obtained from animal derived primary CFs may be difficult to extrapolate into humans owing to the biological differences in the cardiovascular systems.

*1.4 Cardiotoxicity:*

The term 'cardiotoxicity' was first used in the 1940's to describe drug-induced cardiovascular dysfunction associated with anaesthetics and, ironically, medications used to treat heart disease (Chung *et al.,* 2018). As mentioned earlier in section 1.2, the common symptoms of cardiotoxicity are consistent with those of cardiovascular dysfunction – arrhythmias, cardiovascular remodelling, hypertension and heart failure (Zamorano *et al.,* 2016), making it difficult to diagnose, particularly in patients with pre-existing cardiovascular conditions who are at increased risk of developing drug-induced cardiotoxicity (Garcia-Alvarez *et al.,* 2010; Zamorano *et al.,* 2016). The most common method of diagnosing cardiotoxicity is to assess changes in LVEF and cardiac biomarkers – the same methodology used to diagnose cardiovascular disease (Zamorano *et al.,* 2016; Chung *et al.,* 2018). Although the symptoms of cardiotoxicity are widely known, the cellular pathophysiology of drug induced cardiotoxicity remains poorly understood (Varga *et al.,* 2015). Cardiotoxicity is becoming increasingly more common amongst therapeutic drugs. Over the last 40 years, approximately 10% of all medications available for clinical use have been withdrawn or had their use heavily restricted owing to concerns regarding their effect on cardiovascular function. More recent publications have identified a growing link between cardiotoxicity and anti-cancer drugs (Kerkela *et al.,* 2006; Maillet *et al.,* 2016; Zamorano *et al.,* 2016).

*1.4.1 Anti-cancer drug induced cardiotoxicity:*

Recent advances in anti-cancer therapeutics have significantly improved cancer prognosis. However, this has come at a cost as many of these new anti-cancer drugs are associated with increased morbidity and mortality due to off-target effects (Zamorano *et al.,* 2016). Cardiac dysfunction is arguably the most common and severe of these off-target effects and, in some cases, patients are more likely to succumb to these cardiovascular complications than the cancer itself (Gernaat *et al.,* 2017). Cardiotoxicity is the development of impaired cardiac function as a side effect of a therapeutic intervention and is becoming increasingly associated with anti-cancer treatments (Zamorano *et al.,* 2016). It is a relatively new concern in the field of oncology but is a fast-growing concern in terms of safety pharmacology. Such toxicity exists in two forms: on-target toxicity, where the target is directly involved in other biologic systems and inhibition of that target has an indirect effect on non-targeted biological processes; and off-target toxicity, wherein other proteins and kinases are simultaneously inhibited, unintentionally, by the drug (Cheng and Force, 2010). Ideally, targeted anti-cancer treatments would focus on an exclusive aspect of the cancer cell that serves a critical function in tumour growth and/or survival, preserving the healthy surrounding cells. Intended to enhance remission length and reduce side effects and toxicity, these novel strategies were designed to offer refined treatments with greater therapeutic potential to better manage and treat cancers with a poor prognosis. In reality, such therapies did show significant success, but were marred by reports of dose-dependent toxicity associated with these drugs.

*1.4.2 Anthracycline induced cardiotoxicity:*

Anthracyclines are a class of very effective anti-cancer drugs used to treat several cancers, including breast cancer, lymphomas and neuroblastomas (Maillet *et al.,* 2016). The mechanism of action of anthracyclines can be split into two broad categories, the inhibition of topoisomerase II and intercalation of DNA base pairs, both of which prohibit cancer cell transcription and replication (Muppidi *et al.,* 2015). However, anthracyclines have long been associated with cardiotoxicity and the anthracycline, doxorubicin, is believed to be one of the most cardiotoxic drugs in clinical use (Maillet *et al.,* 2016). The symptoms of cardiotoxicity associated with anthracyclines are varied and include cardiac arrhythmias, structural remodelling, reduced contractility and, ultimately, HF (Zamorano *et al.,* 2016). The prevalence of anthracycline-induced cardiotoxicity is dependent on several factors, including age, co-morbidities and drug concentration. Drug concentration has been shown to play a massive role in the development of doxorubicin-induced cardiotoxicity (Swain *et al.,* 2003). A retrospective analysis of patients receiving doxorubicin treatment showed that 5% of patients receiving a cumulative dose of 400mg/$m^2$ developed HF, rising to 26% at 550mg/$m^2$ and 48% at 700mg/$m^2$. Furthermore, the same study also showed that HF was more prevalent in doxorubicin-treated patients over the age of 65, highlighting that advanced age may also increase susceptibility to doxorubicin-induced cardiotoxicity. Of course, one could argue that age itself is not a risk factor, more so the decline in physiological functioning and biological processes that accompany aging, such as diabetes and cardiovascular and renal dysfunction, comorbidities that are known to increase susceptibility to anthracycline-induced cardiotoxicity (Zamorano *et al.,* 2016). The cardiotoxic mechanism of anthracyclines is not yet clear, but the prevailing theory is that the cardiotoxic effects are caused by increased ROS production. This increase in intracellular ROS is believed to be mediated at the level of the mitochondria and involve $Ca^{2+}$ dysregulation, lipid peroxidation and impaired oxidative phosphorylation (OXPHOS), ultimately causing CM cell death (Muppidi *et al.,* 2015; Maillet *et al.,* 2016). This mitochondrial mediated mechanism of anthracycline cardiotoxicity is

interesting and can be directly attributable for impaired cardiac function. CMs are abundant with mitochondria, making cardiac tissue particularly susceptible to drug-induced cardiotoxicity (Muppidi *et al.,* 2015). It is important to note that similarities may exist in the cardiotoxic effects observed across different classes of anti-cancer drugs. Despite the differences in the mechanism of action of anthracyclines and other anti-cancer therapeutics, there may be shared cardiotoxic mechanisms exerted by these drugs. Consequently, our understanding of the pathophysiology of anthracycline-induced cardiotoxicity may serve as a starting point for research into the cardiotoxic mechanism of more recent classes of anti-cancer drugs, such as tyrosine kinase inhibitors (TKIs).

*1.5 Tyrosine kinase inhibitors:*

TKIs are a relatively new class of anti-cancer drugs, with the first TKI, imatinib mesylate (Gleevec®), approved for clinical use in 2001 (Cheng and Force, 2010). Tyrosine kinases are signalling proteins that play a critical role in cancer cell survival (Paul and Mukhopadhyay, 2004). They transfer a phosphate group from adenosine triphosphate (ATP) to the tyrosine residues of specific proteins, activating signalling cascades such as angiogenesis, proliferation and cell differentiation. Such processes are critical to the growth and survival of all cell types, including cancer cells. TKIs work by antagonising the ATP binding pocket, preventing phosphorylation and activation of downstream substrates to prohibit cancer cell proliferation. However, because the ATP binding pocket is a shared entity amongst approximately 500 protein kinases and over 2,000 binding proteins, it is not surprising that TKIs are susceptible to selectivity issues and associated toxicity (Bantscheff *et al.,* 2007). Cardiotoxicity occurs when the kinase inhibited plays a prominent role in cardiac function, the inhibition of which disrupts these physiological processes.

TKIs differ in their selectivity and, as a result, have varying degrees of off-target effects. Type I TKIs are largely non-selective, targeting the ATP pocket al.one. As a result, Type I TKIs are well associated with off-target toxicity. In comparison, Type II TKIs are more selective, simultaneously targeting the ATP binding pocket and a site adjacent to it (Cheng and Force, 2010). The enhanced selectivity of Type II TKIs mean that their association with off target effects is much less. Type II TKIs are not exempt to off-target toxicity, the prevalence of these off-target effects is just much lower in Type II TKIs than in Type I TKIs (Zamorano *et al.,* 2016). In the case of TKIs, one would assume that drugs with increased selectivity would induce less toxicity and therefore be more effective. However, this is not always the case. It may be that targeting multiple tyrosine kinases increases the drug's tumour suppressing effect, but does so at the cost of increasing the risk of off-target effects. Of course, this is entirely dependent upon the pathophysiology of the cancer and the drug used to treat it. Nonetheless, it is apparent that toxicity is a critical issue with TKIs and that better understanding of the mechanism of these drugs is required so to limit the cardiotoxicity associated with their use (Moslehi and Deininger, 2015).

### *1.5.1 Imatinib mesylate:*

Imatinib mesylate is a Type II small molecule TKI approved to treat a vast array of conditions, including Philadelphia chromosome positive chronic myeloid leukemia (Ph+CML), hypereosinophilic syndrome (HES) and myeloproliferative diseases (MPD) associated with platelet derived growth factor receptors (PDGFRs) (Krause and van Etten, 2005; Wolf *et al.,* 2010; Garcia-Alvarez *et al*., 2010). Imatinib gained approval in 2001 and has since revolutionised Ph+CML treatment, prolonging patient survival in a condition that was largely fatal 5 years post-diagnosis before the introduction of imatinib, to 90% survival 5 years post-diagnosis in imatinib-treated patients (Cheng and Force, 2010). Imatinib is a highly selective therapeutic agent inhibiting approximately 10 kinases including the tyrosine

kinase Abl, c-KIT and PDGRFs (Cheng and Force, 2010; Garcia-Alvarez *et al*., 2010; Gotlib *et al*., 2004). It was perceived as a safe and well tolerated therapy with no reports of cardiotoxicity during drug development (Wolf *et al*., 2010). However, despite the enhanced selectivity of this agent, patients receiving imatinib therapy have been reported to develop cardiotoxicity. Kerkelä and colleagues (2006) were the first to report TKI-induced cardiotoxicity. The study reported severe congestive heart failure and reduced cardiac output in 10 patients receiving imatinib treatment, all of whom had normal cardiac function at the beginning of treatment. Further reports of cardiotoxicity in patients receiving imatinib treatment soon followed. Ribivero (2008) found that imatinib treatment caused an increase in BNP, an indicator of cardiac hypertrophy. However, the patients enrolled in this study were of an increased age and presented with pre-existing co-morbidities at the outset of treatment, including oedema, borderline left ventricular hypertrophy, an enlarged left atrium and increased left atrial pressure. Similarly, Garcia-Alvarez (2010) reported left ventricular dysfunction following imatinib treatment in a 46-year-old female presenting with HES. However, this patient also presented with cardiovascular dysfunction at initial diagnosis that worsened with imatinib treatment. The incidence of imatinib-induced cardiotoxicity is relatively low (<3%) and almost exclusively occurs in patients with pre-existing cardiovascular conditions or co-morbidities (Garcia-Alvarez *et al*., 2010; Zamorano *et al*., 2016). With routine cardiac assessments before and during therapy, imatinib is, and can continue to be, a safe and highly successful therapeutic agent for several debilitating conditions (Garcia-Alvarez *et al*., 2010; Pareek *et al*., 2018).

### *1.5.2 Sunitinib malate:*

Sunitinib malate (Sutent®) is an effective Type I TKI approved to treat several cancers, including advanced renal cell carcinomas (ARCC), progressive pancreatic neuroendocrine tumours and gastrointestinal stromal tumours (GIST) in patients unable to

tolerate imatinib or after disease progression (Telli *et al*., 2008; Cohen *et al*., 2011; Blanca *et al*., 2016). Sunitinib has been found to inhibit more than 50 kinases and its targets include vascular endothelial growth factor receptors (VEGFRs), c-KIT and PDGFRs amongst others, but its non-selective, anti-angiogenic and anti-proliferative activity is affiliated with off-target cardiotoxicity as a result of its mechanism of action (Telli *et al*., 2008; Cheng and Force, 2010; Cohen *et al*., 2011; Blanca *et al*., 2016). A Phase III clinical trial conducted by Motzer (2007) found that sunitinib increased completion rates and progression-free survival in ARCC patients in comparison to interferon alpha (the first line treatment for the condition at that time) but was associated with a higher incidence of adverse effects. The off-target effects of sunitinib varied, including a reduction in LVEF, hypertension and other, more common adverse effects (diarrhoea, nausea, vomiting). It should be noted, however, that these adverse effects stopped after cessation of therapy or a reduction in sunitinib dosage. Telli (2008) also reported sunitinib-induced cardiotoxicity in a phase III clinical trial aimed at treating metastatic renal cell carcinoma. The study observed a reduction in LVEF in 21% of participants, with symptomatic grade 3/4 left ventricular systolic dysfunction found in 15% of patients. Not surprisingly, further analysis of these patients experiencing cardiotoxic symptoms revealed that cardiotoxicity was more prevalent in those with pre-existing cardiovascular co-morbidities and in elderly patients. At present the incidence of sunitinib-induced cardiotoxicity is estimated somewhere between 20-60% (Chu *et al*., 2007; Telli *et al*., 2008). However, the relative youth of these drugs mean that accurate long-term data is not yet available.

### *1.5.3 Proposed cardiotoxic mechanism of tyrosine kinase inhibitors:*

Although the cardiotoxic mechanism of TKIs is poorly understood, there is a growing body of evidence suggesting that the cardiotoxic mechanism may be mediated, at least in part, at the level of the mitochondria. Kerkela and colleagues (2006) first proposed

mitochondrial dysfunction as a possible mechanism of cardiotoxicity in 2006. The Kerkela study found evidence of abnormal mitochondria in CMs isolated from patients presenting with imatinib-induced cardiotoxicity. Further analysis obtained from murine models verified these findings and provided insight into the possible cardiotoxic mechanism. Mice, treated with imatinib at a dose believed to be equivalent to the blood concentration in patients treated with imatinib (200mg/kg/day), displayed mitochondrial biogenesis - a hallmark of impaired mitochondrial ATP production. Analysis of mitochondria isolated from cardiac tissue from the imatinib treated mice showed $Ca^{2+}$-induced swelling of the mitochondria and subsequent $Ca^{2+}$-induced opening of the mitochondrial permeability transition pore. This imatinib-induced mitochondrial dysfunction was associated with reduced contractile function and left ventricular dilation, as was seen in humans presenting with imatinib-induced cardiotoxicity. These findings suggest a prominent role for mitochondrial dysfunction in TKI-induced cardiotoxicity. Since then, the link has grown considerably, with several studies evaluating the effect of TKI on $Ca^{2+}$ handling and mitochondrial function. Similar to the findings of Kerkela, Emadi and colleagues (2019) found evidence of mitochondrial toxicity in imatinib treated mice. Emadi reported that imatinib treatment caused mitochondrial swelling, membrane depolarisation and reduced ATP production, with evidence that this toxic mechanism may be mediated by oxidative stress. Soon after, Boutbir *et al*. (2020) also showed that imatinib treatment reduced ATP production and dissipated mitochondrial membrane potential in C2C12 myoblasts. The study showed that imatinib treatment interfered with the activity of Complex I of mitochondrial respiration, increasing mitochondrial superoxide production and inducting mitochondrial toxicity via oxidative stress, providing more support to a potential toxic mechanism involving mitochondrial dysfunction that appears to be conserved amongst different cell types.

In the context of cardiac pathologies, $Ca^{2+}$ handling proteins are becoming increasingly more recognised for the role they play in the pathophysiology of these conditions. This is also true of the pathophysiology of TKI-induced cardiotoxicity, with recent

publications showing that the expression and activity of the $Ca^{2+}$ handling protein, CaMKII, is upregulated following sunitinib and imatinib treatment both *in vitro* and *in vivo* (Barr *et al*., 2014; Mooney *et al*., 2015). CaMKII has already emerged as a prominent figure in the regulation of cardiac physiology, and previous literature has shown that CaMKII is upregulated in cardiac pathologies such as HF (Sossalla *et al*., 2010), atrial fibrillation (AF) (Neef *et al*., 2010) and diabetic cardiomyopathy (Daniels *et al*., 2015; Daniels *et al*., 2018). More recently, sunitinib treatment has been shown to induce cardiac fibrosis in mice, resulting in an increase in left ventricular mass and a reduction in CO (Sourdon *et al*., 2021). Taken together, these findings show strong similarities in the pathophysiology of TKI-induced cardiotoxicity and HF, suggesting that, like in HF, CaMKII may also play a role in the cardiotoxic mechanism of TKIs. The role of CaMKII in mitochondrial activity and its potential role in mediating TKI-induced cardiotoxicity will be covered in more detail in sections 1.6.3 and 1.6.8, respectively.

*1.6 Calcium/calmodulin-dependent protein kinase II (CaMKII):*

CaMKII is a multimeric protein existing in four isoforms (α, β, γ and δ). Although CaMKII is expressed throughout the body, the α and β isoforms are highly expressed in the brain, while the γ and δ isoforms are expressed predominantly in the heart (Pellicena and Schulman, 2014; Zhang, 2017). CaMKII is a dodecameric holoenzyme formed of CaMKII monomers arranged into a pair of stacked hexameric rings, giving the protein a wagon wheel-like appearance (Anderson, Brown and Bers, 2011; Pellicena and Schulman, 2014), as shown in Figure 1.6.1. Each CaMKII monomer is formed of 3 domains, each contributing to the structure and activity of the enzyme (Hoelz *et al*., 2003; Anderson, Brown and Bers, 2011). The association domain is central to the enzyme's structure, forming the wagon wheel-like appearance. The regulatory and catalytic domains control CaMKII activation and, under basal conditions, are closely associated. During $Ca^{2+}$ transients, when $Ca^{2+}$

concentrations are elevated, $Ca^{2+}$ activates calmodulin, forming a $Ca^{2+}$/calmodulin ($Ca^{2+}$/CaM) complex (Clapham, 2007). The $Ca^{2+}$/CaM complex then binds to a corresponding site located within the regulatory domain, relieving autoinhibition and causing a conformational shift in the monomer's structure. This causes activation of the enzyme, exposing binding sites within both the regulatory and catalytic domains. The exposed catalytic domain is then able to phosphorylate targets, mediating $Ca^{2+}$ handling proteins, mitochondrial proteins and ion channel function. The exposed binding sites in the regulatory domain, on the other hand, can manipulate the function of CaMKII itself, mediating post-translational modifications (PTMs) that cause sustained CaMKII activation and resultant CaMKII-mediated pathological effects.

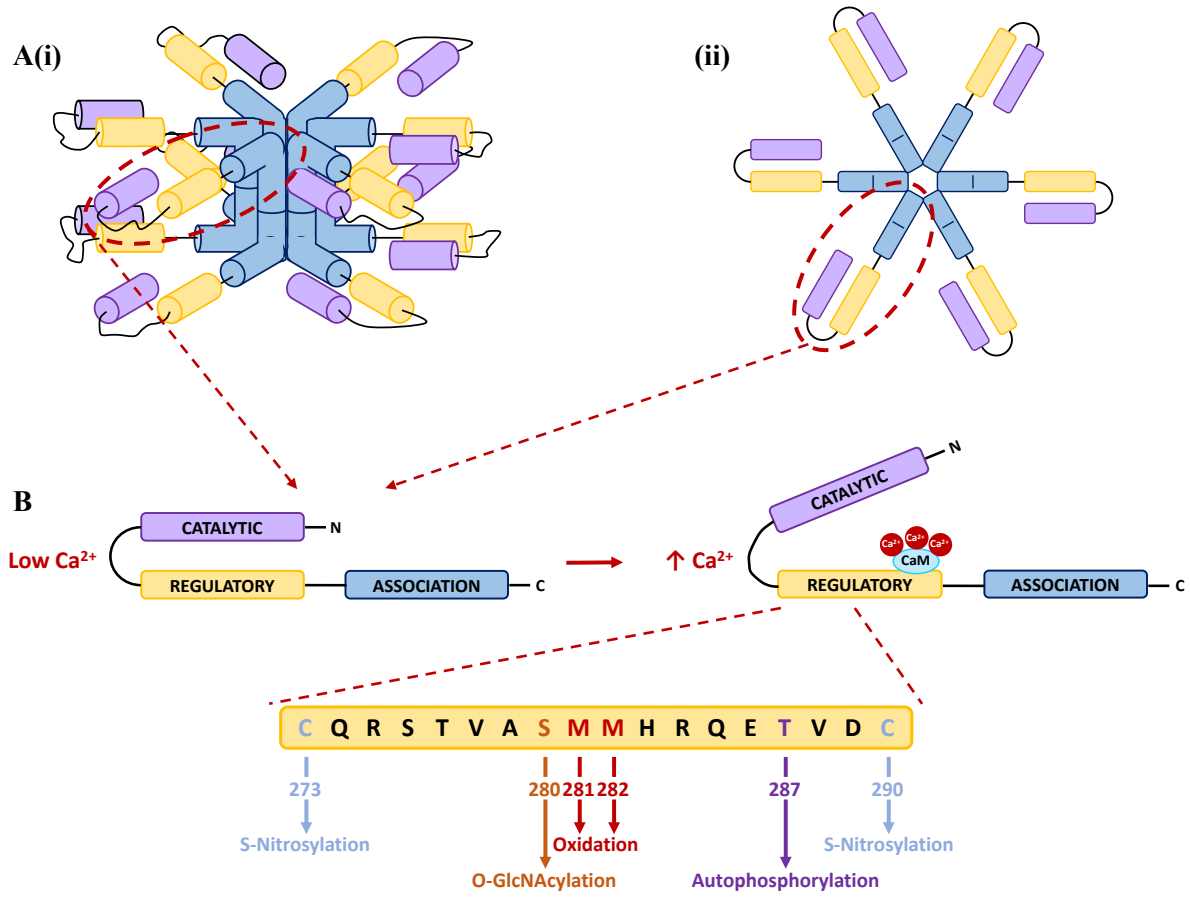


**Figure 1.6.1. A schematic representation of the structure and activation of CaMKII.** CaMKII is a dodecameric holoenzyme formed of CaMKII monomers arranged into a pair of stacked hexameric rings (A(i)) a lateral view of the CaMKII protein structure. A(ii) plan view of the CaMKII protein structure). Under resting $Ca^{2+}$ concentrations, CaMKII is inactivated, and the catalytic and regulatory domains remain closely associated. However, when $Ca^{2+}$ concentrations rise, $Ca^{2+}$ forms a complex with calmodulin that binds to the regulatory domain, relieving autoinhibition. This activates CaMKII and exposes binding sites on the regulatory domain that are susceptible to post-translational modifications (PTMs) that can cause autonomous activation of the enzyme. (B) CaMKII activation and the binding sites inferring autonomous activation via PTMs.

*1.6.1 The activation and autoregulation of CaMKII:*

The $Ca^{2+}$/CaM complex has a relatively weak affinity towards the regulatory domain, making it sensitive to changes in intracellular $Ca^{2+}$. Under normal conditions, when the $Ca^{2+}$ transient ends and the $Ca^{2+}$ concentration recedes, the $Ca^{2+}$/CaM complex dissociates from the regulatory site. This allows the catalytic and regulatory domains to reassociate, de-activating the CaMKII enzyme. PTMs on the exposed regulatory site can, however, prolong the activity of CaMKII, even when $Ca^{2+}$ transients decline. There are four known PTMs that infer autonomous CaMKII activity: phosphorylation, oxidation, O-linked glycosylation (O-GlcNAcylation) and S-nitrosylation. Phosphorylation of the T287 subunit is the most understood PTM to infer autonomous CaMKII activity. The process significantly increases the affinity of the CaMKII enzyme for calmodulin, prolonging the time taken for the $Ca^{2+}$/CaM complex to dissociate from the enzyme (Meyer *et al*., 1992). Phosphorylation of the T287 subunit prohibits the reassociation of the regulatory and catalytic domains, even when the $Ca^{2+}$ transient declines and the $Ca^{2+}$/CaM complex dissociates, maintaining the activation of the enzyme until the phosphate group is removed from the T287 subunit by a protein phosphatase (Lai *et al*., 1987; Strack *et al*., 1997).

Oxidation has also been observed to induce autonomous activation of CaMKII (Erickson *et al*., 2008). This study by Erickson and colleagues showed that CaMKII was activated following stimulation with $H_2O_2$, but only when pre-treated with $Ca^{2+}$ and CaM, and activity was sustained in the presence of the $Ca^{2+}$ chelator, EGTA. Further investigation using mutant variants of CaMKII revealed that the autonomous activity of the protein was induced by oxidation of two methionine residues in the regulatory domain, M281 and M282, and that oxidation of either residue alone was not sufficient to confer activity. In the context of autophosphorylation, the addition of a phosphate group to the T287 subunit has been shown to slow the rate of dissociation of the $Ca^{2+}$/CaM complex, prolonging the activation and activity of CaMKII (Meyer *et al*., 1992). However, this is not true of oxidation of the M281

and M282 subunits (Erickson *et al*., 2008). The findings of Erickson showed that although oxidation of the methionine residues did interfere with the interaction of the regulatory and catalytic domains, sustaining CaMKII activity independent of $Ca^{2+}$/CaM, it had no effect on the affinity of the $Ca^{2+}$/CaM complex for the CaMKII enzyme. Further analysis suggested that the lack of change in this affinity may be caused by the oxidation of a third methionine residue, M308. Similar to autophosphorylated CaMKII, the study also showed that the oxidation of the methionine residues was a reversible reaction, and that the enzyme methionine sulfoxide reductase A (msrA) was responsible for reversing CaMKII oxidation. The study showed that msrA-deficient mice were predisposed to cardiovascular remodelling, had reduced cardiovascular function and greater mortality than control subjects. These data show that, like autophosphorylation, oxidation is a reversible reaction that precludes the association between the catalytic and regulatory domains, independent of $Ca^{2+}$/CaM. However, unlike autophosphorylation, oxidation does not affect the affinity of CaM for the binding sites on the regulatory domain.

Elevated glucose levels, consistent with those of pre-diabetic or diabetic patients, were found to cause autonomous activation of CaMKII (Erickson *et al*., 2013). Erickson found that this high glucose induced autonomous activation of CaMKII was absent in a mutant form of the protein lacking the S279 subunit (Figure 1.6.1), suggesting a prominent role for this serine residue in this potentially novel mechanism. This high glucose induced activation of CaMKII was still present in mutant variants of the protein lacking the T287 and M281/282 subunits, responsible for autonomous activation of CaMKII via phosphorylation and oxidation respectively. This suggests that the activation of CaMKII by elevated glucose concentrations occurs by an entirely separate, unknown mechanism. Previous studies have shown that O-GlcNAcylation is increased in the presence of elevated glucose concentrations (Buse *et al*., 2002; Walgren *et al*., 2002). O-GlcNAcylation is a reversible PTM wherein a N-acetylglucosamine (GlcNAc) monosaccharide is covalently attached to a serine or threonine residue (Chang *et al*., 2020). Taken together, these findings suggest that elevated glucose

causes autonomous activation of CaMKII via O-GlcNAcylation of the S279 subunit in the regulatory domain. This was confirmed by Erickson (2013), who observed an increase in the expression of O-GlcNAcylated CaMKII in CM stimulated with high concentrations of glucose. This increase was not present in CM isolated from the S279 knock-out model or in the presence of the CaMKII inhibitor KN-93, confirming the role of S279 O-GlcNAcylation in this novel mechanism of autonomous CaMKII activation. Again, $Ca^{2+}$ flux was required to induce autonomous CaMKII activation, suggesting that O-GlcNAcylation mediated activation of CaMKII can only occur when autoinhibition has been relieved by $Ca^{2+}$/CaM binding to the regulatory domain, as is the case for autonomous activation of CaMKII by phosphorylation and oxidation.

More recently, a fourth PTM inferring autonomous activation of CaMKII has been reported – S-nitrosylation (Erickson *et al*., 2015). A previous study noted that CaMKII activity was sustained, independent of $Ca^{2+}$, in the presence of NO (Curran *et al*., 2014). Furthermore, the activated CaMKII was found to dysregulate intracellular $Ca^{2+}$ homeostasis via known CaMKII substrates. The study also showed that the sustained CaMKII activation was mediated by NO, suggesting that NO may confer autonomous activation of CaMKII. Shortly thereafter, Erickson reported a novel mechanism whereby S-nitrosylation, the covalent attachment of NO to a thiol group of a cysteine residue, caused autonomous activation of CaMKII (Hess *et al*., 2005; Erickson *et al*., 2015). The study showed that CaMKII incubated with $Ca^{2+}$/CaM and then the NO donor S-Nitrosoglutathione (GNSO), caused activation of the protein and subsequent increased intracellular $Ca^{2+}$ release, consistent with CaMKII activation (Erickson *et al*., 2015). The activation was sustained in the presence of EGTA, indicating autonomous activation of CaMKII. Further analysis using mutant variants of CaMKII revealed that the NO-mediated autonomous activation of CaMKII occurred via S-nitrosylation of the C290 subunit in the regulatory domain. The process increased the affinity of CaMKII for CaM, sustaining the activation of the protein. Interestingly, the study also found a second regulatory role for S-nitrosylation of CaMKII in

addition to causing autonomous activation. The study found that the addition of GNSO prior to $Ca^{2+}$/CaM did not cause CaMKII activation. Mutant variant analysis showed that the addition of GNSO prior to $Ca^{2+}$/CaM resulted in the S-nitrosylation of a different cysteine residue in the regulatory domain, C273. The S-nitrosylation of C273 actually reduced the affinity of CaMKII for CaM, precluding $Ca^{2+}$/CaM binding and maintaining CaMKII in an inactive state. Taken together, these findings show a dual regulatory role for the S-nitrosylation of CaMKII, causing both autonomous activation and inhibition of the enzyme.

*1.6.2 CaMKIIδ regulates calcium handling in cardiac myocytes:*

CaMKIIδ is a prominent $Ca^{2+}$ handling protein that, when activated, is known to phosphorylate numerous intracellular $Ca^{2+}$ regulating proteins and transmembrane ion channels in the heart. These interactions make CaMKIIδ central to ECC in CMs and, as a result, to normal cardiac physiology (Beckendorf *et al*., 2018). The influence of CaMKIIδ on CM $Ca^{2+}$ handling is dynamic, phosphorylating proteins which both increase and decrease the intracellular $Ca^{2+}$ concentration (Figure 1.6.4.1). CaMKIIδ is known to phosphorylate LTCCs, facilitating $Ca^{2+}$ entry into the cytosol (Hudmon *et al*., 2005). This in turn induces further intracellular [$Ca^{2+}$] release from intracellular $Ca^{2+}$ stores, mediated, in part, by phosphorylation of the RyR2 by CaMKIIδ, releasing stored $Ca^{2+}$ from the SR (Currie *et al*., 2004, Neef *et al*., 2010). This increase in intracellular [$Ca^{2+}$] is critical in facilitating cardiac contraction (Bers, 2002; Bers and Grandi, 2009; Aronsen *et al*., 2013; Ottolia *et al*., 2013). In contrast, CaMKIIδ is also known to mediate cardiac relaxation, reducing the intracellular [$Ca^{2+}$] by phosphorylating PLB and relieving PLB inhibitory action on SERCA (Ai *et al*., 2005). This allows extrusion of $Ca^{2+}$ from the cytosol back into the SR via SERCA. This dynamic regulation of $Ca^{2+}$ handling proteins makes CaMKIIδ a central mediator of cardiac contraction (Zhang *et al*., 2003; Sossalla *et al*., 2010; Daniels *et al*., 2018; Beauverger *et al*., 2020).

*1.6.3 CaMKIIδ influences mitochondrial function:*

Mitochondria facilitate the contractile function of CMs by meeting the cells high demand for ATP (Gustafsson and Gotlieb, 2008). They achieve this via OXPHOS, a mitochondrial metabolic pathway that couples electron transfer to proton translocation across the inner mitochondrial membrane, generating ATP as a result (Figure 1.6.3.1) (Bergman and Ben-Shachar, 2016). The metabolically demanding CMs can then utilise the ATP produced by OXPHOS to facilitate cardiac contraction and maintain intracellular ion concentrations (Bers, 2002; Luo and Anderson, 2013; Tran *et al*., 2015). Mitochondria also play and important role in maintaining intracellular [$Ca^{2+}$] homeostasis, sequestering excess cytosolic [$Ca^{2+}$] to prevent $Ca^{2+}$ dysregulation and, in CMs, preserve cardiac contraction (Gustafsson and Gotlieb, 2008). This uptake of cytosolic [$Ca^{2+}$] into the mitochondria may be mediated by CaMKII. Joiner *et al*. (2012) found evidence that CaMKII facilitates $Ca^{2+}$ entry into the mitochondria by phosphorylating the mitochondrial $Ca^{2+}$ uniporter (MCU) (Figure 1.6.4.1). However, it should be noted that these findings were obtained in a pathological model, and more recent findings have disputed this (This will be covered in greater detail in section 1.6.6). Although it is not yet clear whether CaMKII influences mitochondrial function directly, given that the mitochondria sequester excess $Ca^{2+}$ form the cytosol, CaMKII will, at the very least, have an indirect effect on mitochondrial function via its regulation of intracellular [$Ca^{2+}$] through its substrates.

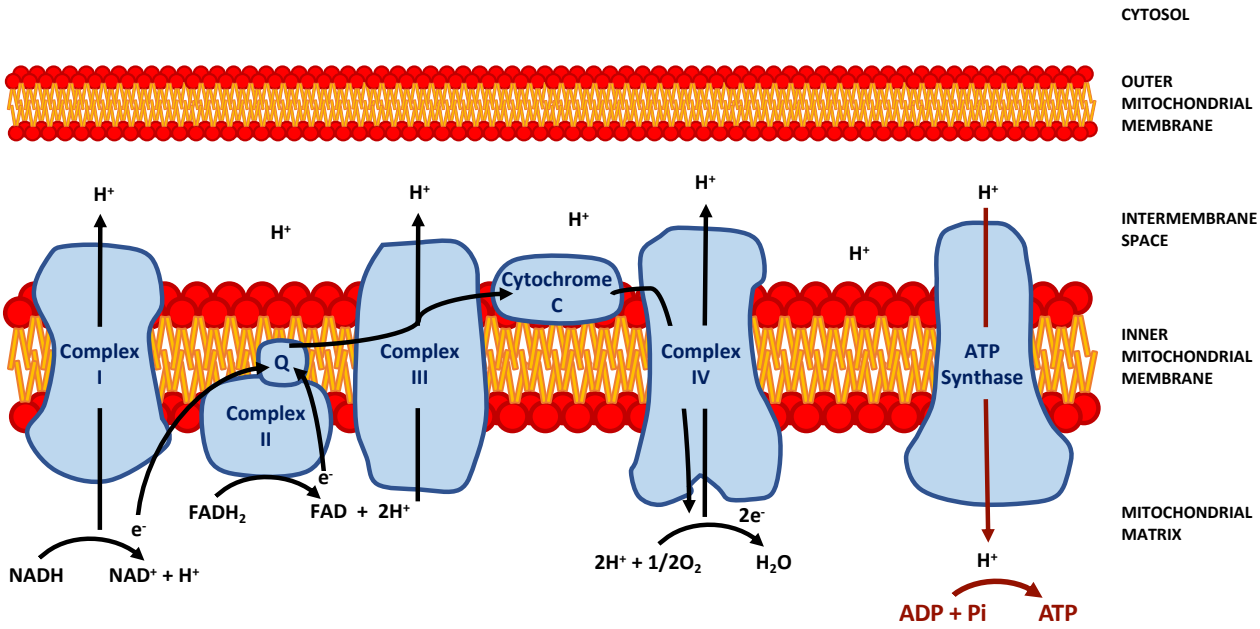


**Figure 1.6.3.1. An overview of oxidative phosphorylation.** Oxidative phosphorylation (OXPHOS) is a mitochondrial metabolic pathway which couples electron transfer to proton translocation across the inner mitochondrial membrane in order to generate ATP. Complexes I, III and IV of the electron transport chain are proton pumps which utilize the energy produced from electron transfer to pump protons ($H^+$) from the mitochondrial matrix, across the inner mitochondrial membrane and into the intermembrane space. NADH initiates the process by depositing its electrons ($e^-$) at Complex I, forming NAD+ and releasing a $H^+$ into the mitochondrial matrix. FADH2's electrons are at a lower energy level so cannot be transferred to Complex I. Instead, they are deposited at Complex II where FADH2 is reduced to FAD, releasing 2 $H^+$ ions. The electrons from Complexes I and II are them passed to the mobile electron carrier, ubiquinone (Q), that travels the inner mitochondrial membrane and deposits the electrons at Complex III. This electron movement through Complex III facilitates the translocation of more $H^+$ ions across the inner mitochondrial membrane. Ubiquinone delivers the electrons to Cytochrome C, a mobile hemoprotein that passes freely through the inner mitochondrial membrane to deliver the electrons to Complex IV. Complex IV passes the electrons to $O_2$, the terminal electron acceptor, which is split to form two $O_2$ atoms that accept $H^+$ ions from within the mitochondrial matrix to form $H_2O$. This proton translocation forms an electrochemical gradient that is used to catalyse ATP production. $H^+$ ions then flow down the concentration gradient into the mitochondrial matrix via ATP synthase, catalysing the conversion of ADP to ATP.

*1.6.4 CaMKIIδ regulates cardiac fibroblast activation:*

The effects of CaMKIIδ are not limited to just CMs. CaMKIIδ is also known to regulate aspects of CF function, specifically CF activation (Zhang *et al*., 2010; Martin *et al*., 2014). Both Zhang and Martin showed that CaMKIIδ induced CF proliferation (Figure 1.6.4.1) and that this could be attenuated via targeted CaMKII inhibition. Furthermore, Zhang found that CaMKIIδ-mediated CF activation coincided with the release of MMPs, inflammatory mediators and collagen secretion – factors that regulate cardiac structure. MMP expression, collagen secretion and inflammatory mediator release are attenuated by CaMKII inhibition, showing a role for these processes in CaMKII-induced CF proliferation. It is evident that CaMKIIδ plays a critical role in cardiovascular function, exerting influence over multiple cardiac cell types. The role of CaMKIIδ in normal physiological functioning, and in an adaptive sense to preserve cardiac function in response to insult or injury, cannot be overlooked. However, the regulatory role that CaMKIIδ has on $Ca^{2+}$ handling and proliferation, and the downstream effect that this has on cellular organelles such as the mitochondria, mean that sustained activation of CaMKIIδ can result in pathophysiological changes in the heart.

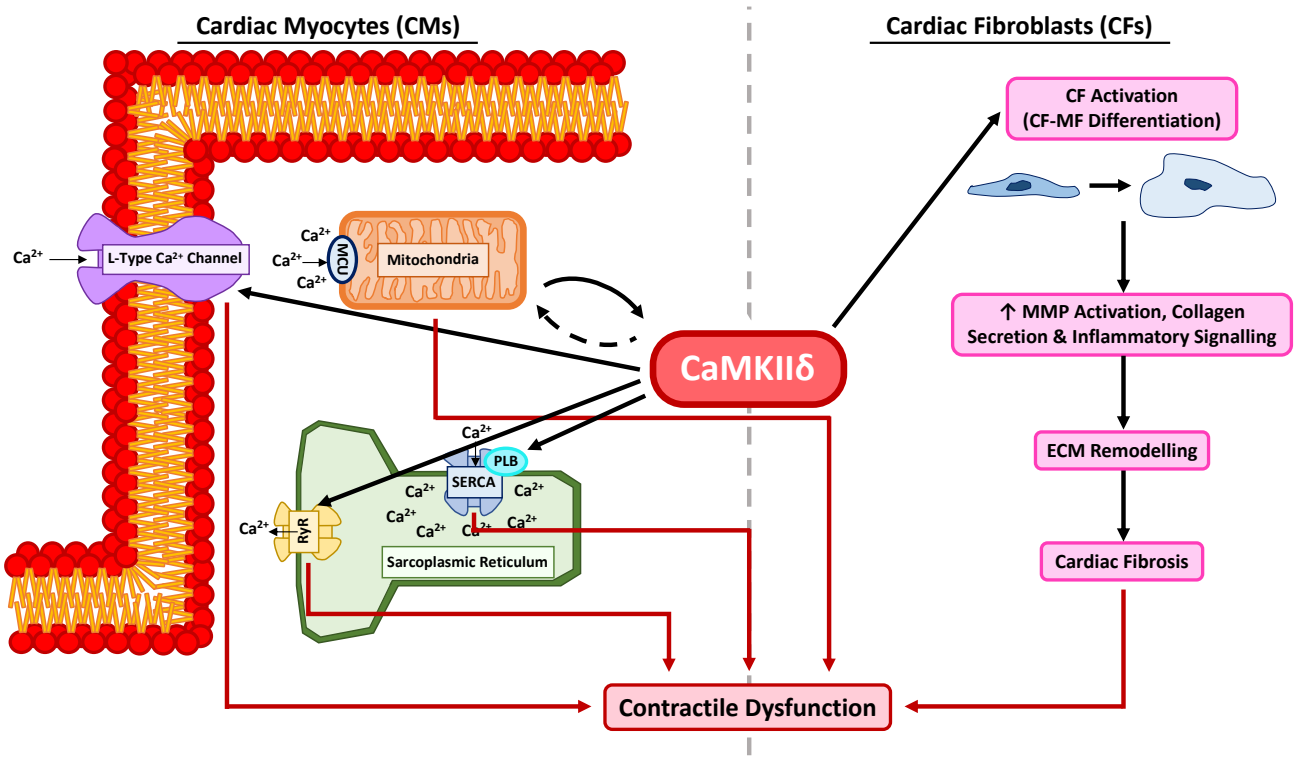


**Figure 1.6.4.1. A schematic representation of CaMKIIδ substrates.** CaMKIIδ is a prominent $Ca^{2+}$ handling protein known to regulate intracellular [$Ca^{2+}$] concentration in cardiac myocytes. CaMKIIδ can increase intracellular [$Ca^{2+}$] via the L-type $Ca^{2+}$ channel and the ryanodine receptor (RyR2), which facilitates stored $Ca^{2+}$ release from the sarcoplasmic reticulum (SR). Conversely, CaMKIIδ can reduce intracellular [$Ca^{2+}$] via phospholamban (PLB), which facilitates $Ca^{2+}$ re-uptake into the SR via the sarco/endoplasmic reticulum $Ca^{2+}$-ATPase (SERCA). Previous studies have suggested that CaMKII may facilitate $Ca^{2+}$ uptake into the mitochondria, though recent publications have refuted this. CaMKIIδ is also known to regulate cardiac fibroblast (CF) activation. CF activation is critical in maintaining the structure and function of the heart via their secretion of factors that synthesise and degrade the extracellular matrix (ECM).

*1.6.5 CaMKIIδ mediates altered calcium handling in cardiac myocytes:*

There is a considerable body of evidence demonstrating that the pathophysiological changes mediating altered $Ca^{2+}$ handling can be caused by autonomous activation of CaMKIIδ. As discussed in the section 1.6.2, CaMKIIδ is known to influence intracellular $Ca^{2+}$ handling via direct interaction and phosphorylation of LTCCs, RyR2 and PLB. In cardiac pathology, there is extensive evidence that sustained CaMKIIδ activation results in hyperphosphorylation and dysregulation of these key $Ca^{2+}$ handling proteins, causing dysregulated $Ca^{2+}$ handling as a result. Ai *et al*. (2005) observed a significant increase in RyR2 phosphorylation, despite a reduction in RyR2 expression, in a rabbit model of HF. The investigation observed an increase in RyR2 phosphorylation at both the CaMKIIδ-specific serine-2815 site and the shared CaMKIIδ/PKA serine-2809 site. The increased RyR2 activation via CaMKIIδ correlates with the increased SR $Ca^{2+}$ leak that is typical of HF. Interestingly, PLB expression does not appear to be significantly altered in HF (Kubo *et al*., 2001; Ai *et al*., 2005). Although PLB activation at the CaMKIIδ-specific threonine-17 site is increased, there is reduced PLB activation at the PKA site, attenuating changes in PLB activity via CaMKIIδ (Ai *et al*., 2005). These changes are consistent with the reduced SR $Ca^{2+}$ content seen in HF. Specifically, increased RyR2 phosphorylation promotes $Ca^{2+}$ leak from the SR, reducing SR $Ca^{2+}$ content. SR $Ca^{2+}$ content is further limited by the reduced expression of SERCA in HF (Kubo *et al*., 2001). This is further confounded by the lack of change in PLB activity, resulting in a net loss in SR $Ca^{2+}$ content that is not mitigated by $Ca^{2+}$ reuptake into the SR via PLB. These changes at the cellular level, mediated by increased CaMKIIδ expression and activation, culminate in increased SR $Ca^{2+}$ leak, reduced SR $Ca^{2+}$ content and ultimately suppressed cardiac contraction in HF.

However, the cellular changes that seemingly underpin the HF mechanism can be reversed via the targeted inhibition of CaMKIIδ, alleviating the functional changes in cardiac performance in HF patients (Sossalla *et al*., 2010). CaMKIIδ inhibition was found to reduce

phosphorylation of the RyR2 at both the serine-2815 and serine-2809 sites. The reduction in RyR2 phosphorylation correlates with reduced SR $Ca^{2+}$ leak and a resultant increase in SR $Ca^{2+}$ content in CMs isolated from failing human hearts. Reduced SR $Ca^{2+}$ leak and increased SR $Ca^{2+}$ content subsequent to CaMKIIδ inhibition was also observed in an animal model of HF (Ai *et al*., 2005). These improvements in SR $Ca^{2+}$ handling, mediated by CaMKII inhibition, profoundly improve cardiac function. Sossalla (2010) found that CaMKIIδ inhibition reduced $Ca^{2+}$ spark frequency and duration, thereby augmenting contractile force in HF. Similar findings were reported by Zhang *et al*. (2003) and Beauverger *et al*. (2020), whom both showed that CaMKIIδ induced cardiovascular dysfunction via activation of the $Ca^{2+}$ handling proteins and known CaMKIIδ substrates, RyR2 and PLB. Furthermore, Beauverger *et al*. (2020) also showed that CaMKII inhibition improved cardiac output in a murine model of dilated cardiomyopathy by reducing activation of these $Ca^{2+}$ handling proteins. These studies show that CaMKIIδ plays a pivotal role in the pathophysiology of CVD and this can be attenuated by CaMKII inhibition. Given the similarity in the pathophysiology of TKI-induced cardiotoxicity, CaMKIIδ may also play a role in the cardiotoxic mechanism of TKIs and serve as a target to reduce the impact of TKI-induced toxicity.

### *1.6.6 The possible role of CaMKIIδ in mitochondrial dysfunction:*

Mitochondrial dysfunction is known to contribute to the pathophysiology of HF and is known to be caused by increased $Ca^{2+}$ entry into the mitochondria. This results in impaired OXPHOS, opening of the mitochondrial membrane transition pore (mPTP), loss of mitochondrial membrane potential and apoptotic cell death (Luo and Anderson, 2013). A previous study found that CaMKII inhibition reduced mitochondrial $Ca^{2+}$ uptake, preventing opening of the mPTP, the loss of mitochondrial membrane potential and reduced apoptotic cell death (Joiner *et al*., 2012). These findings, obtained in a disease model, links CaMKII to

the increased $Ca^{2+}$ entry into the mitochondria, the initiating step in the proposed mechanism of mitochondrial dysfunction in HF. The MCU is understood to be the main mechanism of $Ca^{2+}$ entry into the mitochondria (Finkel *et al*., 2015). Taken together, these findings imply that $Ca^{2+}$ entry into the mitochondria is governed by CaMKII regulation of the MCU. However, a recent publication showed no difference in mitochondrial $Ca^{2+}$ content in mitochondria or CM isolated from CaMKII-deficient mice in comparison to wild type (WT) controls (Nickel *et al*., 2020). Mitochondrial $Ca^{2+}$ content was also unchanged between WT and CaMKII-deficient groups in mitochondria stimulated with $H_2O_2$, a known inducer of $Ca^{2+}$-mediated mitochondrial dysfunction (Guo *et al*., 2016). Collectively, these findings would suggest that CaMKII does not regulate $Ca^{2+}$ entry into the mitochondria directly, at least not in a non-disease setting, and the reduction in $Ca^{2+}$ entry into the mitochondria most likely reflects a reduction in intracellular $Ca^{2+}$ owing to CaMKII inhibition.

*1.6.7 CaMKIIδ mediates cardiovascular remodelling:*

Cardiac fibrosis plays a central role in the pathology of several CVDs, including myocardial infarction, HF and diabetic cardiomyopathy (Murtha *et al*., 2017; Curl *et al*., 2018; Daniels *et al*., 2018; Pyun *et al*., 2018; Beauverger *et al*., 2020). Cardiac fibrosis is caused by CF proliferation and the secretion of collagen, MMPs and inflammatory mediators that facilitate ECM turnover (Zhang *et al*., 2010; Martin *et al*., 2014; Cao *et al*., 2018). This is a hallmark of CF to MF differentiation, and these structural changes in the heart restrict its functioning, causing fibrotic remodelling and ultimately HF. Studies have shown that CF activation, and the fibrotic remodelling that accompanies this in a pathological setting, is mediated by increased activation of CaMKIIδ (Zhang *et al*., 2010; Martin *et al*., 2013; Daniels *et al*., 2018; Beauverger *et al*., 2020). Martin *et al*. (2013) showed that CaMKIIδ expression and activation is significantly increased in hypertrophied hearts. The study showed that the increase in CaMKIIδ expression and activation was associated with CF proliferation and

secretion of MMPs and interstitial collagen. These changes, mediated by CF activation, resulted in evidence of cardiac hypertrophy, contractile dysfunction and fibrosis. The study also showed that CF proliferation could be reduced via CaMKII inhibition. Previous work by Zhang *et al*. (2010) showed similar findings. Zhang *et al*. showed that CaMKII inhibition reduced CF proliferation and also reduced the secretion of MMPs, collagen and inflammatory mediators that are known to mediate fibrotic remodelling. Such findings also give prominence to CaMKII as a novel therapeutic target for CVD that warrants further investigation.

### *1.6.8 CaMKIIδ: A mediator of tyrosine kinase inhibitor-induced cardiotoxicity?*

CaMKII has been well established as a key signalling molecule in cardiac physiology and mediator of cardiac pathology. Recently, imatinib treatment was found to increase CaMKII expression in NRVMs (Barr *et al*., 2014). The increased CaMKII activity was associated with increased intracellular $Ca^{2+}$ and phosphorylation of PLB and RyR, resulting in CM hypertrophy and necrosis. These changes bear a striking resemblance to pathophysiological changes seen in cardiovascular disease, suggesting a similar mechanism may exist. More recently, these findings were replicated in vivo, with chronic imatinib and sunitinib treatment found to significantly increase CaMKII expression and activity in guinea pig heart (Mooney *et al*., 2015). The increase in CaMKII expression correlated with increased phosphorylation of RyR2. The observations reported in these studies of increased CaMKII expression and activity, induced by TKI treatment, are consistent with the known pathological mechanisms of CaMKII. This would infer that CaMKII may be a possible mediator of TKI induced toxicity and warrants further investigation into the role it plays in cardiotoxicity. If a role for CaMKII can be established in the pathophysiology of TKI-induced cardiotoxicity, it may also serve as a target for pharmacological intervention.

*1.7 Hypothesis and aims:*

The overall hypothesis of this project is that CaMKIIδ activation is a key modulator of the cardiotoxic effects of the anti-cancer drugs sunitinib and imatinib and that cardiotoxicity can be reduced or reversed following inhibition of CaMKIIδ.

The aims of this project are to:

1.) Investigate whether sunitinib or imatinib treatment instigate contractile and non-contractile cardiac cell dysfunction and death

2.) Determine whether sunitinib or imatinib increase cellular oxidative stress by increasing ROS generation via effects at a mitochondrial level and, if so, investigate if this correlates with increased oxidation and autonomous activation of CaMKII

3.) Explore whether a role exists for CaMKII in the cardiotoxic mechanism of TKIs and if CaMKII inhibition using KN-93 can reduce or reverse the toxic effects of sunitinib and imatinib and improve cell survival following chronic anti-cancer drug treatment

# Chapter Two: Materials and Methods

*2.1 Materials:*

***Abcam (Cambridge, UK):***

Anti-von Willebrand Factor (vWF) rabbit polyclonal IgG antibody (ab6994), anti-smooth muscle cell actin (SMCa) mouse monoclonal IgG antibody (ab7817), anti-glyceraldehyde 3-phosphate dehydrogenase (GAPDH) mouse monoclonal IgG antibody (ab8245), anti-sarcomeric α actinin rabbit polyclonal IgG antibody (ab137346), 2',7' – dichlorofluorescin diacetate (DCFDA) cellular ROS assay kit

***Badrilla (Leeds, UK):***

Anti-Phos-CaMKII rabbit polyclonal IgG antibody (A010-50), anti-phospholamban (PLB) mouse monoclonal IgG antibody

***BD Biosciences (Berkshire, UK):***

APC annexin V, annexin V binding buffer

***BDH Limited (Poole, UK):***

Glucose, sodium dihydrogen orthophosphate ($NaH_2PO_4$), methanol

***Bio-Rad Laboratories Ltd. (Watford, UK):***

4-20% Mini-PROTEAN TGX Precast Protein Gels

***Cambridge Bioscience Ltd (Cambridge, UK):***

Sunitinib malate

***Eurogentec (Southampton, UK):***

Custom anti-CaMKIIδ rabbit polyclonal antibody

***Insight Biotechnology Limited (Wembley, UK):***

Anti-Ox-CaMKII rabbit polyclonal IgG antibody (GTX36254)

***Jackson ImmunoResearch (Cambridge, UK):***

AffiniPure donkey anti-mouse IgG (H+L) HRP-conjugated (715-035-150), AffiniPure donkey anti-rabbit IgG (H+L) HRP-conjugated (111-035-144)

***Promocell GmbH (Heidelberg, Germany):***

Human cardiac myocytes, myocyte growth medium kit, DetachKit, Cryo-SFM cryopreservation medium

***Sigma-Aldrich (Missouri, USA):***

Potassium chloride (KCl), 4-(2-hydroxyethyl)-1-piperazineethanesulfonic acid (HEPES), magnesium chloride hexahydrate ($MgCl_2.6H_2O$), taurine, creatinine, protease XIV (P5147), dithiothreitol (DTT), tween 20, tris base, p-coumeric acid, luminol, hydrogen peroxide ($H_2O_2$), thiazolyl blue tetrazolium bromide (MTT), triton X-100, formaldehyde, imatinib mesylate, ethylene glycol-bis(2-aminoethylether)-N N N′N′-tetraacetic acid (EGTA), angiotensin II (human), autocamtide 2-related inhibitory peptide, KN-93, anti-vimentin mouse monoclonal IgM antibody (V5255), anti-tubulin mouse monoclonal IgG antibody (T5168), potassium dihydrogen phosphate ($KH_2PO_4$), potassium hydroxide (KOH), magnesium sulfate heptahydrate ($MgSO_4•7H_2O$), sodium bicarbonate ($NaHCO_3$), d-sucrose, 4′,6-diamidino-2-phenylindole (DAPI), dimethyl sulfoxide (DMSO)

***Thermo Fisher Scientific (Massachusetts, USA):***

Sodium dodecyl sulphate (SDS), sodium chloride (NaCl), glycine, bovine serum albumin (BSA), phosphate buffered saline (PBS) tablets, Dulbecco's modified eagle medium (DMEM), probenecid, MitoSOX Red™, PageRuler™ plus prestained protein ladder, Alexa fluor® 488 goat anti-mouse IgG (H+L) (A-11001), Alexa fluor® 488 goat anti-rabbit IgG (H+L) (A-11008), NuPAGE LDS sample buffer (4x), anti-ryanodine receptor (RyR) monoclonal IgG antibody (MA3-916), NuPAGE Novex 10% BisTris Gels (1.0 mm, 10 well),

NuPAGE™ 3-(N-morpholino)propanesulfonic acid (MOPS) SDS Running Buffer (for Bis-Tris Gels only) (20X), penicillin/streptomycin antibiotics, foetal calf serum (FCS)

***vWR International (Leicestershire, UK):***

Methanol

***Worthington Biochemical Corporation (New Jersey, USA):***

Collagenase type I (LS004196)

*2.2 Buffer/solution composition:*

***$Ca^{2+}$ Free KB solution:*** 70mM KOH, 40mM KCl, 10mM Hepes, 3mM $MgCl_2.6H_2O$, 20mM Taurine, 50mM L-glutamic acid, 10 mM Glucose and 20mM $KH_2PO_4$, 1mM EGTA in $dH_2O$, adjusted to pH=7.2. Filter sterilised and warmed to 37°C prior to use.

***Digestion Buffer:*** Krebs containing 0.08% (w/v) collagenase Type I and 0.003% (w/v) protease XIV. Filter sterilised and warmed to 37°C prior to use.

***ECL1:*** 100mM Tris base (pH=8.5), 2.5mM luminol (in DMSO) and 1.25mM coumaric acid (in DMSO) in $dH_20$.

***ECL2:*** 100mM Tris base and 0.64mM $H_2O_2$ in $dH_2O$.

***Fluo4 Buffer containing 2μM Fluo4-AM:*** 1mM MgCl, 1.5mM CaCl, 0.3mM probenecid and 0.1% (w/v) BSA in HBSS. Fluo4-AM $Ca^{2+}$ indicator dye was diluted in Fluo4 Buffer to a final concentration of 2μM immediately before use.

***Hank's Buffered Saline solution (HBSS)****:* 136.9mM NaCl, 5.4mM KCl, 1.3mM $CaCl_2$, 0.4mM $MgSO_4•7H_2O$, 0.5mM $MgCl_2.6H_2O$, 0.3mM $Na_2HPO_4.2H_2O$, 0.4mM $KH_2PO_4$, 5.6mM glucose, 4.2mM $NaHCO_3$, adjusted to pH=7.2.

***Krebs:*** 120mM NaCl, 5.4mM KCl, 20mM HEPES, 3.5mM $MgCl_2.6H_2O$, 20mM Taurine, 10mM Creatinine, 11.1 mM Glucose and 0.52mM $NaH_2PO_4$ in $dH_2O$, adjusted to pH=7.4. Filter sterilised and warmed to 37°C prior to use.

***Lithium Dodecyl Sulfate (LDS) Sample Buffer:*** 25% (v/v) 4x Nu PAGE LDS Sample Buffer and 75mM DTT in $dH_2O$.

***3-(N-morpholino)propanesulfonic acid (MOPS) Buffer:*** Stock 20x buffer was diluted 1:20 in $dH_2O$ to produce 1x MOPS buffer.

***Mitochondrial Respiration (MiR) Buffer:*** 0.5mM EGTA, 3mM $MgCl_2 \cdot 6H_2O$, 60mM lactobionic acid, 20mM taurine, 10mM $KH_2PO_4$, 20mM HEPES, 110mM d-sucrose, 0.1% (w/v) BSA, adjusted to pH=7.1.

***PBS:*** 1x PBS tablet per 100ml $dH_2O$, adjusted to pH=7.4.

***Running Buffer:*** 3.5mM SDS, 192mM glycine and 25mM Tris base in $dH_2O$.

***Stripping Buffer:*** 31mM Tris base, 35mM SDS in $dH_2O$, adjusted to pH=6.7.

***Transfer Buffer:*** 192mM glycine, 25mM Tris base, 20% (v/v) methanol and 80% (v/v) $dH_2O$.

***Tris-buffered Saline-Tween 20 (TBS-T) (0.1%):*** 20mM Tris base, 150mM NaCl, adjusted to pH=7.4, and 0.1% (v/v) Tween 20.

***Wash Buffer:*** Krebs containing 1mM EGTA and 1% (v/v) penicillin/streptomycin. Filter sterilised and warmed to 37°C prior to use.

*2.3 Methods:*

*2.3.1 Animal ethics:*

All procedures were performed under sterile conditions and conformed to the Guide for the Care and Use of Laboratory Animals published by the US National Institutes of Health (NIH Publication No. 85-23, revised 1996) and Directive 2010/63/EU of the European Parliament.

*2.3.2 Adult primary cardiac fibroblast isolation:*

CFs were isolated from adult Sprague-Dawley rats (weighing between 237-345g, average weight = 287g) via bulk collagenase digestion (Lawan *et al*., 2011). Rats were sacrificed via cervical dislocation and the heart recovered immediately while still beating and held in wash buffer. The aorta and atria were excised, and the remaining cardiac tissue cleansed using wash buffer to remove any remaining blood. Minced cardiac tissue was incubated in 10ml of digestion buffer for 10 minutes in a shaker bath (37°C) to facilitate digestion. The digested tissue was then centrifuged for 3 minutes at 600g. The first collection of supernatant was discarded and the digestion process repeated. The remaining supernatant was collected and held on ice in 10ml of wash buffer. The digestion process was repeated until all of the digestion buffer had been utilised. The supernatant was centrifuged for 10 minutes at 2,000g to pellet the cells. The isolated CF were then reconstituted in 10ml of CF growth medium (DMEM supplemented with 20% (v/v) FCS, 2% (v/v) penicillin/ streptomycin and 1% (v/v) L-glutamine) before being plated in a T75 culture flask and incubated (37°C, 5% $CO_2$). The CF growth media was replenished after 4-5 hours of incubation to remove non-adherent cells. A second media change was conducted 24 hours post-isolation to remove any remaining cell debris, with further media changes conducted at 48-hour intervals thereafter as per the standard cell culture protocol.

*2.3.3 Cardiac myocyte isolation:*

CMs were isolated from adult Sprague-Dawley rats (weighing between 297-337g, average weight = 322g) via a Langendorff perfusion method (Li *et al*., 2020). The Langendorff perfusion system was first primed with Krebs to remove any air bubbles. Rats were sacrificed via injection with dolethal + heparin and the heart and lungs excised immediately while maintaining a good length of the descending thoracic aorta (~10mm). Tissue was washed in ice-cold Krebs solution + heparin, and while the heart was still beating, the ascending aorta was cut just before the brachiocephalic artery to provide sufficient length for cannulation. The heart was then cannulated via the aorta onto the Langendorff perfusion system and held in place with a bulldog clip. The heart was then perfused with Krebs solution + 0.1% (w/v) BSA at a flow rate of 7ml/minute to remove any remaining blood. The heart was then perfused with Krebs supplemented with 0.1% (w/v) BSA, 0.08% (w/v) collagenase Type I and 0.007% (w/v) protease XIV to facilitate digestion of the cardiac tissue. Digestion continued until the heart appeared flaccid, pale and slightly swollen and the perfusate was more viscous (approximately 15-20 minutes). The heart was then cut down from the cannula, resecting the atria and aorta, and held in 10ml $Ca^{2+}$ free KB solution + 0.1% BSA. The ventricular tissue was minced and then titrated using a Pasteur pipette. The cells were then left to rest horizontally in KB solution + 0.1% BSA in a 50ml falcon tube at room temperature for 1 hour. The KB + 0.1% BSA solution can then be carefully aspirated, and the remaining settled cell pellet processed for downstream applications.

*2.3.4 Swiss 3T3 cell culture:*

Swiss 3T3 cells (S3T3s) (generously gifted by Professor M. Helen Grant, University of Strathclyde) were cultured in S3T3 growth medium (DMEM supplemented with 10% (v/v) FBS, 2% (v/v) penicillin/streptomycin and 1% (v/v) L-glutamine and 1% (v/v) non-essential

amino acids (NEAA)) with media changes conducted at 48-hour intervals until the cells reached 70-80% confluence. Cells were then trypsinised using 5ml of TrypLE™ Express (37°C) and then collected in 10ml of S3T3 growth media. The cells were centrifuged for 5 minutes at 2,000g to pellet the cells. The cells were reconstituted in S3T3 growth medium and counted using a haemocytometer.

*2.3.5 Cardiac fibroblast cell culture:*

CFs were cultured in their respective growth medium (see section 2.3.2 for details) with media changes conducted at 48-hour intervals until the cells reached 70-80% confluence. Once confluent, the cells were dissociated using 5ml of TrypLE™ Express (37°C). The cells were collected in 10ml CF growth media and centrifuged for 5 minutes at 2,000g to pellet the cells. The cells were reconstituted in growth medium and counted using a haemocytometer.

*2.3.6 Progenitor cardiac myocyte cell culture:*

PCMs were cultured in Promocell myocyte growth medium containing 5% FCS, recombinant human epidermal growth factor (0.5 ng/ml), recombinant human basic fibroblast growth factor (2 ng/ml) and recombinant human insulin (5 µg/ml). Media changes were conducted at 48-hour intervals until the cells reached 70-80% confluence. PCMs were then passaged using the recommended Promocell DetachKit. Briefly, PCMs were washed with Hepes BSS and then detached using Trypsin/EDTA at room temperature. PCMs were then harvested in Trypsin Neutralisation Buffer and centrifuged at 1,000g for 3 minutes to pellet the cells. The cells were reconstituted in myocyte growth medium and counted using a haemocytometer.

*2.3.7 Cryopreservation:*

Cell stocks were stored in liquid $N_2$. Cells were trypsinised and pelleted as per their respective culture protocols described previously. CF and S3T3 pellets were then reconstituted in freezing media (90% FBS, 10% DMSO) and aliquoted into cryogenic vials at a density of $1x10^6$ cells/ml. PCM pellet was reconstituted in Cryo-SFM cryopreservation medium at a density of $1x10^6$ cells/ml. The vials were then stored at -80°C for 24 hours before being transferred into liquid $N_2$ for cryopreservation.

*2.3.8 In vitro drug treatment:*

Cells were treated with sunitinib malate and imatinib mesylate for 18 hours. For serum free (SF) samples, the culture medium was removed and replaced with SF media (DMEM supplemented with 2% penicillin/streptomycin and 1% L-glutamine). Cells were then cultured for 4 hours prior to the addition of drugs. For serum containing (SC) samples, drugs were added to the existing SC culture medium. For CF and S3T3 treated samples, drugs were diluted in SF medium. For CM treated samples, drugs were diluted in complete CM growth medium.

*2.3.9 Brightfield imaging:*

Cell phenotype and growth was monitored using a Nikon Eclipse (TE300) inverted microscope (Nikon, Tokyo, Japan) and a Leica EC3 digital camera affixed to a Leica DM IL LED inverted microscope (Leica Biosystems, Wetzlar, Germany). Imaging was conducted at x10 or x20 magnification.

*2.3.10 MTT assays:*

MTT assays were conducted to determine changes in cell viability following treatment with TKIs (Green and Leeuwenburgh, 2002; Burke *et al*., 2019; Sirangelo *et al*., 2020). CFs (P1-P3) and PCMs (P3-P4) were seeded in a 96-well plate at a density of $2.5x10^4$ cells/well and cultured in their respective growth medium for 24 hours. The following day, cells were treated as per the drug treatment protocol with increasing concentrations of sunitinib and imatinib (0.1-10μM). Following drug treatment, the culture medium was aspirated and replaced with fresh growth medium containing MTT (10μg/ml). The plate was then wrapped in aluminium foil to omit light and incubated (37°C, 5% $CO_2$) for 2 hours. In living cells, mitochondrial dehydrogenases convert MTT to purple MTT formazan crystals. The MTT formazan crystals were then re-solubilised by adding 100μl of DMSO to each well. The plate was then re-covered with aluminium foil and returned to the incubator (37°C, 5% $CO_2$) for 5 minutes. Cell viability was then assessed via optical density at a wavelength of 570nm.

*2.3.11 Fluorescence-activated cell sorting:*

Fluorescence-activated cell sorting (FACS) was used to determine cell viability by sorting healthy, apoptotic and necrotic cells by propidium iodide (PI) and annexin V fluorescent labelling (Wang *et al*., 2010; Kumar *et al*., 2018). PI can fluorescently tag the DNA of necrotic cells due to the loss of membrane integrity, whereas annexin V can tag phospholipids that have translocated from the internal membrane to the cell surface during early apoptosis. Detection of both PI and annexin V fluorescence indicates late apoptosis whereas detection of no PI or annexin V fluorescence indicates healthy cells. Cells were plated in 12-well plates at a density of $1x10^5$ cells/ml in their respective growth medium and cultured for 24 hours. Cells were then treated with imatinib mesylate and sunitinib malate (0.1-10μM) for 18 hours as described previously. Cells were also treated with $H_2O_2$ for 18

hours to provide single stain controls (750µM Annexin V control and 1500µM PI control). The single stain controls allow the gates for fluorescent tagging to be set, so that the cells can be sorted into healthy, early apoptotic, late apoptotic or necrotic fractions, and for compensation for any potential fluorescence spillover to be set. Once treated, the media from each well was collected into individual FACS tubes. Treated cells were then dissociated with 300µl of TrypleExpress (37°C) and collected into their respective FACS tubes alongside the previously collected media. Wells were then washed with 1ml of PBS to ensure all cells were recovered and the PBS collected and added to the corresponding FACS tube before being centrifuged at 1,000rpm for 5 minutes. Cells were then washed twice with PBS (the supernatant was discarded, the cells washed with 1ml of PBS and centrifuged at 1,000rpm for 5 minutes). After the second wash, 100µl of annexin V binding buffer was added to each FACS tube. 5µl of APC-conjugated annexin V was then added to all FACS tubes except the control (unstained) and the PI single stain (1200µM $H_2O_2$ treated) samples. The samples were then covered with aluminium foil to omit light and incubated for 15 minutes at room temperature. 400µl of 1:500 PI in binding buffer was added to all FACS tubes except the control (unstained) and annexin V single stain (750µM $H_2O_2$ treated) samples. 400µl of binding buffer was added to the control (unstained) and annexin V single stain (750µM $H_2O_2$ treated) samples. The samples were then analysed using an Attune NxT Flow Cytometer (Thermo Fisher Scientific, UK) and FlowJo v9 software (FlowJo LLC, Oregon, USA). Instrument settings were as follows; FSC: 40, SSC: 320, BL2 (Wavelength 574/26): 260, RL1 (Wavelength 670/14): 340.

*2.3.12 Immunofluorescence:*

Immunofluorescent staining was used to detect cell marker and protein expression (Camelliti *et al.*, 2005; Brown *et al.*, 2021). Cells were seeded in 12-well plates containing 13mm glass coverslips at a density of $1.5x10^4$ cells/ml and cultured until 40-60% confluent. Cells were then treated as per the drug treatment protocol with sunitinib or imatinib (1-

10μM). Following treatment, the cells were washed with PBS and then fixed with 3.6% (v/v) formaldehyde in PBS for 10 minutes at room temperature. Cells were washed again with PBS before being permeabilised with 0.25% Triton X-100 in PBS for 10 minutes at room temperature. The cells were again washed with PBS before being blocked in 1% (w/v) BSA in PBS for 30 minutes at room temperature. Cells were then incubated with primary antibody diluted in 1% (w/v) BSA in PBS (Table 1) overnight at room temperature.

Table 1. Antibodies and corresponding conditions optimised for immunofluorescence.

| Antibody: | Species: | Primary Antibody Dilution: | Secondary Antibody Dilution: |
|---|---|---|---|
| **Vimentin** | Mouse | 1:400 | 1:100 |
| **vWF** | Rabbit | 1:100 | 1:100 |
| **SMCa** | Mouse | 1:200 | 1:100 |
| **PLB** | Mouse | 1:100 | 1:100 |
| **RyR** | Mouse | 1:100 | 1:100 |
| **Sarcomeric α-Actinin** | Rabbit | 1:500 | 1:100 |

The following morning, coverslips were washed 3 times with PBS before being blocked again with 1% (w/v) BSA in PBS for 15 minutes at room temperature. Coverslips were then incubated with the corresponding Alexa fluor™ 488 secondary antibody (Table 1) in 1% (w/v) BSA in PBS for 60 minutes at room temperature while covered to omit light. Coverslips were again washed 3x with PBS and then stained with DAPI (1:2,000) for 5 minutes in darkness. Coverslips were then washed 2x with PBS before being mounted onto glass coverslips with Mowiol® and stored at 4°C until imaged. Samples were imaged using the EVOS™ FL Auto Imaging System (Thermo Fisher, Renfrew, UK) at x20 magnification.

*2.3.13 Intracellular calcium release assay:*

Cells were seeded in a black sided, clear bottomed 96-well plate at a density of $2.5x10^4$ cells/well and cultured for 24 hours. The following day, the culture medium was aspirated, and the cells washed twice with HBSS. Cells were then incubated with 2μM Fluo4-AM $Ca^{2+}$ indicator dye in Fluo4 buffer for 2 hours (37°C, 5% $CO_2$). Cells were then washed twice with Fluo4 buffer before adding 80μl of Fluo4 buffer to each well. A compound plate was prepared using the ligands of interest, diluted to 3x the final concentration in Fluo4 buffer. The plate reader transfers 40μl of compound to each well, diluting the compound 1:3 to reach a 1x desired final concentration for each sample. Ligand-induced $Ca^{2+}$ mobilisation was then measured using a Flexstation 3 microplate reader (Molecular Devices, Wokingham, UK) and SoftMax® Pro software, version 5.4.3. Raw $Ca^{2+}$ trace data was plotted using GraphPad Prism (version 7.0a). Changes in $Ca^{2+}$ flux were determined by subtracting the minimum from the maximum $Ca^{2+}$ fluorescent value. Samples were compared against untreated control.

*2.3.14 SDS-PAGE Western blot:*

Cell marker and protein expression and activation was also confirmed via Western Blot (Yao *et al*., 2011; Daniels *et al*., 2018). CFs (P1-P3) and CMs (P3-P5) were seeded in 12-well plates at a density of $1x10^5$ cells/ml and cultured in CF or CM growth medium until 70-80% confluent. Cells were then treated as per the in vitro drug treatment protocol (section 2.3.8). Cells were washed with phosphate buffered saline (PBS) and lysed in 150μl of LDS sample buffer. Cells were then scraped, lysed using a 21-gauge syringe and then heated at 100°C for 5 min. The lysates were then stored at -20°C until required.

*2.3.14.1 Cardiac fibroblast SDS-PAGE Western blot:*

CF lysates were loaded on to 4-20% Mini-PROTEAN TGX Precast Protein Gels and subjected to electrophoresis at 120V for 110 minutes in running buffer using a Mini-PROTEAN Tetra chamber (Bio-Rad Laboratories Ltd., Watford, UK) at room temperature. Proteins were then transferred to nitrocellulose membranes in transfer buffer using a MiniTrans-Blot Electrophoretic Transfer Cell (Bio-Rad Laboratories Ltd., Watford, UK) at a constant current of 280mA for 110 minutes at room temperature. Membranes were then blocked in 5% (w/v) BSA in TBS-T (0.1%) for 120 minutes at room temperature. The membranes were then transferred into 50ml falcon tubes and incubated with the appropriate primary antibody (Table 2) in 0.5% (w/ v) BSA in TBS-T (0.1%) and rotated overnight at 4°C.

Table 2. Antibodies and corresponding conditions optimised for immunoblotting.

| Antibody: | Species: | Primary Antibody Dilution: | Wash Procedure: | Secondary Antibody Dilution: |
|---|---|---|---|---|
| **CaMKIIδ** | Rabbit | 1:5,000 | 6x 5 Minute Washes | 1:7,500 |
| **Phos-CaMKII** | Rabbit | 1:5,000 | 6x 5 Minute Washes | 1:7,500 |
| **Ox-CaMKII** | Rabbit | 1:5,000 | 6x 5 Minute Washes | 1:7,500 |
| **GAPDH** | Mouse | 1:100,000 | 3x 5 Minute Washes | 1:7,500 |
| **Vimentin** | Mouse | 1:80,000 | 3x 5 Minute Washes | 1:7,500 |
| **vWF** | Rabbit | 1:100,000 | 3x 5 Minute Washes | 1:7,500 |
| **SMCa** | Mouse | 1:100,000 | 3x 5 Minute Washes | 1:7,500 |
| **PLB** | Mouse | 1:1,000 | 3x 5 Minute Washes | 1:7,500 |
| **RyR** | Mouse | 1:1,000 | 3x 5 Minute Washes | 1:7,500 |
| **Sarcomeric α-Actinin** | Rabbit | 1:3,000 | 3x 5 Minute Washes | 1:7,500 |

The following morning, the membranes were subjected to the relevant washing procedure (Table 2) followed by incubation in the corresponding secondary antibody (Table X2) in 0.5% (w/v) BSA in TBS-T (0.1%) for 90 minutes at room temperature. The membranes were again subjected to the relevant washing procedure before being developed via chemiluminescence (1:1 dilution of ECL1 and ECL2) using Ultracruz® autoradiography film (Santa Cruz Biotechnology, Heidelberg, Germany) and a JP-33 automatic film processor (JPI Healthcare Solutions, New York, USA). Membranes were then stripped in 15ml of stripping buffer and 105µl of β-mercaptoethanol for 30 minutes on an

incubated (60°C) shaking platform. Once stripped, the membranes were washed (4x 5 minute washes in TBS-T (0.1%)), blocked for 120 minutes at room temperature in 5% (w/v) BSA in TBS-T (0.1%) and incubated in the relevant primary and secondary antibodies (Table 2) as before. X-ray film was scanned on a HP Deskjet 2540 printer scanner and densitometry was carried out using Image J software (Schneider *et al*., 2012). Blotting data was normalised as indicated in the relevant figure legends and samples processed as percentage of control untreated signal.

*2.3.14.2 Progenitor cardiac myocyte SDS-PAGE Western blot:*

PCM lysates were loaded on to NuPAGE Novex 10% BisTris gels and subjected to electrophoresis at 200V for 90 minutes in MOPS buffer using a Mini Gel Tank and Blot Module Set (Invitrogen™, Renfrewshire, UK) at room temperature. Proteins were then transferred to nitrocellulose membranes in transfer buffer using the same Mini Gel Tank and Blot Module Set as before at a voltage of 25V for 60 minutes. Membranes were then blocked in 5% (w/v) BSA in TBS-T (0.1%) for 120 minutes at room temperature. The membranes were then transferred into 50ml falcon tubes and incubated with the appropriate primary antibody (Table 2) in 0.5% (w/ v) BSA in TBS-T (0.1%) and rotated overnight at 4°C.

The following morning, the membranes were subjected to the relevant washing procedure (Table 2) followed by incubation in the corresponding secondary antibody (Table X2) in 0.5% (w/v) BSA in TBS-T (0.1%) for 90 minutes at room temperature. The membranes were again subjected to the relevant washing procedure before being developed via chemiluminescence (1:1 dilution of ECL1 and ECL2) using Ultracruz® autoradiography film (Santa Cruz Biotechnology, Heidelberg, Germany) and a JP-33 automatic film processor (JPI Healthcare Solutions, New York, USA). Membranes were then stripped in 15ml of stripping buffer and 105µl of β-mercaptoethanol for 30 minutes on an

incubated (60°C) shaking platform. Once stripped, the membranes were washed (4x 5 minute washes in TBS-T (0.1%)), blocked for 120 minutes at room temperature in 5% (w/v) BSA in TBS-T (0.1%) and incubated in the relevant primary and secondary antibodies (Table 2) as before. X-ray film was scanned on a HP Deskjet 2540 printer scanner and densitometry was carried out using Image J software (Schneider *et al*., 2012). Blotting data was normalised as indicated in the relevant figure legends and samples processed as percentage of control untreated signal.

*2.3.15 DCFDA cellular reactive oxygen species detection assay:*

The DCFDA assay was used to determine whether there were any changesin intracellular ROS production following TKI treatment (Li *et al*., 2018). Cells were seeded in a black sided, clear bottomed 96-well plate at a density of $2.5x10^4$ cells/well and cultured in their respective growth medium for 24 hours. Cellular ROS production was then assessed using the 2',7' –dichlorofluorescin diacetate (DCFDA) cellular ROS assay kit (Abcam, Cambridge, UK). The culture medium was removed from the wells and the cells washed using the 1x buffer supplied with the kit. The cells were then incubated with 25μM DCFDA in 1x buffer for 45 minutes (37°C, 5% $CO_2$). Once the fluorescent dye has diffused into the cell, the cells were then washed again with 1x buffer to remove excess dye. The cells were then treated with the compounds of interest, diluted to the desired concentration in 1x supplemented buffer (1x buffer supplemented with 10% FBS) for 4 hours while covered in aluminium foil to omit light (37°C, 5% $CO_2$). Fluorescence was then determined using a Flexstation 3 microplate reader (Molecular Devices, Wokingham, UK) at Ex/Em: 485/535nm. Fluorescent values (RFU) were plotted using GraphPad Prism (version 7.0a).

*2.3.16 Live cell imaging of mitochondrial superoxide using MitoSOX red:*

MitoSOX Red was used to determine changes in mitochondrial superoxide production in cardiac cells following treatment with TKIs (Mukhopadhyay *et al*., 2007; Mukhopadhyay *et al*., 2009). Cells were seeded in an 8-well chamber at a density of $1x10^4$ cells/well and cultured in growth medium for 24 hours. Cells were then treated with the compounds of interest as per the drug treatment protocol with 1-10μM sunitinib and imatinib. The treated samples were then washed with HBSS before being incubated with 3μM MitoSOX Red (diluted in HBSS) for 5 minutes at room temperature in the absence of light. MitoSOX Red permeates live cells where it selectively targets the mitochondria. Within the mitochondria, MitoSOX Red is oxidised exclusively by superoxide, producing red fluorescence. Cell images were then recorded using WinFluor V4 0.8 live cell imaging software. Samples were normalised by selecting 10 cells from each sample and measuring fluorescence intensity for each cell. A blinded process was used for cell selection. Fluorescence intensity was then measured using imageJ software (Schneider *et al*., 2012) and normalised against control.

*2.3.17 Co-localisation:*

Co-localisation was used to investigate whether TKI treatment resulted in changes in CaMKII localisation at the mitochondria (Dunn *et al*., 2011). Cells were seeded in 12-well plates containing 13mm glass coverslips at a density of $1.5x10^4$ cells/ml and cultured until 40-60% confluent. Cells were then treated as per the drug treatment protocol with sunitinib (1μM) or imatinib (10μM). Following treatment, the cells were washed with PBS and then fixed with 3.6% (v/v) formaldehyde in PBS for 10 minutes at room temperature. Cells were washed again with PBS before being permeabilised with 0.25% Triton X-100 in PBS for 10 minutes at room temperature. The cells were again washed with PBS before being blocked in 1% (w/v) BSA in PBS for 30 minutes at room temperature. Cells were then double stained

with CaMKIIδ/ATPIF1 or Ox-CaMKII/ATPIF1 primary antibodies diluted in 1% (w/v) BSA in PBS (Table 3) overnight at room temperature.

Table 3. Optimised antibody concentrations for co-localisation experiments.

| Antibody: | Species: | Primary Antibody Dilution: | Secondary Antibody Dilution: |
|---|---|---|---|
| **CaMKIIδ** | Rabbit | 1:100 | 1:100 |
| **Ox-CaMKII** | Rabbit | 1:100 | 1:100 |
| **ATPIF1** | Mouse | 1:200 | 1:100 |

The following morning, coverslips were washed 3 times with PBS before being blocked again with 1% (w/v) BSA in PBS for 15 minutes at room temperature. Coverslips were then incubated with the corresponding Alexa fluor™ 488 secondary antibodies (Table 3) in 1% (w/v) BSA in PBS for 60 minutes at room temperature while covered to omit light. Coverslips were again washed 3x with PBS and then stained with DAPI (1:2,000) for 5 minutes in the absence of light. Coverslips were then washed 2x with PBS before being mounted onto glass coverslips with Mowiol® and stored at 4°C until imaged.

Coverslips were imaged using a Leica SP8 confocal microscope at 40x magnification. The images were processed via ImageJ software (Schneider *et al*., 2012). Co-localisation and changes therein were determined via Pearson's correlation, established using the Just Another Co-localisation Plugin (JACoP) (Bolte and Cordelieres, 2006).

*2.3.18 Measuring mitochondrial respiration:*

Cell samples were cultured in T75 flasks. The cells were trypsinised as per their relevant protocols and then re-suspended in MiR buffer. The cells were then counted using a haemocytometer and the sample volumes adjusted with MiR so that the treatment and control samples had equal cell densities ($1x10^6$ cells/ml). Mitochondrial respiration was measured using the Oxygraph O2k respirometer (Oroboros Instrumens, Austria), a common and robust measure of mitochondrial function that provides the investigator with a comprehensive overview of the bioenergetics of intact cells (Brand and Nicholls, 2011; Djafarzadeh and Jakob, 2017). The instrument measures the $O_2$ concentration within the chamber and, from this, calculates the real-time rate of $O_2$ consumption. The instrument also allows for the injection of substrates, uncouplers and inhibitors into the chambers, which enables the user to determine cellular bioenergetics (Figure 2.3.18.1A). The Oxygraph O2k has two oxygen sensing chambers which allow for the real-time analysis of two samples – one treated sample and one control sample for comparison.

Mitochondrial respiration was measured using the 'high-resolution respirometry' and 'oxygen consumption of intact cells' protocols described by Djafarzadeh and Jakob (2017), as described previously by Paech *et al*. (2017). Briefly, the intact cells were placed in a polarographic $O_2$ sensing chamber and sealed. Basal cellular respiration was then recorded until a stable oxygen flux signal was achieved. Then oligomycin (2.5μM final concentration) was added to the chamber to inhibit ATP production (Figure 2.3.18.1). Again, cellular respiration was then recorded until a stable oxygen flux signal was achieved. The uncoupler carbonyl cyanide m-chlorophenyl hydrazone (CCCP) was then titrated (0.5μM increments) until the oxygen flux signal reaches maximal respiration and begins to decline (Figure 2.3.18.1). At this point, rotenone (0.5μM final concentration) and antimycin A (2.5μM final concentration) were added to inhibit mitochondrial respiration (Figure 2.3.18.1). The average rate of oxygen consumption from each state of cellular respiration is then plotted using

GraphPad Prism (version 7.0a). From this, cellular bioenergetics can be calculated as shown in Figure 2.3.18.1B and are corrected to show mitochondrial respiration only by subtracting the rate of oxygen consumption for non-mitochondrial respiration. Cellular bioenergetics are then compared between treated and control samples.

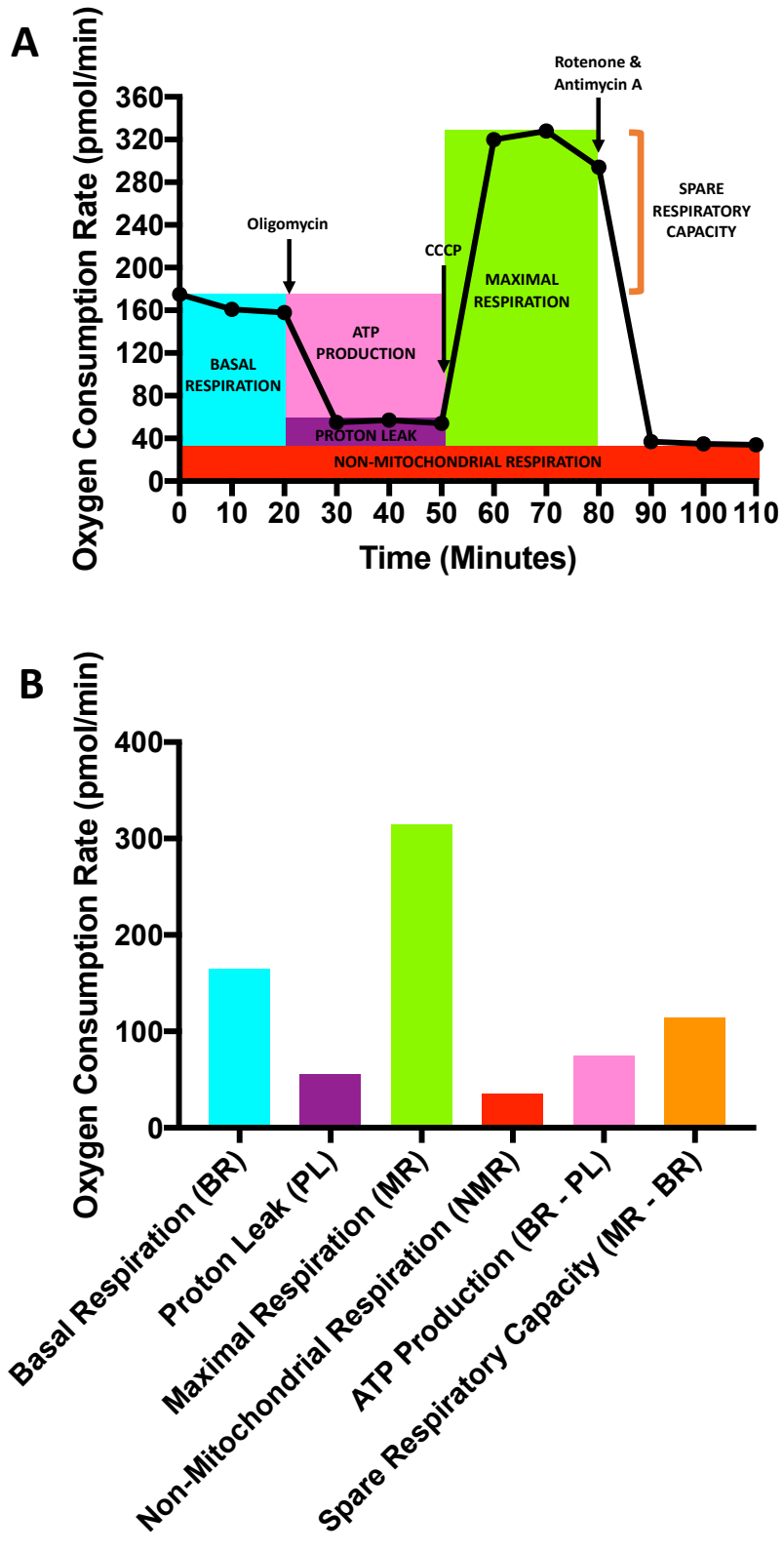


**Figure 2.3.18.1. An overview of the mitochondrial respiration protocol.** (A) An overview of mitochondrial respiration detailing the methodology used to determine the different stages of respiration and the uncouplers and inhibitors used to determine these. (B) An example of the findings of this method and how ATP production and spare respiratory capacity can be estimated from these.

*2.4 Data Analysis:*

Data are presented as mean values ± S.E.M of n observations, where n represents the number of samples. Comparisons were assessed by one-way ANOVA with post hoc Dunnett's test using GraphPad Prism (version 7.0a). P-values $<0.05$ were considered significant.

# Chapter Three: Investigating the effect of tyrosine kinase inhibitor treatment on cardiac cells

*3.1 Introduction*

Tyrosine kinase inhibitors (TKIs) have transformed cancer therapy since the approval of the first TKI, imatinib mesylate (Gleevec®), in 2001 (Cheng and Force, 2010). However, the success of such agents has been marred by reports of associated cardiotoxicity as a result of their mechanism of action. TKIs antagonise the ATP binding pocket, preventing activation of the kinase and subsequent downstream phosphorylation. As the ATP binding pocket is a shared entity amongst approximately 500 kinases, it is not surprising that agents targeting this communal locale are susceptible to selectivity issues and associated toxicity (Bantscheff *et al*., 2007). Both sunitinib and imatinib are affiliated with cardiotoxicity, although the prevalence of toxicity varies in accordance with the selectivity of the drug.

Kerkela and colleagues first reported CM cell death in imatinib-treated human and murine CMs in 2006. The study found that imatinib treatment caused CM cell death via mitochondrial dysfunction. Similar findings were also reported by Chu (2007) and Cohen (2011), both of whom observed CM cell death subsequent to sunitinib treatment; again, citing toxicity at the level of the mitochondria as a possible mechanism. Reduced cardiac contractility is a hallmark of TKI-induced cardiotoxicity and is consistent with these findings. It is clear that CM dysfunction is central to the pathology of TKI-induced cardiotoxicity, however, the effect of these drugs on other cardiac cell types cannot be overlooked.

Despite the plethora of research assessing the effect of sunitinib and imatinib on CMs, little is known of wider ranging effects, particularly on cardiac non-myocytes. CFs are one of the most abundant cell types within the heart and are responsible for maintaining cardiac structure. CFs regulate the structure of the ECM through the secretion of factors that synthesize and degrade the collagen framework (Camelliti *et al*., 2005). This dynamic process is critical to both cardiac repair and pathology and is consistent with one of the hallmark characteristics of TKI-induced cardiotoxicity – ECM remodelling. In understanding

how TKIs mediate their cardiotoxic effects it is essential to study both the myocytes and non-myocytes of the heart. Of the little research conducted on CFs, Burke and colleagues (2019) have shown that both sunitinib and imatinib significantly reduce CF viability, highlighting the potential role CF toxicity may play in the pathology of TKI-induced cardiotoxicity.

The experimental results presented in this chapter examine the morphological and cell marker changes upon sunitinib and imatinib treatment on both the contractile and non-contractile cells of the heart. Changes in cardiac cell viability following TKI-treatment are also assessed.

*3.2 Characterising healthy cardiac fibroblasts in culture*

In both the healthy and diseased heart, CFs are central in establishing and preserving cardiac structure and function (Camelliti *et al*., 2005; Souders *et al*., 2009). Healthy, quiescent CFs are flat, spindle shaped cells with multiple projections originating from the main cell body. However, in response to cardiac stress or disease, CFs become activated and undergo a morphological change in order to preserve cardiac function (Vasquez *et al*., 2011). CF activation induces cardiac remodelling and is a well-known mediator of cardiovascular disease. Extensive cardiac remodelling is also observed in patients presenting with TKI-induced cardiotoxicity. This phenomenon suggests that the cardiotoxic mechanism of TKIs likely impact both the contractile and non-contractile cells of the heart. In order to assess the effect TKI treatment has on CFs, the phenotype of healthy CFs must first be established. CFs were isolated from adult male Sprague-Dawley rats as described previously and CF phenotype determined via cell imaging.

Isolated CFs initially appear as small, round bright entities that adhere readily to the culture vessel after approximately 4 hrs (Figure 3.2.1). Initially, cell debris is observed in the culture vessel from the isolation process; however, this is typically eliminated after the second medium change, 24 hrs post-isolation. At this point, it is not uncommon to see some CFs sparsely distributed throughout the culture vessel (Day 1). As the culture process continues, the isolated CFs grow in clusters (Day 3). The isolated CFs are representative of healthy CFs – flat, spindle shaped cells with protrusions emanating from the main cell body (Figure 3.2.1 (Day 3)). As the cells reach confluence, their appearance becomes ‘cobble-stone’ like (Day 6) with the cells located in close proximity to each other, affording the cells their primary function. It should be noted that CFs are typically passaged at 70-80% confluence, however, the cells are grown close to confluence for experimental use in end-stage assays such as those to investigate cell viability. The image of the cells at Day 6 highlights the ‘cobble-stone’ like appearance the cells adopt as they reach confluence.

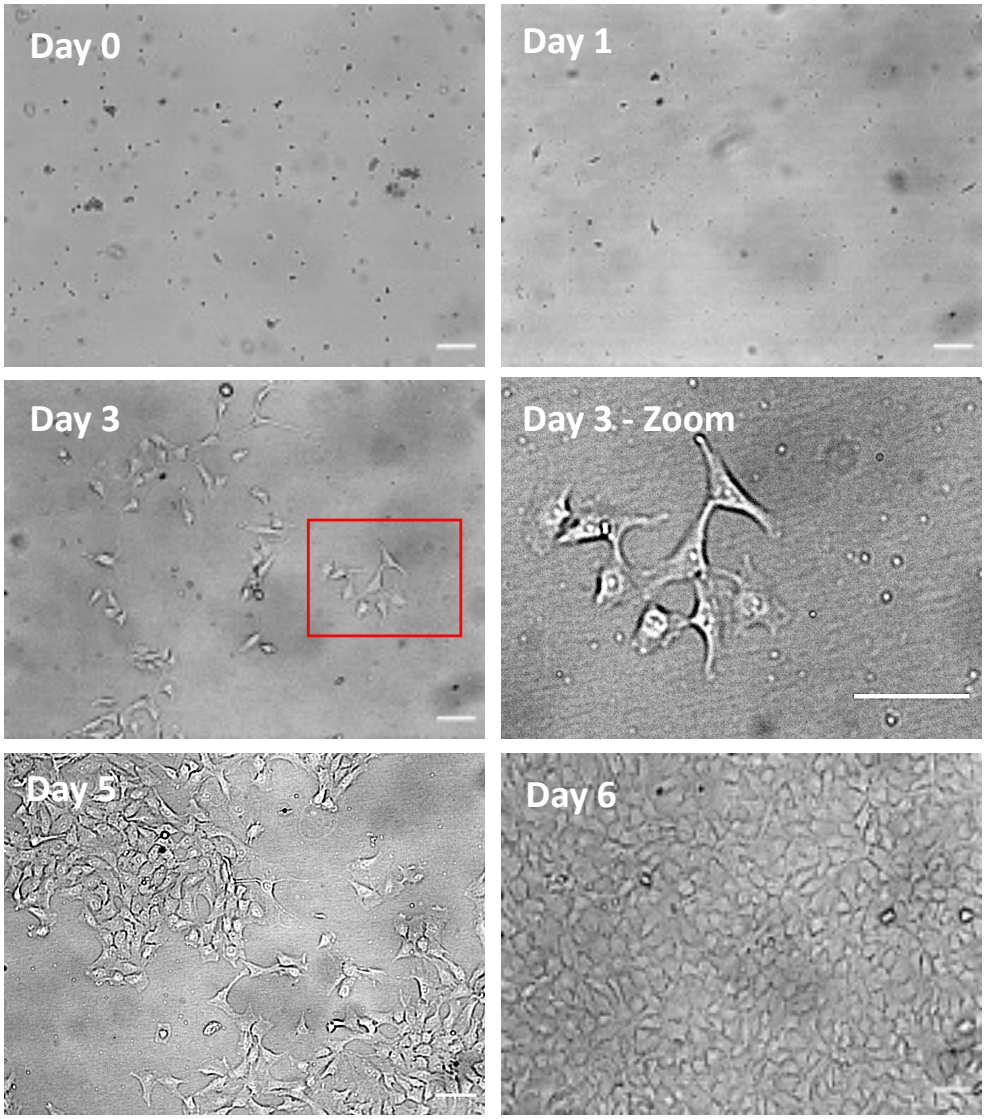


**Figure 3.2.1. Brightfield imaging of cardiac fibroblast phenotype post-isolation and throughout culture until the first passage.** CFs were isolated from male Sprague-Dawley rats via the bulk collagenase digestion method. Images were obtained after each media change, beginning 4 hours post-isolation (Day 0), again 24 hours post-isolation (Day 1) and thereafter at 48hour intervals thereafter until the CFs were ready for passage. Images obtained using a Nikon Eclipse (TE300) inverted microscope (x10 magnification). Scale bar 100μm (n=3).

In response to cardiac stress, the typically quiescent CFs undergo CF to MF differentiation. This biochemical process serves as an adaptive mechanism to preserve cardiac function in response to pathological signalling and can serve as an indicator of CVD (Berk *et al*., 2007; Bradley *et al*., 2018). The activated CFs, commonly referred to as MFs, are structurally and functionally different to the undifferentiated cell type. In comparison to CFs, MFs exert a larger, more rounded and transparent phenotype. MFs are also known to contain prominent focal adhesions and actin stress fibres, giving them a more striated appearance (Vasquez *et al*., 2011). These morphological differences are shown in the comparison between isolated CFs and MFs in Figure 3.2.2. CF to MF transition can occur in culture over time, usually at higher passage numbers (>P3), though on occasion this differentiation can occur at lower passage numbers. It is therefore important to distinguish between these healthy CFs and MFs.

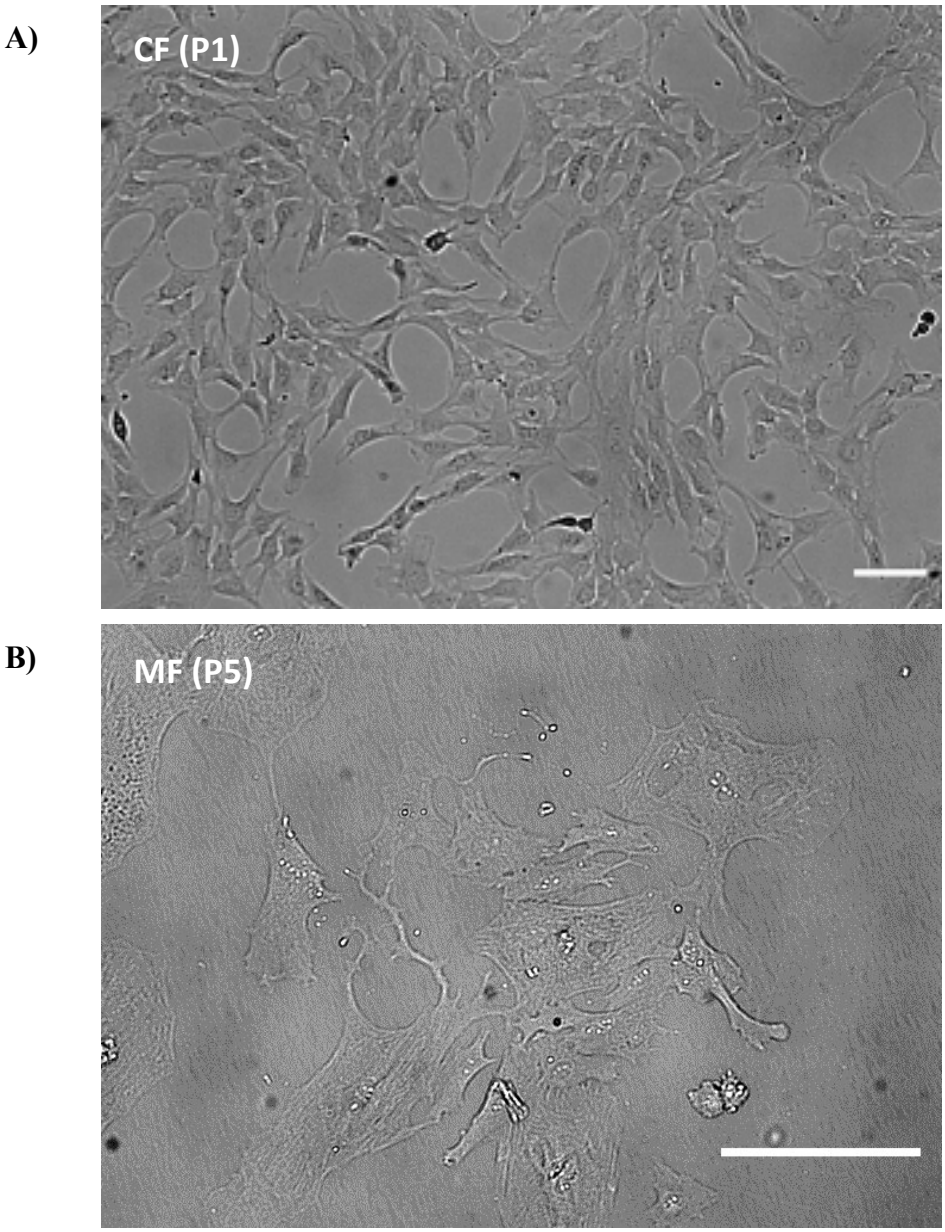


**Figure 3.2.2. Phenotypic characterization of cardiac fibroblasts and myofibroblasts in culture.** CFs were isolated from male Sprague-Dawley rats via the bulk collagenase digestion method. (A) CFs were cultured in CF growth medium until 40-70% confluent (CFs (P1)). CFs were monitored after each passage to assess changes in phenotype as the cells undergo senescence. (B) At passage 5, the CFs have transformed into MFs (P5). Images obtained using a Nikon Eclipse (TE300) inverted microscope (x10 magnification). Scale bar 100μm (n=1).

CFs exist across multiple tissues and organs of the body and exhibit some degree of heterogeneity according to their source. This can make CFs difficult to characterise (Doppler *et al*., 2017). Typically, CFs are characterised by their phenotype and by immunofluorescence staining of recognised positive markers. A positive vimentin stain, a sensitive but non-selective marker for CFs, is used to characterise CFs. However, the non-selective nature of vimentin and the heterogenicity of CFs means that further staining with negative controls should be conducted (Humeres and Frangogiannis, 2019). In addition to a positive vimentin stain, the exclusion of non-CF markers such as vascular smooth muscle, endothelial and haematopoietic cell markers is required to accurately characterise CFs. Isolated CFs were stained with vimentin, α-smooth muscle cell actin (SMCa) and von Willebrand factor (vWF). MFs were stained in parallel with these cell markers in order to differentiate marker expression between healthy CFs and MFs.

Immunofluorescence showed a strong positive stain for vimentin in untreated isolated CFs, consistent with healthy, undifferentiated CFs (Figure 3.2.3). To exclude the possibility of contamination with SMCs or ECs, CFs were also stained for SMCa (a marker of SMC phenotype) and vWF (a marker of EC phenotype). Staining was compared across CFs, MFs, SMCs and ECs. Although a positive stain for both SMCa and vWF was obtained in CFs, staining for SMCa was visibly less than that obtained in the positive controls for SMCs and vWF staining in CF was of a very different pattern than that seen in the positive controls for ECs (Figure 3.2.3). In both CFs and MFs, vWF staining presented as a dull diffuse signal throughout the cytoplasm whereas in ECs vWF staining presented as a speckled pattern, largely located around the nucleus of the cells. In CFs, SMCa staining was also less than that obtained in the phenotypically transformed MFs.

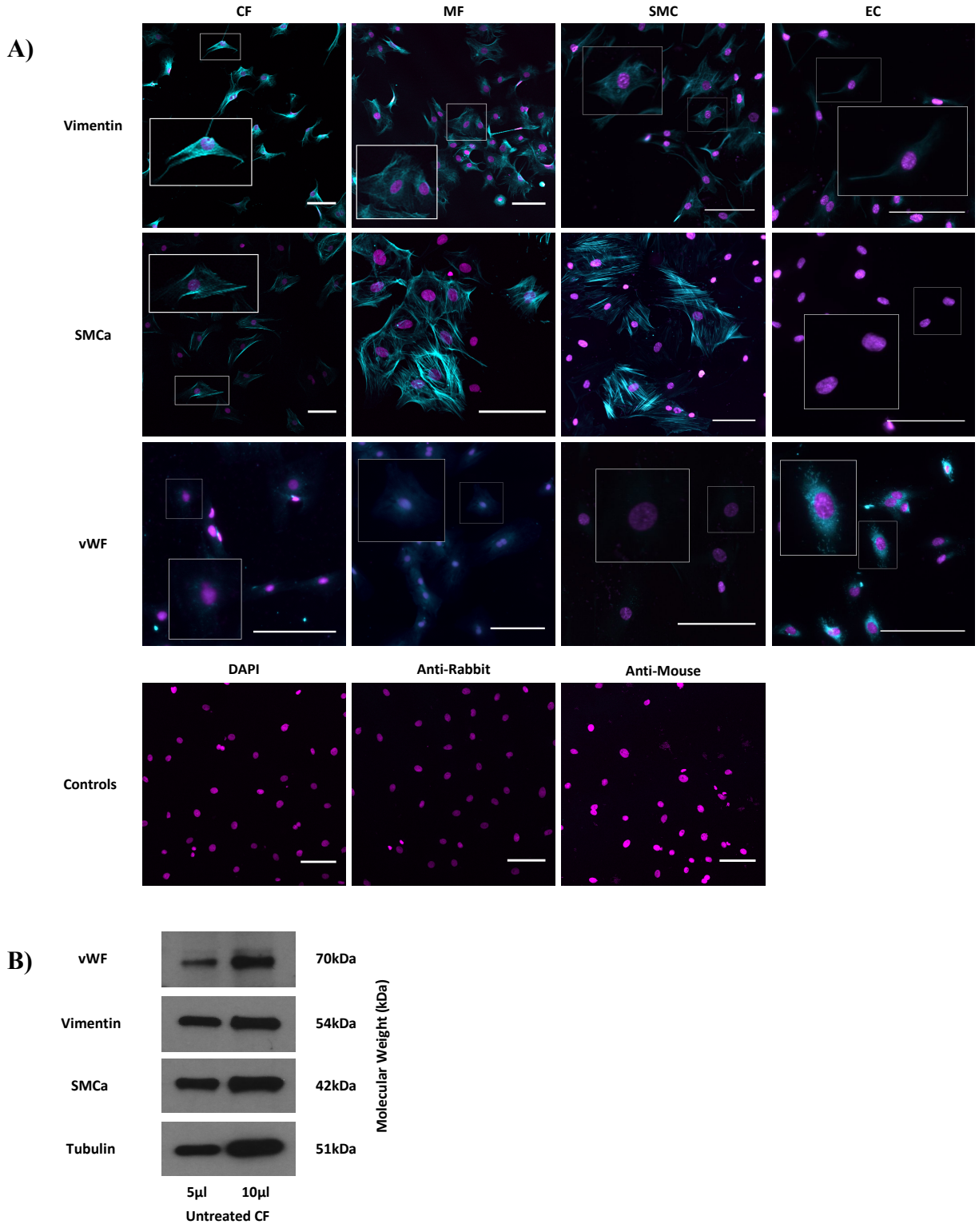


**Figure 3.2.3. Assessment of cardiac fibroblast and myofibroblast phenotype.** (A) CFs phenotype was confirmed via immunofluorescence by staining for vimentin, smooth muscle cell alpha actin (SMCa) and von Willebrand Factor (vWF). Staining was compared between CFs and myofibroblasts (MFs). Smooth muscle cells (SMCs) and human umbilical vein endothelial cells (HUVECs) were used as positive controls. Cells treated with DAPI alone and secondary antibodies alone were used as negative controls. (B) Confirmation of CF marker expression via immunoblotting (n=3). Scale bar 100µm. Images are from one experiment, representative of two others.

*3.3 TKI treatment impacts cardiac fibroblast morphology*

Having established the phenotype and marker expression of healthy isolated CFs, the effect of sunitinib and imatinib treatment on CF morphology was then investigated. Due to the mitogenic properties of serum, cell signalling pathways are often evaluated in the absence of serum. However, concerns have been raised regarding the physiological relevance of such data, with the serum content known to influence experimental outcome (Whorwood *et al*., 2001; Levin *et al*., 2010; Pirkmajer and Chibalin, 2011). With this in mind, one of the objectives of this study was to determine what effect, if any, serum starvation may have in influencing TKI-induced toxicity. This project is unique in that we are interested in the effects of these drugs from both physiological and cell signalling perspectives, combining the effect these drugs have on the cardiac cells with the cellular processes that underpin the cardiotoxic mechanism.

In the absence of serum, sunitinib treatment resulted in changes in CF phenotype from 0.3μM sunitinib in a concentration dependent manner (Figure 3.3.1). Sunitinib-treated CFs appeared larger and more transparent, with the formation of vacuole-like structures evident in the main cell body. Obvious cell loss was evident from 1μM sunitinib, with a concentration dependent cell loss (1-10μM). In comparison, CFs appeared to be less affected by imatinib treatment than sunitinib treatment, even in the absence of serum. Imatinib treatment induced changes in cell phenotype from 3μM imatinib, with obvious cell loss apparent at 10μM imatinib (Figure 3.3.1).

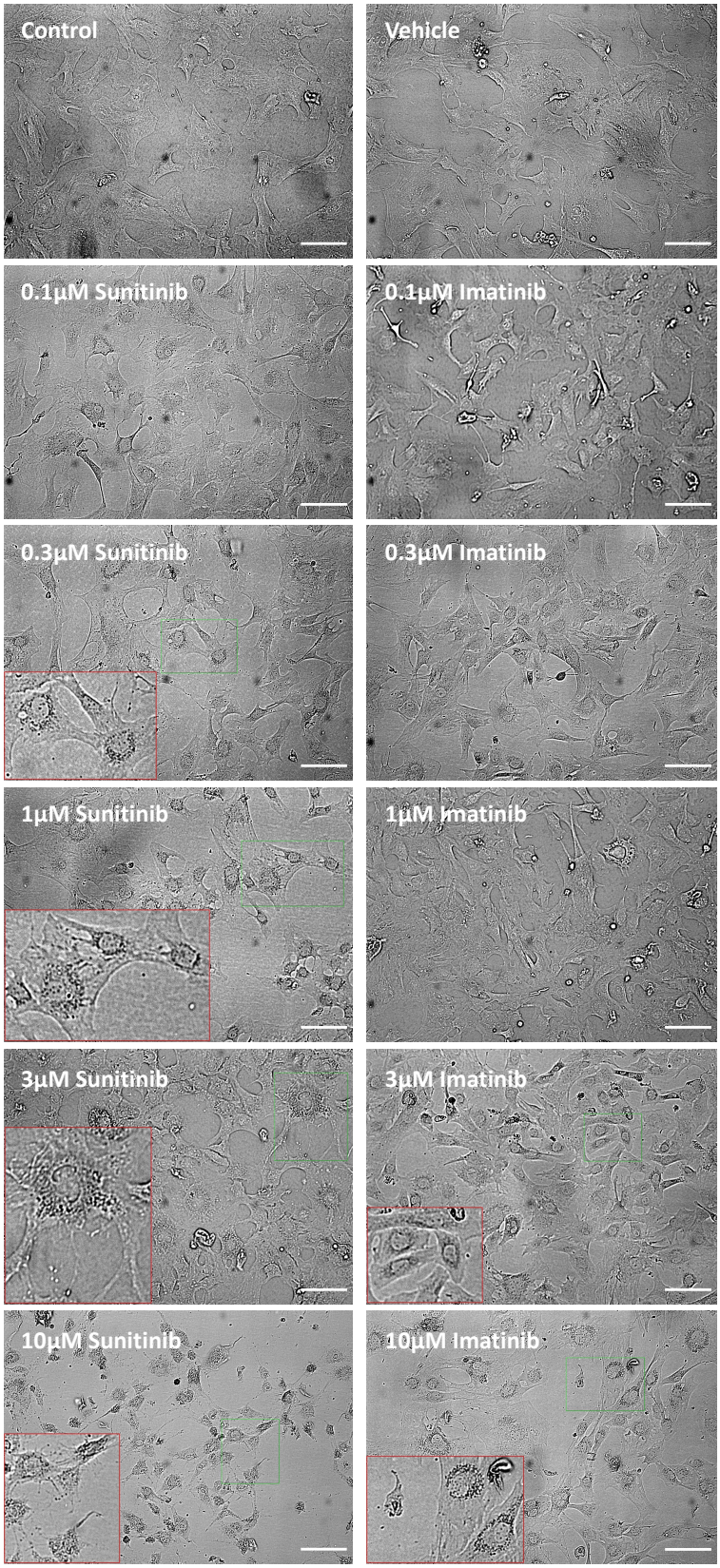


**Figure 3.3.1. Determining the effect of TKI treatment on cardiac fibroblast phenotype in the absence of serum.** CFs were cultured in CF growth medium until 70% confluent and then serum starved for 4 hours prior to drug treatment. CFs were treated with sunitinib or imatinib (0.1-10µM) in the absence of serum for 18 hours. Images obtained using a Nikon Eclipse (TE300) inverted microscope (x10 magnification). Scale bar 100µm (n=3).

Figure 3.3.1 clearly shows that both drugs effect CF morphology, with cell death also apparent in both sunitinib and imatinib treated CFs. To determine what effect the inclusion of serum has on CFs treated with sunitinib and imatinib, the experiment was repeated. In the presence of serum, sunitinib-induced changes in CF phenotype were evident from 1μM sunitinib and became more apparent as the concentration of the drug increased (Figure 3.3.2). Sunitinib treatment resulted in similar characteristics of cell toxicity as seen in the absence of serum. However, the effects were not apparent until higher concentrations of sunitinib were applied, suggesting a protective effect of serum. As seen in Figure 3.3.1, CFs appeared larger and more transparent, and vacuole-like structures were again evident in the main cell body, albeit only at notably higher concentrations of sunitinib than those concentrations required to exert similar effects in the absence or serum. Obvious cell loss was apparent at 10μM sunitinib (Figure 3.3.2). In comparison, imatinib treatment appeared to have no discernible effect on CF phenotype or cell viability in the presence of serum.

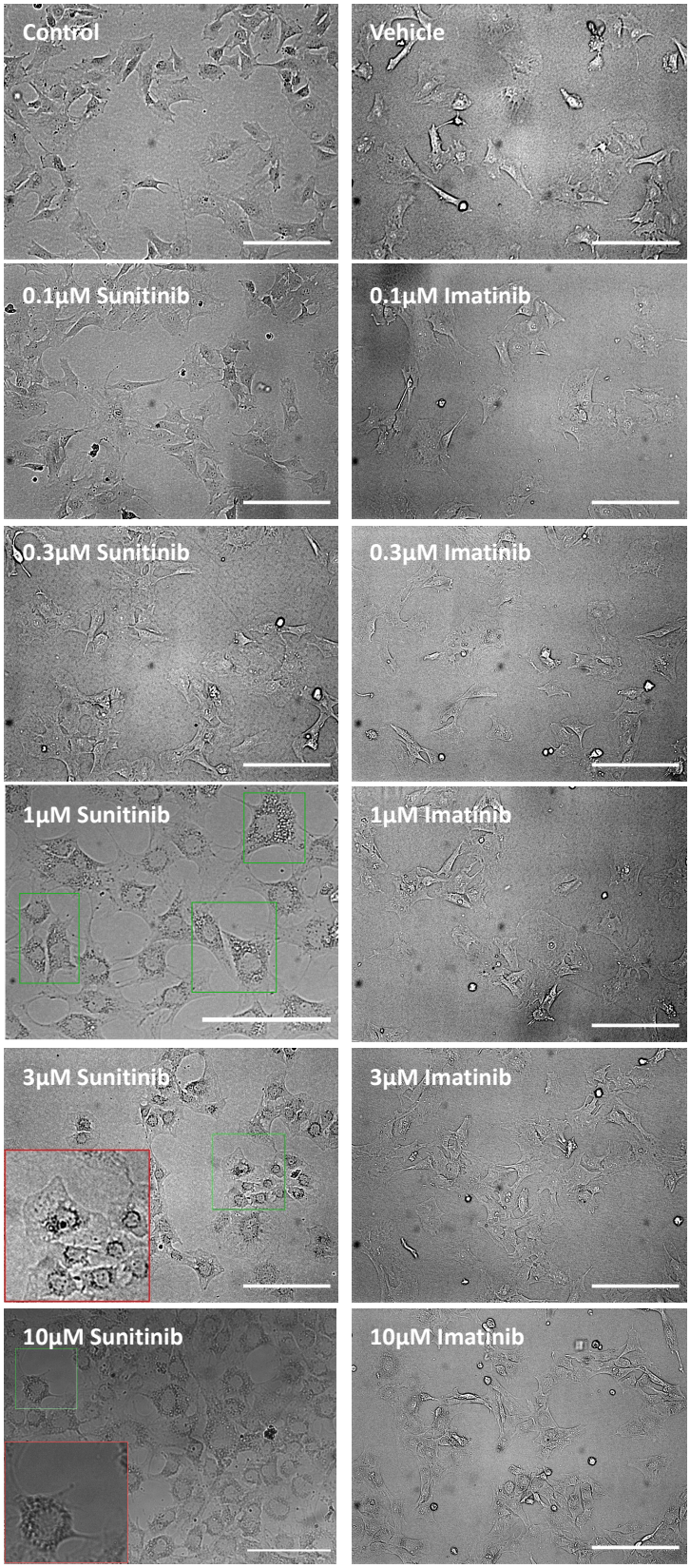


**Figure 3.3.2. Determining the effect of TKI treatment on cardiac fibroblast phenotype in the presence of serum.** CFs were cultured in CF growth medium until 70% confluent. CFs were then treated with sunitinib or imatinib (0.1-10µM) in the presence of serum for 18 hours. Images obtained using a Nikon Eclipse (TE300) inverted microscope (x10 magnification). Scale bar 100µm

The images presented in Figures 11 and 12 show that TKI treatment affects the phenotype of CFs, both in the presence and absence of serum. To further evaluate whether these changes in CF phenotype correlated with changes in marker expression, CFs were treated with sunitinib or imatinib (1μM and 10μM) and then stained with vimentin, SMCa and vWF.

Immunofluorescence of CF cells treated with sunitinib and imatinib showed a positive stain for vimentin, SMCa and vWF (Figure 3.3.3). Vimentin and SMCa stains did not appear to be affected by sunitinib or imatinib treatment. However, both sunitinib and imatinib treatment seemed to cause a visible increase in vWF marker expression (Figure 3.3.3).

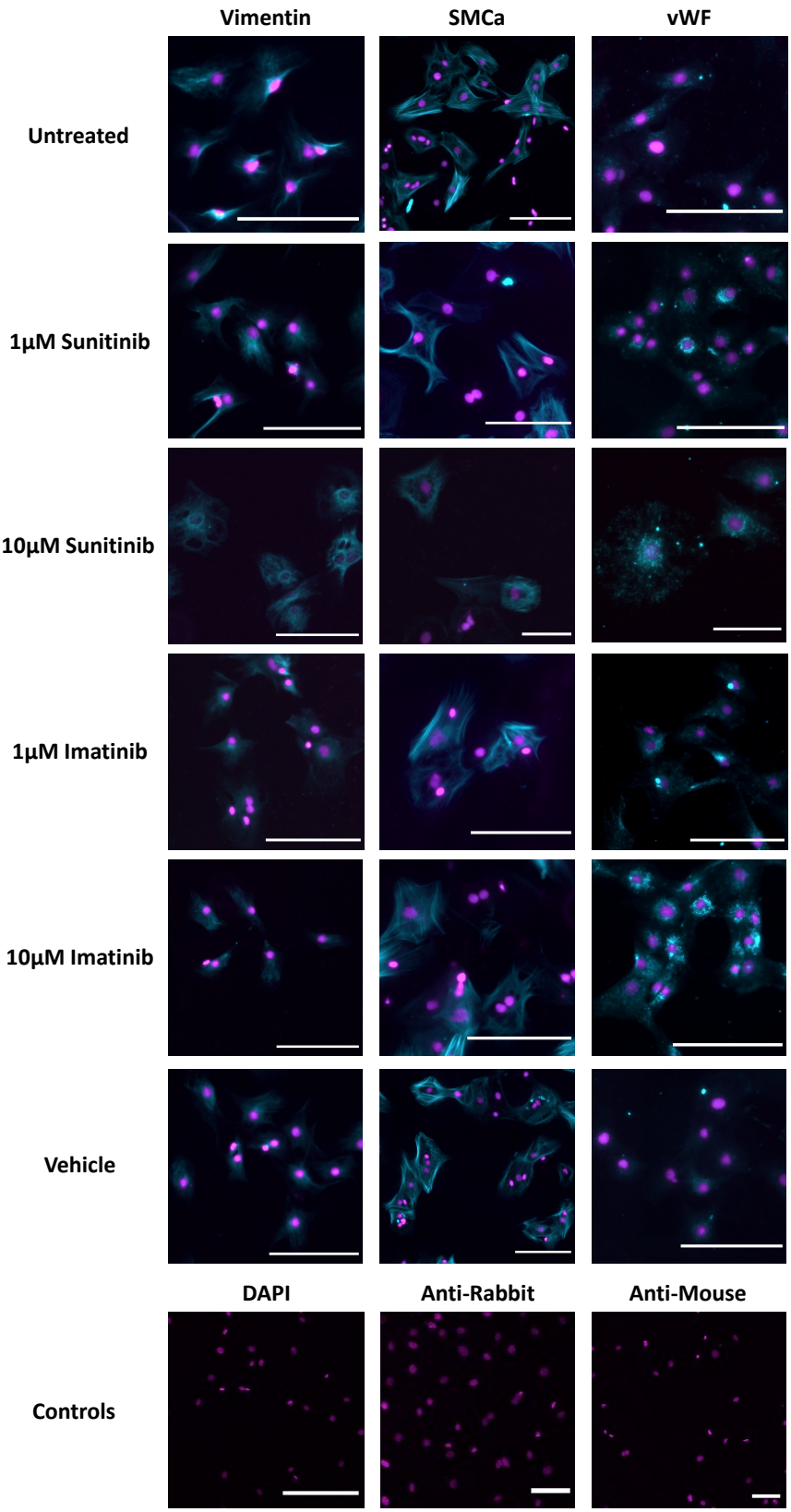


**Figure 3.3.3. Investigating the effect of TKI treatment on cardiac fibroblast marker expression via immunofluorescence.** CFs (P1-P2) were treated with sunitinib or imatinib (1-10µM) and then stained with the CF markers vimentin, SMCa and vWF to determine any changes in marker expression. Cells treated with DAPI alone and secondary antibodies alone were used as negative controls. Scale bar 100µm (n=2).

In order to quantify whether these observed changes in cell marker expression following TKI treatment were significantly different to untreated CFs, sunitinib and imatinib treated CF lysates were analysed via immunoblotting using the same antibodies for CF marker expression. Quantitative immunoblotting revealed that neither sunitinib nor imatinib had any significant effect on CF marker expression (Figure 3.3.4). The apparent increase in vWF expression (Figure 3.3.3) was not statistically significant (Figure 3.3.4) and likely reflects changes in cell phenotype induced by TKI treatment.

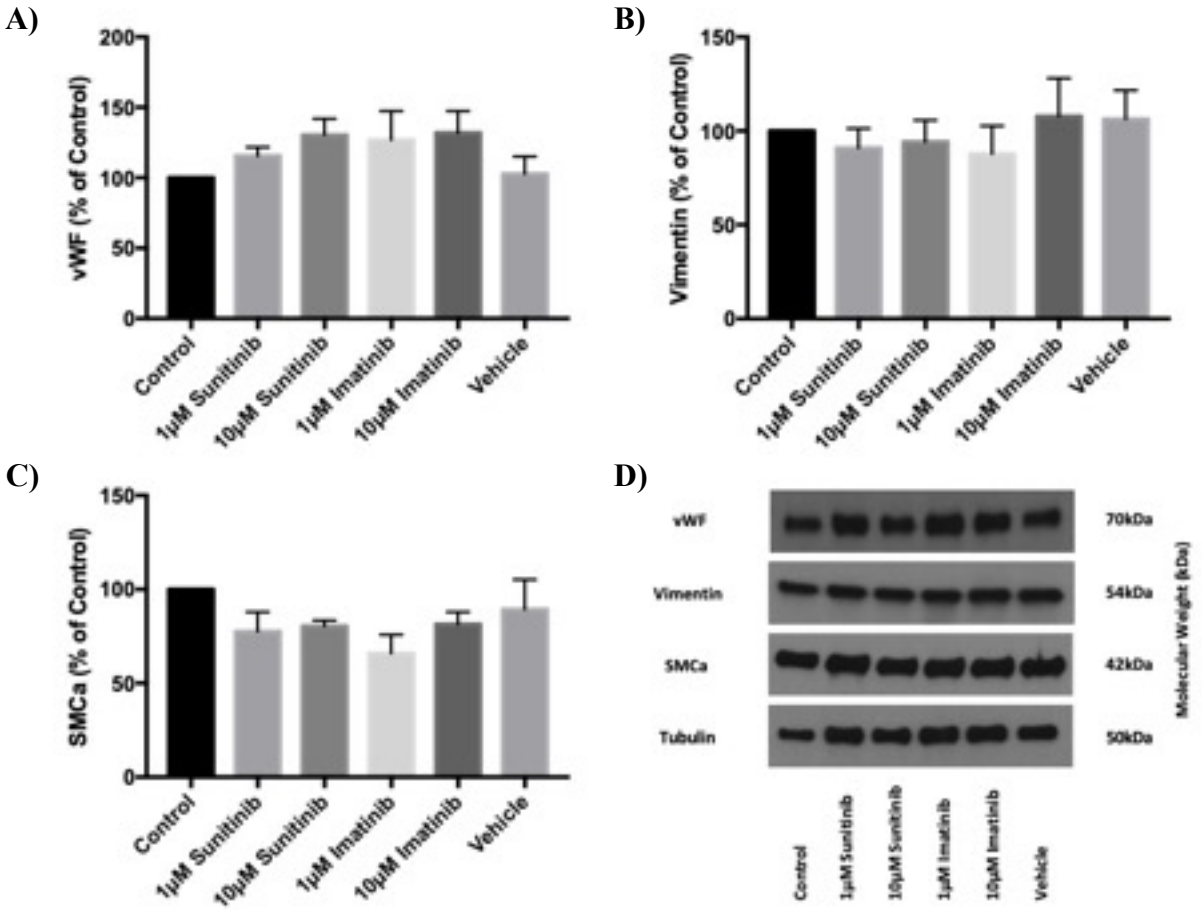


**Figure 3.3.4. Determining the effect of TKI treatment on cardiac fibroblast cell marker expression via western blot.** Following the indicated treatments with either sunitinib or imatinib, vWF, vimentin and SMCa expression was determined via quantitative immunoblotting (A) vWF expression. (B) Vimentin expression. (C) SMCa expression. All samples normalised to tubulin expression. (D) Representative immunoblot showing vWF, vimentin, SMCa and tubulin expression TKI treatment. Results are expressed as mean ± S.E.M and are normalised to control (n=3).

*3.4 TKI treatment causes cardiac fibroblast cell death*

Kerkela (2006) has shown that TKI treatment causes CM apoptosis via impaired mitochondrial function, yet little is known regarding the wider ranging effect of drug treatment on cardiac non-myocytes. Having determined that TKI treatment affects CF morphology, viability assays were then conducted to assess whether the change in phenotype impacted CF function. CFs were treated with sunitinib or imatinib and subjected to an MTT assay. The MTT assay is a widely used colorimetric assay that determines cell viability via the cell's metabolic activity; viable cells are able to reduce MTT to its inactive form, dead cells cannot. It has previously been utilised by several groups to assess the toxicity of anti-cancer drugs on cardiac cells (Green and Leeuwenburgh, 2002; Burke *et al*., 2019; Sirangelo *et al*., 2020). Before investigating the effect of TKI treatment on CFs, the MTT assay was first optimised using hydrogen peroxide ($H_2O_2$).

MTT assays showed that $H_2O_2$ significantly reduced CF viability in a concentration dependent manner in the mM range (Figure 3.4.1). A significant reduction in viability was also seen in CFs cultured in water, a positive control used for this experiment.

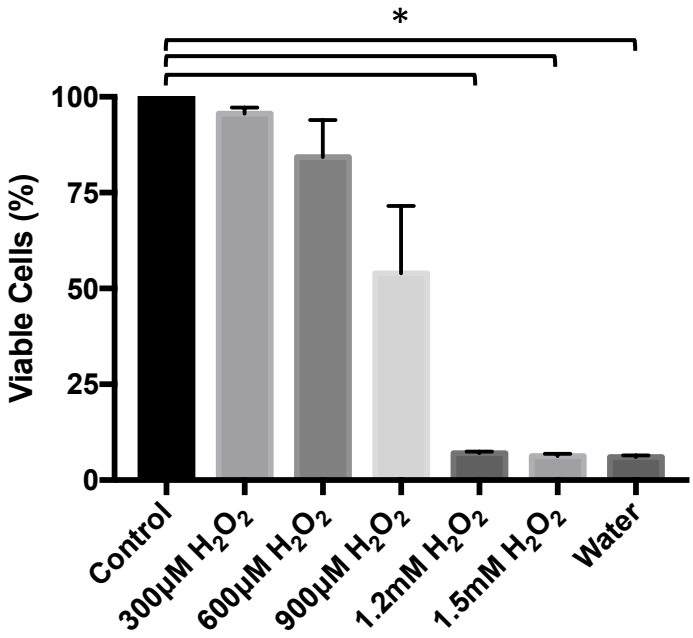


**Figure 3.4.1. MTT optimisation using hydrogen peroxide.** CFs were treated with hydrogen peroxide ($H_2O_2$ (300μM-1.5mM)) in the presence of serum for 18 hours. Water was used as a positive control. Cell proliferation was assessed via MTT assays. Results are expressed as mean ± S.E.M and are normalised to control (n=3, *$p<0.05$).

Having confirmed that the MTT assay was working optimally, CFs were treated with sunitinib or imatinib (0.1-10μM) and then viability was evaluated via MTT assays. Assays were conducted in the presence of serum.

MTT assays revealed that sunitinib, but not imatinib, reduced CF viability (Figure 3.4.2). CF viability was significantly reduced at 3μM (87.7±1.8%) and 10μM (74.0±2.3%) sunitinib (vs untreated control), consistent with the cell loss observed using brightfield imaging (Figure 3.3.2).

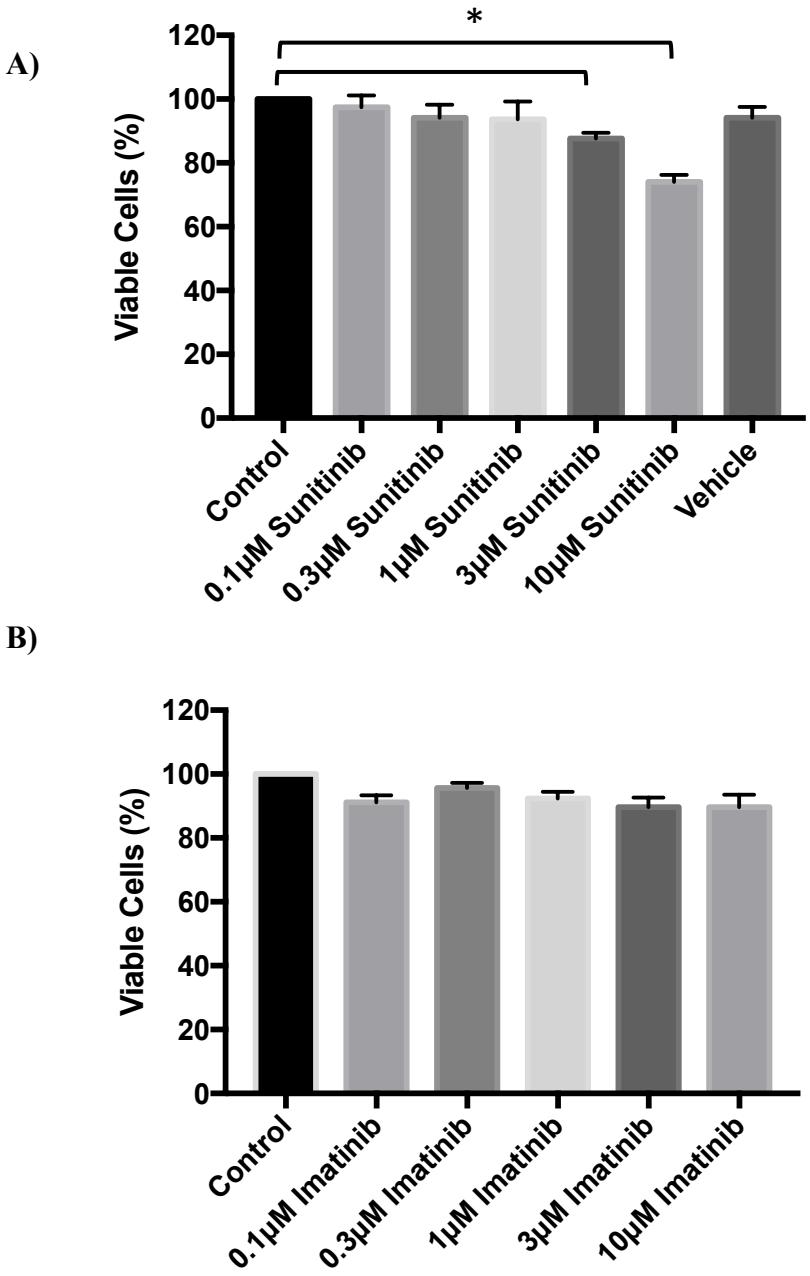


**Figure 3.4.2. Investigating the effect of sunitinib or imatinib treatment on cardiac fibroblast viability.** CFs were treated with sunitinib or imatinib (0.1-10μM) in the presence of serum for 18 hours. Cell proliferation was assessed via MTT assays. (A) sunitinib treated CFs (B) imatinib treated CFs. Results are expressed as mean ± S.E.M and are normalised to control (n=3, *p<0.05).

These results suggest that the changes in CF phenotype induced by TKI treatment (Figure 3.3.2) correlate with reduced cell viability (Figure 3.4.2). However, it is worth highlighting that the consistency and reliability of the MTT assay has been called into question (Kumar *et al*., 2018). As a result, it has been recommended that changes in cell viability be validated by an alternative measurement of cellular toxicity, such as flow cytometry analysis. Flow cytometry is viewed as a more reliable method of assessing cellular toxicity that simultaneously provides greater insight into the mechanism of cell death. During early apoptosis, phosphatidylserine (PS) translocates from the cytoplasmic side of the cell membrane to the cell surface. Annexin V (AnV) has high affinity for PS and positive staining indicates early apoptosis. During necrosis, the loss of membrane integrity allows PI to intercalate DNA and fluoresce. Positive staining of both PI and AnV indicates late apoptosis whereas the extrusion of both PI and AnV indicates healthy cells (Wang *et al*., 2010; Kumar *et al*., 2018). Flow cytometry was first optimised using $H_2O_2$ treated CFs.

Figure 3.4.3 shows the parameters used for flow cytometry analysis. $H_2O_2$ treatment (0.3-1.5mM $H_2O_2$) caused a reduction in the number of healthy CFs with a concomitant increase in the number of apoptotic and necrotic CFs (Figure 3.4.4).

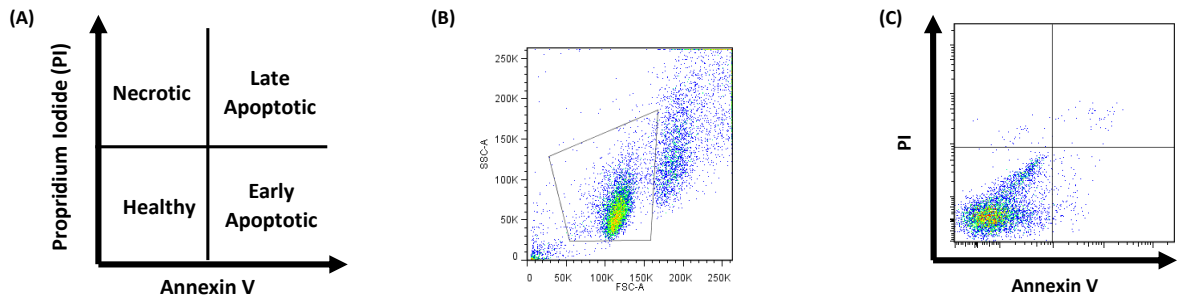


**Figure 3.4.3. The parameters used for flow cytometry.** (A) Illustration of the gates used for FACS analysis. (B) An example of the population pool used for FACS analysis. (C) A representative example of untreated CFs stained with annexin V and PI.

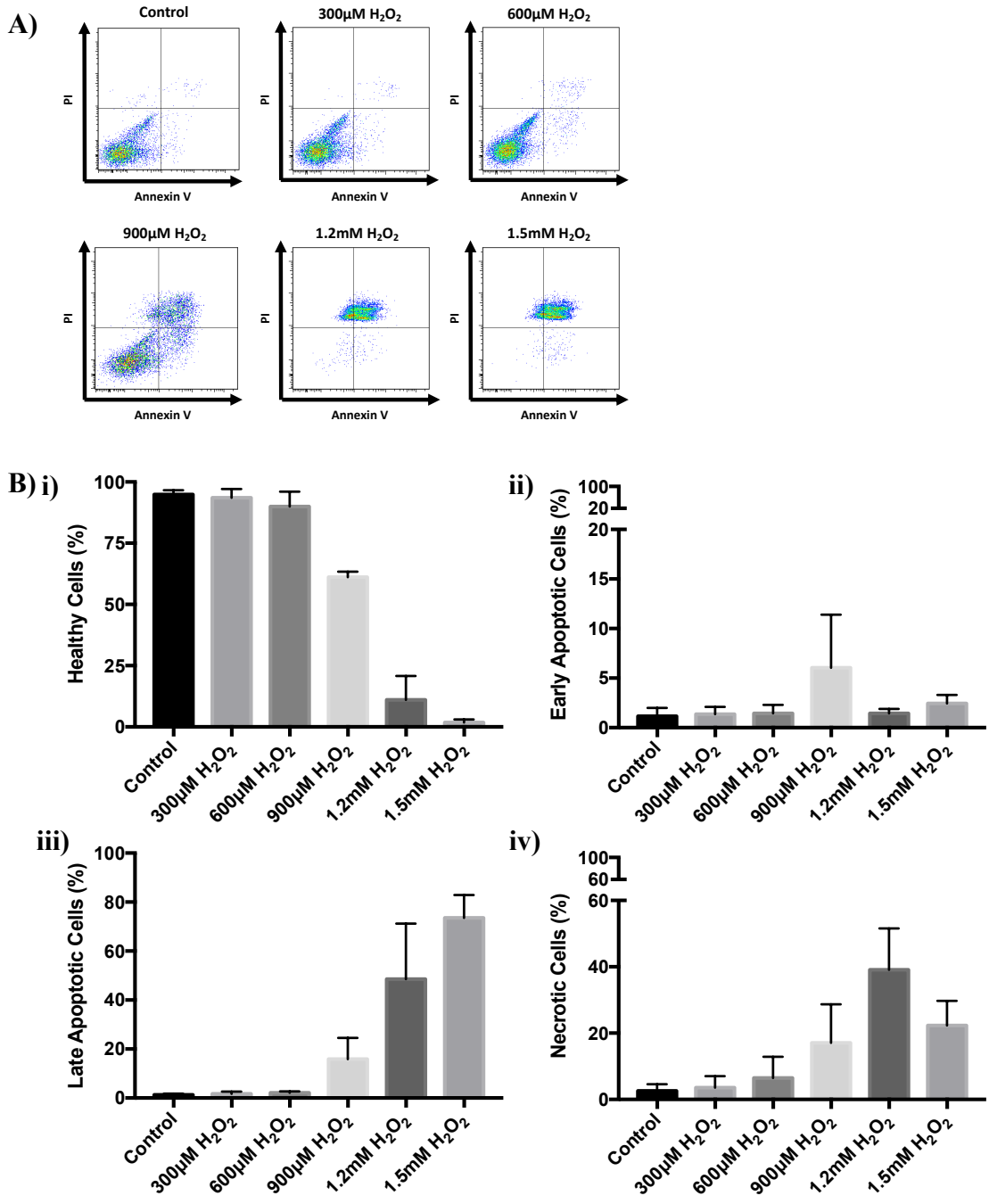


**Figure 3.4.4. Optimisation of flow cytometry using cardiac fibroblasts treated with hydrogen peroxide.** CFs were treated with $H_2O_2$ (300µM-1.5mM) in the presence of serum for 18 hours. Cell proliferation was then determined by propidium iodide (PI) and annexin V (AnxV) staining. (A) Representative flow cytometry dot plots with double Annexin V-FITC/PI staining (B) Histograms detailing the percentage of (i) healthy (ii) early apoptotic (iii) late apoptotic and (iv) necrotic cells following $H_2O_2$ treatment. Results are mean ± S.E.M (n=2).

Having optimised conditions for flow cytometry, CFs were treated with sunitinib or imatinib (0.1-10μM) and then stained with Annexin V and PI. Sunitinib treatment caused a reduction in the number of healthy CFs (Figure 3.4.5) with a concomitant increase in the number of early and late apoptotic cells at 3μM and 10μM treatments. There was also an increase in necrotic cells at 3μM sunitinib with evidence for significant necrosis at 10μM sunitinib (Figure 3.4.5). Imatinib treatment had no significant effect on CF viability (Figure 3.4.6). These finds are consistent with those obtained from MTT assays (Figure 3.4.2).

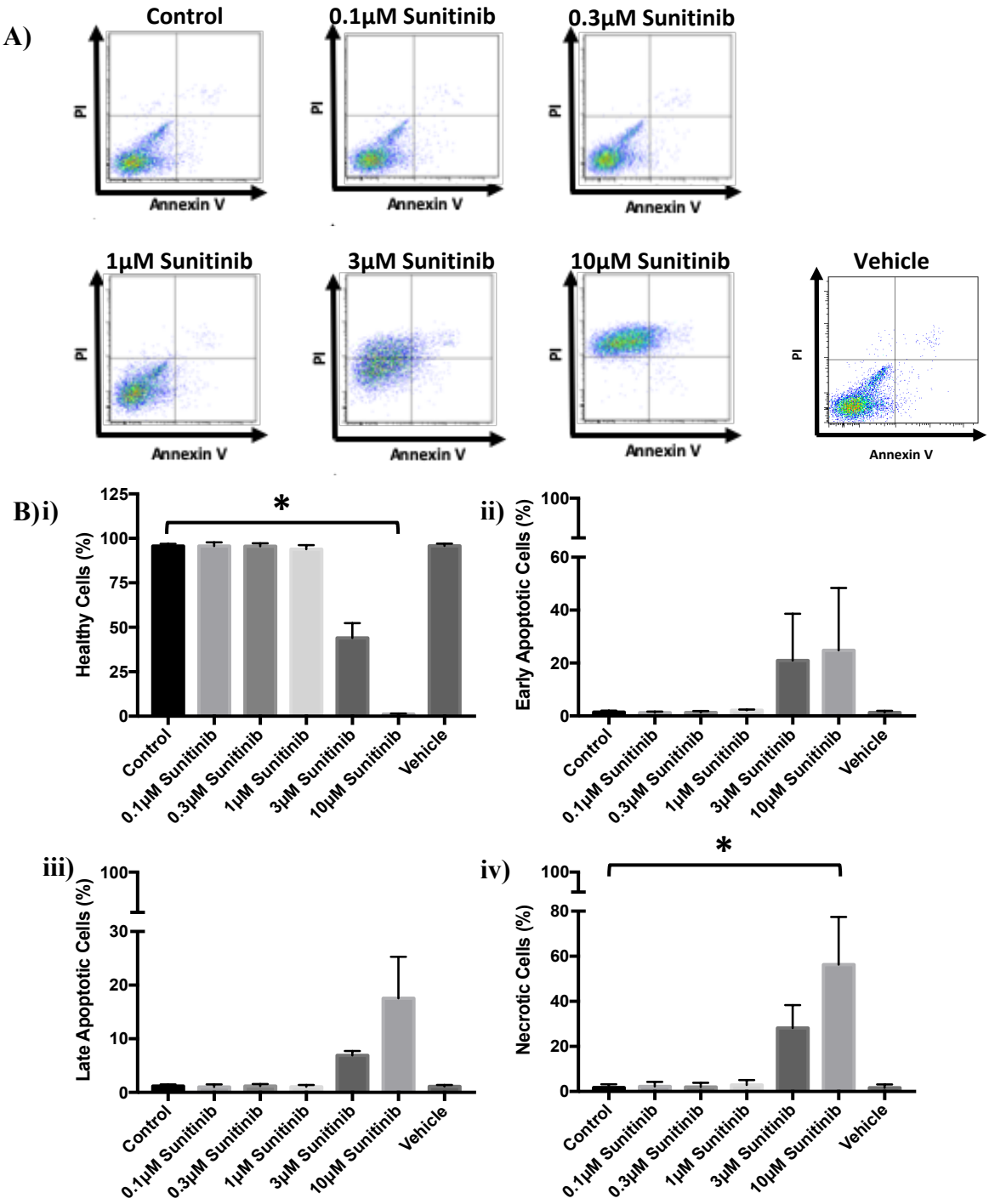


**Figure 3.4.5. Investigating the effect of sunitinib treatment on cardiac fibroblast cell death parameters.** CFs were treated with sunitinib (0.1-10µM) in the presence of serum for 18 h. Cell viability was determined by PI and AnV staining. (A) Representative flow cytometry dot plots with double Annexin V-APC/PI staining for cells treated with sunitinib. (B) Histograms detailing the percentage of (i) healthy (ii) early apoptotic (iii) late apoptotic and (iv) necrotic cells following sunitinib treatment. Results are expressed as mean ± S.E.M (n=3, *p<0.05).

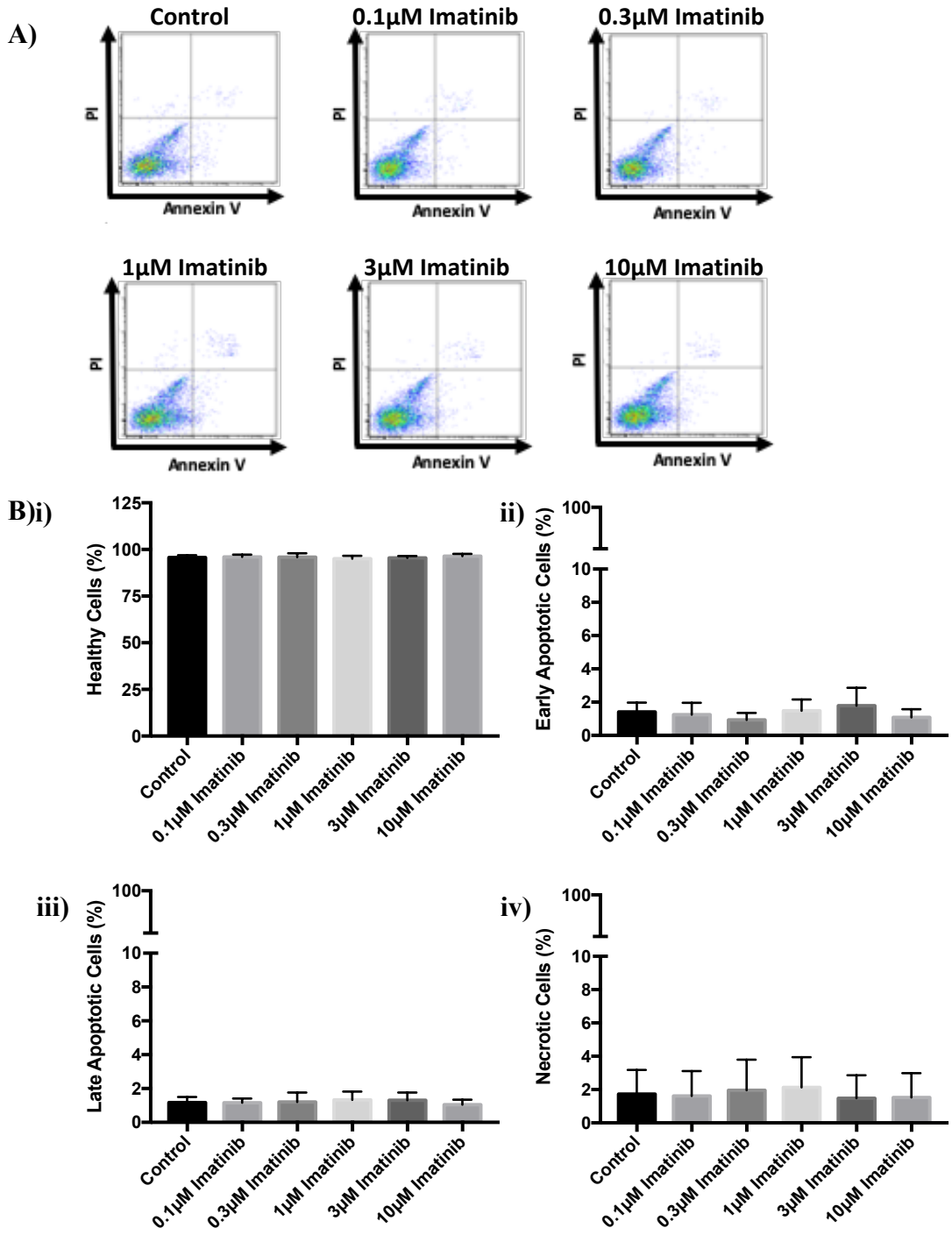


**Figure 3.4.6. Investigating the effect of sunitinib treatment on cardiac fibroblast cell death parameters.** CFs were treated with imatinib (0.1-10µM) in the presence of serum for 18 h. Cell viability was then determined by PI and AnV staining. (A) Representative flow cytometry dot plots with double Annexin V-APC/PI staining for cells treated with sunitinib. (B) Histograms detailing the percentage of (i) healthy (ii) early apoptotic (iii) late apoptotic and (iv) necrotic cells following imatinib treatment. Results are expressed as mean ± S.E.M (n=3).

*3.5 TKI treatment impacts upon myofibroblast phenotype*

Fibrotic remodelling is a well-known mediator of cardiovascular disease and its role in the aetiology of many cardiovascular disorders is well established (Hein *et al*., 2003; Puls *et al*., 2020). MFs promote fibrotic remodelling via the secretion of growth factors, pro-inflammatory mediators and factors that regulate the ECM, ultimately preserving cardiac function via structural remodelling to compensate for the damaged or diseased cardiac tissue. It is well documented in the literature that patients with pre-existing cardiac disease are more susceptible to TKI-induced cardiotoxicity (Ribiverio *et al*., 2008; Garcia-Alvarez *et al*., 2010). For example, in patients with imatinib-resistant, metastatic GIST, sunitinib was found to induce a cardiovascular event (congestive HF, myocardial infarction (MI) or cardiac death) in 75% of patients with cardiovascular risk factors in comparison to 7% in those without (Chu *et al*., 2007). Given that CF to MF differentiation can serve as an indicator of cardiac pathology, it is plausible that the effect of TKI treatment on MFs may be different to that observed in CFs. To assess this, MFs were treated with sunitinib or imatinib (10μM) and then subjected to brightfield imaging to determine any changes in cell phenotype.

Brightfield imaging revealed that sunitinib treatment induced a visible change in MF morphology and viability, causing visible cell loss (Figure 3.5.1). Surviving cells showed similar toxic characteristics as observed in CFs treated with sunitinib, with vacuole-like structures evident in the main cell body following treatment with 10μM sunitinib. In contrast, imatinib was notably less toxic than sunitinib treatment, consistent with what was seen in TKI-treated CFs (Figure 3.3.2). Imatinib treatment did, however, cause the membrane of the MFs to appear serrated (Figure 3.5.1). The cell membrane of untreated and vehicle treated MFs were not serrated. In contrast, 10μM imatinib treatment did not have any discernible effect on CF phenotype (Figure 3.3.2), suggesting that MFs may be more susceptible to TKI-induced toxicity than CFs (Figure 3.5.1).

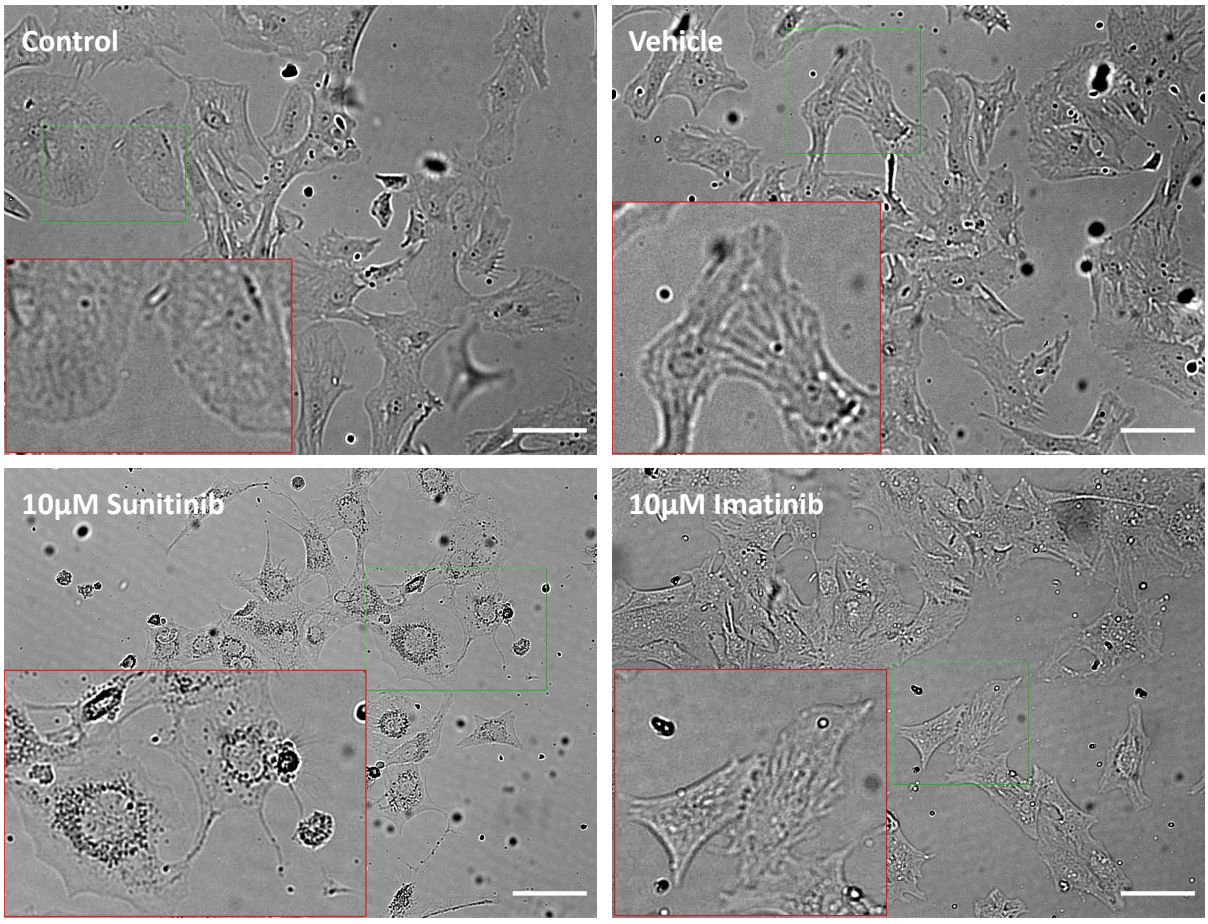


**Figure 3.5.1. Determining the effect of TKI treatment on myofibroblast phenotype.** MFs (P5) were cultured in CF growth medium until 70% confluent. MFs were then treated with sunitinib or imatinib (10µM) in the presence of serum for 18 hours. Images obtained using a Nikon Eclipse (TE300) inverted microscope (x10 magnification). Scale bar 100µm (n=1).

Immunofluorescence of MFs showed a positive stain for SMCa, vimentin and vWF (Figure 3.5.2). The images suggest that TKI treatment may increase SMCa expression, though marker expression was lost at 10μM sunitinib. Expression of vimentin and vWF was also lost at 10μM sunitinib, indicative of cell death. This is consistent with the visible cell loss seen at 10μM sunitinib in Figure 3.5.1, supporting the theory that MFs may be more susceptible to TKI-induced toxicity than CFs. Vimentin and vWF stains did not appear to be affected by sunitinib or imatinib treatment (Figure 3.5.2).

The results presented here suggest that TKI treatment does affect MFs and warrants further investigation. However, the effect of sunitinib or imatinib on MFs was out-with the scope of this investigation. These preliminary findings support the theory that MFs may be more susceptible to TKI-induced toxicity than CFs and this merits follow-up in a future project. It is also worth highlighting that many studies do not discriminate between CFs and MFs (Ma *et al*., 2012; Thottakara *et al*., 2020) which, as these preliminary findings suggest, can influence the outcome of the study as the cell types behave quite differently. The work concerning the effect of TKIs on MFs presented thus far was supplemental and for that reason was not evaluated beyond this point.

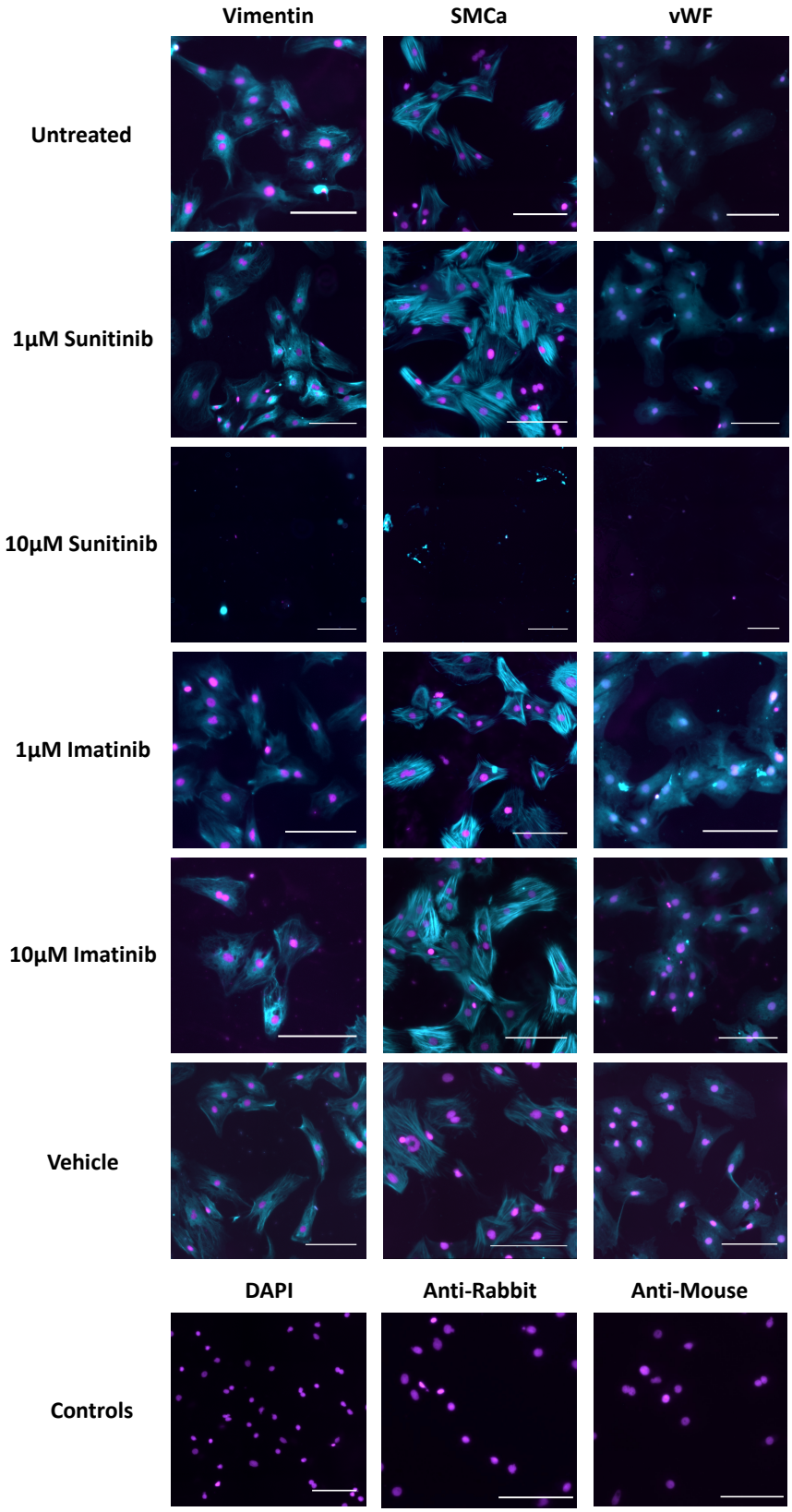


**Figure 3.5.2. Determining the effect of TKI treatment on myofibroblast marker expression via immunofluorescence.** MFs (P5-P6) were treated with sunitinib or imatinib (1-10µM) and then stained with vimentin, SMCa and vWF to determine any changes in marker expression. Cells treated with DAPI alone and secondary antibodies alone were used as negative controls. Scale bar 100µm (n=2).

*3.6 TKI treatment impacts upon progenitor cardiac myocyte morphology*

Cardiac function is facilitated by the dynamic interaction of the contractile and non-contractile cells that comprise the heart, allowing for proper form and function (Souders *et al*., 2009). CMs are the contractile cells of the heart and are responsible for the coordinated contractions that supply the body with oxygenated and nutrient rich blood. A Previous study conducted in mice showed that TKI treatment can cause CM cell death, resulting in left-ventricular contractile dysfunction (Kerkela *et al*., 2009). The same study also reported significant left ventricular dysfunction in patients receiving imatinib therapy. TKI-induced CM toxicity has been reported by others (Chu *et al*., 2007; Kerkela *et al*., 2009; Barr *et al*., 2014) but the mechanism by which this occurs is not yet clear. This is due, in part, to the differences between experimental models and the human heart.

Cardiovascular research is heavily reliant upon animal derived neonatal CMs, PCMs or iPSCs (Guo *et al*., 2018). However, owing to the discrepancies in functional characteristics between these cell types and the adult, human heart, both are limited in terms of the translation of data obtained. Alternatively, primary AVMs can be isolated via bulk collagenase or Langendorff methods, but these too are restricted by the low yield of CMs and the limited time they can be maintained in culture (Mitcheson *et al*., 1998). Freshly isolated adult CMs are typically contractile, rod-shaped cells (Figure 3.6.1A). Although progress has been made in extending the period that adult CMs can be maintained in culture via methods such as maintaining the cells at low temperature (4°C) and inhibiting myosin II ATPase (Abi-Gerges *et al*., 2013), such techniques interfere with normal cellular processes and call into question the validity of results obtained by those methods. Taking these considerations into account, it is imperative to carefully assess the benefits and restrictions of using either (i) NRVMs or PCMs, (ii) iPSCs or (iii) AVMs in cardiovascular research. The

strengths and limitations afforded by each cell type must be balanced with the research questions and experimental applications required.

This study has opted to use human derived PCMs rather than isolated adult CMs. PCMs are ventricular derived, progenitor-like cells and are not fully differentiated. They are highly proliferative and express cardiac markers of early-stage differentiation such as sarcomeric alpha-actin, but it is not known if these cells express markers of adult CMs such as the $Ca^{2+}$ handling proteins RyR2 and PLB. Before assessing the effect of TKI treatment on PCMs, the phenotype of the healthy PCMs in culture must first be established. For reference, the phenotype of healthy, adult CMs isolated from rats was also established to allow comparison between the two cell types.

The morphology of PCMs is quite different to that of adult rod-shaped CMs (Figure 3.6.1). The PCMs are somewhat similar in phenotype to that of CFs, spindle shaped with multiple projections originating from the main cell body (Figure 3.6.1B). The cells are however larger than that of CFs. Although these cells have a different morphology to that of freshly isolated CMs, these cells can be maintained in culture and are suitable for long-term treatments (Srivastava *et al*., 2016). Pertinent to the current study, PCMs have been successfully used to investigate the cardiotoxic properties of anti-cancer agents (Seemann *et al*., 2013).

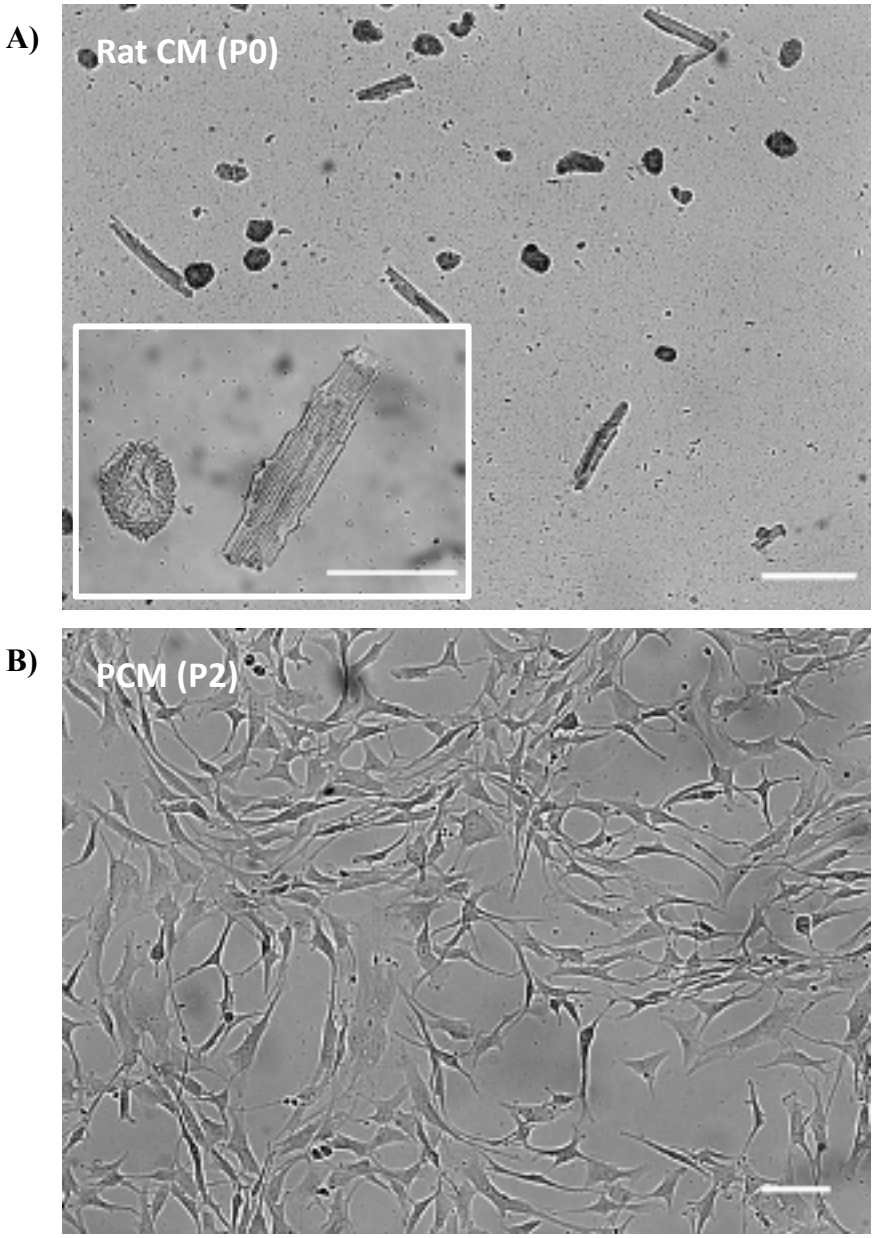


**Figure 3.6.1. Phenotypic characterization of progenitor cardiac myocyte and adult rat cardiac myocyte in culture.** CMs were isolated from adult Sprague-Dawley rats using the Langendorff perfusion method to allow for comparison of the phenotype of adult CMs and PCMs. (A) P0 adult rat CMs. (B) P2 PCMs. Images obtained using a Nikon Eclipse (TE300) inverted microscope (x10 magnification). Scale bar 100μm (n=3).

Following phenotypic assessment of healthy PCMs in culture, further characterisation was performed to assess specific protein marker expression in these cells. Given that PCMs are not fully differentiated, expression of mature CMs proteins, RyR and PLB (two $Ca^{2+}$ handling proteins that are central to cardiac contraction in adult CMs (Bers, 2002)), was also examined.

Immunohistological staining showed a strong positive stain for sarcomeric α-actinin and vimentin in CMs in culture, as suggested by the manufacturer (Figure 3.6.2A). Consistent with the undifferentiated, progenitor-like status of these cells, PCMs did not express RyR2, though a very faint PLB signal was seen. Protein expression was confirmed with immunoblotting (Figure 3.6.2B). Immunoblotting showed a strong signal for both sarcomeric α-actinin and vimentin. No signal was found for RyR2 or PLB in untreated PCM lysates. Figure 3.6.2C shows comparative signals for RyR2 and PLB in fully differentiated, adult rat CMs and CFs. Although a very faint signal for RyR2 and PLB was observed in Figure 3.6.2A, immunoblotting did not corroborate these findings. Regardless, Figure 3.6.2C shows that any apparent signal for mature $Ca^{2+}$ handling proteins in PCMs is negligible in comparison to adult CMs.

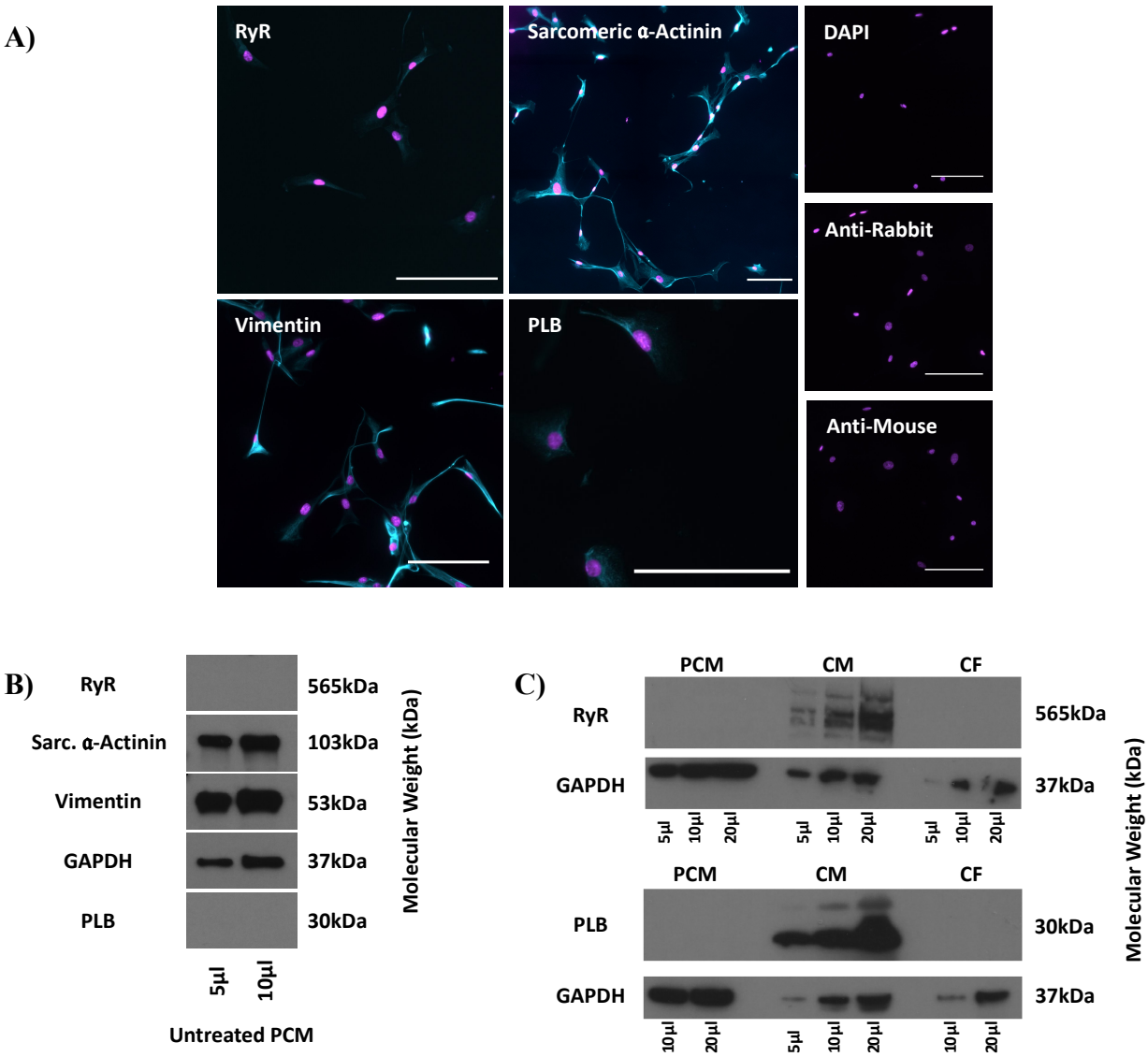


**Figure 3.6.2. Assessment of progenitor cardiac myocyte marker expression.** (A) PCM marker expression was confirmed via immunofluorescence by staining for sarcomeric α-actinin and vimentin, as recommended by the supplier. Cells treated with DAPI alone and secondary antibodies alone were used as negative controls. (B) Confirmation of CF marker expression via immunoblotting (n=3). (C) Comparison of the expression of $Ca^{2+}$ handling proteins across untreated cardiac cell lysates (n=1). Scale bar 100µm. Images are from one experiment, representative of two others. This figure was prepared in part by Dr Sandy MacMillan (University of Strathclyde).

Having established the phenotype and marker expression of healthy PCMs in culture, the effect of TKI-treatment on PCM phenotype was then evaluated. Changes in PCM phenotype were apparent at 3μM sunitinib and continued in a concentration dependent manner (Figure 3.6.3). At 3μM and 10μM sunitinib, cells can be seen to lose the spindle shaped morphology and appear larger, transparent and rounded. PCMs were also found to have serrated edges following sunitinib treatment at 3μM and 10μM sunitinib (highlighted Figure 3.6.3). Similar to effects on CFs, imatinib treatment was found to be less potent than sunitinib treatment in PCMs. Serrated edges were also seen in PCMs treated with 10μM imatinib, though the effect was more subtle than that seen following sunitinib treatment. These observations are somewhat consistent with TKI treated CFs (Figure 3.3.2); with sunitinib treatment appearing to induce more potent effects than imatinib treatment. However, it would appear that PCMs are less sensitive to TKI treatment than CFs, with no visible cell loss at any of the concentrations tested with sunitinib or imatinib (Figure 3.6.3).

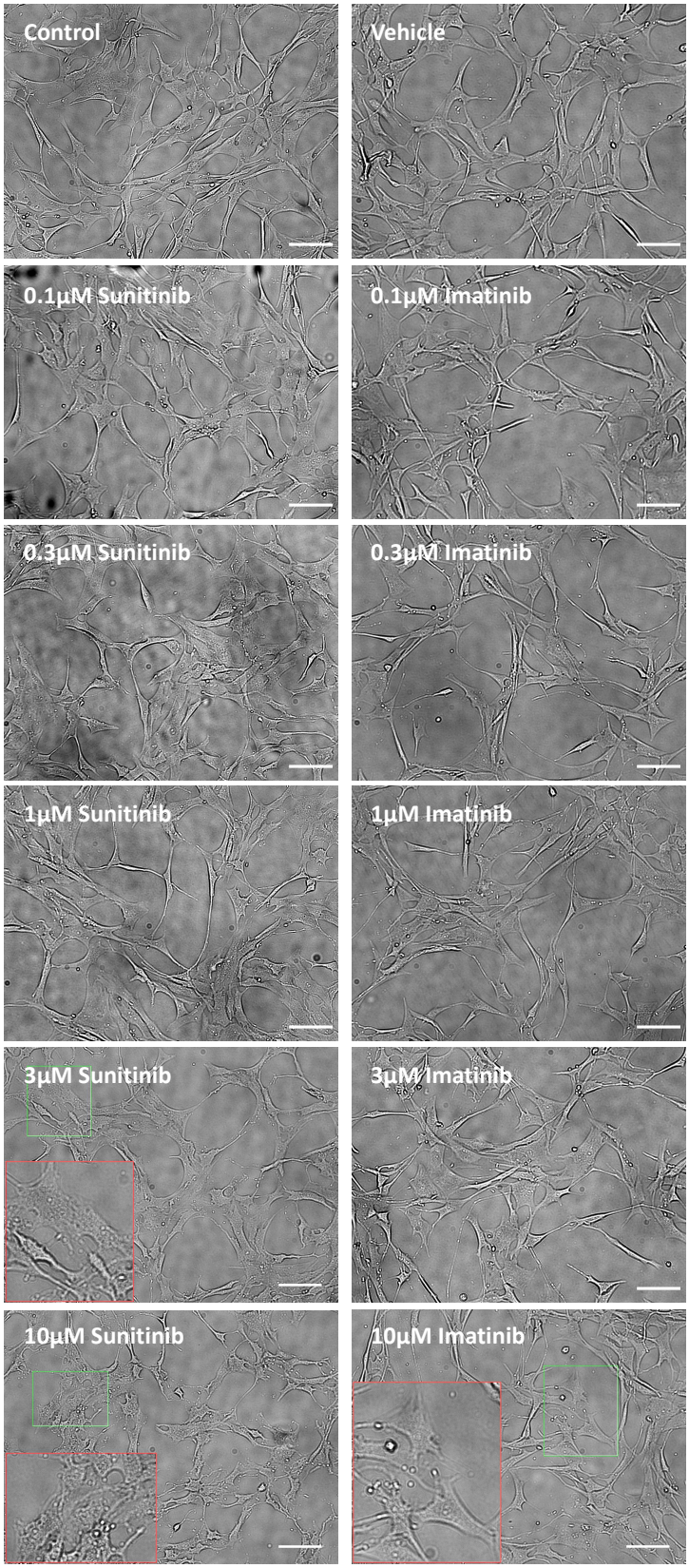


**Figure 3.6.3. Investigating the effect of TKI treatment on progenitor cardiac myocyte phenotype in the presence of serum.** PCMs were cultured until 70% confluent and then treated with sunitinib or imatinib (0.1-10µM) in the presence of serum for 18 hours. Images obtained using a Nikon Eclipse (TE300) inverted microscope (x10 magnification). Scale bar 100µm (n=3).

Having established that TKI treatment induced changes in PCM morphology, it was then assessed whether these changes coincided with changes in cell marker expression. PCMs were treated with sunitinib or imatinib (0.1-10μM) and then stained with sarcomeric alpha-actinin and vimentin. immunofluorescence suggested that both sunitinib and imatinib treatment may increase sarcomeric α-actinin expression in PCMs (Figure 3.6.4). No visible change in vimentin expression was evident following sunitinib or imatinib treatment.

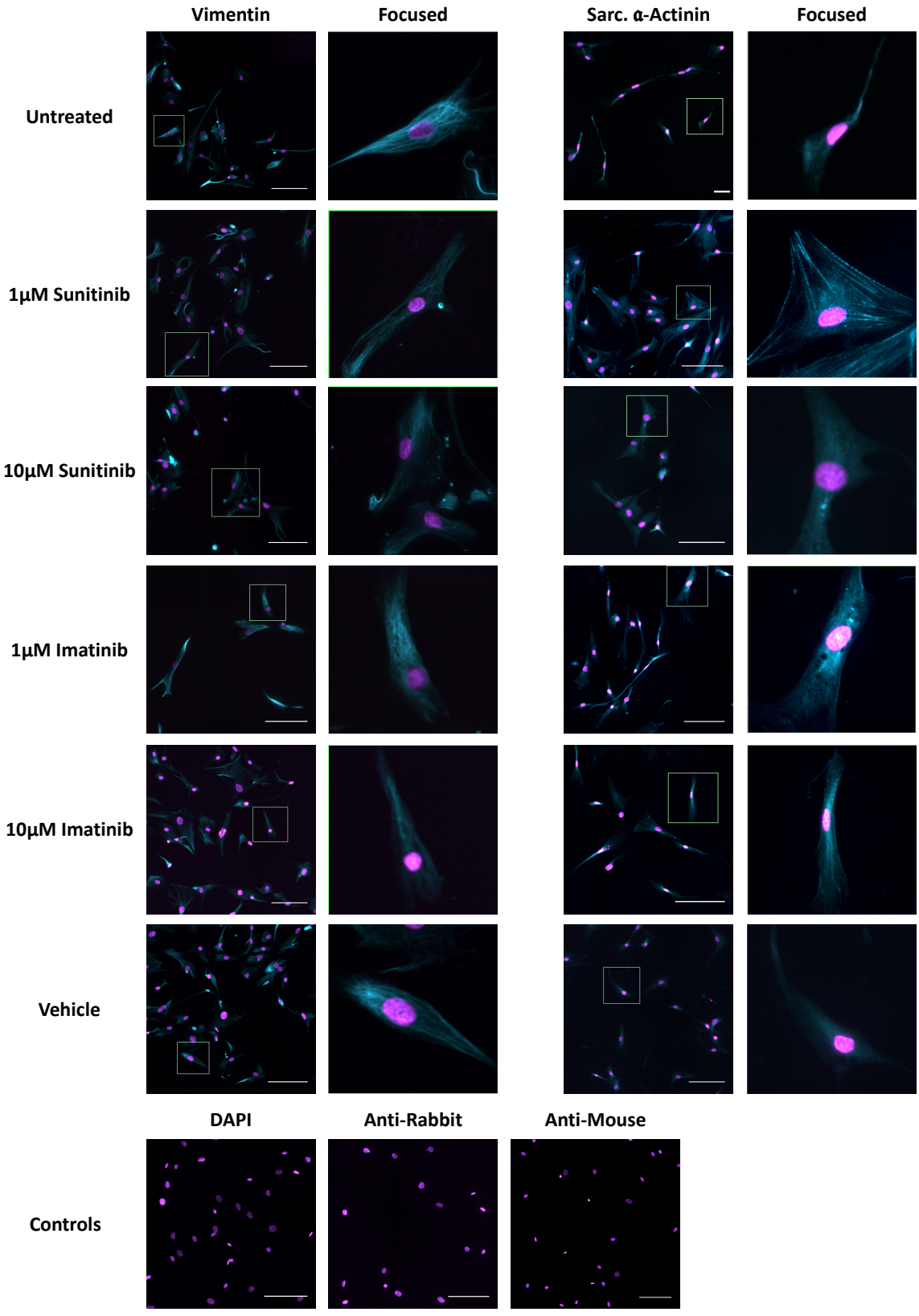


**Figure 3.6.4. Evaluating the effect of TKI treatment on progenitor cardiac myocyte marker expression via immunofluorescence.** PCMs (P3-P4) were treated with sunitinib or imatinib (1-10μM) and then stained with sarcomeric α-actinin and vimentin to determine any changes in marker expression. Cells treated with DAPI alone and secondary antibodies alone were used as negative controls. Scale bar 100μm (n=2).

From immunofluorescence alone, it was difficult to ascertain whether TKI treatments caused any changes in PCM marker expression (Figure 3.6.4). In order to assess whether there were any measurable changes in marker expression, quantitative immunoblotting was performed for both sarcomeric α-actinin and vimentin expression in PCMs treated with sunitinib or imatinib (1&10μM). Immunoblotting revealed that neither sunitinib nor imatinib had any significant effect on PCM marker expression (Figure 3.6.5). The apparent increase in sarcomeric α-actinin expression (Figure 3.6.4) was not statistically significant (Figure 3.6.5) and, similar to what was seen in CFs (Figures 3.3.3 and 3.3.4), it would appear that the apparent changes in cell phenotype induced by TKI treatment were not significant enough to alter cell marker expression.

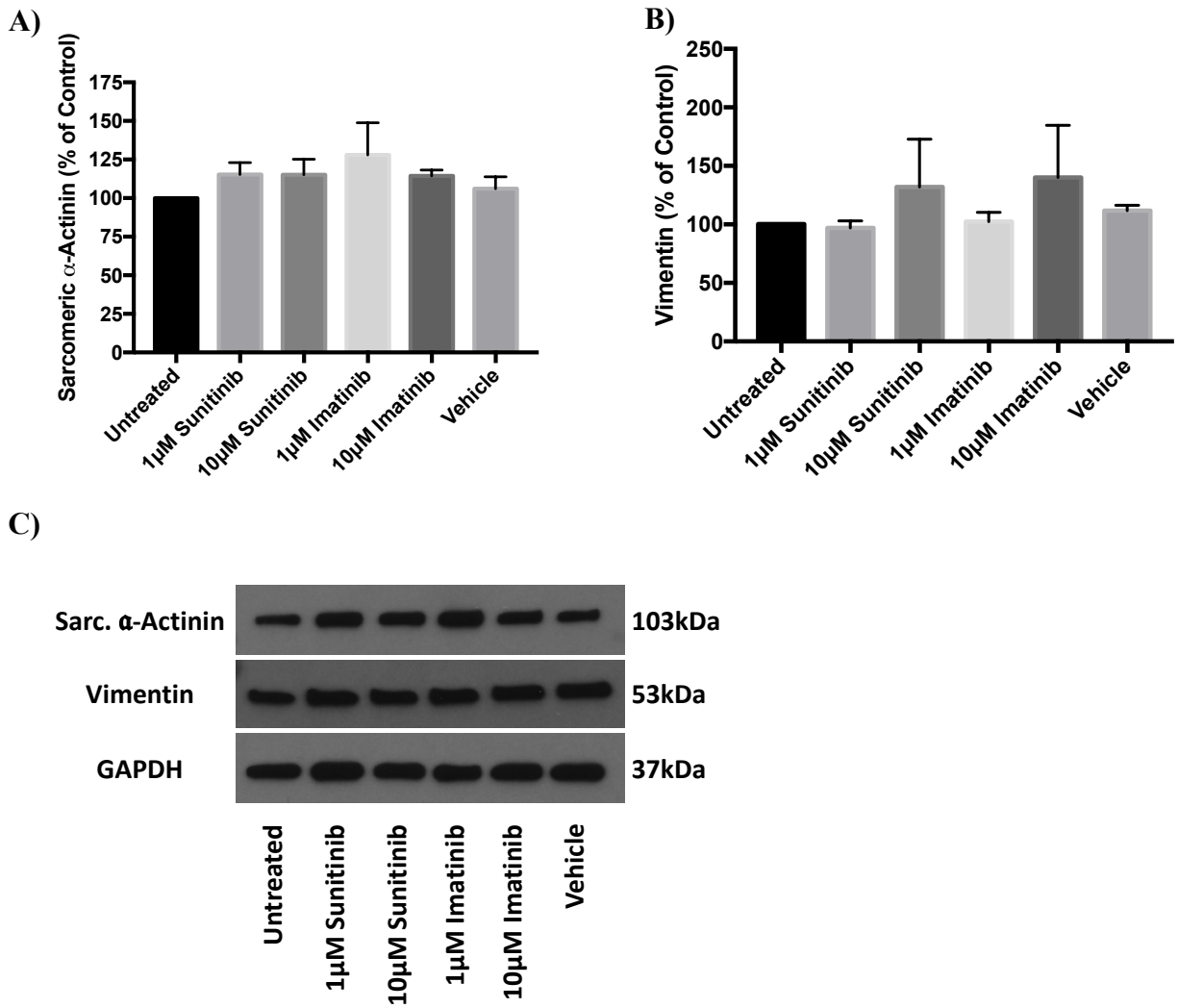


**Figure 3.6.5. Determining the effect of TKI treatment on progenitor cardiac myocyte marker expression via western blot.** Following the indicated treatments with either sunitinib or imatinib, sarcomeric α-actinin and vimentin expression was determined via quantitative immunoblotting (A) sarcomeric α-actinin expression. (B) Vimentin expression. All samples normalised to GAPDH expression. (C) Representative immunoblot showing PCM marker expression following TKI treatment. Results are expressed as mean ± S.E.M and are normalised to control (n=3).

*3.7 TKI treatment causes progenitor cardiac myocyte cell death*

TKIs are known to induce CM cell death. Kerkela (2006) showed that imatinib treatment induced necrosis and, to a lesser extent, apoptosis in NRVMs, with evidence implicating mitochondrial dysfunction as a possible mediator of cell death. Similarly, Chu (2007) found that sunitinib treatment increased apoptosis in NRVM. The study by Chu *et al*. also provided evidence of mitochondrial mediated cell death, with increased caspase-9 activation and cytochrome c release, indicative of activation of the intrinsic mitochondrial apoptotic pathway. PCMs have been used previously to investigate the toxicity of radiation therapy and anthracycline treatment (Seemann *et al*., 2013). However, the effect of TKI treatment on this cell type has not yet been reported. Having determined that TKI treatment affects PCM phenotype, MTT assays were then conducted to assess whether the change in phenotype impacted PCM viability.

MTT assays revealed that sunitinib, but not imatinib, reduced PCM viability (Figure 3.7.1). PCM viability was significantly reduced at 1μM (91.2±0.9%), 3μM (90.0±0.5%) and 10μM (83.2±0.9%) sunitinib vs untreated control. These findings are consistent with the sunitinib induced changes in cell phenotype observed in Figure 3.6.3. It should be noted that at comparable concentrations, sunitinib treatment induced a greater reduction in cell viability in CFs (Figure 3.4.2) than in PCMs (Figure 3.7.1).

.

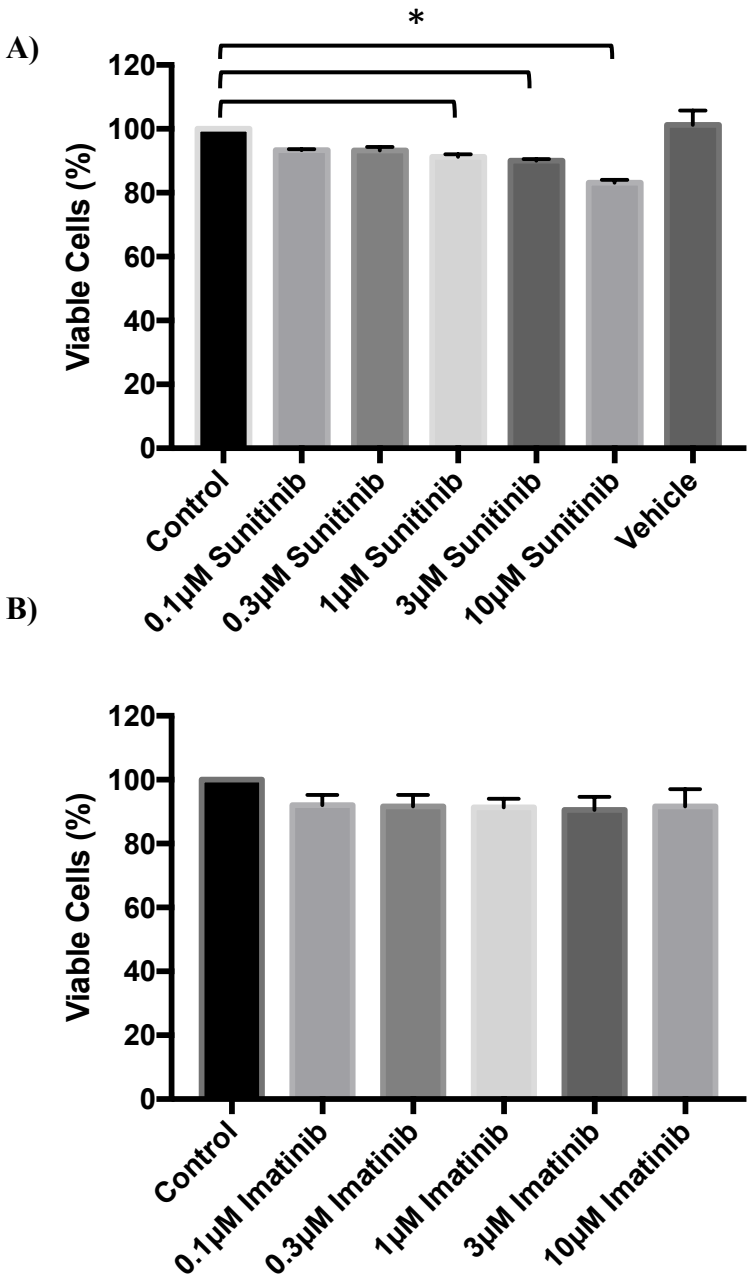


**Figure 3.7.1. Investigating the effect of sunitinib or imatinib treatment on progenitor cardiac myocyte viability.** PCMs were treated with sunitinib or imatinib (0.1-10μM) in the presence of serum for 18 h. Cell proliferation was assessed via MTT assays. (A) sunitinib treated PCMs (B) imatinib treated PCMs. Results are expressed as mean ± S.E.M and are normalised to control (n=3, *p<0.05).

Having established that sunitinib treatment is toxic to PCMs, the mode of sunitinib-induced cell death was investigated further. The mechanism of cell death is dependent on several underlying factors such as the cell type and the selectivity and concentration of the drug used (Fulda and Debatin, 2006). The literature has also shown that the mode of cell death can be influenced by underlying health conditions and risk factors (Chu *et al*., 2007). Given that the mode of cell death associated with cell death in healthy PCMs is not yet known, and in order to corroborate the findings of the MTT assays, PCMs were treated with sunitinib or imatinib (0.1-10μM) and then stained with Annexin V and PI, before being subjected to flow cytometry analysis.

Sunitinib treatment caused a reduction in the number of healthy cells (Figure 3.7.2) from 1μM, with cell number reducing in a concentration dependent manner. The findings presented in Figure 3.7.2 show that both the apoptotic and necrotic cell death pathways are activated following sunitinib treatment. It is also clear that the necrotic pathway is the prominent mechanism of cell death in PCMs treated with sunitinib. The number of necrotic cells significantly increased from 0.3μM sunitinib upwards in a largely concentration dependent manner (Figure 3.7.2). The number of late apoptotic cells was also significantly increased at 10μM sunitinib. Imatinib treatment had no significant effect on PCMs at any of the concentrations tested (Figure 3.7.3), consistent with the findings presented in Figure 3.7.1.

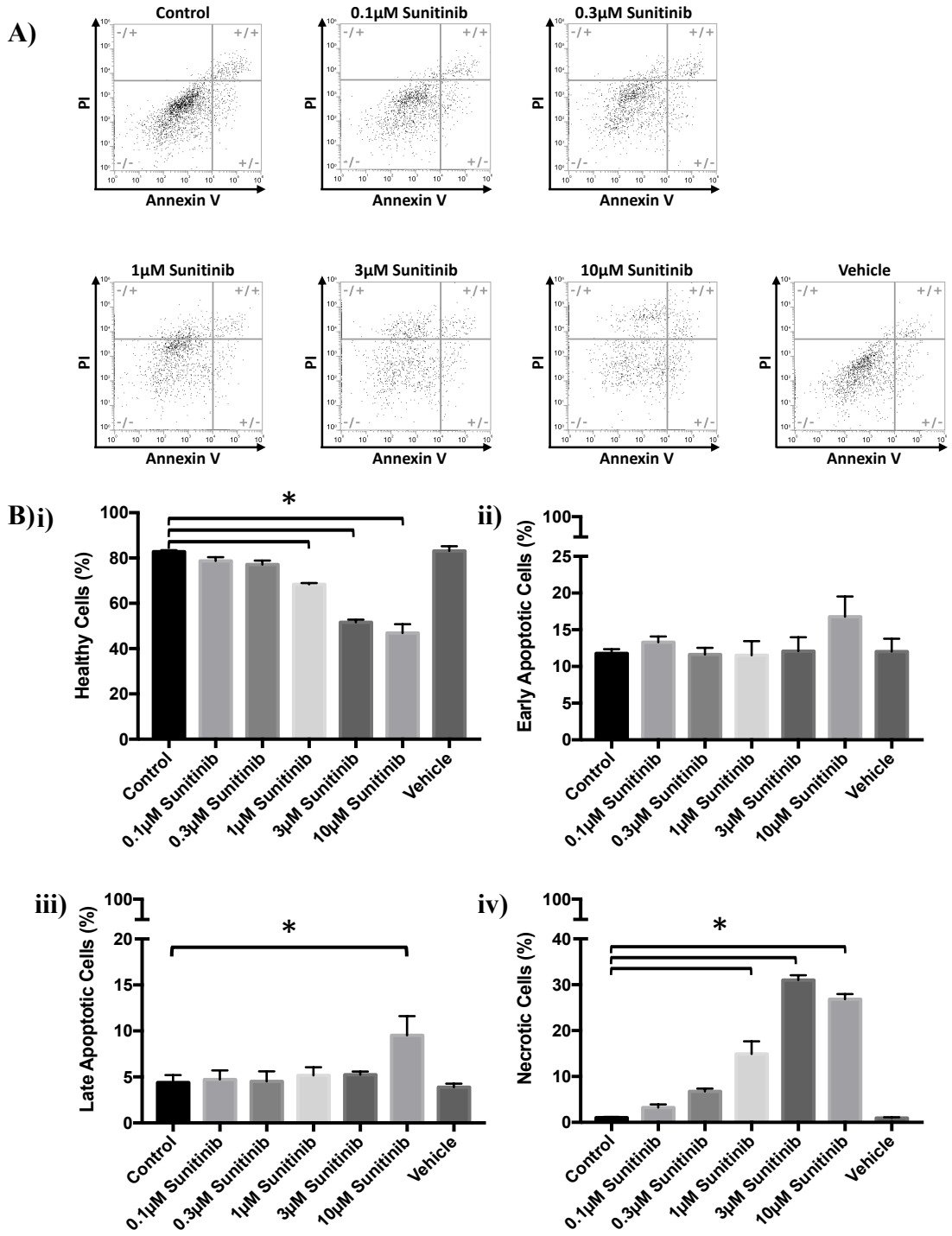


**Figure 3.7.2. Investigating the effect of sunitinib treatment on progenitor cardiac myocyte cell death parameters.** PCMs were treated with sunitinib (0.1-10µM) in the presence of serum for 18 h. Cell viability was determined by PI and AnV staining. (A) Representative flow cytometry dot plots with double Annexin V-APC/PI staining for cells treated with sunitinib. (B) Histograms detailing the percentage of (i) healthy (ii) early apoptotic (iii) late apoptotic and (iv) necrotic cells following sunitinib treatment. Results are expressed as mean ± S.E.M (n=3, *p<0.05).

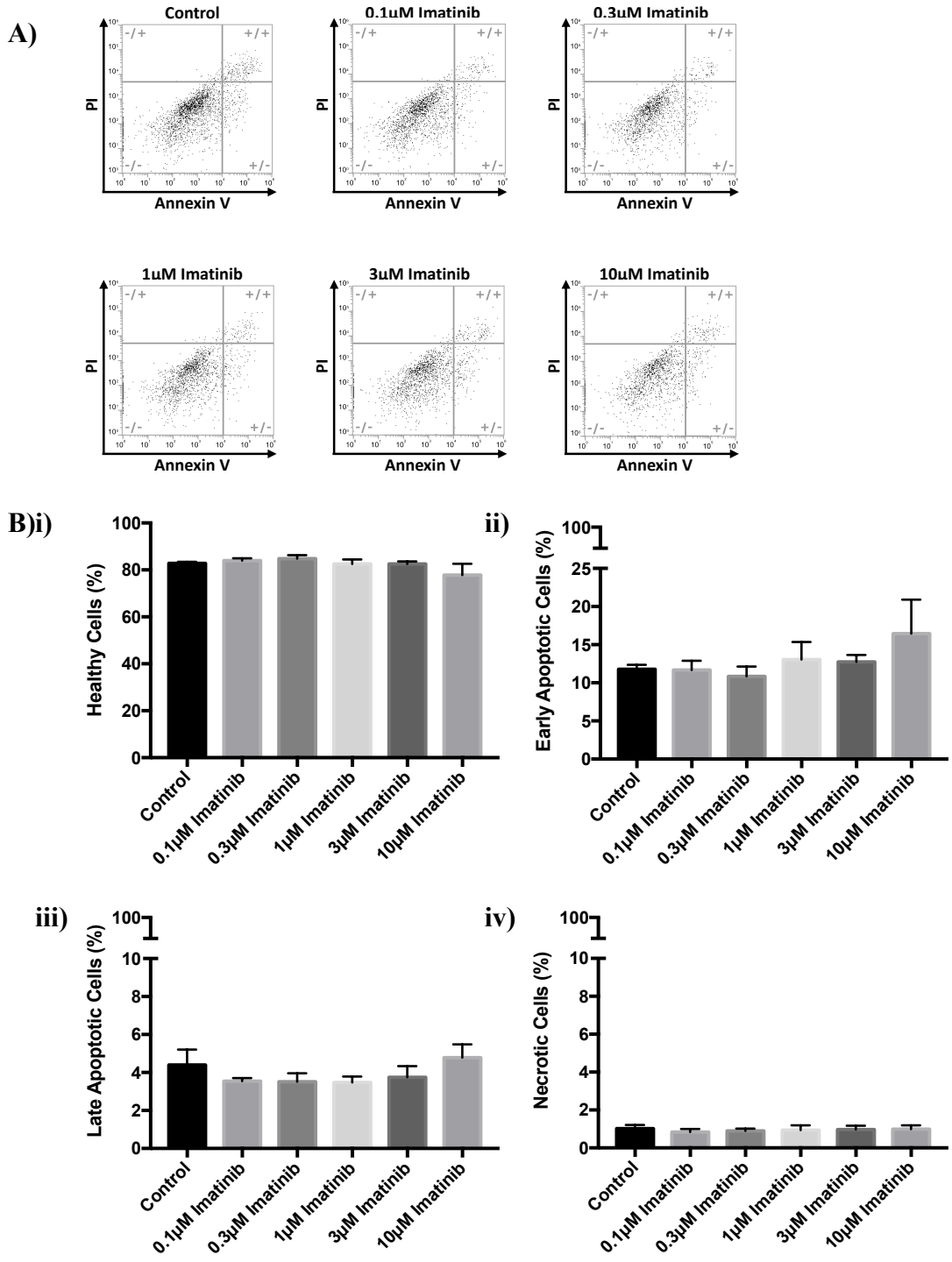


**Figure 3.7.3. Investigating the effect of imatinib treatment on progenitor cardiac myocyte cell death parameters.** PCMs were treated with imatinib (0.1-10μM) in the presence of serum for 18 hours. Cell viability was then determined by PI and AnV staining. (A) Representative flow cytometry dot plots with double Annexin V-APC/PI staining for cells treated with sunitinib. (B) Histograms detailing the percentage of (i) healthy (ii) early apoptotic (iii) late apoptotic and (iv) necrotic cells following imatinib treatment. Results are expressed as mean ± S.E.M (n=3).

*3.8 Discussion*

The aim of this chapter was to determine whether sunitinib or imatinib treatment had any effect on the contractile and non-contractile cells of the heart. The cardiotoxic mechanism of these drugs is still poorly understood and research concerning the wider ranging effects of these TKIs, specifically their effect on cardiac non-myocytes, is lacking. The results presented in this chapter evaluate the effect of TKI treatment on the phenotype and viability of CFs, the most abundant non-contractile cell in the heart. This study is also believed to be the first to compare the effects of sunitinib or imatinib treatment on CFs and PCMs.

Initial experiments were performed to characterise the phenotype and marker expression of healthy, untreated cardiac cells. Immunohistological staining of isolated CFs showed a strong positive stain for vimentin (Figure 3.2.3). Vimentin is the accepted cell marker for CFs, though it is expressed by other cell types (Doppler *et al*., 2017). Previous studies have also used the expression of secreted factors, such as periostin, to differentiate between CFs and the activated form of the cell type, MFs (Furtado *et al*., 2014; Ivey and Tallquist, 2016; Kaur *et al*., 2016). However, the fact these proteins are secreted in response to CF activation can make them difficult to identify and quantify and the results subjective. In the absence of a selective marker for CFs, the exclusion of smooth muscle and endothelial cell markers in addition to a positive vimentin stain is required for CF characterisation, and CFs and MFs can be differentiated by the increased expression of SMCa that accompanies CF to MF transition (Humeres and Frangogiannis, 2019). In the current study, a positive stain for both SMCa and vWF was observed in CFs (Figure 3.2.3). However, it should be noted that staining for SMCa was significantly less than that obtained in the positive controls for SMCs and vWF staining was of a very different pattern than that seen in the positive controls for HUVECs (Figure 3.2.3). Staining of vWF and SMCa in CFs was also less than that obtained in the phenotypically transformed MFs. Low expression of non-CF cell markers

has been reported previously. CFs isolated from mice displayed an enlarged, outstretched phenotype when cultured on plates (Shinde *et al*., 2017). These cells also expressed SMCa, displayed increased collagen mRNA and MMP and TIMP genes that are associated with ECM remodelling. In comparison, mouse CFs cultured on low-tension collagen pads displayed an elongated spindle-shaped phenotype that is classically associated with CFs. These cells also expressed SMCa, collagen mRNA and MMP and TIMP genes, though these were notably reduced in comparison to CF cultured on plates. The study concluded that the high-tension environment of culturing on plasticware increased SMCa incorporation into the cytoskeletal stress fibres. However, the study does not offer a direct comparison between CFs and MFs. Although these findings indicate possible CF to MF differentiation induced via the culture conditions, the extent of CF differentiation cannot be determined. The study does, however, go on to examine CFs cultured in both high-tension and low-tension conditions following stimulation with the pro-inflammatory cytokine TGF-β1. TGF-β1 is known to be upregulated in fibrotic remodelling and is thought to be a central mediator in CF to MF differentiation (Villarreal and Dillmann, 1992; Squires *et al*., 2005, Khalil *et al*., 2017; Nagaraju *et al*., 2019). TGF-β1 stimulation was observed to further increase SMCa expression and collagen mRNA synthesis – consistent with CF to MF differentiation (Shinde *et al*., 2017). These observations are largely consistent with the findings of this study. Findings presented here suggest that although culture conditions may have some effect on CF phenotype and marker expression, the phenotype and marker expression of MF is markedly different to that of CF in culture.

Anti-cancer treatment induced changes in cell marker expression have been reported previously. Seeman (2013) reported an increase in vWF expression in cardiac sections of irradiated mice hearts. The study determined that the increase in vWF expression indicated radiation-induced microvasculature damage. The investigation found that irradiation did not, however, cause cardiac fibrosis, a common manifestation of radiation-induced cardiotoxicity (Jaworski *et al*., 2013). vWF has a pro-thrombotic function, binding to both collagen and the

platelet receptor to mediate platelet adherence to the damaged vasculature (Ruggeri, 2007). Increased thrombosis is also recognised as an off-target effect of several cancer therapies, including TKIs and radiation (Zamorano *et al*., 2016). Changes in vascular function are also thought to contribute to cardiac fibrosis (Jaworski *et al*., 2013). Though the increase in vWF expression seen in the current study following TKI-treatment of CFs was not significant (Figures 3.3.3 and 3.3.4), it is important to recognise that these experiments are examining isolated cells. When considered alongside the findings of Seeman (2013), it is possible that an increase in the expression of vWF may serve as an early indicator of anti-cancer treatment induced cardiotoxicity, before the onset of cardiac fibrosis.

It is well established that culture conditions have a significant impact on cell viability (Larsson *et al*., 2020). Serum has been shown to exert a protective effect on cells in culture, with Lordan and Higginbotham (2012) showing that serum protected human myeloid leukemia cells from nanomaterial cytotoxicity. In contrast, White (2020) reported that serum starvation had a positive effect on prostate cancer cells, activating a survival mechanism to anti-tumour drugs. The results shown in Figures 3.3.1 and 3.3.2 highlight two observations, firstly, that serum starvation has a marked effect on cell health; and secondly, sunitinib is more toxic than imatinib regardless of whether serum is present or not. Serum starvation is commonly used in cell signalling research. It allows researchers to synchronise the cell cycle phase, achieving basal cellular activity to evaluate any effect an agonist of interest has on an isolated pathway (Pirkmajer and Chibalin, 2011). However, serum starvation does so at the expense of physiological relevance and can change the experimental outcome entirely (Whorwood *et al*., 2001; Levin *et al*., 2010; Pirkmajer and Chibalin, 2011). On its own, serum starvation has also been shown to induce phenotype differentiation and apoptosis (Pirkmajer and Chibalin, 2011; Huang *et al*., 2018). Huang reported that, over time, serum starvation significantly increased the percentage of early and late apoptotic cells and these changes coincided with cell cycle arrest, reduced cell proliferation and changes in cell phenotype. There is evidence suggesting that this toxicity may be mediated by a reduction in the ratio of

the anti-apoptotic Bcl-2 to the pro-apoptotic Bax (Braun *et al*., 2011; Huang *et al*., 2018). These findings are consistent with the results obtained in this study and account for the increased susceptibility of CF to TKI-treatment seen in the absence of serum in Figure 3.3.1.

In agreement with the findings presented in this chapter, several other publications have also shown that the Type I TKI sunitinib is more toxic than the Type II TKI imatinib (Will *et al*., 2008; Zamorano *et al*., 2016; Burke *et al*., 2019). The increased susceptibility to sunitinib treatment in comparison to imatinib is not limited to CFs and is also seen in TKI-treated MFs and PCMs. Burke and colleagues (2019) also found sunitinib to be more toxic towards CFs than imatinib. The study found that sunitinib treatment affected CF phenotype and both sunitinib and imatinib significantly reduced CF viability at 3μM and 10μM respectively. These results are largely consistent with the findings of this study. In the presence of serum, both this investigation and that of Burke (2019) found that sunitinib induced toxicity at 3μM, continuing in a concentration dependent manner. However, the study by Burke found that imatinib treatment affected CF phenotype and significantly reduced CF viability at 10μM. In comparison, Figure 3.3.2 shows that imatinib treatment did not have any effect on CFs at any of the concentrations tested. However, it should be noted that differences exist in the CF isolation method, serum content and treatment length used in both studies. Burke used the Langendorff isolation technique, a typically non-sterile protocol. In addition, the medium contained 10% serum in comparison to the 20% used in this investigation. The impact of reduced serum has been discussed previously (Huang *et al*., 2018). It should also be noted that the treatment length is significantly longer in the study by Burke (24-48 hr) than was performed in this study (18 hr). These differences may account for the differences seen in imatinib treatment between the two findings.

Given that contractile dysfunction is a common manifestation of TKI-induced cardiotoxicity, it is not surprising that the effect of TKI treatment on CMs is well documented in the literature. Chu and colleagues (2007) have shown that sunitinib treatment affects cell

morphology in both human and animal CMs. The same study also found a significant reduction in cell viability in cultured NRVMs at 1μM sunitinib. Chu observed a significant increase in the number of apoptotic cells (1μM sunitinib, 44 hr treatment) and a concentration dependent increase in the activation of caspase-9 (1&10μM sunitinib, 40 hr treatment), a mediator of the intrinsic mitochondrial apoptotic pathway. Although the cell type and treatment length are different to those used in this investigation, toxicity exists in the same concentration range. The findings of Chu show that the mitochondrial apoptotic pathway is activated by sunitinib treatment. However, the results presented in this chapter show sunitinib treatment significantly increases necrotic cell death in both CFs (Figure 3.4.5) and PCMs (Figure 3.7.2), though a significant increase is the number of late apoptotic PCMs is also seen at 10μM sunitinib (Figure 3.7.2).

Although the study by Chu did not assess changes in necrotic cell death directly, it did report changes consistent with necrotic cell death. Transmission electronmicroscopy of cardiac tissue sections from sunitinib mice showed abnormal CMs – mitochondrial swelling and intracellular vacuolisation (Chu *et al.*, 2007). Similar findings were reported by Kerkela (2006) in CMs isolated from mice treated with clinically relevant concentrations of imatinib. Imatinib treatment was found to induce mitochondrial swelling, intracellular vacuolisation and loss of plasma membrane integrity. These changes are characteristic of necrotic cell death (Yuan *et al.*, 2003), and are consistent with the TKI-induced changes in CFs and MFs phenotype observed in this study.

Kerkela (2006) reported a significant increase in both apoptotic and necrotic CMs death following imatinib treatment. The study proposed that the energy depletion in imatinib treated CMs may have influenced the mode of cell death. Kerkela postulated that the 65% reduction in ATP concentration could have prevented the activation of the intrinsic apoptotic pathway, an energy requiring process. These findings somewhat contradict those of the current study. Although this study has observed an increase in both apoptotic and necrotic

cell death following sunitinib treatment, imatinib treatment was observed to have no significant effect on either CFs or PCMs. However, in the study conducted by Kerkela, the treatment time was notably longer (24 hr).

Susceptibility to TKI-induced cardiotoxicity is largely influenced by underlying health conditions (Zamorano *et al*., 2016). It is also possible that the mechanism of cell death could also be influenced by similar comorbidities. This theory is supported by findings of Chu (2007) who observed a significant increase in apoptotic cell death in the hearts of mice treated with sunitinib and the vasoconstrictor, phenylephrine. Apoptosis was not significantly increased via sunitinib treatment alone, despite increased mitochondrial cytochrome C release.

### *3.9 Conclusion*

The results presented in this chapter show that TKI-treatment affects both the contractile and non-contractile cells of the heart and is believed to be the first study to compare this directly. These findings also show sunitinib is significantly more toxic than imatinib, consistent with the selectivity profiles of both drugs, and that serum starvation can markedly exacerbate drug-induced toxicity. Sunitinib induced toxicity appears to be a largely necrotic mechanism, in both CFs and PCMs. These results also indicate that MFs are more susceptible to TKI-induced toxicity than CFs, supporting the observation that those with pre-existing cardiovascular conditions are more likely to experience TKI-induced cardiotoxicity.

# Chapter Four: Investigating the cardiotoxic mechanism of tyrosine kinase inhibitors

*4.1 Introduction*

The findings presented in Chapter 3 clearly show that TKIs, particularly sunitinib, affect the phenotype and reduce the viability of CFs and PCMs. However, the cardiotoxic mechanism which causes cell death in these cell types is poorly understood, though anecdotal evidence from within the literature has highlighted that $Ca^{2+}$ dysregulation and mitochondrial dysfunction may contribute towards the toxic mechanism of TKIs (Kerkela *et al*., 2006; Chu *et al*., 2007; Barr *et al*., 2014). Altered $Ca^{2+}$ handling is a key feature of cardiovascular dysfunction and, as such, it is not unreasonable to predict that TKI treatment might affect global $Ca^{2+}$responses in the heart. A central mediator of $Ca^{2+}$-induced signaling in the heart is the enzyme CaMKII. CaMKII has already emerged as a prominent enzyme central to the regulation of both normal cardiac physiology and pathology (Neef *et al*., 2010; Sossalla *et al*., 2010; Anderson, 2015). CaMKII is overexpressed and significantly activated across a number of cardiac pathologies such as hypertrophic remodeling (Barr *et al*., 2014; Pyun *et al*., 2018; Suetomi *et al*., 2018; Beauverger *et al*., 2020), atrial fibrillation (Neef *et al*., 2010) and myocardial infarction (Luczack *et al*., 2020). It is possible that TKIs, which in the long-term can cause very similar pathological (toxic) effects in the heart to those observed in CVD, might actually target CaMKII either directly or indirectly, impacting on its expression, activity or both. CaMKIIδ is the most prominent isoform in the heart and the role that it plays in CM contractility is well established. CaMKIIδ is known to influence cardiac contraction by phosphorylating a number of $Ca^{2+}$ handling substrates. Two of the most prominent substrates for CaMKII are RyR2 and PLB (Currie *et al*., 2004; Ai *et al*., 2005; Bers and Grandi, 2009; Neef *et al*., 2010; Mooney *et al*., 2015), and both of these proteins are pivotal in regulating intracellular $Ca^{2+}$ concentration, influencing mitochondrial ATP production and thus controlling cardiac contractility. The role of CaMKII in non-myocytes is extensive and includes regulation of vascular dysfunction (McCluskey *et al*., 2015), CF proliferation (Martin *et al*., 2014) and inflammatory signaling (Martin *et al*., 2018). CF are one of the most

abundant cell type within the heart and are responsible for maintaining cardiac structure. CFs regulate the structure of the ECM through the secretion of factors that synthesize and degrade the collagen framework that underpins cardiac structure (Camelliti *et al*., 2005). This dynamic process is critical to both cardiac repair and pathology and is consistent with one of the hallmark characteristics of TKI-induced cardiotoxicity – ECM remodeling. In understanding how TKIs influence their cardiotoxic effects, it is essential to study both myocytes and non-myocytes of the heart; particularly as the findings presented in Chapter 3 clearly show that TKIs cause morphological changes and reduce the viability of both CFs and PCMs at concentrations considered clinically relevant.

Previous studies have suggested that the cardiotoxic effect of TKIs may be mediated at the level of the mitochondria (Kerkela *et al*., 2006; Chu *et al*., 2007; Will *et al*., 2008). Evidence suggests that mitochondrial dysfunction may occur secondary to changes in $Ca^{2+}$ mobilisation (Kerkela *et al*., 2006; Chu *et al*., 2007). Kerkela (2006) observed $Ca^{2+}$ induced swelling of the mitochondria, caused by $Ca^{2+}$-induced opening of the mitochondrial permeability transition pore in mitochondria isolated from imatinib treated mice. These mitochondrial abnormalities were found to induce mitochondrial biogenesis (an adaptation that occurs when ATP production can no longer meet demand (Jornayvaz and Shulman, 2010)) and was associated with reduced cardiac contractility and left ventricular dilation. The same study reported abnormal mitochondria, left ventricular dysfunction and reduced cardiac output in imatinib treated patients, none of which had known cardiac dysfunction prior to imatinib treatment. Chu (2007) also reported mitochondrial abnormalities in sunitinib treated patients. Sunitinib treatment induced mitochondrial swelling and apoptotic cell death, an almost identical mechanism to that seen in the study by Kerkela (2006). However, the study by Chu (2007) did not investigate intracellular $Ca^{2+}$ so it is not known if mitochondrial dysfunction was mediated by changes in $Ca^{2+}$ mobility.

It is also possible that the changes in $Ca^{2+}$ mobility at the level of the mitochondria may be mediated by CaMKII. Mooney and colleagues (2015) showed that chronic imatinib and sunitinib therapy significantly increased CaMKIIδ expression and activity in guinea pig whole heart homogenate prepared from imatinib and sunitinib-treated animals and this correlated with significant cardiac dysfunction *in vivo*. This result was supported by *in vitro* effects of imatinib whereby increased CaMKIIδ activation was evident in imatinib treated NRVMs (Barr *et al*., 2014). The increased CaMKIIδ activity was associated with increased phosphorylation of PLB and RyR2, with resultant myocyte hypertrophy and necrotic cell death.

In addition to regulating intracellular $Ca^{2+}$, CaMKII may also facilitate direct $Ca^{2+}$ entry into the mitochondria by phosphorylating the mitochondrial $Ca^{2+}$ uniporter (Joiner *et al*., 2012). Luo and Anderson (2013) presented a mechanism in which CaMKII-mediated mitochondrial dysfunction causes CM cell death in heart failure (Figure 4.1.1). They proposed that increased $Ca^{2+}$ entry into the mitochondria, induced by CaMKII phosphorylation of the mitochondrial uniporter, impaired mitochondrial energy production. Specifically, $Ca^{2+}$ overload is proposed to cause electron transport chain uncoupling at complexes I and III, increasing ROS production. It is also possible that the increased ROS production may increase CaMKII production via oxidation in a positive feedback mechanism. These changes may then trigger opening of the mitochondrial permeability transition pore and collapse of the inner mitochondrial membrane potential. This could cause cell death via the apoptotic pathway, mediated by cytochrome c release. This proposed mechanism is based largely on the findings of Joiner (2012), who not only found evidence of a CaMKII-mediated mechanism of mitochondrial dysfunction in heart failure but showed that inhibition of CaMKII can actually protect against mitochondrial dysfunction and reduce myocardial cell death in a mouse model of heart failure. The changes in protein expression and

mitochondrial function bear a striking similarity to the changes seen in TKI-induced cardiotoxicity.

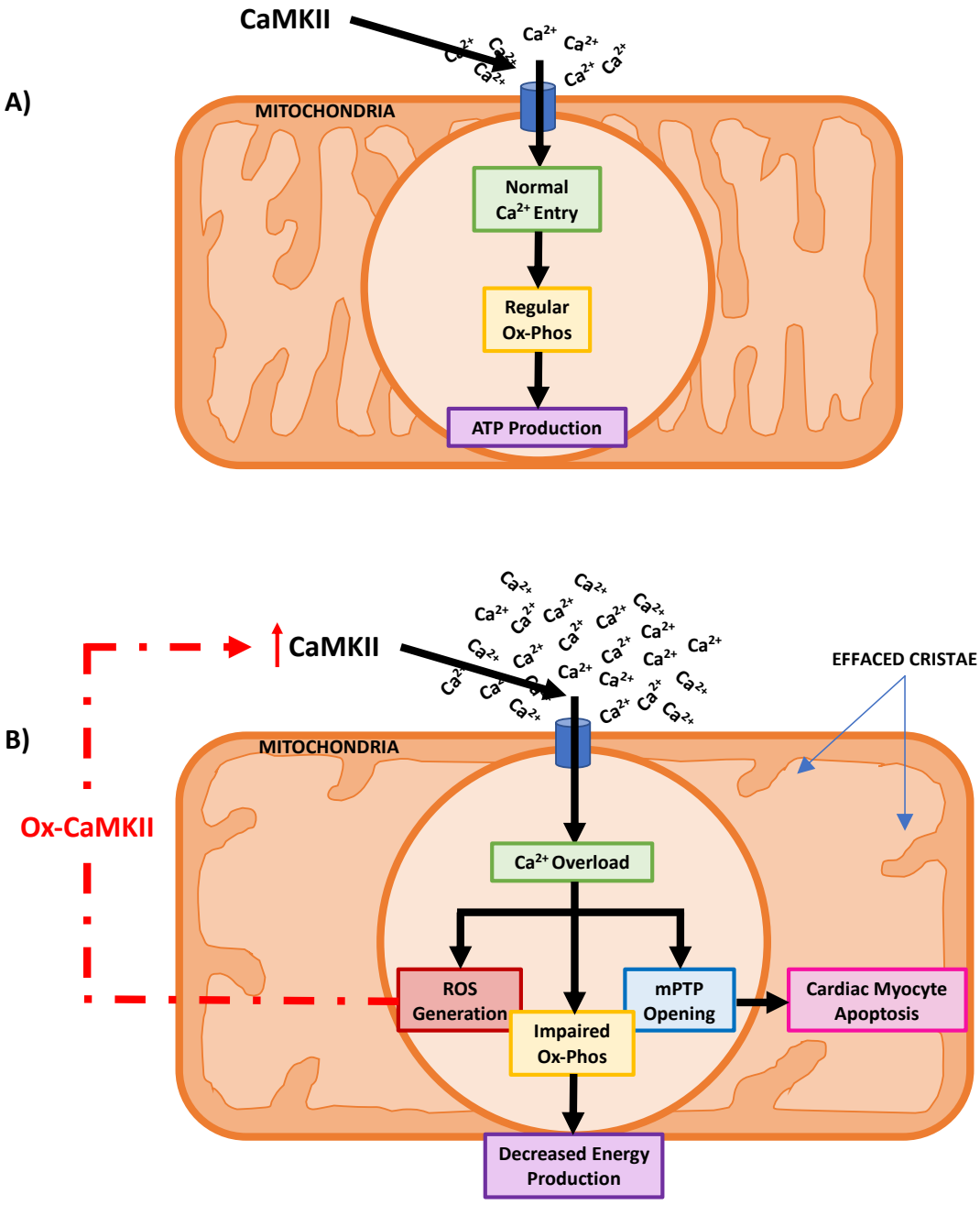


**Figure 4.1.1. Comparing mitochondrial function in healthy and failing cardiac myocytes.** Representative diagrams showing the biological processes occurring in (A) mitochondria in CMs in healthy hearts and (B) mitochondria in CMs in failing hearts. In failing hearts, CMs appear swollen and with effaced cristae. The cristae house the complexes of the electron transport chain and therefore play a critical role in ATP production. Changes in the cristae will consequently have a negative impact mitochondrial ATP production. Mitochondria swelling is caused by increased $Ca^{2+}$ entry into the mitochondria, mediated by CaMKII. This impairs mitochondrial bioenergetics, increasing ROS production and triggering the opening of the mitochondrial permeability transition pore. Cell death ensues via cytochrome c release. Figure developed from Luo and Anderson (2013) and Kuhlbrandt (2015).

The effect of sunitinib on CM function has been extensively studied, yet little is known of wider ranging effects, particularly on cardiac non-myocytes. It has already been established that CaMKIIδ regulates CF activation and can contribute to a disease phenotype (Martin *et al*., 2014; Pyun *et al*., 2018; Luczak *et al*., 2020). It therefore seems possible that CaMKIIδ may also play a key role in TKI-mediated effects in non-myocytes of the heart resulting in cardiotoxicity, perhaps in a mechanism similar to that seen in CMs involving mitochondrial dysfunction.

Having established that TKI treatment affects the phenotype and viability of both CFs and PCMs in Chapter 3, the experimental results presented in this chapter investigate a possible cardiotoxic mechanism mediated by the $Ca^{2+}$ handling protein, CaMKII. This chapter will determine what effect, if any, sunitinib or imatinib treatment has on intracellular $Ca^{2+}$ mobilisation, CaMKII expression and activation and mitochondrial ROS production in both cell types. This chapter will also assess whether CaMKII inhibition can reduce or reverse TKI-induced cardiac cell death.

*4.2 TKI treatment increases intracellular calcium mobilisation in cardiac cells*

In order to determine whether TKI treatment had any effect on intracellular $Ca^{2+}$release, CFs were loaded with Fluo-4 AM $Ca^{2+}$ indicator dye and then stimulated with sunitinib or imatinib (0.1-100μM). Fluo-4 AM is a cell permeant, fluorescent $Ca^{2+}$ indicator with low basal fluorescence and is sensitive to changes in cytosolic $Ca^{2+}$ (Lock *et al*., 2015). It has previously been used to determine changes in intracellular $Ca^{2+}$ following doxorubicin treatment in human cardiac cells (Burridge *et al*., 2016; Maillet *et al*., 2016). Ang II, a known inducer of intracellular $Ca^{2+}$ release (Aiello and Cingolani, 2001; Zhuo *et al*., 2006; Currie *et al*., 2016), was used as a positive control. Imatinib stimulation was found to have no significant effect on $Ca^{2+}$ release at any of the concentrations tested ((0.1-100μM) Figure 4.2.1). In contrast, sunitinib stimulation did significantly increase intracellular $Ca^{2+}$ release in CFs at 100μM sunitinib. However, it should be noted that although stimulation with 100μM sunitinib appeared to significantly increase intracellular $Ca^{2+}$ release, and that previous studies have investigated the effect of sunitinib treatment at similar concentrations in CFs (Burke *et al*., 2019), this concentration is way beyond what is considered clinically relevant.

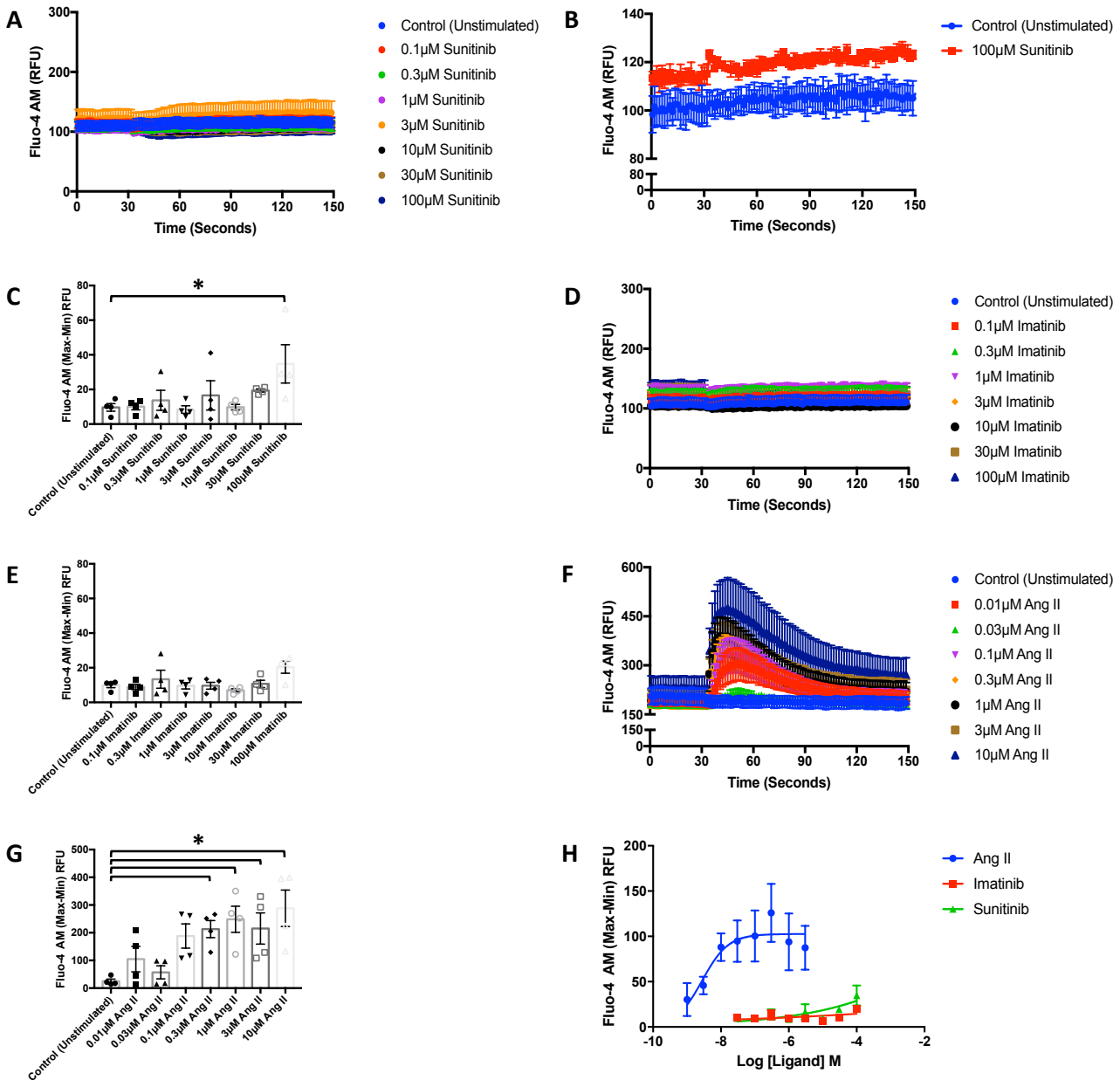


**Figure 4.2.1. Investigating the effect of sunitinib or imatinib stimulation on intracellular calcium mobilisation in cardiac fibroblasts.** (A) Representative trace of intracellular $Ca^{2+}$ release following increasing concentrations of sunitinib (0.1-100μM). (B) Comparison of maximal (100μM) sunitinib Ang II-induced $Ca^{2+}$ mobilisation vs control (unstimulated). (C) Effects of increasing concentrations of sunitinib (0.1-100μM) on $Ca^{2+}$ mobilisation. (D) Representative trace of intracellular $Ca^{2+}$ release following increasing concentrations of imatinib (0.1-100μM). (E) Effects of increasing concentrations of imatinib (0.1-100μM) on $Ca^{2+}$ mobilisation. (F) Representative trace of intracellular $Ca^{2+}$ release following increasing concentrations of angiotensin II (Ang II) (0.01-10μM). (G) Effects of increasing concentrations of Ang II (0.01-10μM) on $Ca^{2+}$ mobilisation. (H) Dose response curve showing the effect of sunitinib, imatinib and Ang II on intracellular $Ca^{2+}$. Calcium mobilisation was determined by measuring fluorescence at Ex:494/Em:525nm. Results are expressed as mean ± S.E.M of 4 biological replicates, *p<0.05.

These results show that TKI stimulation had little effect on intracellular $Ca^{2+}$ release, at least not concentrations that could be considered clinically relevant. Given that symptoms of TKI-induced cardiotoxicity do not present until months or even years after treatment begins (Kerkela *et al*., 2006; Telli *et al*., 2008), it is not surprising that acute TKI stimulation does not impact $Ca^{2+}$ mobility. It is likely that any change in intracellular $Ca^{2+}$ would occur gradually over time and may occur secondary to changes in $Ca^{2+}$ handling protein expression or activity. In order to assess this, CFs were pre-treated with sunitinib or imatinib for 18 hours and then stimulated with a sub-maximal (≈80%) concentration of Ang II (0.3μM) to invoke intracellular $Ca^{2+}$ release. Baseline $Ca^{2+}$ concentration was recorded for 30 seconds prior to stimulation with Ang II. Ang II-induced $Ca^{2+}$ flux was then recorded over the next 2 minutes. Responses were compared with Ang II responses in untreated CFs. Given the yellow colour of sunitinib, background fluorescence was also assessed for both sunitinib (1μM) and imatinib (10μM) by diluting the maximum drug concentration in assay buffer without cells and measuring fluorescence excitation. This ensures that any change in intracellular $Ca^{2+}$ release is not confounded by intrinsic drug fluorescence, an important quality assurance step that is often missed in studies dealing with drugs that exhibit this property (Maillet *et al*., 2016). Sunitinib pre-treatment resulted in a concentration-dependent increase in Ang II-evoked intracellular $Ca^{2+}$ release (Figure 4.2.2B and 4.2.2C) with significance observed at 1μM sunitinib (Figure 4.2.2C and 4.2.2F). In contrast, imatinib pre-treatment, even at higher concentrations, did not result in any significant effect on Ang II-evoked $Ca^{2+}$ release (Figure 4.2.2D and 4.2.2E). Background fluorescent measurements demonstrated no interference from either sunitinib (Figure 4.2.2G) or imatinib (Figure 4.2.2H).

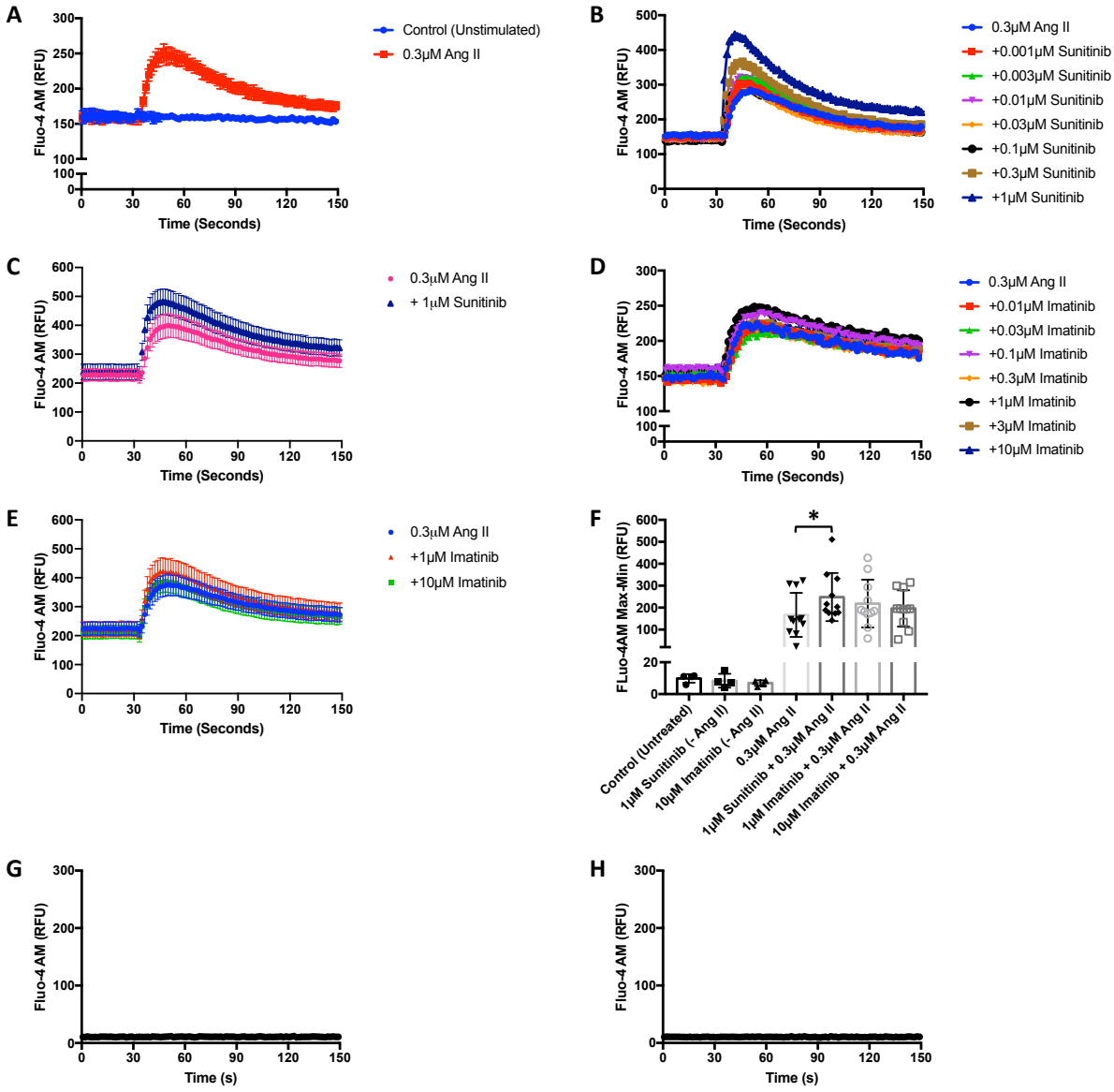


**Figure 4.2.2. Determining whether TKI pre-treatment influences angiotensin II–induced intracellular calcium mobilisation in cardiac fibroblasts.** (A) Representative trace of $Ca^{2+}$ mobilisation in response to 0.3μM Ang II stimulation. (B) Representative trace of intracellular $Ca^{2+}$ release in response to 0.3μM Ang II stimulation following pre-treatment with increasing concentrations of sunitinib (0.001-1μM). (C) Comparison of maximal (1μM) sunitinib Ang II-induced $Ca^{2+}$ mobilisation vs control. (D) Representative trace of intracellular $Ca^{2+}$ release in response to 0.3μM Ang II stimulation following pre-treatment with increasing concentrations of imatinib (0.001-1μM). (E) Comparison of high concentration (1&10μM) imatinib Ang II-induced $Ca^{2+}$ mobilisation vs control. (F) Effects of sunitinib and imatinib pre-treatment on Ang II-induced $Ca^{2+}$ mobilisation. (G). Sunitinib (1μM) background fluorescence. (H) Imatinib (10μM) background fluorescence. Calcium mobilisation was determined by measuring fluorescence at Ex:494/Em:525nm. Results are expressed as mean ± S.E.M of 6 biological replicates, *p<0.05.

Having established that sunitinib pre-treatment had significantly increased intracellular $Ca^{2+}$ release in CFs, the study then sought to investigate whether a similar effect was observed in PCMs. First, the effect of Ang II stimulation (0.01-10μM) on PCMs was investigated to determine a suitable sub-maximal concentration for assessing Ang II-induced $Ca^{2+}$ release in TKI pre-treated PCMs. Ang II significantly increased intracellular $Ca^{2+}$ release at all of the concentrations tested (Figure 4.2.3). 0.3μM Ang II induced a sub-maximal response (again ≈80%) and was therefore deemed an appropriate concentration to investigate the effect of TKI pre-treatment on Ang II-induced $Ca^{2+}$ mobilisation in PCMs.

Having optimised a sub-maximal concentration of Ang II, PCMs were then pre-treated with sunitinib (0.001-1μM) or imatinib (0.01-10μM) and then stimulated with 0.3μM Ang II. Previous studies have already shown that TKI treatment significantly alters $Ca^{2+}$ mobility (Kerkela *et al*., 2006) and that this correlates with changes in cardiac contraction (Doherty *et al*., 2013). However, in this study, TKI-pre-treatment had no influence on Ang II-induced intracellular $Ca^{2+}$ release in PCMs (Figure 4.2.4).

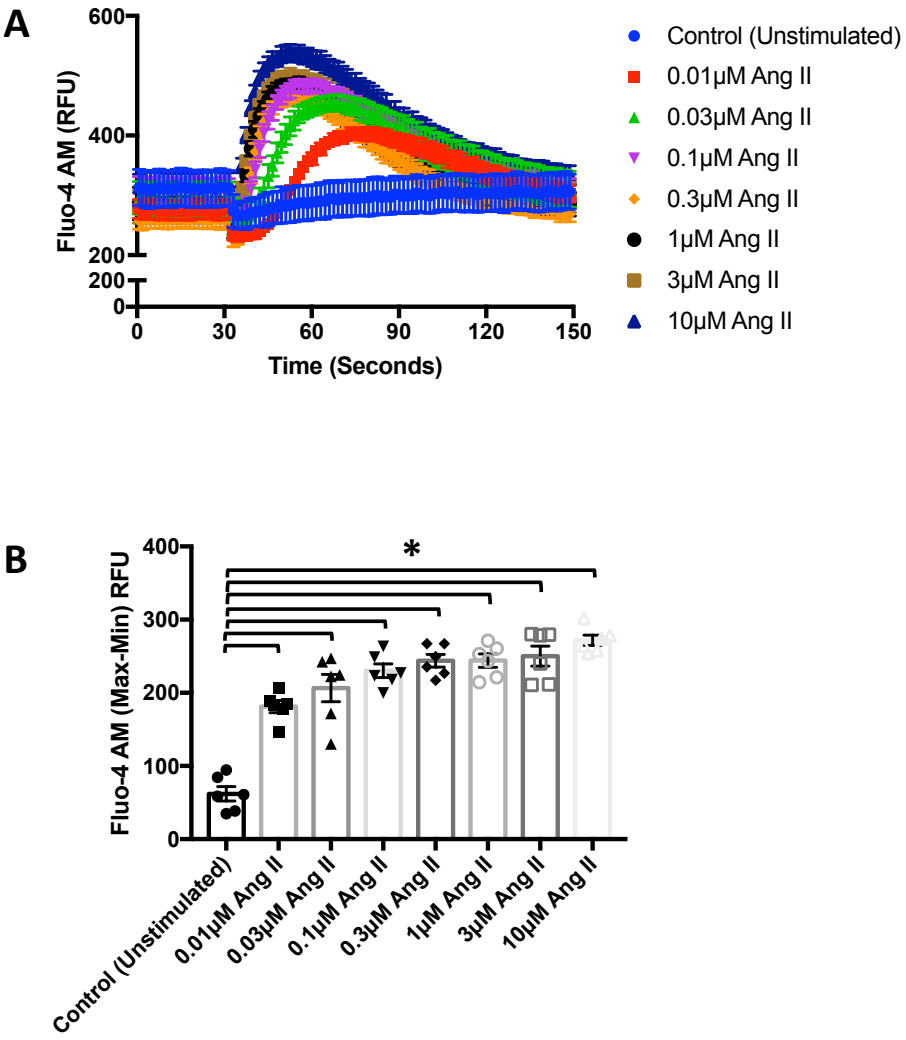


**Figure 4.2.3. Investigating the effect of angiotensin II stimulation on intracellular calcium mobilisation in progenitor cardiac myocytes.** (A) Representative trace of intracellular $Ca^{2+}$ release following increasing concentrations of Ang II (0.01-10μM). (B) Effect of increasing concentrations of Ang II (0.01-10μM) on $Ca^{2+}$ mobilisation. Calcium mobilisation was determined by measuring fluorescence at Ex:494/Em:525nm. Results are expressed as mean ± S.E.M of 4 biological replicates, *p<0.05.

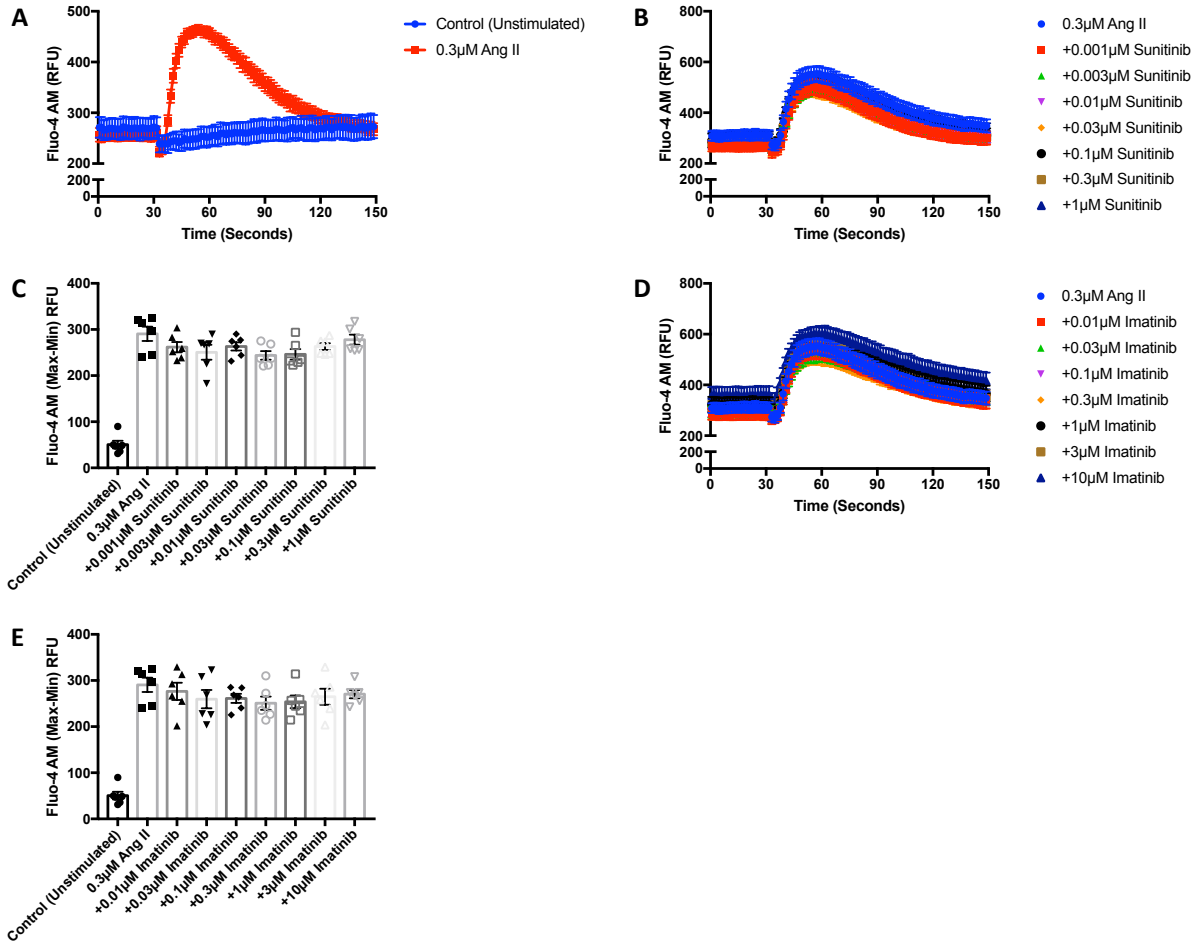


**Figure 4.2.4. Determining whether TKI pre-treatment influences angiotensin II–induced intracellular calcium mobilisation in progenitor cardiac myocytes**. (A) Representative trace of $Ca^{2+}$ mobilisation in response to 0.3μM Ang II stimulation. (B) Representative trace of intracellular $Ca^{2+}$ release in response to 0.3μM Ang II stimulation following pre-treatment with increasing concentrations of sunitinib (0.001-1μM). (C) Effects of sunitinib pre-treatment on Ang II-induced $Ca^{2+}$ mobilisation. (D) Representative trace of intracellular $Ca^{2+}$ release in response to 0.3μM Ang II stimulation following pre-treatment with increasing concentrations of imatinib (0.001-1μM). (E) Effects of imatinib pre-treatment on Ang II-induced $Ca^{2+}$ mobilisation. $Ca^{2+}$ mobilisation was determined by measuring fluorescence at Ex:494/Em:525nm. Results are expressed as mean ± S.E.M of 6 biological replicates, *p<0.05.

*4.3 TKI treatment alters CaMKII activation in cardiac cells*

Having established that TKI treatment increases intracellular $Ca^{2+}$, the study then sought to determine whether the changes in $Ca^{2+}$ mobility correlated with changes in CaMKII activation or expression, as has been established in numerous cardiac pathologies (Neef *et al*., 2010; Sag *et al*., 2011; Barr *et al*., 2014; Martin *et al*., 2014; Curl *et al*., 2018; Daniels *et al*., 2018; Pyun *et al*., 2018; Beauverger *et al*., 2020; Luczack *et al*., 2020). Before determining the effect of TKI treatment, the optimal conditions for the CaMKIIδ (the most prominent isoform in the heart), oxidised CaMKII (Ox-CaMKII) and phosphorylated CaMKII (Phos-CaMKII) antibodies were confirmed using untreated CF lysates (Figure 4.3.1). GAPDH was used as a loading control. CaMKII was found to be highly expressed in CFs, with a volume of 10µl of CF lysate found to elicit sufficient protein expression for all three antibodies using the conditions optimised by the lab group previously.

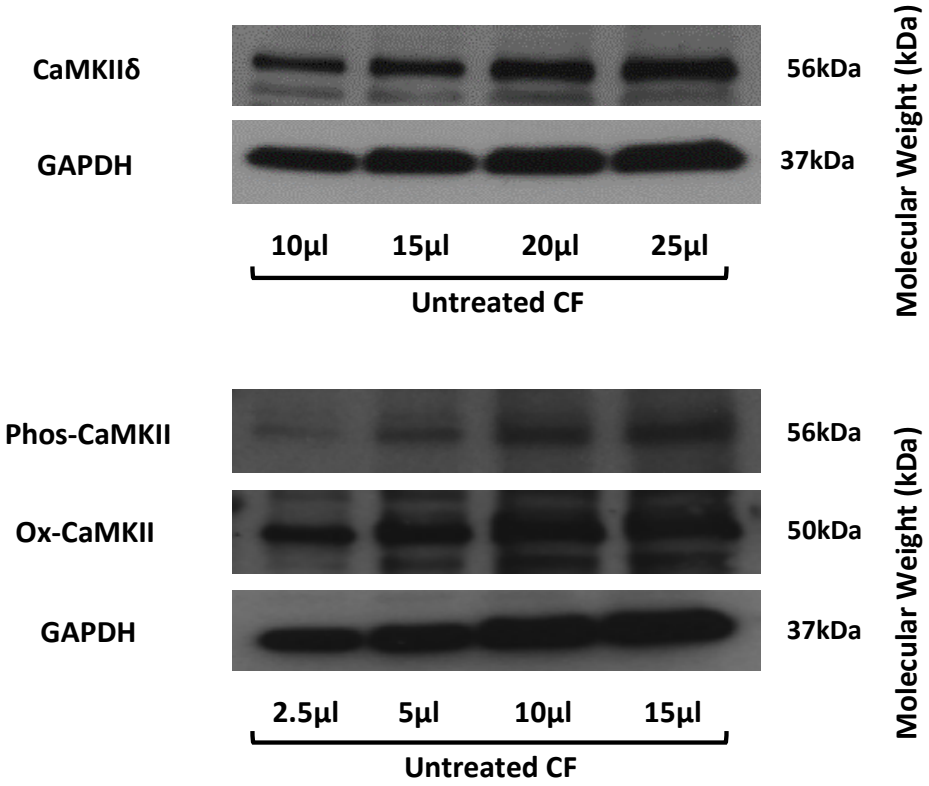


**Figure 4.3.1. Verification of CaMKII antibody conditions using untreated cardiac fibroblast lysates.** Untreated CF lysates were run on 4-20% Mini-PROTEAN TGX Precast Protein Gels. (A) CaMKIIδ optimisation using 10-well gels. (B) Phos-CaMKII and Ox-CaMKII optimisation using 15-well gels (n=1).

Having verified the antibody conditions, the study then sought to investigate the effect of TKI treatment on CaMKII expression and activation in CFs. Surprisingly, sunitinib treatment (0.1-10μM) did not affect CaMKII activation or expression (Figure 4.3.2). Imatinib treatment had no discernible effect on CaMKII either (Figure 4.3.3), though this was as to be expected as imatinib treatment had little impact on intracellular $Ca^{2+}$ (Figure 4.2.2). However, given the effect of sunitinib on intracellular $Ca^{2+}$ in CFs (Figure 4.2.2), the lack of any corresponding effect one of the predominant $Ca^{2+}$ handling proteins in the heart was unexpected.

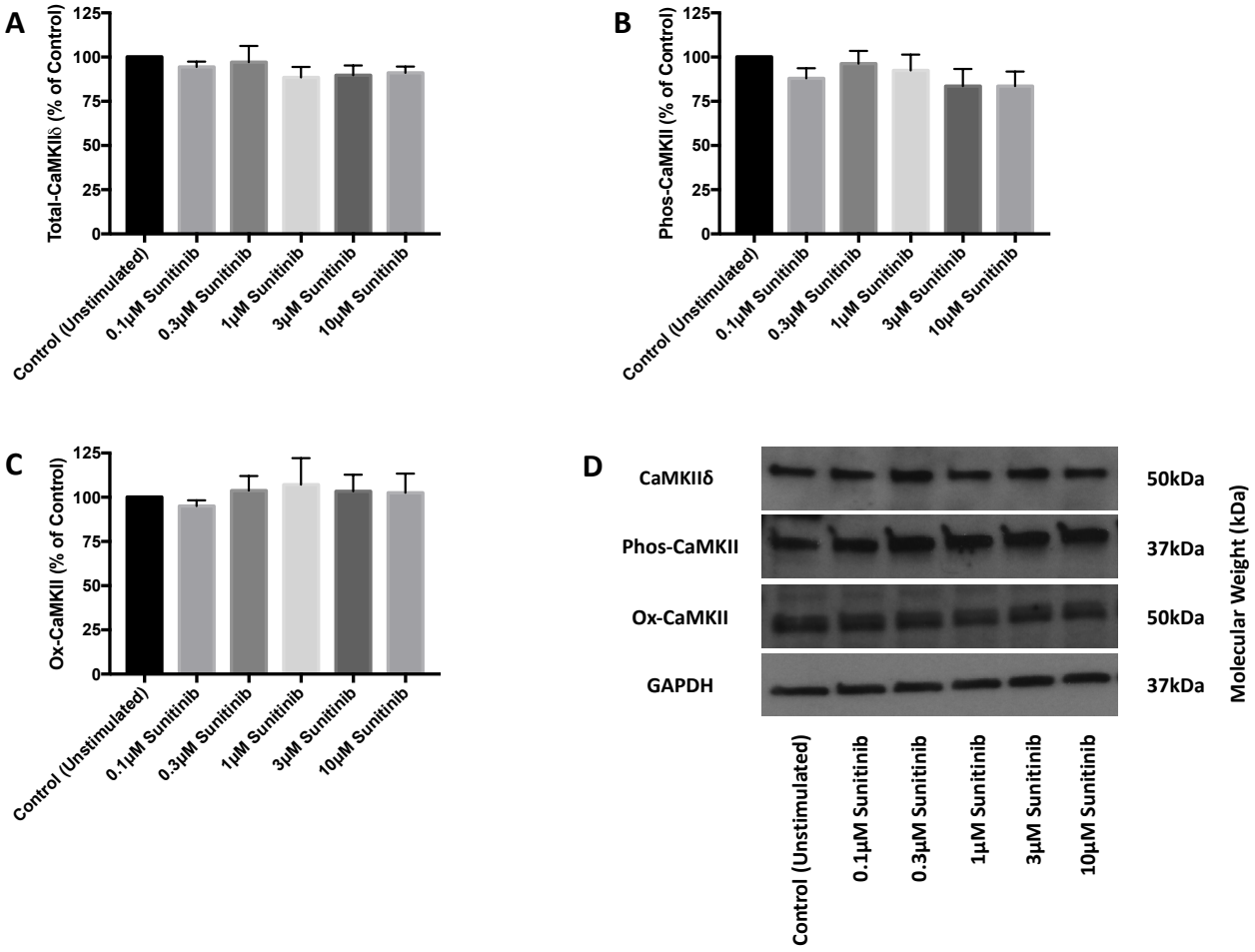


**Figure 4.3.2. Investigating the effect of sunitinib treatment on CaMKII activation and expression in cardiac fibroblasts.** Following the indicated treatments with sunitinib, CaMKIIδ expression or CaMKII activation via phosphorylation or oxidation was determined via quantitative immunoblotting (A) CaMKIIδ expression (B) Phos-CaMKII expression (C) Ox-CaMKII expression. All samples were normalised to GAPDH (D) Representative immunoblot showing CaMKIIδ expression and CaMKII activation following sunitinib treatment (0.1-10μM). Results are expressed as mean ratios protein:GAPDH ± S.E.M and are normalised to control (n=5).

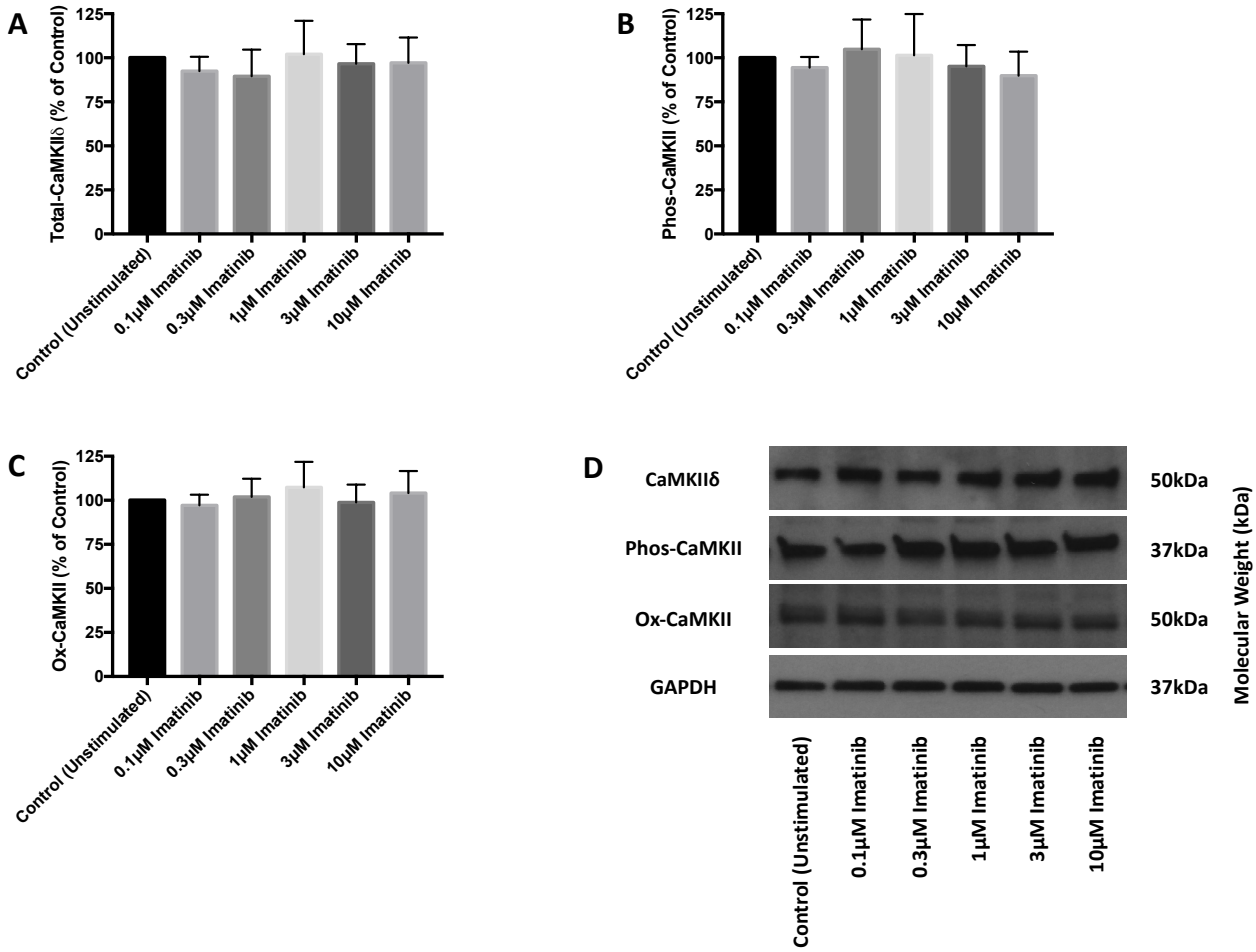


**Figure 4.3.3. Investigating the effect of imatinib treatment on CaMKII activation and expression in cardiac fibroblasts.** Following the indicated treatments with imatinib, CaMKIIδ expression or CaMKII activation via phosphorylation or oxidation was determined via quantitative immunoblotting (A) CaMKIIδ expression (B) Phos-CaMKII expression (C) Ox-CaMKII expression. All samples were normalised to GAPDH (D) Representative immunoblot showing CaMKIIδ expression and CaMKII activation following imatinib treatment (0.1-10μM). Results are expressed as mean ratios protein:GAPDH ± S.E.M and are normalised to control (n=5).

After scrutinising the sample preparation protocol, it became apparent that the inclusion of DTT may be obscuring changes in TKI-induced CaMKII activation. DTT is a reducing agent commonly used in sample buffer to disrupt protein disulphide bonds (Konigsberg, 1972). However, it is possible that the inclusion of DTT in Ox-CaMKII samples may be masking changes in protein oxidation. In order to investigate whether the inclusion of DTT had any effect on the outcome of Ox-CaMKII blotting experiments, TKI treated CF lysates were subjected to electrophoresis in both the presence and absence of DTT and the results compared. Given that no significant effect had been seen in any of the experiments conducted this far at concentrations less than 1μM, a more concise concentration range was used, comparing an effective low (1μM) and high (10μM) concentration of each drug. This was retained for all future blotting experiments.

The exclusion of DTT had a profound effect on Ox-CaMKII expression (Figure 4.3.4). In the absence of DTT, sunitinib treatment appeared to notably increase Ox-CaMKII expression; however, in the presence of DTT, this effect was masked. The exclusion of DTT did not reveal any change in Ox-CaMKII expression in imatinib treated samples, though this is consistent with the findings of previous experiments and the contrast in potency of both drugs.

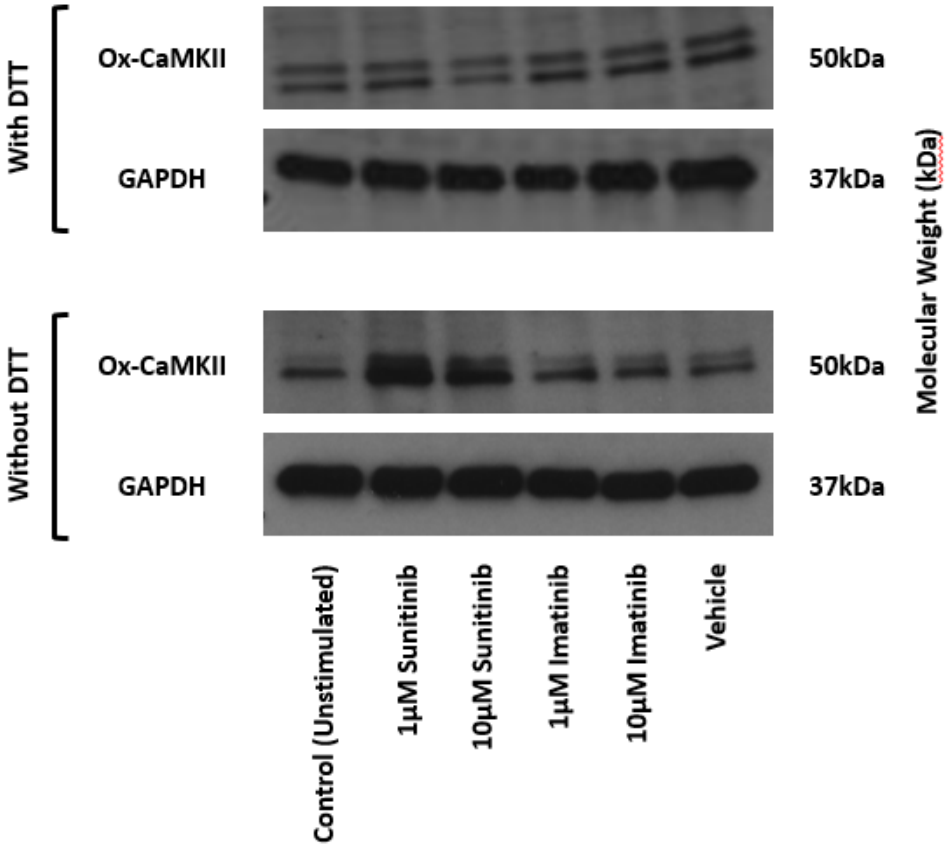


**Figure 4.3.4. Comparing the effect of dithiothreitol inclusion in the expression of Ox-CaMKII in cardiac fibroblasts.** Following the indicated treatments with sunitinib or imatinib, samples were prepared in both the presence and absence of the reducing agent DTT (75mM). Ox-CaMKII expression was then determined via immunoblotting (n=2).

Having determined that changes in Ox-CaMKII expression may have been concealed by the inclusion of DTT in TKI-treated CF samples, fresh samples were prepared, and the blotting process repeated. Samples used to determine CaMKIIδ and Phos-CaMKII expression contained 75mM DTT, Ox-CaMKII expression samples did not. Using the revised sample preparation method, TKI treatment did not alter CaMKIIδ expression in CFs (Figure 4.3.5) nor was phosphorylation of CaMKII affected. Interestingly though, sunitinib treatment did increase CaMKII activation via oxidation at 1μM sunitinib. There was a subsequent decrease in oxidation at 10μM sunitinib likely due to cell death as indicated by the lower signal for GAPDH (Figures 4.3.5C and 4.3.5D). Imatinib treatment had no discernible effect on CaMKII expression or activation.

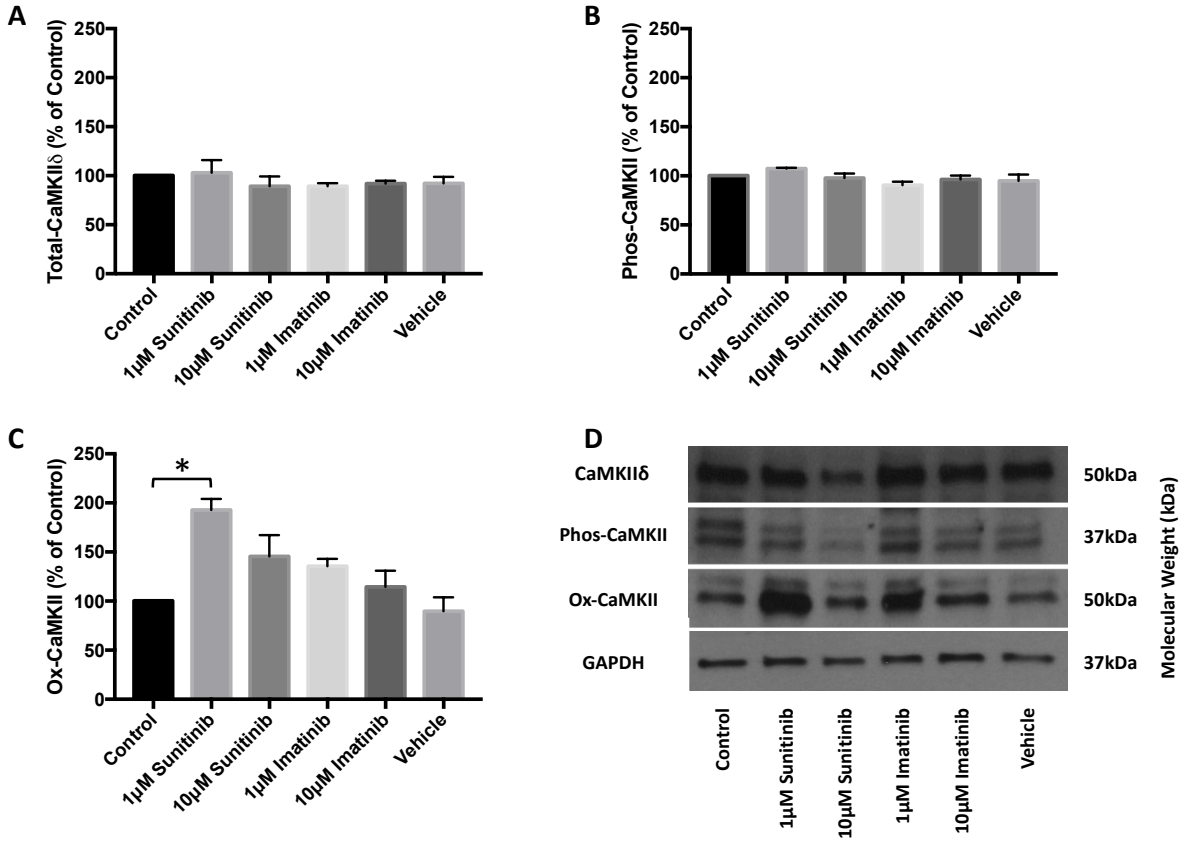


**Figure 4.3.5. Determining the effect of sunitinib or imatinib treatment on CaMKII activation and expression in cardiac fibroblasts.** Following the indicated treatments with either sunitinib or imatinib, CaMKIIδ expression or CaMKII activation via phosphorylation or oxidation was determined via quantitative immunoblotting (A) CaMKIIδ expression, normalised to GAPDH (B) Phos-CaMKII expression, normalised to CaMKIIδ (C) Ox-CaMKII expression, normalised to CaMKIIδ (D) Representative immunoblot showing CaMKIIδ expression and CaMKII activation following TKI treatment. Results are expressed as mean ratios protein:GAPDH ± S.E.M and are normalised to control (n=3, *p<0.05).

Having established that sunitinib treatment increases Ox-CaMKII expression in CFs, the study then investigated whether similar effects were seen in PCMs. TKI-induced changes in intracellular $Ca^{2+}$ have been reported previously (Kerkela *et al*., 2006), suggesting changes in $Ca^{2+}$ handling protein expression or activity or both in this cell type. Prior to investigating the effect of TKI treatment, antibody conditions were optimised in untreated PCMs (Figure 4.3.6). The expression of CaMKII in PCMs was much lower than it is in CFs, meaning a greater sample volume was required. 20µl was found to be the optimum volume. The low protein content also meant that the stripping process could not be carried out. Instead, membranes had to be cut in order to obtain a loading control. At this point, the lab group had all reported experiencing inconsistent results with the GAPDH antibody. As a result, tubulin was used as a loading control for these optimisation experiments while a replacement GAPDH antibody was sourced from the supplier.

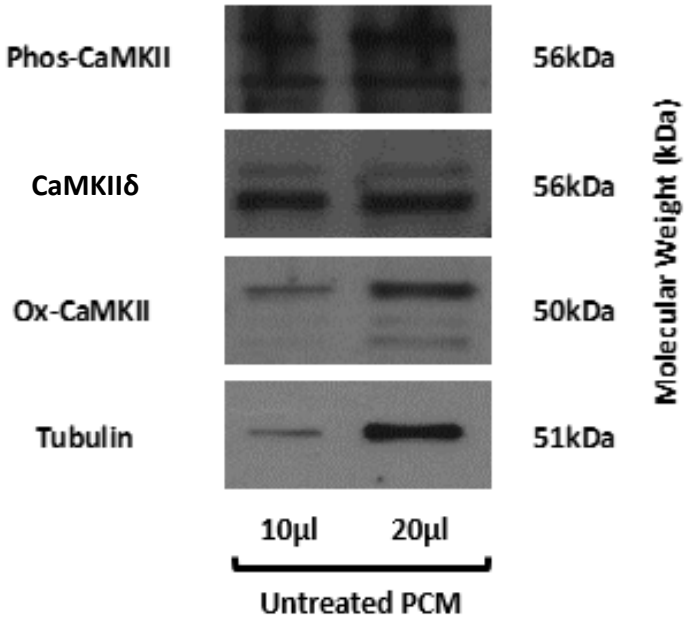


**Figure 4.3.6. Optimisation of CaMKII antibodies using untreated progenitor cardiac myocytes.** Untreated PCM lysates were run on 10% NuPAGE Novex BisTris Gels and then proteins identified using CaMKIIδ antibodies (n=3).

Having optimised the antibody conditions for PCMs, the effect of TKI treatment was then investigated. TKI treatment had very little effect on CaMKIIδ expression (Figure 4.3.7A) or oxidation of CaMKII (Figure 4.3.7C). Surprisingly, sunitinib treatment reduced CaMKII phosphorylation at 10μM sunitinib. Again, the reduction in CaMKII phosphorylation was likely due to cell death, as indicated by the lower signal for GAPDH (Figures 4.3.7B and 4.3.7D). Imatinib treatment had no discernible effect on CaMKII phosphorylation in PCMs.

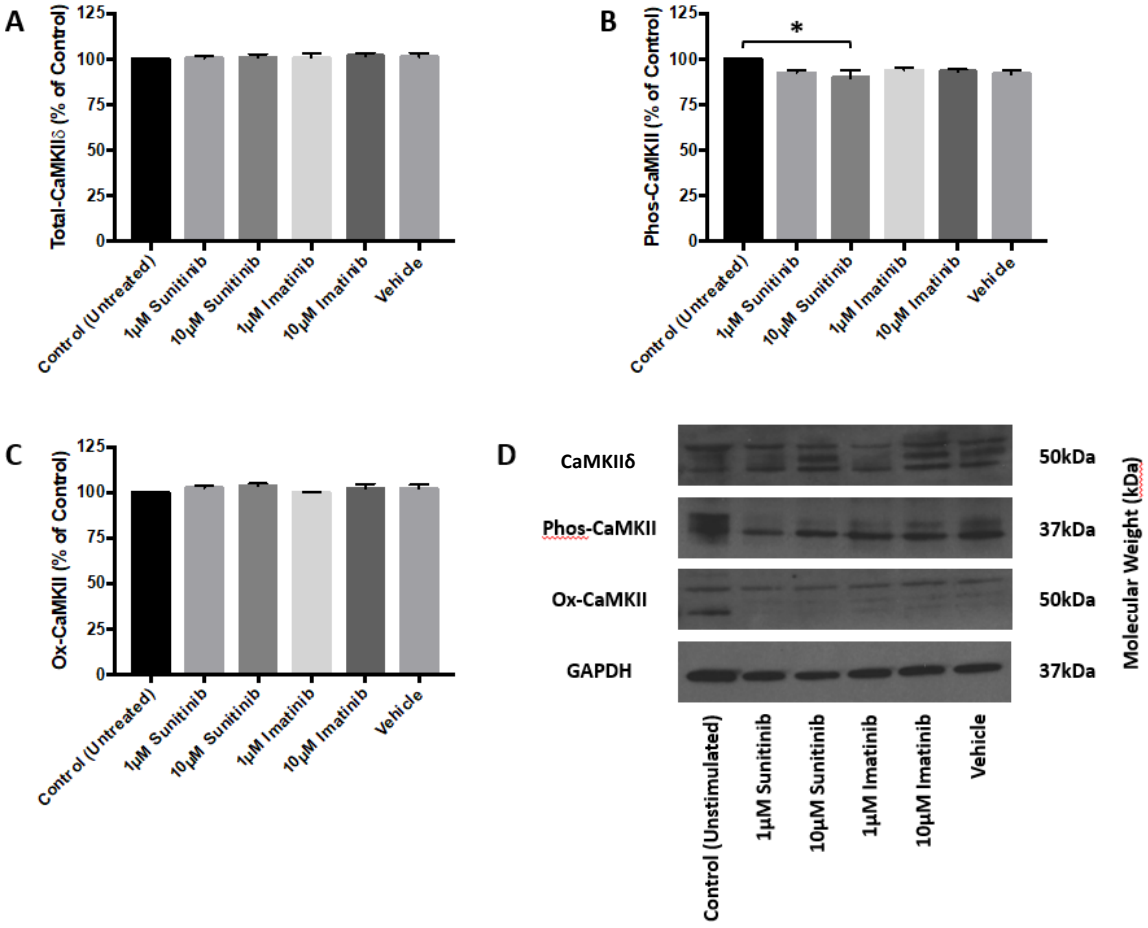


**Figure 4.3.7. Determining the effect of sunitinib or imatinib treatment on CaMKII activation and expression in progenitor cardiac myocytes.** Following the indicated treatments with either sunitinib or imatinib, CaMKIIδ expression or CaMKII activation via phosphorylation or oxidation was determined via quantitative immunoblotting (A) CaMKIIδ expression (B) Phos-CaMKII expression (C) Ox-CaMKII expression. Samples were all normalised to GAPDH. (D) Representative immunoblot showing CaMKIIδ expression and CaMKII activation following TKI treatment. Results are expressed as mean ratios protein:GAPDH ± S.E.M and are normalised to control (n=3, *p<0.05).

*4.4 The cardiotoxic mechanism of tyrosine kinase inhibitors involve mitochondrial dysfunction*

Having established that TKI treatment increases $Ca^{2+}$ mobility and CaMKII activation, the next part of the project sought to investigate whether these changes in $Ca^{2+}$ handling had any effect on mitochondrial function. $Ca^{2+}$-mediated mitochondrial dysfunction has been described in the pathophysiology of HF (Luo and Anderson, 2013) and, given the similarities between HF and TKI-induced cardiotoxicity, may also form part of the cardiotoxic mechanism of TKIs. ROS are critical to both normal cardiac physiology and disease. In a physiological setting, ROS are known to play a key role in excitation contraction coupling and cardiac myocyte maturation via redox signalling (Burgoyne *et al*., 2012). Mitochondria are an important source of ROS and cardiac tissue, in particular, is rich in mitochondria (Peoples *et al*., 2019). The mitochondrial electron transport chain is the main source of ROS in cardiac tissue. Physiologically speaking, ROS are a natural by-product of aerobic respiration. However, when ROS production becomes excessive or unregulated, it can have a damaging effect. In a pathological setting, increased ROS can cause oxidative stress and mediate CM cell death via mitochondrial dysfunction (Joiner *et al*., 2012; Luo and Anderson, 2013). These pathological changes have been seen in both cardiomyopathy (Kwong *et al*., 2014) and HF (Tsutsui *et al*., 2011).

Increased ROS production may also be a part of the cardiotoxic mechanism of TKIs. Changes in cell morphology following TKI treatment are consistent with the changes seen in CMs in heart failure, a process mediated largely by increased ROS production at the level of the mitochondria. Furthermore, increased ROS production has been observed in TKI treated human derived CMs previously (Dougherty *et al*., 2013). The DCFDA assay has previously been used to determine changes in intracellular ROS production in cardiac progenitor cells

(Li *et al*., 2018). It is a fluorescence-based assay used to quantitatively determine ROS in live cell samples. Given that increased ROS generation may contribute to the cardiotoxic mechanism of TKIs, this study utilised the assay to determine changes in intracellular ROS following TKI treatment in CFs. The assay was optimised using $H_2O_2$, a compound known to stimulate ROS production (Al Ghouleh *et al*., 2013). The assay was first optimised using S3T3s, a non-primary murine fibroblast cell line that has been used previously to investigate the cardiotoxic effect of anthracyclines (Tsiftsoglou *et al*., 1986). Optimisation showed a concentration dependent increase in intracellular ROS, reaching significance at 100μM $H_2O_2$ (Figure 4.4.1A). A significant increase in ROS production was also observed with the positive control, tert-Butyl hydrogen peroxide (TBHP). Having shown that the assay was sensitive to changes in intracellular ROS production, the optimisation process was repeated using CFs. CFs stimulated with $H_2O_2$ showed a significant increase in ROS production at 100μM $H_2O_2$ (Figure 4.4.1B). However, the manufacturer recommended positive control (50μM TBHP) failed to produce a positive effect in CFs.

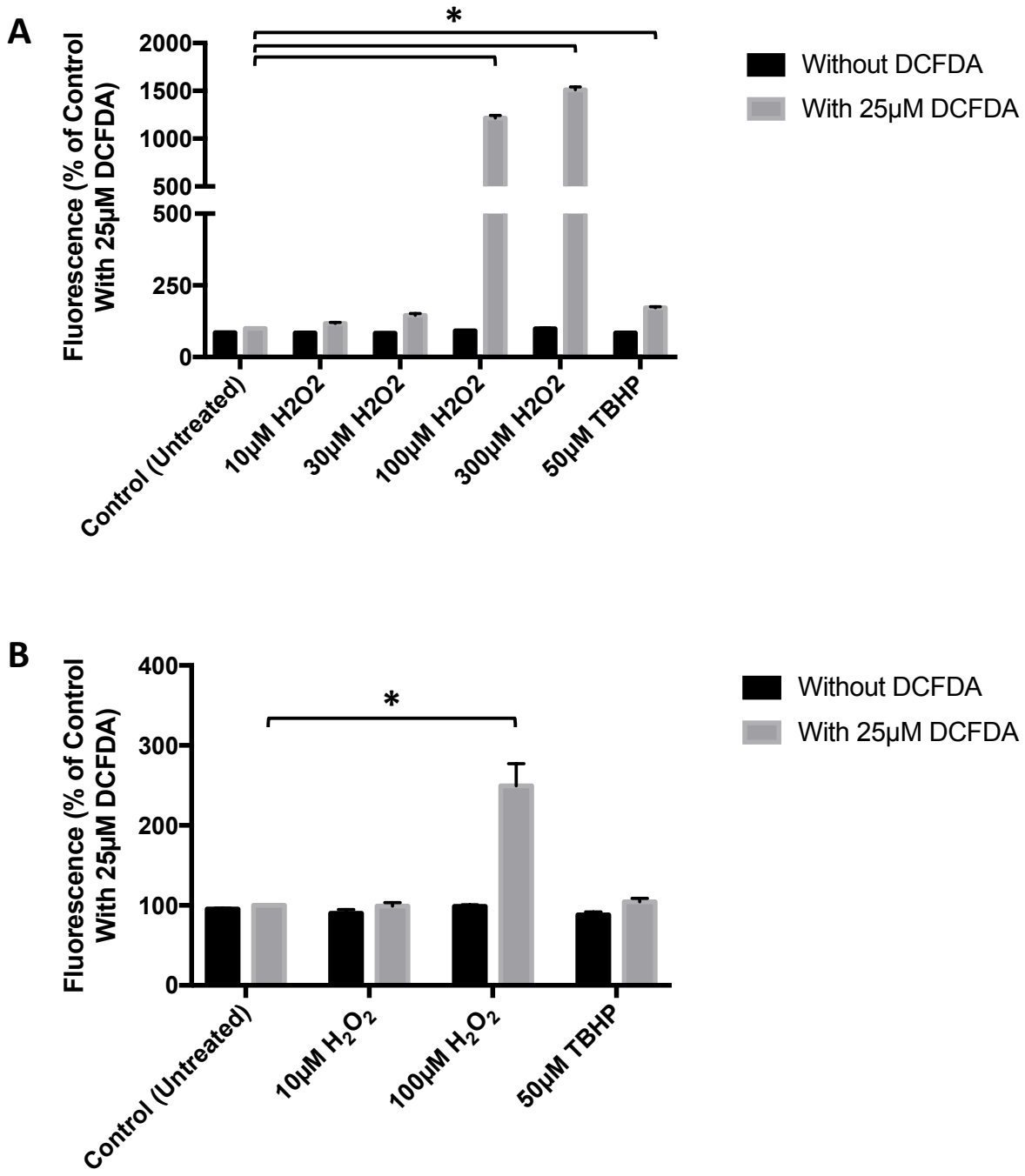


**Figure 4.4.1. Optimisation of the DCFDA assay using hydrogen peroxide.** Cells were incubated with or without 25µM DCFDA before stimulation with $H_2O_2$. (A) S3T3s stimulated with 10-300µM $H_2O_2$. (B) CFs stimulated with 10-100µM $H_2O_2$. 50µM TBHP was used as a positive control. Intracellular ROS was detected by reading signals at EX485/Em535nm. Results presented as percentage of control (untreated) containing 25µM DCFDA (n=3, *$p<0.05$, compared to control (untreated) containing 25µM DCFDA).

The optimised DCFDA assay was then used to determine whether stimulation with sunitinib or imatinib (1-10μM) had any effect on intracellular ROS production in CFs. For these experiments, 100μM $H_2O_2$ was used as a positive control as optimisation experiments showed that TBHP failed to evoke a positive response. Sunitinib stimulation increased intracellular ROS production in a concentration dependent manner, reaching significance at 10μM sunitinib (Figure 4.4.2A). However, a significant increase in fluorescence was also seen at 10μM sunitinib in samples not containing the fluorescent agent DCFDA. These findings suggest that the fluorescent measurement may be confounded by the colour of the drug in solution. Imatinib stimulation, on the other hand, did not affect intracellular ROS production in CFs (Figure 4.4.2B).

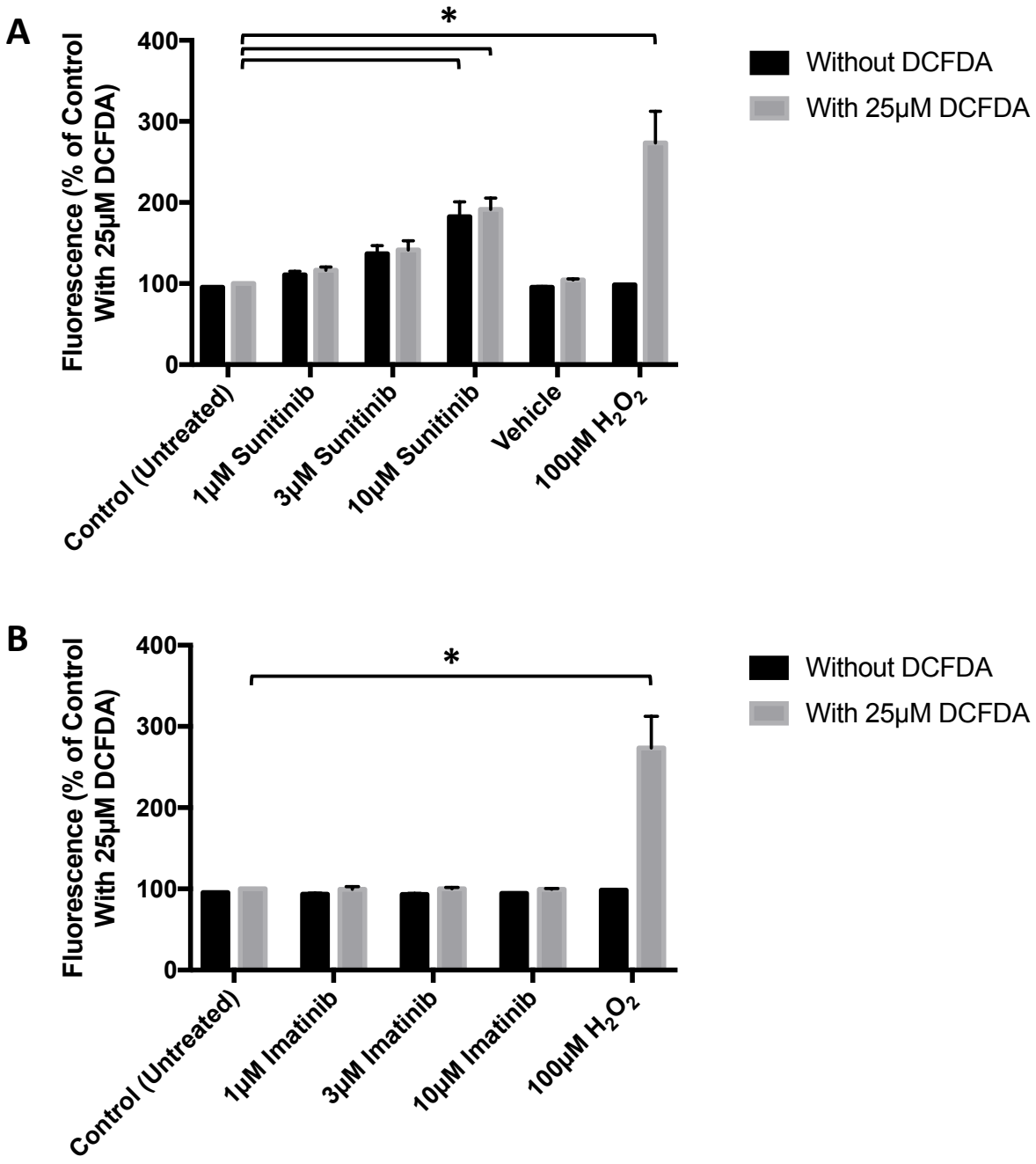


**Figure 4.4.2. Investigating the effect of sunitinib or imatinib treatment on reactive oxygen species production in cardiac fibroblasts.** CFs were incubated with or without 25μM DCFDA before stimulation with (A) sunitinib (1-10μM) or (B) imatinib (1-10μM). 100μM $H_2O_2$ was used as a positive control. Intracellular ROS was detected by reading signals at EX485/Em535nm. Results presented as percentage of control (untreated) containing 25μM DCFDA (n=3, *$p<0.05$, compared to control (untreated) containing 25μM DCFDA).

The anti-cancer drug, doxorubicin, is known to be auto-fluorescent (Mukhopadhyay *et al*., 2007) and the auto-fluorescent properties of the drug have been reported to interfere with in vitro assays previously (Luis *et al*., 2019). Interestingly, doxorubicin is recommended as a positive control by the manufacturer of the DCFDA assay kit used in this study (Abcam (ab113851)). Given the intrinsic fluorescence of doxorubicin, it is possible that the positive response it produces in the DCFDA assay does not reflect an accurate increase in intracellular ROS production but rather an increase in the amount of fluorescent drug present, similar to what was observed with sunitinib (Figure 4.4.2A). In order to investigate this, CFs were stimulated with 10μM doxorubicin, with and without pre-treatment with DCFDA. Although this experiment only has an n number of 2 and does not allow for statistical analysis, the findings indicate that the intrinsic fluorescence of doxorubicin, like sunitinib, interferes with the outcome of the DCFDA assay (Figure 4.4.3). These findings suggest that the DCFDA assay is flawed. Given that the results from the assay appear to be influenced by the colour of the drug itself, the study cannot conclude whether TKI treatment has any effect on intracellular ROS production using this method. As the assay is not reliable, it was not pertinent to assess the effect of TKI treatment on PCMs using the DCFDA assay.

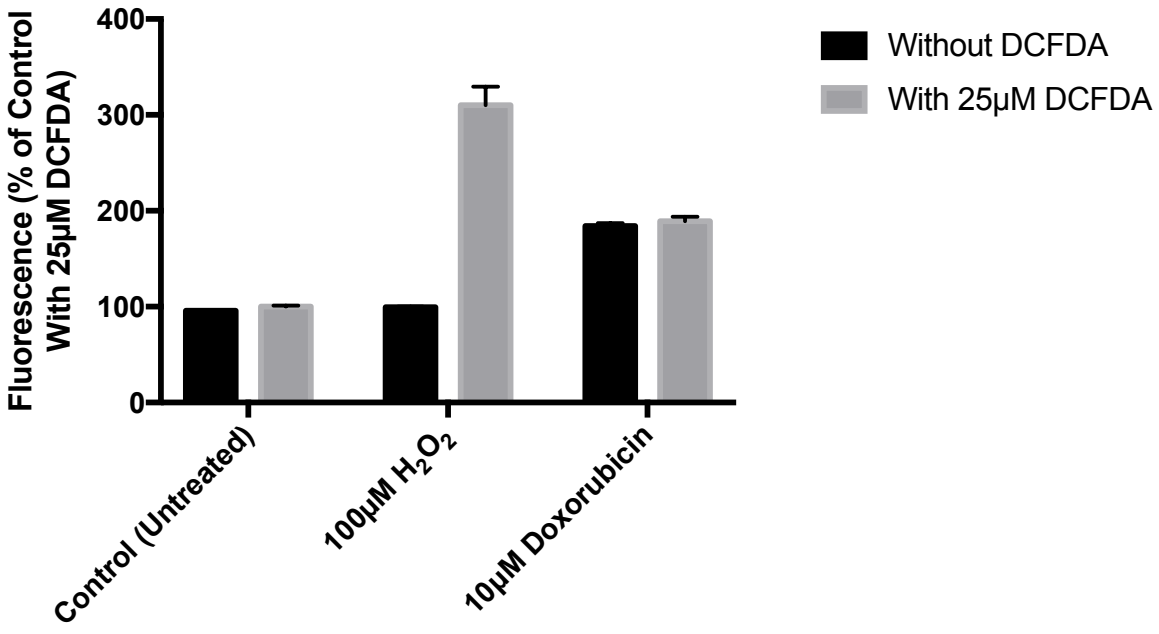


**Figure 4.4.3. Investigating whether intrinsic drug fluorescence introduces bias to the DCFDA assay.** CFs were incubated with or without 25µM DCFDA before stimulation with 10µM doxorubicin. 100µM $H_2O_2$ was used as a positive control. Intracellular ROS was detected by reading signals at EX485/Em535nm. Results presented as percentage of control (untreated) containing 25µM DCFDA (n=2).

The findings of this project have so far shown that sunitinib treatment significantly increases intracellular $Ca^{2+}$ release and Ox-CaMKII activation. However, due to the issues surrounding intrinsic drug fluorescence with the DCFDA assay, it is not yet known whether these changes affect mitochondrial function and/or ROS production. The study therefore opted to investigate the effect of TKI treatment on ROS production directly at the level of the mitochondria using the mitochondrial superoxide indicator, MitoSOX Red.

MitoSOX Red has previously been used to investigate superoxide production following anthracycline treatment in both animal and human derived cardiac cells (Mukhopadhyay *et al*., 2007; Mukhopadhyay *et al*., 2009). S3T3s were used to optimise the concentration of MitoSOX Red and determine an appropriate positive control. The manufacturers recommended concentration of 5μM MitoSOX Red produced an optimal uptake of fluorescent probe while maintaining its mitochondrial specificity (Figure 4.4.4A-C). Previous research has shown that MitoSOX Red can cause uncoupling and lose its membrane specific localisation when applied at elevated concentrations (Roelofs *et al*., 2015). When this happens, the findings obtained using this fluorescent probe are no longer a true reflection of superoxide production within the mitochondrial matrix. It is therefore imperative to properly optimise the concentration of MitoSOX Red for each cell type. The mitochondrial complex III inhibitor antimycin A was found to increase mitochondrial superoxide production (Figure 4.4.4D-F), as has been described previously (Boveris and Cadenas, 1975). As such, antimycin A was determined to be a suitable positive control for subsequent experiments.

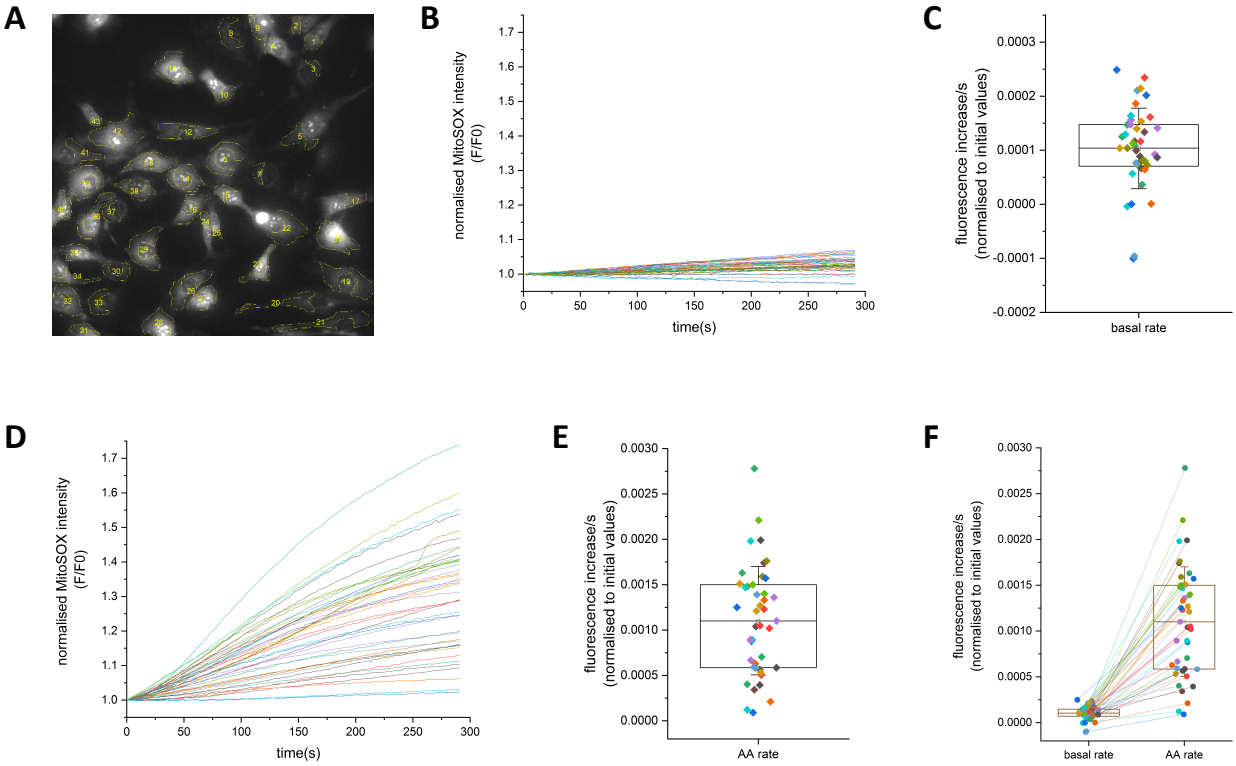


**Figure 4.4.4. Optimisation of MitoSOX Red using Swiss 3T3 cells.** S3T3s (P15-18) were incubated with 5μM MitoSOX Red for 5 min then recorded for 5 min using WinFluor V4 0.8 live cell imaging software. (A) Representative image of S3T3s incubated with 5μM MitoSOX Red. (B) Fold change in fluorescence intensity in untreated S3T3s. (C) Changes in fluorescence intensity normalised to initial values in untreated S3T3s over the 5 min recording period. (D) Fold change in fluorescence intensity in S3T3s treated with 10μM antimycin A. (E) Changes in fluorescence intensity normalised to initial values in S3T3s treated with 10μM antimycin A over the 5 min recording period. (F) Changes in fluorescence intensity in S3T3s incubated for 5 min with 5μM MitoSOX Red and then treated with 10μM antimycin A for 5 min, normalised to initial values. This figure has been generated from one data set and is representative of two other experiments (n=3).

Having identified a suitable positive control, the optimisation process was repeated using CFs. The optimisation process found that 3μM MitoSOX Red was the optimal concentration for detecting changes in superoxide production in CFs (Figure 4.4.5C and 4.4.5E), concentrations lower than 3μM failed to provide sufficient uptake of the fluorescent probe for live cell imaging (Figure 4.4.5B). Concentrations above 3μM did provide sufficient uptake of dye for live cell imaging (Figure 4.4.5E) but were associated with nuclear re-localisation of MitoSOX Red, consistent with toxic concentrations (Figure 4.4.5D).

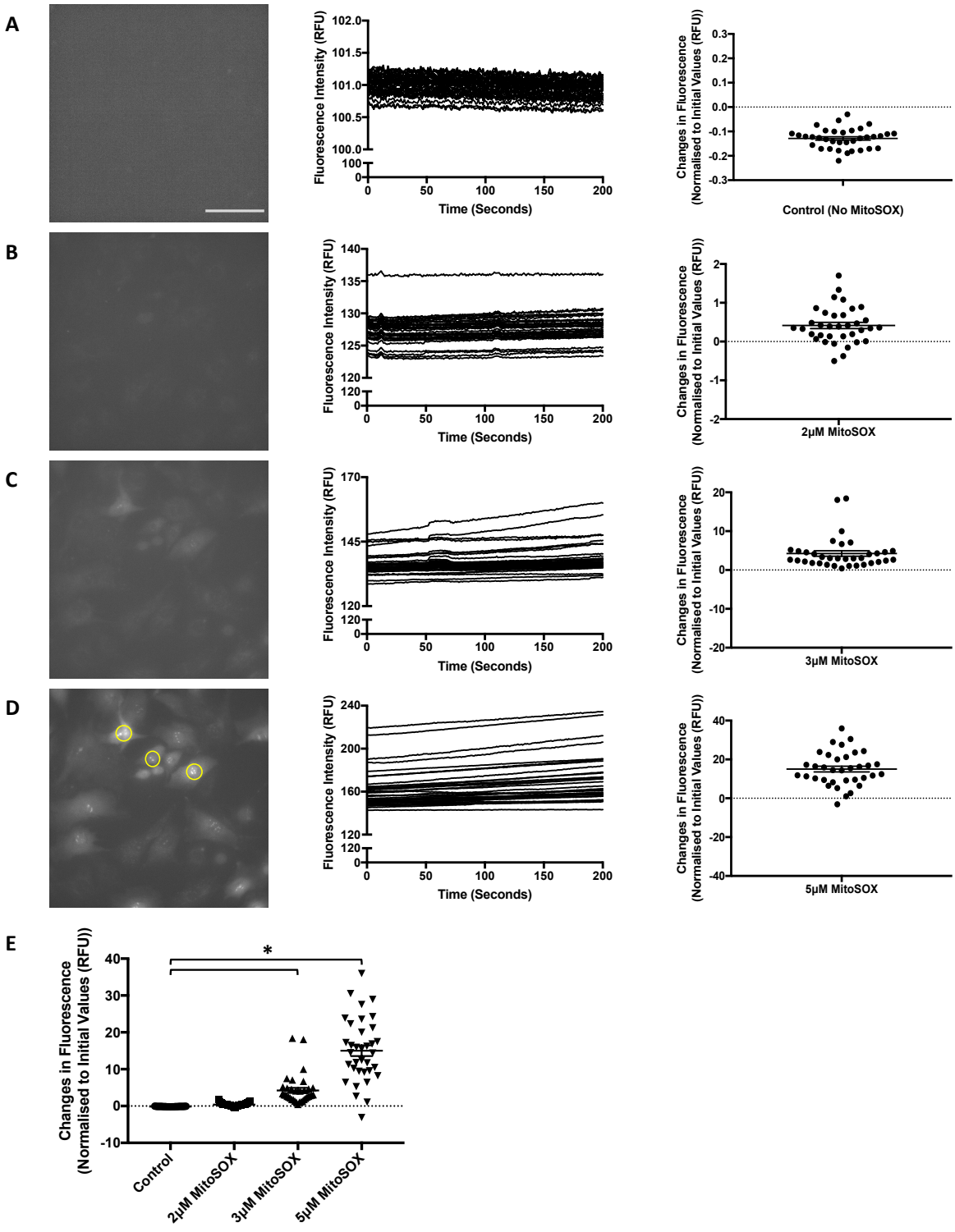


**Figure 4.4.5. Optimising MitoSOX Red concentration in untreated cardiac fibroblasts.** CFs (P1-2) were incubated with increasing concentrations of MitoSOX Red for 5 min then recorded for 5 min using WinFluor V4 0.8 live cell imaging software. (A) CFs without MitoSOX Red (B) 2μM MitoSOX Red. (C) 3μM MitoSOX Red. (D) 5μM MitoSOX Red. (E) Changes in fluorescence intensity normalised to initial values across the 5 min recording period following incubation with increasing concentrations of MitoSOX Red. This figure has been generated from one data set and is representative of two other experiments (n=3, *p<0.05 in comparison to control (without MitoSOX Red)).

The optimised conditions for MitoSOX Red live cell imaging were then used to determine the effect TKI treatment has on superoxide production in CFs. Live cell imaging revealed that both sunitinib and imatinib significantly increased mitochondrial superoxide production in CFs (Figure 4.4.6B and 4.4.6C). This is evident at all concentrations tested and the fold-changes observed following TKI treatment were markedly higher than that observed with the mitochondrial complex III inhibitor Antimycin A, which was used as a positive control for increased superoxide production (Figure 4.4.6A). Sunitinib resulted in considerably higher fluorescence than imatinib (Figure 4.4.6B versus 4.4.6C), again suggesting the increased potency and cardiotoxic potential of sunitinib when compared with imatinib.

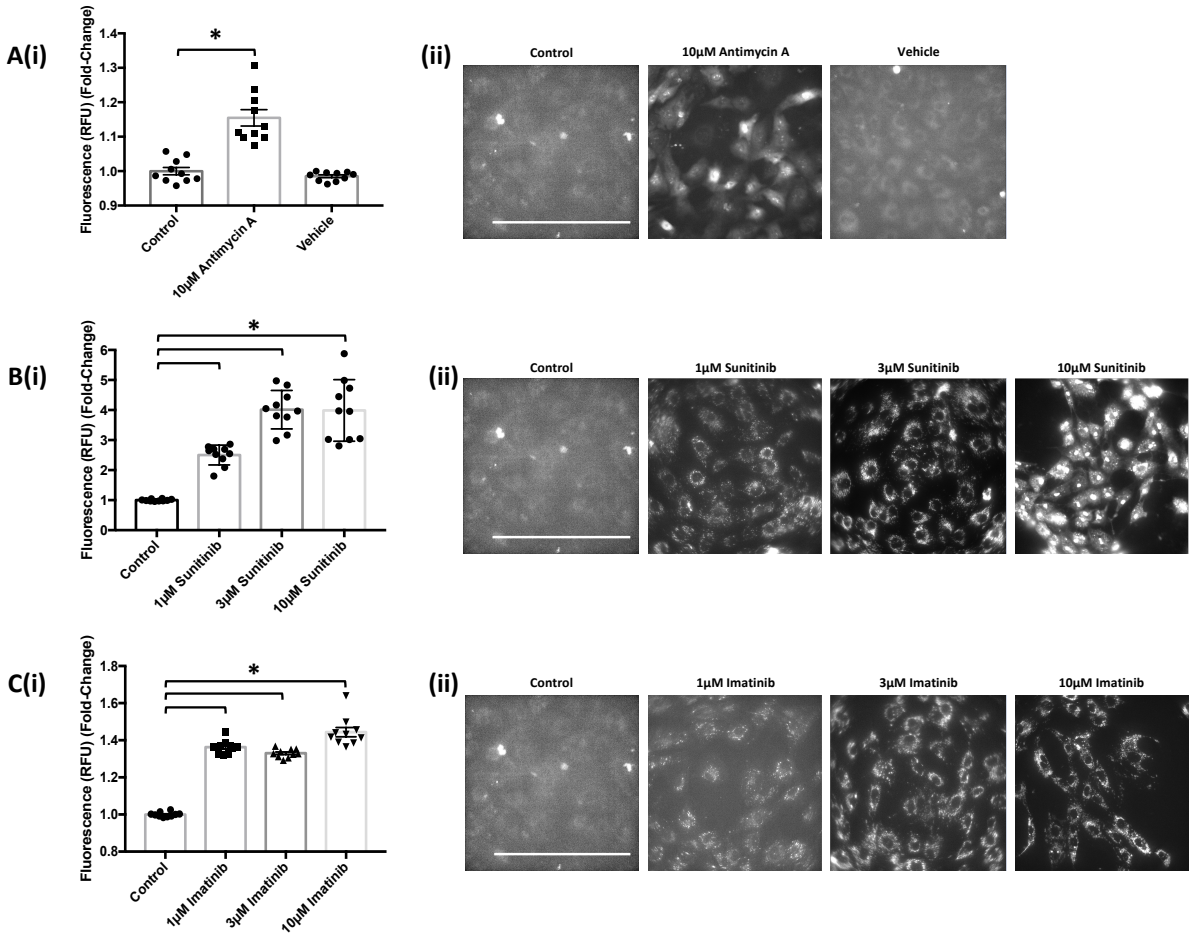


**Figure 4.4.6. Investigating the effect of sunitinib or imatinib treatment on mitochondrial superoxide production in cardiac fibroblasts.** (A(i)) Histogram showing superoxide production assessed via fluorescence intensity in antimycin A and vehicle treated CFs (A(ii)) Representative images of MitoSOX Red analysis of antimycin A and vehicle treated samples. (B(i)) Superoxide production assessed via fluorescence intensity in sunitinib treated CFs (B(ii)) Representative images of MitoSOX Red analysis of sunitinib treated samples. (C(i)) Superoxide production assessed via fluorescence intensity in imatinib treated CFs (C(ii)) Representative images of MitoSOX Red analysis of imatinib treated samples. Scale bar 100μm. Results shown are mean data from one experiment (One n number = fluorescent intensity of 10 cells randomly selected from each image), representative of two other experiments (*$p<0.05$).

Having established that TKI treatment impacts intracellular $Ca^{2+}$ handling and increases mitochondrial superoxide production, the study then sought to investigate the role that CaMKII may play in this paradigm. To do this, CFs were pre-treated with KN-93, a known inhibitor of CaMKII, and then treated with high concentrations of sunitinib or imatinib (10μM). Interestingly, when CFs were pre-treated with KN-93, sunitinib-mediated superoxide production was significantly reduced (Figure 4.4.7A). Moreover, in CFs treated with 10μM imatinib, KN-93 pre-treatment completely abolished the imatinib-induced increase in mitochondrial superoxide production (Figure 4.4.7B).

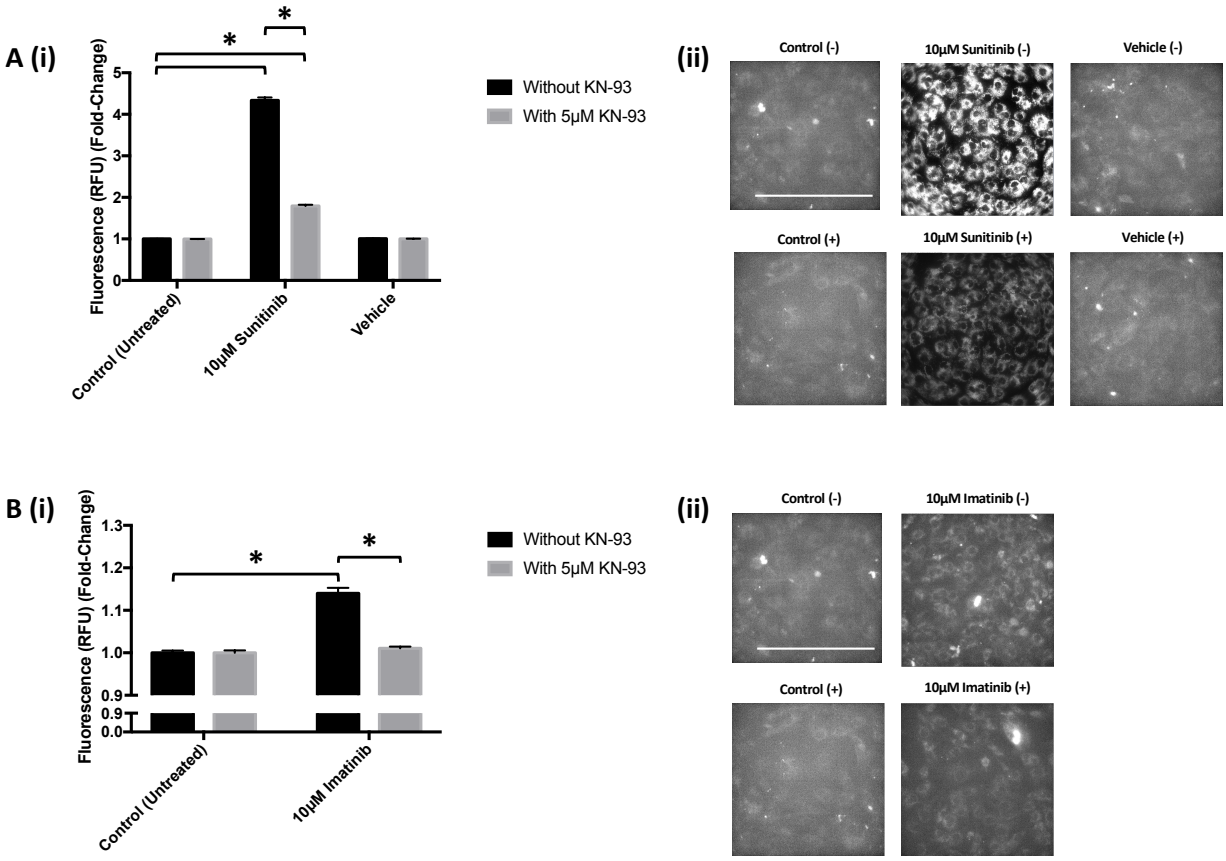


**Figure 4.4.7. Investigating the effect of CaMKII inhibition on mitochondrial superoxide production in sunitinib or imatinib treated cardiac fibroblasts.** (A(i)) Superoxide production assessed via fluorescence intensity in sunitinib treated CFs in the presence (+) or absence (-) of 5μM KN-93. (A(ii)) Representative images of MitoSOX Red analysis of sunitinib treated samples in the presence (+) or absence (-) of KN-93. (B(i)) Superoxide production assessed via fluorescence intensity in imatinib treated CFs in the presence (+) or absence (-) of KN-93. (B(ii)) Representative images of MitoSOX Red analysis of imatinib treated samples in the presence (+) or absence (-) of KN-93. Scale bar 100μm. Results shown are mean data from one experiment (One n number = fluorescent intensity of 10 cells randomly selected from each image), representative of two other experiments (*$p<0.05$).

These findings suggest a relationship between CaMKII and the mitochondria in the cardiotoxic mechanism of TKIs, particularly with regard to sunitinib. However, it is not known whether CaMKII affects the mitochondria directly or acts via a secondary mediator. In order to better characterise the relationship between CaMKII and the mitochondria, co-localisation analysis was performed. Co-localisation is frequently used to investigate intracellular transport and protein function (Dunn *et al*., 2011). By measuring the interaction between CaMKII and the mitochondrial marker, ATPIF1, this study sought to determine whether TKI treatment caused (i) CaMKII translocation to the mitochondria, (ii) increased mitochondrial CaMKII activation or (iii) if the effects CaMKII has on mitochondrial superoxide production are mediated by pathophysiological changes upstream of the mitochondria. Before performing co-localisation experiments, CaMKIIδ, Ox-CaMKII and ATPIF1 antibodies were first optimised for fluorescent imaging in CFs. For this experiment, the Phos-CaMKII antibody was not optimised for use as there has been no evidence to support changes in Phos-CaMKII expression or activation following TKI treatment. Furthermore, the ATPIF1 antibody is used to identify ATP synthase, a critical part of the mitochondrial electron transport chain (Brand and Nicholls, 2011). As such, the ATPIF1 antibody was used as a mitochondrial marker. Optimisation showed a strong, positive signal for all 3 antibodies (Figure 4.4.8). In the case of CaMKIIδ and Ox-CaMKII, the protein is found throughout the cytoplasm. It should be noted that the signal for Ox-CaMKII is less than that of CaMKIIδ, though the Ox-CaMKII signal is still strong. The ATPIF1 signal, on the other hand, shows predominant perinuclear localisation. There are mitochondria located throughout the cytosol, but they appear to be largely concentrated around the nucleus of the cell. Having determined suitable antibody concentrations for co-localisation, CFs were then treated with sunitinib (1μM) or imatinib (10μM) and then co-stained with CaMKIIδ/ATPIF1 or Ox-CaMKII/ATPIF1 before imaging via confocal microscopy.

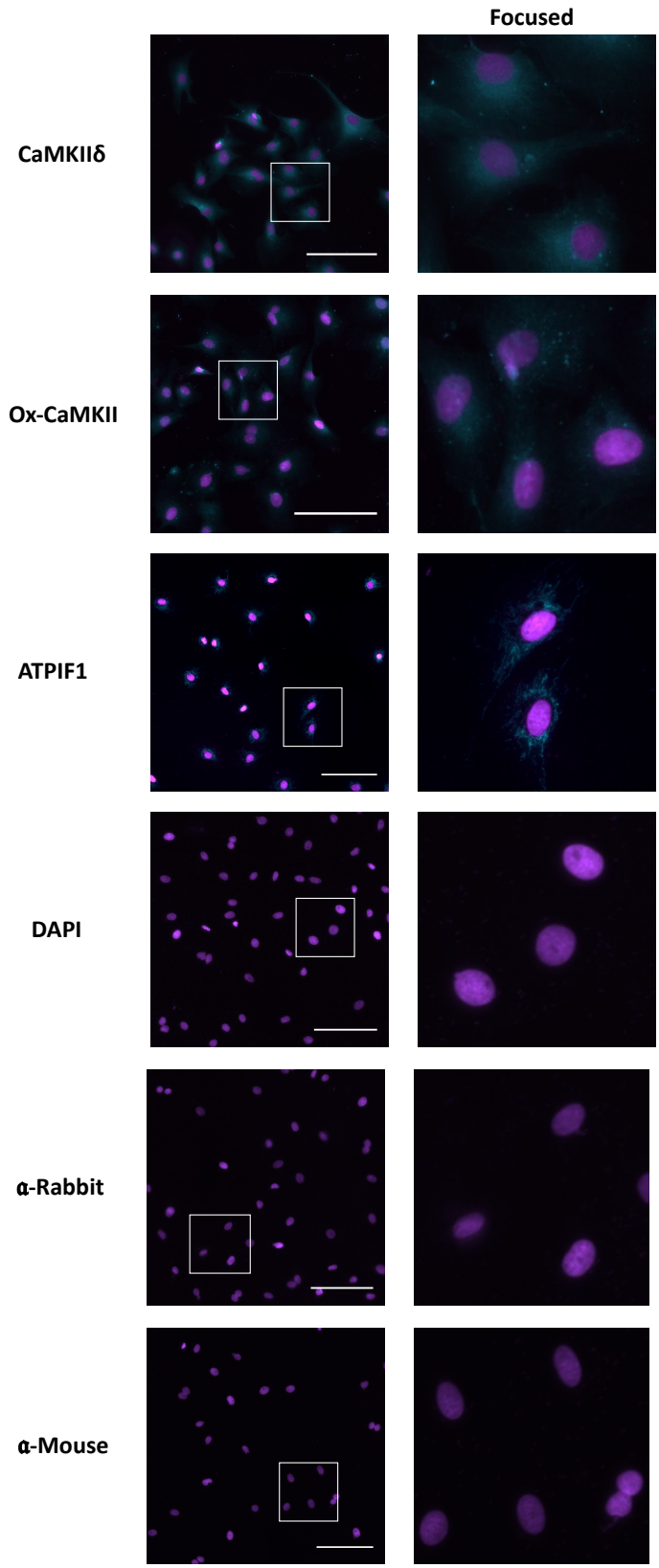


**Figure 4.4.8. Optimisation of antibodies for cardiac fibroblast co-localisation experiments.** Untreated CFs were stained with CaMKIIδ, Ox-CaMKII or the mitochondrial marker ATPIF1. DAPI was used as a nuclear counterstain. Cells treated with DAPI alone and secondary antibodies alone were used as negative controls (n=3). Scale bar 100μm. Images are from one experiment, representative of two others.

Confocal microscopy revealed that neither sunitinib nor imatinib treatment had any effect on CaMKIIδ co-localisation at the mitochondria (Figure 4.4.9). Likewise, there was no change in Ox-CaMKII co-localisation at the mitochondria following TKI treatment either. In both cases, the correlation between the two variables can be described as moderate at best (Akoglu, 2018). In both the vehicle and TKI treated images, CaMKII and the mitochondrial marker can be seen throughout the cytosol. The positioning of these proteins, portrayed clearly in these images, show that CaMKII is located in close proximity to the mitochondria and is unchanged by TKI treatment.

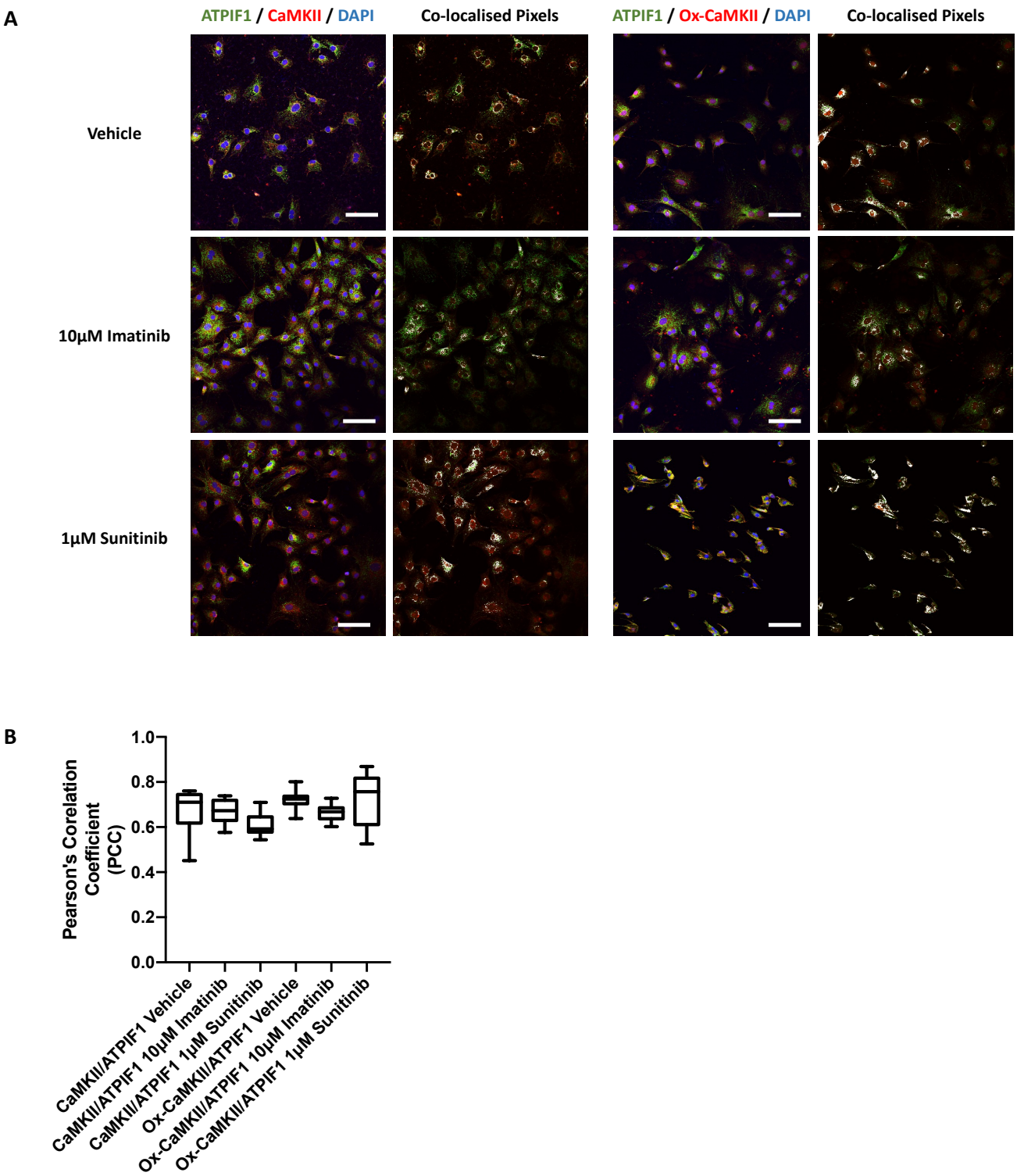


**Figure 4.4.9. Investigating whether TKI treatment influences CaMKII translocation to the mitochondria in cardiac fibroblasts.** CFs were treated with sunitinib (1μM) or imatinib (10μM) and then double stained with CaMKIIδ/ATPIF1 or Ox-CaMKII/ATPIF1. (A) Representative co-localisation images. (B) Protein interaction determined via Pearson's correlation coefficient. DAPI was used as a nuclear counterstain. Cells treated with DAPI alone and secondary antibodies alone were used as negative controls (n=3). Scale bar 100μm. Images are from one experiment, representative of two others.

Having established that TKI treatment does not affect CaMKII co-localisation with the mitochondria, the study then sought to investigate whether this relationship is altered by TKI treatment in PCMs. CaMKIIδ, Ox-CaMKII and ATPIF1 antibodies were first optimised for fluorescent imaging in PCMs. All three antibodies produced a strong, positive signal (Figure 4.4.10. Again, CaMKIIδ and Ox-CaMKII were found throughout the cytoplasm. Interestingly, the mitochondrial marker, ATPIF1, was evenly distributed throughout the cell in PCMs. This is in contrast to what was seen in CFs where ATPIF1 was predominantly concentrated around the nucleus (Figure 4.4.10). The change in PCM ATPIF1 expression is, however, consistent with what is seen in CM cell types, given that CMs are densely populated with mitochondria to facilitate their contractile function (Stride *et al*., 2013).

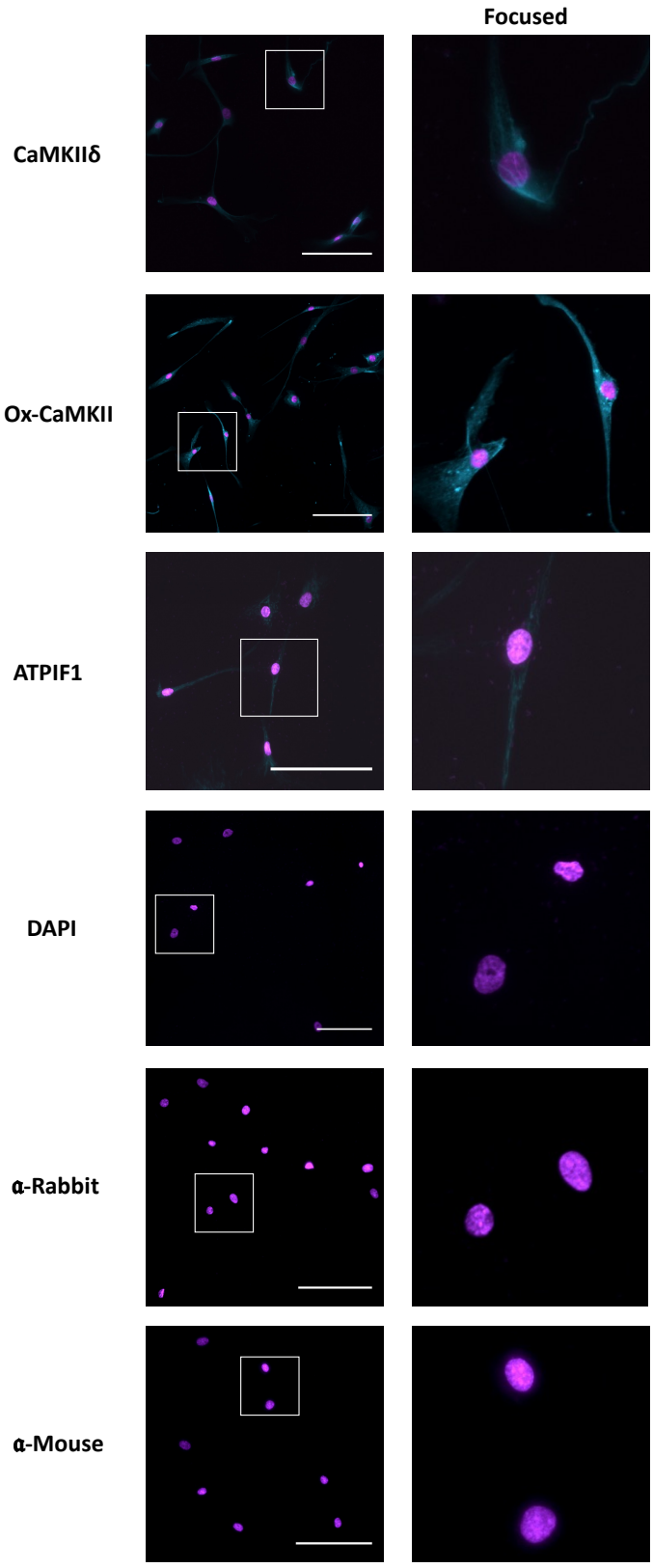


**Figure 4.4.10 Optimisation of antibodies for progenitor cardiac myocyte co-localisation experiments.** Untreated PCMs were stained with CaMKIIδ, Ox-CaMKII or the mitochondrial marker ATPIF1. DAPI was used as a nuclear counterstain. Cells treated with DAPI alone and secondary antibodies alone were used as negative controls (n=3). Scale bar 100μm. Images are from one experiment, representative of two others.

The optimised antibody conditions were then used to determine changes in co-localisation subsequent to TKI treatment. The images show that CaMKIIδ/ATPIF1 co-localisation is unaffected by TKI treatment (Figure 4.4.11A). Interestingly, sunitinib treatment appears to reduce Ox-CaMKII/ATPIF1 co-localisation in PCMs. This assumption is confirmed via the Pearson's correlation coefficient, showing a modest, yet significant, reduction in Ox-CaMKII/ATPIF1 co-localisation (Figure 4.4.11B). Imatinib treatment did not affect Ox-CaMKII/ATPIF1 co-localisation in PCMs.

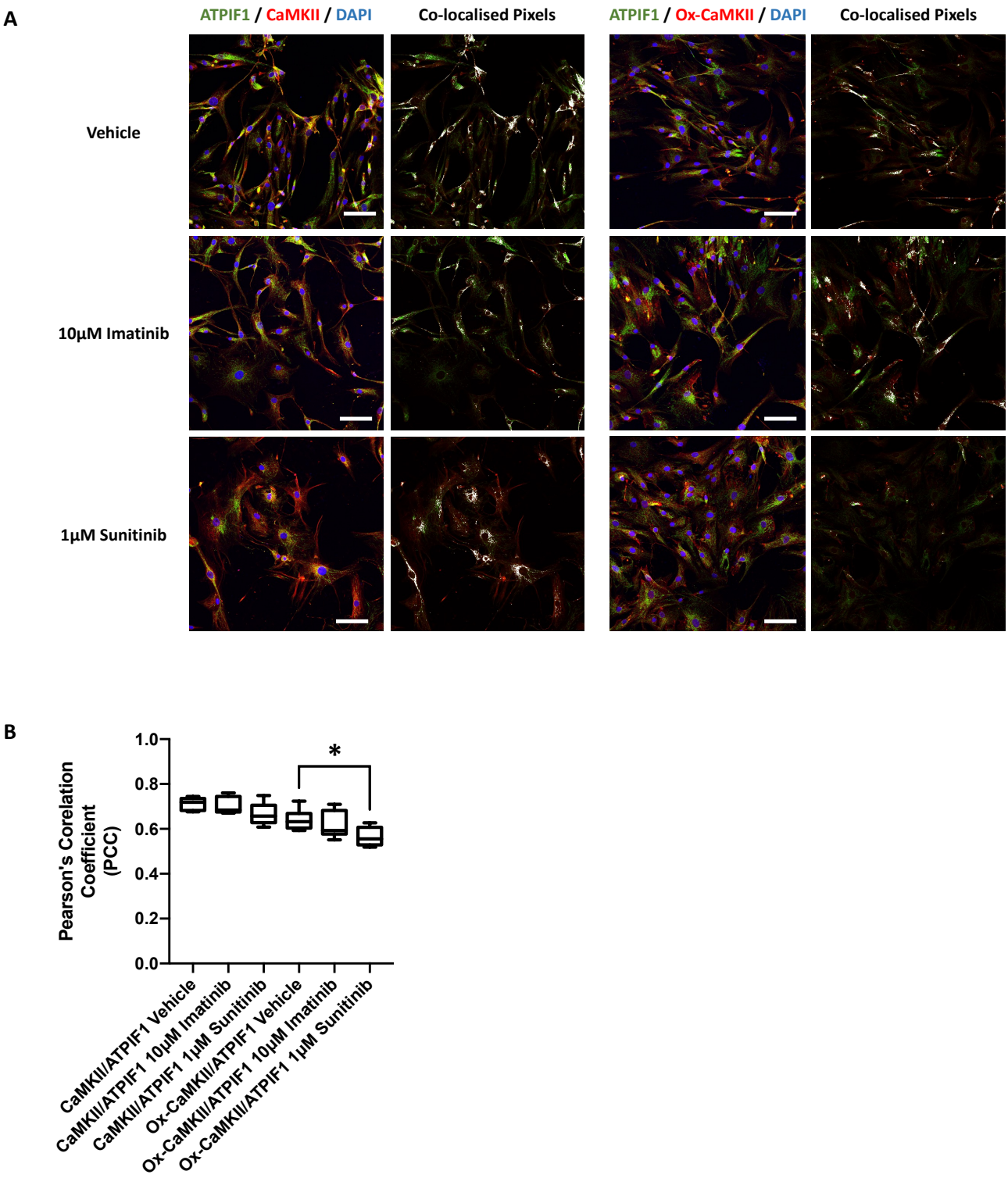


**Figure 4.4.11. Investigating whether TKI treatment influences CaMKII translocation to the mitochondria in progenitor cardiac myocytes.** PCMs were treated with sunitinib (1μM) or imatinib (10μM) and then co-stained with CaMKIIδ/ATPIF1 or Ox-CaMKII/ATPIF1. (A) Representative co-localisation images. (B) Protein interaction determined via Pearson's correlation coefficient. DAPI was used as a nuclear counterstain. Cells treated with DAPI alone and secondary antibodies alone were used as negative controls (n=3, *p<0.05). Scale bar 100μm. Images are from one experiment, representative of two others.

The results presented in this chapter support a role for the mitochondria in the cardiotoxic mechanism of TKIs, particularly sunitinib, in both cell types. In CFs, TKI treatment was found to increase mitochondrial superoxide production, indicative of mitochondrial dysfunction. These findings also highlighted a role for CaMKII, showing that this increase in mitochondrial superoxide production could be attenuated by CaMKII inhibition. In PCMs, the evidence of mitochondrial dysfunction was, admittedly, less clear, though one could argue that the sunitinib-induced reduction in Ox-CaMKII/ATPIF1 co-localisation may reflect a reduction in the mitochondrial marker ATPIF1. ATPIF1 is used to detect ATP synthase, a critical component of the mitochondrial electron transport chain that affords the mitochondria their primary function – ATP production. Therefore, a reduction in ATPIF1 expression would be consistent with a reduction in ATP production, as has been reported previously (Kerkela *et al*., 2006). These findings therefore warrant further investigation into the effect TKI treatment has on mitochondrial function.

OXPHOS is a mitochondrial metabolic pathway which couples electron transfer to proton translocation across the inner mitochondrial membrane to facilitate ATP production (Bergman and Ben-Shachar, 2016). The process requires oxygen and, as such, mitochondrial respiration can be measured to assess mitochondrial activity (Djafarzadeh and Jakob, 2017). The Oroboros O2k is a high-resolution oxygraph that has been used previously to infer TKI-induced changes in mitochondrial function in a liver tumour cell line (Paech *et al*., 2017). Having established that TKI treatment increases mitochondrial superoxide production, this study planned to utilise the Oroboros O2k to explore TKI-mediated effects on mitochondrial function in more detail. The protocol used to assess mitochondrial respiration was first optimised using untreated CFs. The optimisation process proved successful and found that the substrates, uncouplers and inhibitors were suitable in inducing the different states of mitochondrial bioenergetics in CFs (Figure 4.4.12). However, the optimisation process did reveal that the untreated CFs had limited spare respiratory

capacity, suggesting they were stressed and already working close to their full potential to meet metabolic demand. Unfortunately, due to the impact of the COVID-19 pandemic, the optimisation process could not be repeated and the effect of TKI treatment could not be assessed in either CFs or PCMs. These experiments were conducted in the laboratory of Dr John Mercer (University of Glasgow) and restrictions implemented as a result of the pandemic meant that the facilities at the University of Glasgow could not be accessed. Regrettably, this meant that the work assessing the impact of TKI treatment on mitochondrial bioenergetics could not be completed.

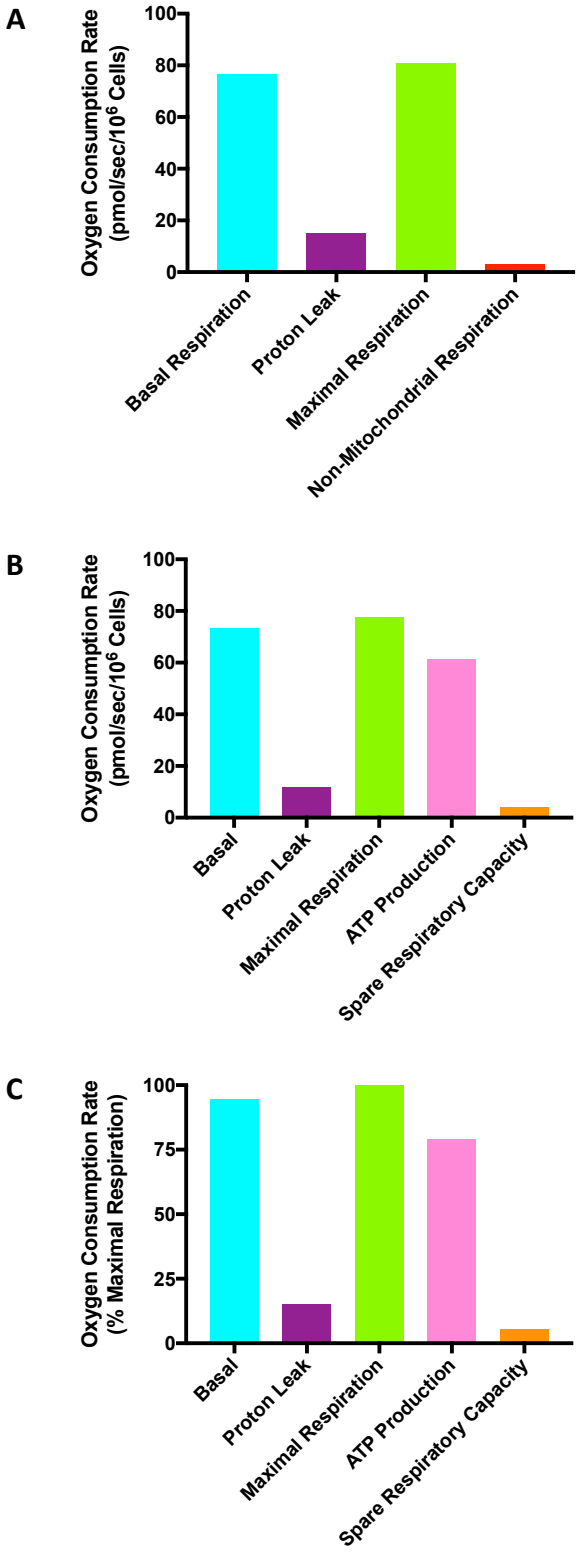


**Figure 4.4.12. Optimisation of the protocol for assessing mitochondrial bioenergetics in untreated cardiac fibroblasts.** (A) Raw data obtained from the Oroboros O2k. The raw data was then used to calculate the cellular bioenergetics as described in Chapter 2, Section 2.3.15 (Graph colours correspond with those used to explain how cellular bioenergetics are calculated (Figure 2.3.18.1)). (B) Oxygen consumption relative to CF cellular bioenergetics, corrected for non-mitochondrial respiration. (C) Oxygen consumption, presented as a percentage of maximal respiration (maximum oxygen consumption) (n=1).

*4.5 KN-93 pre-treatment does not reduce TKI-induced cardiac cell death*

The results presented thus far suggest that CaMKII may mediate the cardiotoxic effects of TKIs. There is evidence that sunitinib can cause activation of CaMKII via oxidation in CFs (Figure 4.3.5). CaMKII inhibition via KN-93 significantly reduced superoxide production in sunitinib treated CFs and completely abolished the increased superoxide production in imatinib treated CFs (Figure 4.4.7), suggesting a potential cardioprotective effect at the level of the mitochondria. CaMKII inhibition has previously shown therapeutic potential in numerous animal models of cardiac pathology. Daniels (2018) showed that CaMKII inhibition improved cardiac contractility and relaxation in a rat model of diabetic cardiomyopathy. Similarly, Beauverger (2020) found that CaMKII inhibition significantly improved cardiac output in a murine model of dilated cardiomyopathy. The therapeutic potential of CaMKII inhibition has also been highlighted in a cellular setting, with CaMKII inhibition preventing CM hypertrophy in a cellular model of HF (Pyun *et al*., 2018). In the current study, the reduction in superoxide generation following CaMKII inhibition may correlate with reduced cell death or perhaps prevent the toxic effect on cardiac cells completely.

In order to determine whether CaMKII mediates the cardiotoxic mechanism of TKIs and if targeted CaMKII inhibition can reduce or reverse cellular toxicity, CFs were pre-treated with the CaMKII inhibitor KN-93 before treatment with sunitinib or imatinib (0.1-10μM). Treated cells were then analysed via FACS, as described previously in Chapter 2 (section 2.3.11). In KN-93 pre-treated CFs, sunitinib treatment significantly reduced the number of healthy cells across all of the concentrations tested (Figure 4.5.1Bi). The reduction in healthy cells was accompanied by a concurrent increase in the number of early (Figure 4.5.1Bii) and late apoptotic cells (Figure 4.5.1Biii) at 10μM sunitinib and an increase

in necrotic cells from 1μM sunitinib (Figure 4.5.1Biv). For the most part, the mechanism of sunitinib toxicity appears to be caused by necrotic cell death. However, at 10μM sunitinib, cell death appears to occur largely by apoptosis and not by the predominantly necrotic mechanism seen at lower concentrations. Imatinib treatment on the other hand appears to have little effect on CFs in the presence of KN-93. 10μM imatinib did cause a small but significant increase in the number of early apoptotic cells (Figure 4.5.2Bii), though this occurred alongside a concomitant reduction in the number of late apoptotic cells (Figure 4.5.2Biii).

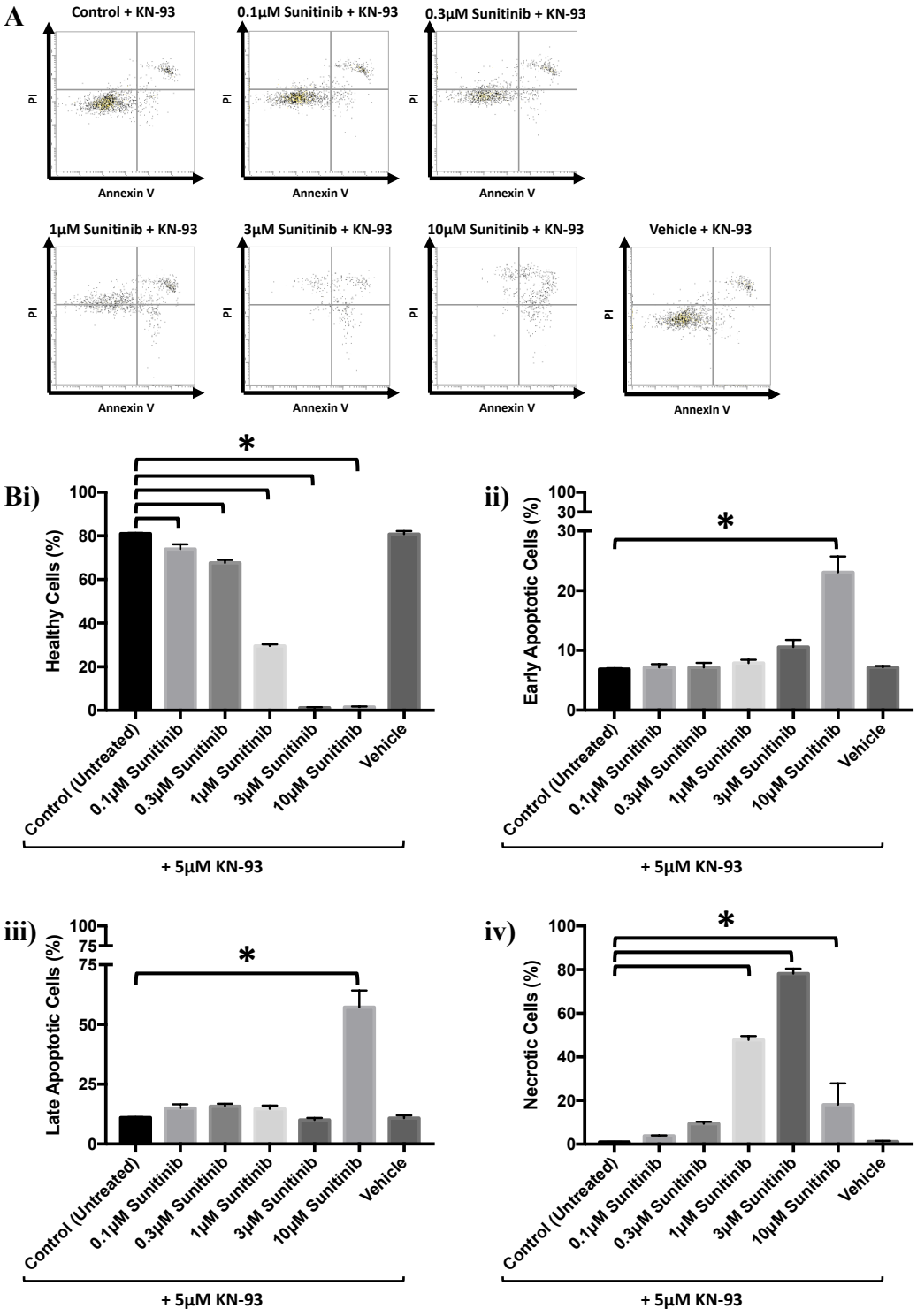


**Figure 4.5.1. Investigating whether CaMKII inhibition has any effect on sunitinib-induced cell death parameters in cardiac fibroblasts.** CFs were pre-treated with 5µM KN-93 and then treated with sunitinib (0.1-10µM) in the presence of serum. Cell viability was determined by PI and AnV staining. (A) Representative flow cytometry dot plots with double Annexin V-APC/PI staining for cells treated with sunitinib + 5µM KN-93. (B) Histograms detailing the percentage of (i) healthy (ii) early apoptotic (iii) late apoptotic and (iv) necrotic cells following treatment with sunitinib + 5µM KN-93. Results are expressed as mean ± S.E.M (n=3, *p<0.05).

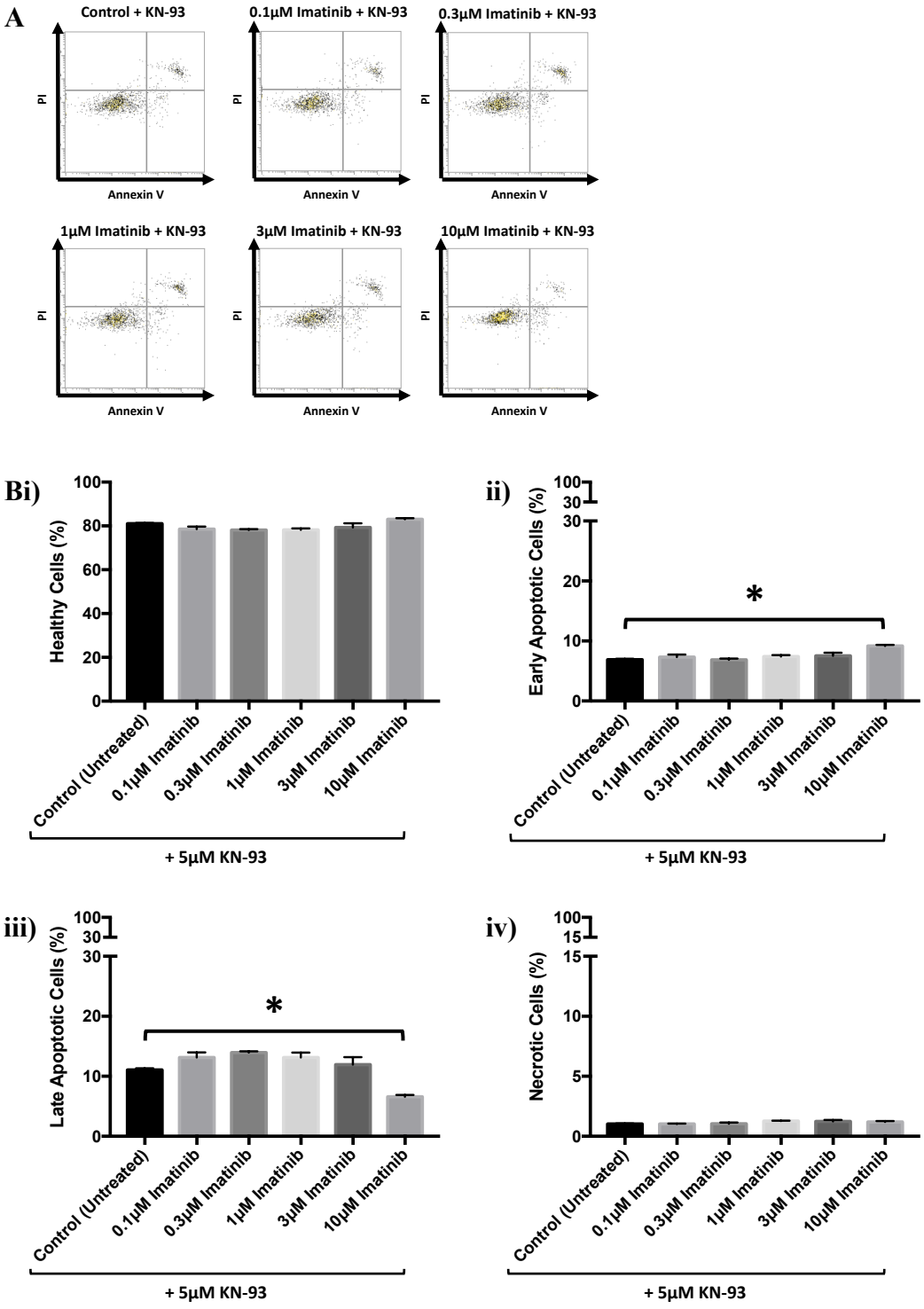


**Figure 4.5.2. Investigating whether CaMKII inhibition has any effect on imatinib-induced cell death parameters in cardiac fibroblasts.** CFs were pre-treated with 5µM KN-93 and then treated with imatinib (0.1-10µM) in the presence of serum. Cell viability was determined by PI and AnV staining. (A) Representative flow cytometry dot plots with double Annexin V-APC/PI staining for cells treated with imatinib + 5µM KN-93. (B) Histograms detailing the percentage of (i) healthy (ii) early apoptotic (iii) late apoptotic and (iv) necrotic cells following treatment with imatinib + 5µM KN-93. Results are expressed as mean ± S.E.M (n=3, *p<0.05).

A comparison of CFs treated with TKIs, both with and without KN-93 pre-treatment, shows clear differences between the number healthy, apoptotic and necrotic cells. However, these results must be interpreted cautiously. The data sets were obtained using two different instruments; TKI-treated CF samples without KN-93 pre-treatment were obtained using the BD FACSCanto II Flow Cytometer, while TKI-treated CF samples with KN-93 pre-treatment were procured using the much newer Attune NxT Flow Cytometer. Although the two sample sets seem quite different, a similar pattern exists in both the presence and absence of KN-93. Both in the presence and absence of KN-93, the toxic effect of sunitinib treatment is clear at higher concentrations (3-10μM), reducing the number of healthy cells and increasing the number of apoptotic and necrotic cells (Figure 4.5.3). Imatinib treatment, both in the presence and absence of KN-93, was much less potent, no effect observed (Figure 4.5.4). Though a slight difference was seen in the ratio of early to late apoptotic cells in the presence of KN-93, generally speaking there was no change in the number of healthy, apoptotic or necrotic cells following imatinib treatment, both with KN-93 pre-treatment and without.

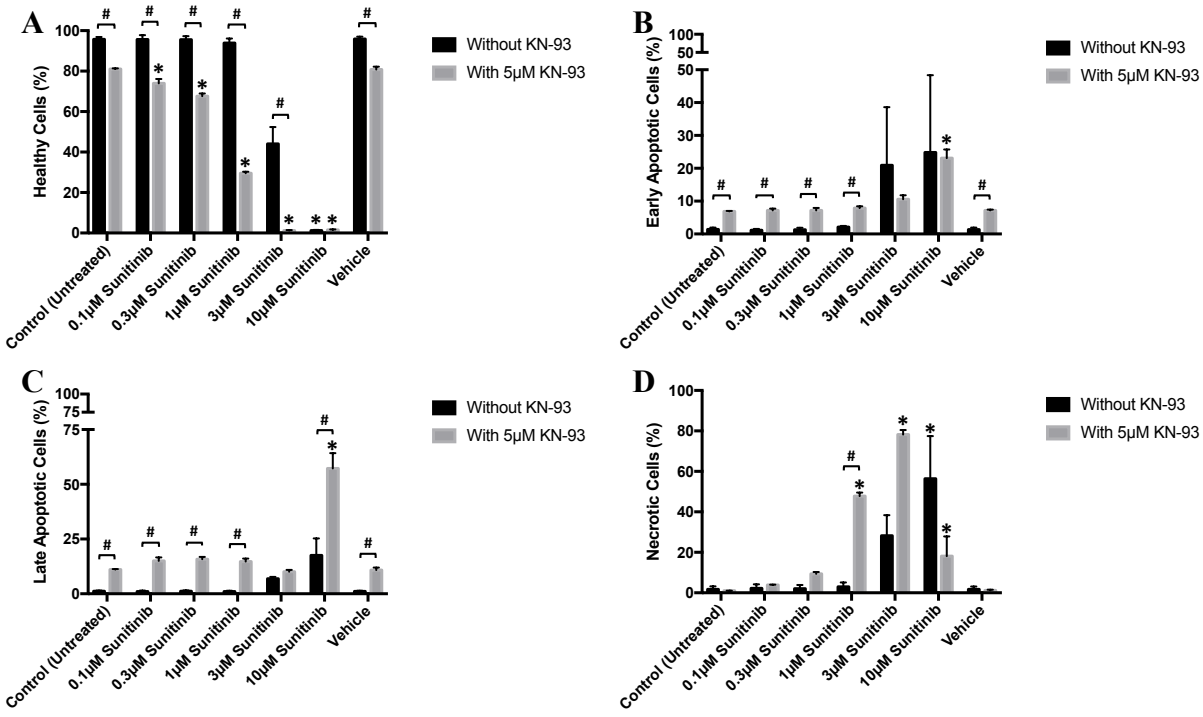


**Figure 4.5.3. A comparison of the effect of CaMKII inhibition via KN-93 on sunitinib-induced cell death parameters in cardiac fibroblasts.** CFs were treated with sunitinib (0.1-10μM) in the presence of serum, with and without pre-treated with 5μM KN-93. Cell viability was determined by double Annexin V-APC/PI staining. Histograms detailing the percentage of (A) healthy (B) early apoptotic (C) late apoptotic and (D) necrotic cells. Results are expressed as mean ± S.E.M (n=3, *$p<0.05$ vs respective untreated control, $^{\#}p<0.05$ non-KN-93 pre-treated sample vs KN-93 pre-treated sample).

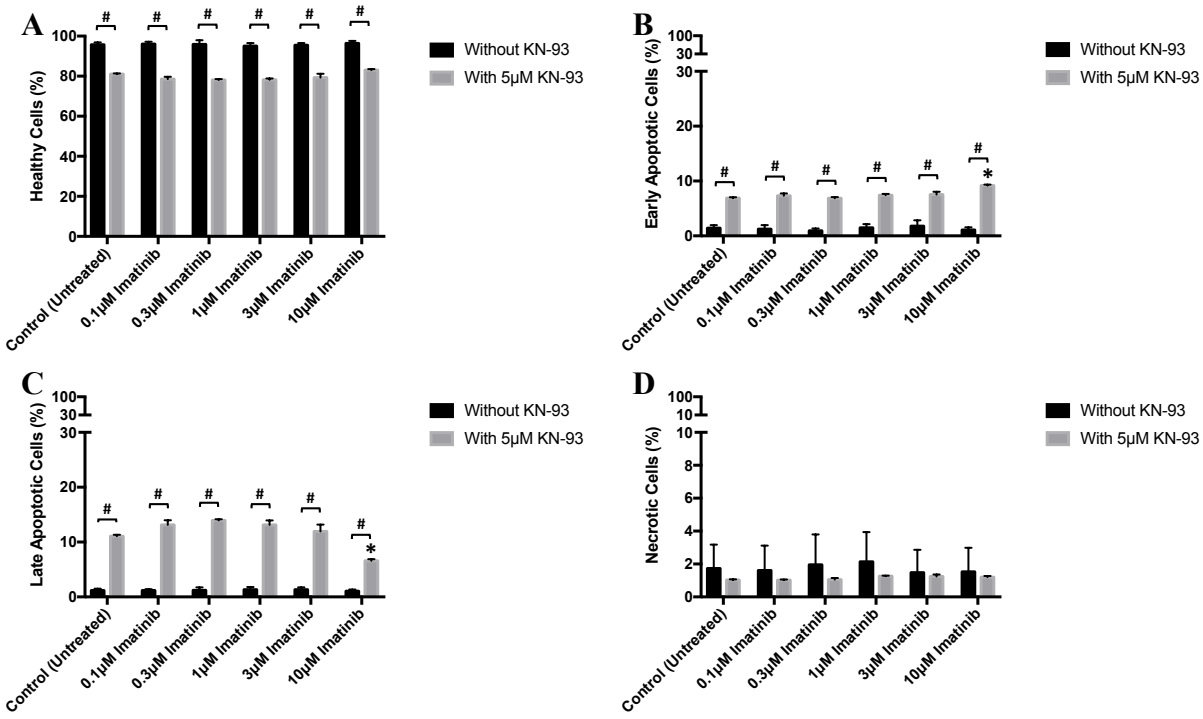


**Figure 4.5.4. A comparison of the effect of CaMKII inhibition via KN-93 on imatinib-induced cell death parameters in cardiac fibroblasts.** CFs were treated with imatinib (0.1-10μM) in the presence of serum, with and without pre-treated with 5μM KN-93. Cell viability was determined by double Annexin V-APC/PI staining. Histograms detailing the percentage of (A) healthy (B) early apoptotic (C) late apoptotic and (D) necrotic cells. Results are expressed as mean ± S.E.M (n=3, *$p<0.05$ vs respective untreated control, $^{\#}p<0.05$ non-KN-93 pre-treated sample vs KN-93 pre-treated sample).

The effect of KN-93 pre-treatment was also evaluated in PCMs, allowing the comparison between the two cell types. In the presence of KN-93, sunitinib treatment significantly reduced the number of healthy PCMs, reaching significance at 0.3μM sunitinib (Figure 4.5.5Bi). The reduction in healthy cells was accompanied by a concurrent increase in the number of late apoptotic cells at 10μM sunitinib (Figure 4.5.5Biii) and the number of necrotic cells from 1μM sunitinib (Figure 4.5.5Biv). Imatinib treatment, in the presence of KN-93, had no effect on PCM viability (Figure 4.5.6).

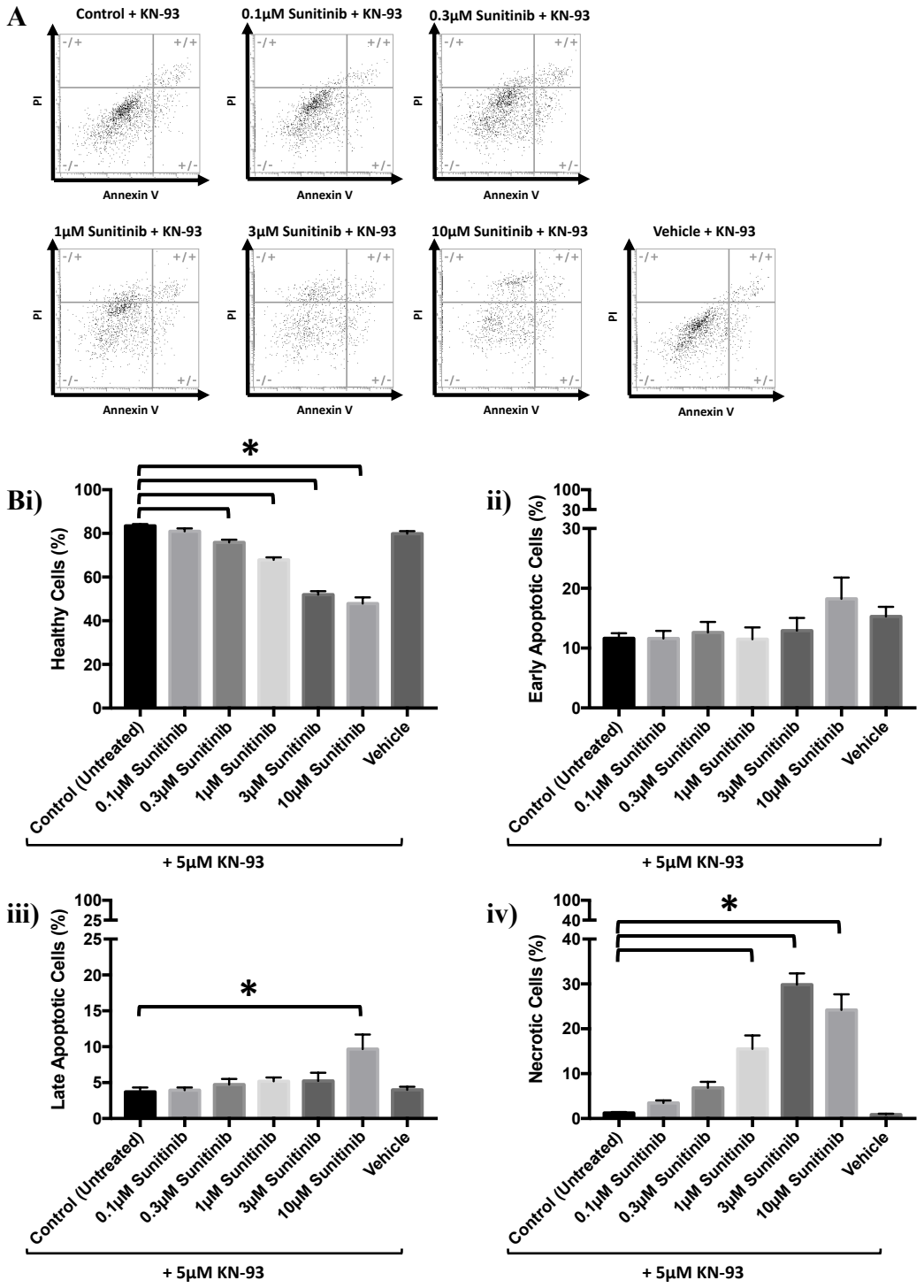


**Figure 4.5.5. Investigating whether CaMKII inhibition has any effect on sunitinib-induced cell death parameters in progenitor cardiac myocytes.** PCMs were pre-treated with 5µM KN-93 and then treated with sunitinib (0.1-10µM) in the presence of serum. Cell viability was determined by PI and AnV staining. (A) Representative flow cytometry dot plots with double Annexin V-APC/PI staining for cells treated with sunitinib + 5µM KN-93. (B) Histograms detailing the percentage of (i) healthy (ii) early apoptotic (iii) late apoptotic and (iv) necrotic cells following treatment with sunitinib + 5µM KN-93. Results are expressed as mean ± S.E.M (n=3, *p<0.05).

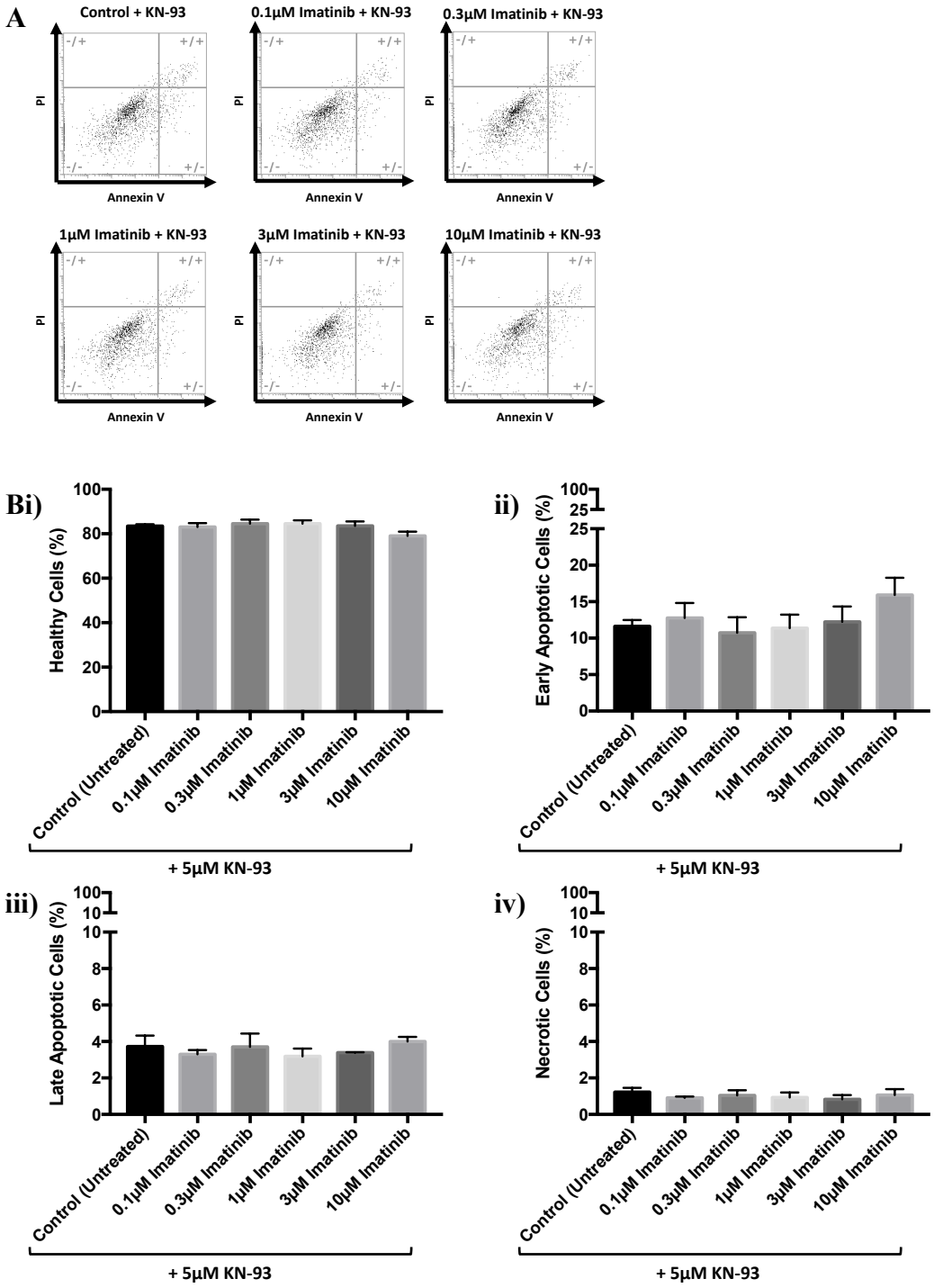


**Figure 4.5.6. Investigating whether CaMKII inhibition has any effect on imatinib-induced cell death parameters in progenitor cardiac myocytes.** PCMs were pre-treated with 5µM KN-93 and then treated with imatinib (0.1-10µM) in the presence of serum. Cell viability was determined by PI and AnV staining. (A) Representative flow cytometry dot plots with double Annexin V-APC/PI staining for cells treated with imatinib + 5µM KN-93. (B) Histograms detailing the percentage of (i) healthy (ii) early apoptotic (iii) late apoptotic and (iv) necrotic cells following treatment with imatinib + 5µM KN-93. Results are expressed as mean ± S.E.M (n=3).

A comparison of the effect of KN-93 pre-treatment in PCMs shows no difference. Both in the presence and absence of KN-93, sunitinib treatment showed a significant reduction in the number of healthy PCMs at concentrations of 1μM and above, with an affiliated increase in the number necrotic cells at the same concentrations (Figure 4.5.7). Also, a significant increase in the number of late apoptotic cells was seen at 10μM sunitinib in both instances. Imatinib treatment had no effect in PCMs viability, both in the presence and absence of KN-93 (Figure 4.5.8).

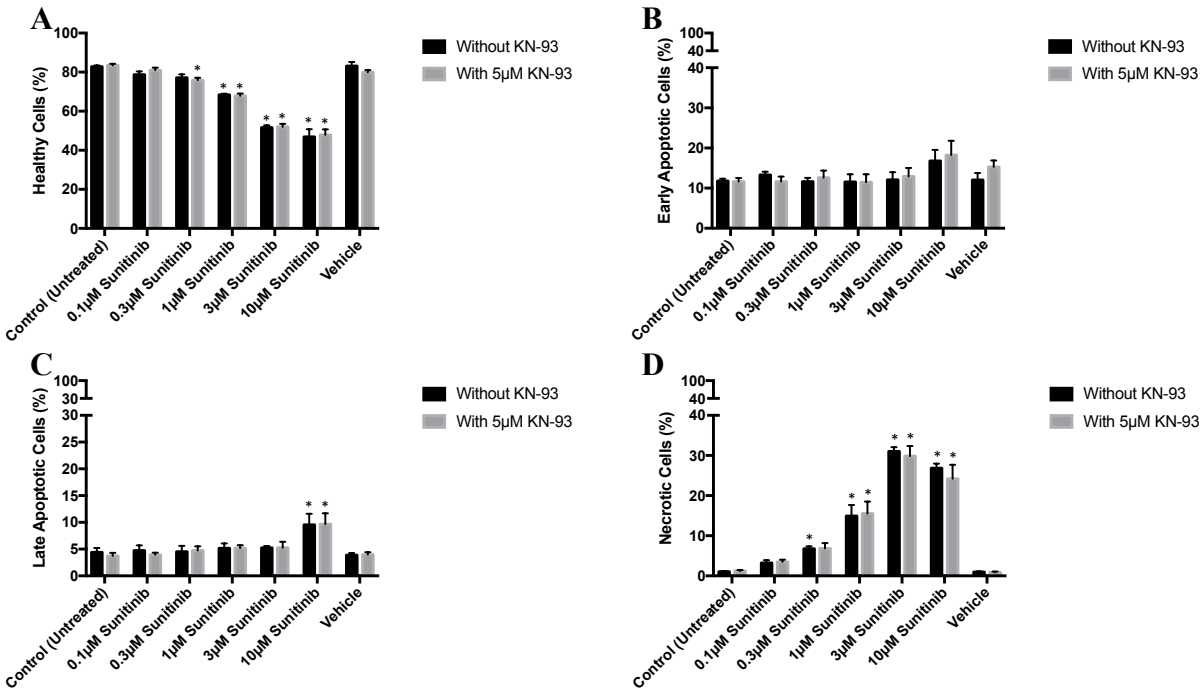


**Figure 4.5.7. A comparison of the effect of CaMKII inhibition via KN-93 on sunitinib-induced cell death parameters in progenitor cardiac myocytes.** PCMs were treated with sunitinib (0.1-10μM) in the presence of serum, with and without pre-treatment with 5μM KN-93. Cell viability was determined by double Annexin V-APC/PI staining. Histograms detailing the percentage of (A) healthy (B) early apoptotic (C) late apoptotic and (D) necrotic cells. Results are expressed as mean ± S.E.M (n=3, *p<0.05 vs respective untreated control).

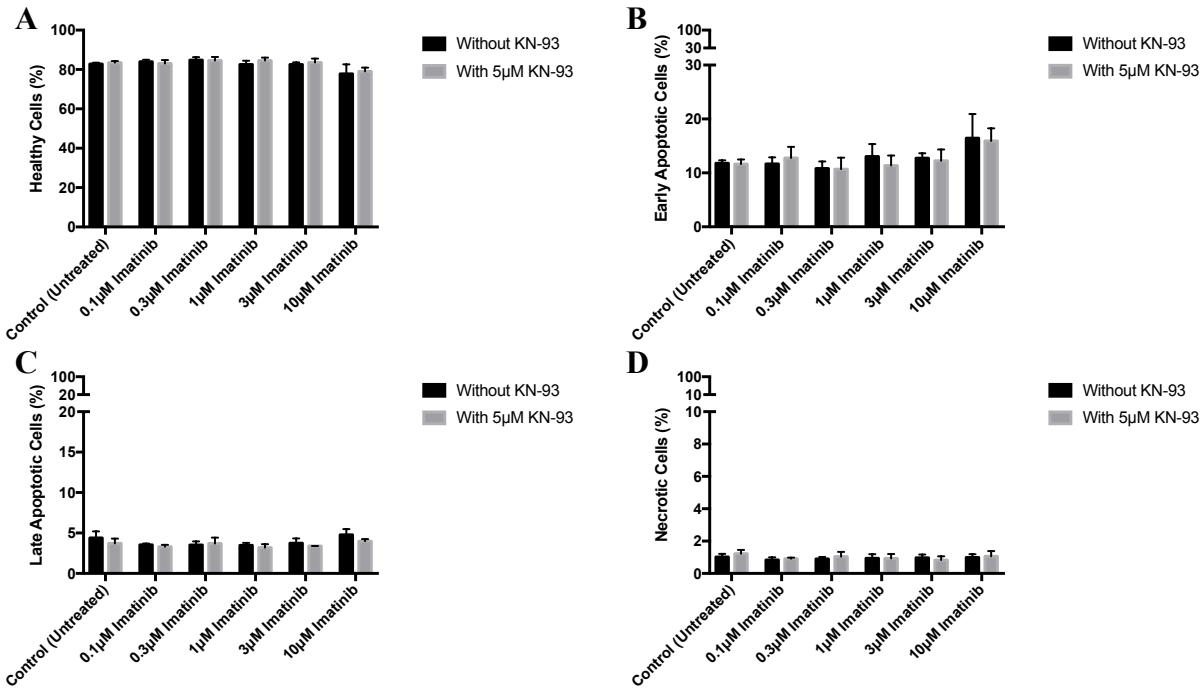


**Figure 4.5.8. A comparison of the effect of CaMKII inhibition via KN-93 on imatinib-induced cell death parameters in progenitor cardiac myocytes.** PCMs were treated with imatinib (0.1-10μM) in the presence of serum, with and without pre-treated with 5μM KN-93. Cell viability was determined by double Annexin V-APC/PI staining. Histograms detailing the percentage of (A) healthy (B) early apoptotic (C) late apoptotic and (D) necrotic cells. Results are expressed as mean ± S.E.M (n=3).

*4.6 CaMKII inhibition via KN-93 does not attenuate sunitinib-induced changes in intracellular calcium*

Having established that CaMKII inhibition did not attenuate sunitinib induced cell death, the effect of CaMKII inhibition on the proposed cardiotoxic mechanism of TKIs was further investigated. The proposed hypothesis is that TKIs mediate cardiotoxicity at the level of the mitochondria, and the proposed mitochondrial toxicity is believed to be initiated by changes in intracellular $Ca^{2+}$and may involve changes in CaMKII. The findings presented in this study support a $Ca^{2+}$-mediated, mitochondrial mechanism involving aberrant CaMKII activity, as do those of Kerkela (2006) and Mooney (2015). However, inhibition of the $Ca^{2+}$ handling protein, CaMKII, did not reduce TKI-mediated cell death. This suggests that either (i) CaMKII does not mediate the cardiotoxic mechanism of TKIs; or (ii) The inhibition of CaMKII was not sufficient to attenuate cell death. To evaluate this, the effect of CaMKII inhibition on TKI-induced changes in intracellular $Ca^{2+}$ was assessed. In CFs pre-treated with KN-93, sunitinib treatment increased intracellular $Ca^{2+}$ mobilisation, reaching significance at 1μM (Figure 4.6.1A and 4.6.1B). Imatinib meanwhile had no effect on intracellular $Ca^{2+}$ in KN-93 pre-treated CFs (Figure 4.6.1C and 4.6.1D).

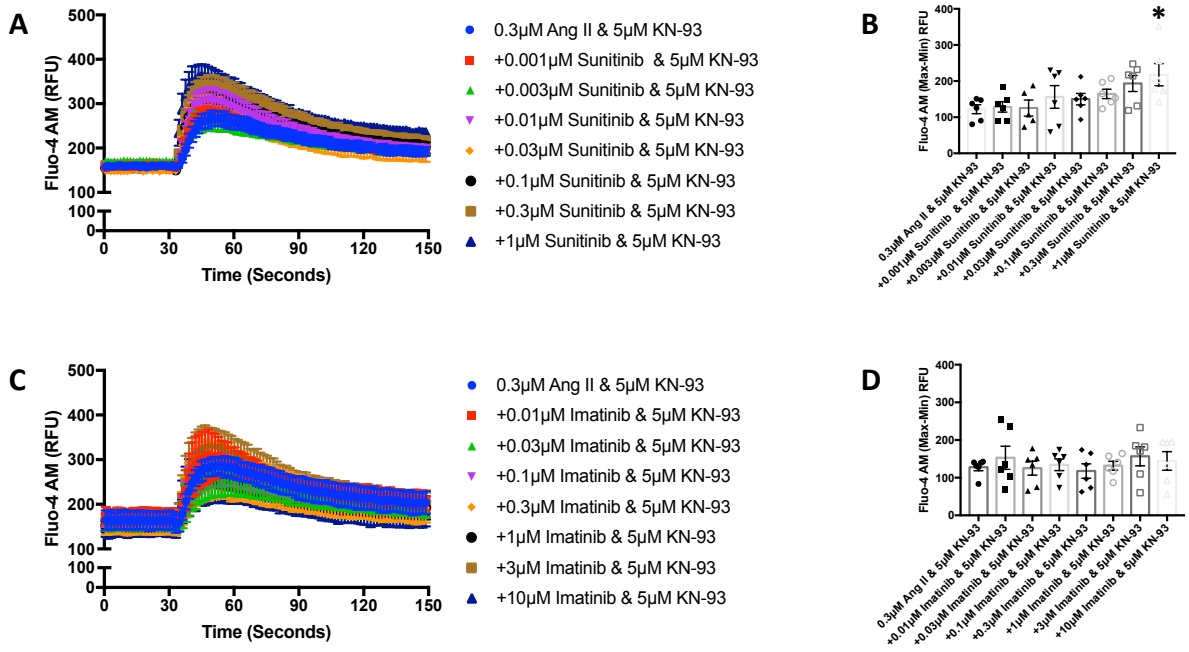


**Figure 4.6.1. Determining the effect of CaMKII inhibition on angiotensin II–induced intracellular calcium mobilisation in cardiac fibroblasts pre-treated with sunitinib or imatinib.** (A) Representative trace of intracellular $Ca^{2+}$ release in response to 0.3μM Ang II stimulation following pre-treatment with increasing concentrations of sunitinib (0.001-1μM) and 5μM KN-93. (B) Changes in $Ca^{2+}$ flux following 0.3μM Ang II stimulation in CFs treated with sunitinib and KN-93. (C) Representative trace of intracellular $Ca^{2+}$ release in response to 0.3μM Ang II stimulation following pre-treatment with increasing concentrations of imatinib (0.01-10μM) and 5μM KN-93. (D) Changes in $Ca^{2+}$ flux following 0.3μM Ang II stimulation in CFs treated with imatinib and KN-93. $Ca^{2+}$ mobilisation was determined by measuring fluorescence at Ex:494/Em:525nm. Results are expressed as mean ± S.E.M (n=4, *p<0.05 vs respective untreated control).

A comparison of KN-93 pre-treatment on Ang II induced $Ca^{2+}$ mobilisation in TKI treated CFs shows no significant change (Figure 4.6.2). Though it is clear that KN-93 pre-treatment does reduce $Ca^{2+}$ mobilisation, the reduction is not statistically significant. This may explain why CaMKII inhibition did not mitigate TKI-induced CF cell death. More comprehensive CaMKII inhibition strategies must be utilised to verify this in future. Given that no change in $Ca^{2+}$ mobility was seen in PCMs, the effect of CaMKII inhibition was not evaluated further in this cell type.

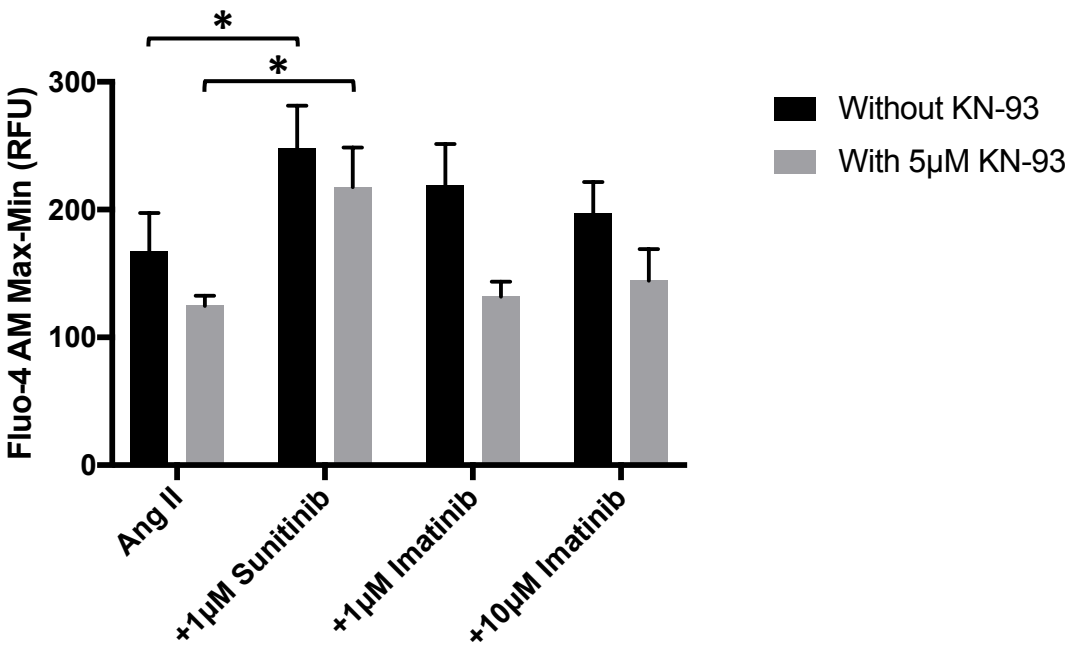


**Figure 4.6.2. A comparison of the effect of CaMKII inhibition via KN-93 on angiotensin II-induced intracellular calcium release in cardiac fibroblasts pre-treated with sunitinib or imatinib.** A comparison of $Ca^{2+}$ flux in CFs treated with sunitinib (1μM) and imatinib (1&10μM), in the presence of serum, with and without pre-treated with 5μM KN-93. $Ca^{2+}$ mobilisation was determined by measuring fluorescence at Ex:494/Em:525nm. Results are expressed as mean ± S.E.M (n=4, *p<0.05 vs respective untreated control).

*4.7 Discussion*

The aim of this chapter was to investigate the cardiotoxic mechanism of the TKIs sunitinib and imatinib and establish whether the pathophysiological changes that underpin TKI-induced cardiotoxicity differ between cell types. Several studies have shown that TKI treatment impairs mitochondrial function, but it is not clear whether these effects are caused by mitochondrial toxicity directly or are a consequence of pathological changes upstream of the organelle. The findings presented in this chapter investigate the effect of TKI treatment at the level of the mitochondria and highlight a potential role for CaMKII in mediating the cardiotoxic mechanism of TKIs. The findings presented in this chapter also compare the proposed cardiotoxic mechanism in both CFs and PCMs.

$Ca^{2+}$ plays a key role in several cellular processes, including proliferation (Pinto *et al*., 2016), differentiation (Bae *et al*., 2018), angiogenesis (Kohn *et al*., 1995), muscle contraction and cell death (Bootman *et al*., 2012). These processes are critical to both healthy and cancerous cells, playing a critical role in tumour survival and progression in several cancers. Unsurprisingly then, changes in intracellular [$Ca^{2+}$] are well documented following anticancer drug treatment. The molecular mechanism of the anthracycline, doxorubicin, is known to involve changes in $Ca^{2+}$ homeostasis, affecting both the cancer cells as part of the therapeutic mechanism and the healthy cells as an off-target effect (Micallef and Baron, 2020). This is reflected in the findings of Maillet (2016), who observed a 2.5-fold increase in intracellular [$Ca^{2+}$] concentration in CMs following treatment with 5μM doxorubicin and associated cell death. The findings of this project show similar changes in intracellular [$Ca^{2+}$] handling following sunitinib treatment in CFs (Figure 4.2.2), suggesting that altered $Ca^{2+}$ homeostasis may also be part of the cardiotoxic mechanism of this class of anticancer drug. TKI-induced changes in $Ca^{2+}$ homeostasis was also reported by Kerkela (2006), who

observed $Ca^{2+}$ induced swelling of the mitochondria and opening of the mitochondrial permeability transition pore.

This altered $Ca^{2+}$ handling mediates cell death via the mitochondria. Specifically, the $Ca^{2+}$ flux activates the intrinsic apoptotic pathway, causing cell death via the release of cytochrome c from the mitochondria and caspase activation (Micallef and Baron, 2020). This is a well-established mechanism of cardiac cell death and has been linked to the pathology of HF (Joiner *et al*., 2012; Lu *et al*., 2016) and doxorubicin induced cardiotoxicity (Maillet *et al*., 2016; Micallef and Baron, 2020). It is also thought to involve changes in mitochondrial ROS production. Maillet *et al*. (2016) showed that doxorubicin treatment increased superoxide production in a concentration-dependent manner, with a significant increase in superoxide production seen at 5μM doxorubicin, the same concentration of doxorubicin shown to increase intracellular $Ca^{2+}$ mobility. Mukhopadhyay (2009) also found that doxorubicin increased superoxide production in mitochondria isolated from doxorubicin treated mice. In both of these studies, the increase in superoxide production was associated with reduced cell viability (Mukhopadhyay *et al*., 2009; Maillet *et al*., 2016).

TKI treatment has also been shown to increase mitochondrial ROS production. Doherty (2013) showed that the TKIs crizotinib and nilotinib increased ROS generation in cardiac cells and suggested that the change in ROS production may instigate cell death. Interestingly, the same study did not find a significant change in ROS production following sunitinib treatment, contradicting the findings of this project (Figure 4.4.6). However, it should be noted that the fluorescent dihydroethidium (DHE) dye method used to measure ROS production in the study by Doherty was different to the MitoSOX method used here. Furthermore, Paech (2017) reported that the TKIs sunitinib, imatinib, lapatinib and erlotinib increased ROS production in Hep G2 cells, while imatinib, lapatinib and erlotinib increased

superoxide production, as determined by MitoSOX Red. Surprisingly, Paech was not able to measure changes in superoxide production following sunitinib treatment due to drug auto-fluorescence that interfered with the assay. This was not the case in this project. Here, background readings prior to the addition of MitoSOX Red did not show any issues with drug auto-fluorescence. Though differences exist in the protocols used in this study and that of Paech. The protocol used in this project includes two wash steps prior to loading the MitoSOX Red dye in order to remove any fluorescent drug or medium containing phenol red that could interfere with the fluorescent imaging. The protocol used by Paech did not include these wash steps.

Drug auto-fluorescence did, however, interfere with the DCFDA assay conducted in this study. The assay appeared to show a concentration dependent increase in intracellular ROS production with sunitinib treatment (Figure 4.4.2). However, sunitinib treatment also showed increased fluorescence intensity in the absence of the ROS sensitive, fluorogenic dye, DCFDA. Maillet (2016) also used the DCFDA assay to determine changes in intracellular ROS production, showing a significant increase at 10μM doxorubicin. However, the study did not evaluate possible drug auto-fluorescence. Given that doxorubicin has been associated with auto-fluorescence previously (Mukhopadhyay *et al*., 2007), it is likely that the findings of Maillet were impacted. This in turn may mitigate the proposed role ROS play in the cardiotoxic mechanism of doxorubicin, based on the findings of Maillet. These findings highlight that it is imperative to properly control fluorescent based assays, particularly when drug auto-fluorescence may be a factor. Despite the interference of sunitinib auto-fluorescence in the DCFDA assay, the results of the MitoSOX experiments clearly show an increase in mitochondrial ROS following TKI treatment, consistent with the proposed mechanism of TKI-induced cardiotoxicity.

TKI treatment has also been associated with changes in the expression and activation of the $Ca^{2+}$ handling protein, CaMKII (Mooney *et al*., 2015). CaMKII is known to affect both CMs and CFs, causing impaired cardiac contraction and cardiovascular remodelling. These changes in cardiovascular function are also known symptoms of cardiotoxicity (Kerkela *et al*., 2006; Chu *et al*., 2007; Zamorano *et al*., 2016; Dobbin *et al*., 2018), suggesting a possible role for CaMKII in the toxic mechanism. The findings presented in this study show that TKI treatment did not affect CaMKII expression in either cell type, but sunitinib treatment did increase CaMKII activation via oxidation in CFs. These findings somewhat contradict those of Mooney *et al*. (2015), who found increased CaMKII expression following sunitinib and imatinib treatment. Mooney also found that the increased CaMKII expression was associated with increased phosphorylation of the $Ca^{2+}$ release channel, RyR2. This is consistent with the increase in $Ca^{2+}$ flux seen in this study following sunitinib treatment. It should be noted, however, that there were significant differences in the experimental model used by Mooney and that of the isolated, single cell model used in this study. Mooney used whole-heart cardiac lysates from TKI-treated guinea pigs. The whole heart lysate encompasses all cardiac cell types. Cardiac cells, in particular, are known to influence one another which causes the cells to behave differently when together than they do on their own (Pellman *et al*., 2016). This can significantly alter findings and may account for the differences in CaMKII expression in this study (Figures 4.3.5 and 4.3.7) and that of Mooney.

Palomeque *et al*. (2009) showed that Ang II-induced ROS production increased CaMKII activation, and that this mechanism caused cell death via apoptosis. Ang II is known to facilitate changes in $Ca^{2+}$ flux (Aiello and Cingolani, 2001; Zhuo *et al*., 2006; Currie *et al*., 2016), and Palomeque showed that Ang II also increased ROS production and CaMKII activation. This mechanism bears a striking resemblance to the findings reported in this thesis (Figures 4.3.5, 4.4.6 and 4.4.7). Furthermore, increased CaMKII activation may

compound mitochondrial toxicity in a positive feedback loop. The mitochondrial $Ca^{2+}$ uniporter (MCU) is believed to be a substrate for CaMKII and is the main $Ca^{2+}$ entry point into the mitochondria (Joiner *et al*., 2012). Thereby an increase in CaMKII activation via mitochondrial ROS may in fact increase $Ca^{2+}$ entry into the mitochondria, exacerbating mitochondrial dysfunction in a positive feedback mechanism. As a result, CaMKII may serve as a therapeutic target to reduce or reverse the cardiotoxic mechanism of TKIs.

CaMKII has shown therapeutic potential as a drug target for alleviating symptoms of HF (Kashiwase *et al*., 2005; Sossalla *et al*., 2010; Zhang *et al*., 2010; Suetomi *et al*., 2018; Beauverger *et al*., 2020). Previous studies have shown that CaMKII inhibition improves cardiac contractility in HF (Sossalla *et al*., 2010; Daniels *et al*., 2018; Beauverger *et al*., 2020). Sossalla *et al*. (2010) showed that CaMKII inhibition via KN-93 was associated with increased SR $Ca^{2+}$ content, mediated by reduced RyR phosphorylation. This increase in SR $Ca^{2+}$ content improved contractility in CMs isolated from the hearts of HF patients. More recently, a novel CaMKII inhibitor, RA306, was found to increase cardiac output in a murine model of dilated cardiomyopathy (Beauverger *et al*., 2020). However, inhibition of CaMKII using KN-93 did not attenuate TKI-induced cardiac cell death in this project (Figures 4.5.3, 4.5.4, 4.5.6 and 4.5.8). Further investigation in the present study showed that although CaMKII inhibition did reduce intracellular [$Ca^{2+}$] flux, the reduction was not significant and [$Ca^{2+}$] flux remained significantly increased vs untreated control, even in the presence of KN-93 (Figure 4.5.8). This may explain why CaMKII inhibition did not ameliorate TKI-induced cell death. In the findings of both Sossalla and Beauverger, CaMKII inhibition attenuated intracellular [$Ca^{2+}$] by significantly altering $Ca^{2+}$ handling protein activation. A recent study by Daniels (2018) compared the effect of two different CaMKII inhibitors in restoring cardiac contractility in type II diabetic cardiac muscle. The study found that KN-93, the CaMKII inhibitor used in this project, partially restored cardiac contractility while autocamptide-2 related inhibitor peptide (AIP), an alternative CaMKII inhibitor, fully restored cardiac

contractility. This variance in the efficacy of two inhibitors may be explained by their different mechanisms of action. The seemingly less effective of the two, KN-93, acts outside of the catalytic domain, inhibiting CaMKII activation by blocking calmodulin binding (Daniels *et al*., 2018). In contrast, AIP acts on the catalytic domain, prohibiting the interaction of the activated CaMKII with its substrates. AIP therefore prohibits the autonomous activity of CaMKII that is associated with cardiovascular pathology (Erickson *et al*., 2013; Zhang, 2017; Daniels *et al*., 2018). It is therefore possible that more efficient CaMKII inhibition may reduce or reverse TKI-induced cell death.

The CF data presented in this chapter supports a TKI-induced cardiotoxic mechanism that involves $Ca^{2+}$ dysregulation (Figure 4.2.2), CaMKII activation (Figure 4.3.5) and mitochondrial dysfunction (Figure 4.4.6). However, parallel data obtained in PCMs does not (Figures 4.2.4 and 4.3.7). This is very much in contrast to what has been reported in the literature, with several studies reporting evidence of impaired $Ca^{2+}$ handling, mitochondrial dysfunction and even CaMKII activation in the cardiotoxic mechanism of TKIs obtained in CM cellular models. Kerkela *et al*. (2006) were the first to report mitochondrial abnormalities in NRVMs. The study by Kerkela showed that imatinib treatment collapsed the mitochondrial membrane potential, reducing ATP production and ultimately causing cell death. The same study also highlighted mitochondrial dysfunction in both human and murine hearts following imatinib treatment, with evidence of $Ca^{2+}$ induced swelling of the mitochondria in imatinib treated mice that was associated with impaired ATP production, contractile dysfunction and cardiovascular remodelling. These observations made this study the first to highlight the possible role of altered $Ca^{2+}$ handling and mitochondrial dysfunction in the cardiotoxic mechanism of TKIs. Soon after, Chu *et al*. (2007) also reported sunitinib treatment induced mitochondrial dysfunction and apoptotic cell death in NRVMs. Together, these studies highlight the role of mitochondrial dysfunction in the cardiotoxic mechanism of TKIs and suggest that these changes in mitochondrial function may be mediated by abnormal $Ca^{2+}$

handling. More recently, Barr *et al*. (2014) provided further evidence of $Ca^{2+}$ dysregulation in CMs treated with imatinib. This study showed that imatinib treated CMs had increased peak systolic $Ca^{2+}$ and prolonged $Ca^{2+}$ transients and these changes correlated with increased expression of ANP, a biomarker of cardiac hypertrophy – a common clinical feature of TKI-induced cardiotoxicity. Moreover, the study linked these changes in $Ca^{2+}$ handling to increased activation of the known CaMKII substrates RyR2 and PLB at sites specific to CaMKII activation (Ai *et al*., 2005; Barr *et al*., 2014). The study also showed that CaMKII inhibition via AIP or a dominant negative CaMKII construct significantly reduced ANP expression in imatinib treated NRVMs. Although the study did not assess CaMKII expression or activation directly, these results suggest that CaMKII may mediate the cardiotoxic mechanism of imatinib, and that inhibition of CaMKII can reduce or reverse TKI-induced cardiovascular hypertrophy. Taken together these results show that in CMs, TKI treatment induces abnormal $Ca^{2+}$ handling and mitochondrial dysfunction and highlights a possible role for CaMKII in the cardiotoxic mechanism. These results are almost identical to those obtained in CFs in this study, suggesting that siilar pathophysiological changes exist in both cell types in the cardiotoxic mechanism of TKIs. One must question then why this study did not observe similar findings in TKI treated PCMs in this study. The answer likely stems from the cell model itself and the differences in phenotype and protein expression between progenitor and adult cells (Bers, 2002; Zhang *et al*., 2003; Bootman *et al*., 2012; Luo and Anderson, 2013; Dewenter *et al*., 2017). It is known from findings presented in Chapter 3 that PCMs do not express the key $Ca^{2+}$ handling proteins RyR2 and PLB that are pivotal to intracellular [$Ca^{2+}$] handling in CMs (Chapter 3, Figure 3.6.2). We know from the study by Barr *et al*. (2014) that activation of these $Ca^{2+}$ handling proteins is central to the $Ca^{2+}$ dysregulation and resultant mitochondrial dysfunction that appears to form part of the cardiotoxic mechanism of TKIs. This therefore may explain why similar findings were not obtained from TKI treated PCMs in this study.

Although this study did not observe TKI-induced changes in $Ca^{2+}$ mobility or CaMKII expression or activation, it did find that sunitinib treatment significantly reduced Ox-CaMKII/ATPIF1 co-localisation (Figure 4.4.11). The images show no obvious re-localisation of Ox-CaMKII or ATPIF1 (Figure 4.4.11A). Therefore, the reduction in Ox-CaMKII/ATPIF1 co-localisation suggest that sunitinib treatment affects the expression of one, or perhaps both, of these proteins. However, we know that both CaMKIIδ and Ox-CaMKII expression is not affected by TKI treatment, certainly not at the concentrations used in these co-localisation experiments (Figure 4.3.7). Therefore, if the reduction in Ox-CaMKII/ATPIF1 co-localisation is to be explained by a change in the expression of the variables, it is likely that of ATPIF1. This is consistent with previous reports of mitochondrial dysfunction in TKI-treated CMs (Kerkela *et al*., 2006; Chu *et al*., 2007; Paech *et al*., 2017).

ATPIF1 expression has been shown to be increased in failing mouse and human hearts (Pavez-Giani *et al*., 2021). This mitochondrial protein is known to have pro-survival properties, conserving ATP and preserving cell viability during ischaemia (Formentini *et al*., 2012). However, a recent publication by Pavez-Giani *et al*. (2021) suggested that ATPIF1 is a mediator of HF, inducing mitochondrial superoxide production, mitochondrial biogenesis, impaired $Ca^{2+}$ handling and CM hypertrophy via the activation of CaMKII and its downstream mediator, PLB. Though this study did not assess changes in ATPIF1 expression in either cell type, TKI-treatment was observed to induce similar pathophysiology in CFs – increased $Ca^{2+}$ mobility (Figure 4.2.2), CaMKII activation (Figure 4.3.5) and mitochondrial superoxide production (Figure 4.4.6), meaning ATPIF1 expression may also be altered following TKI treatment. In contrast, similar pathophysiological changes were not observed in TKI-treated PCMs (Figures 4.2.4 and 4.3.7). If anything, ATPIF1 expression may have been reduced following TKI-treatment (Figure 4.4.11). However, as has already been established, PCMs do not express the mature $Ca^{2+}$ handling proteins (Chapter 3, Figure 3.6.2 that Pavez-Giani *et al*. have shown to play a role in these pathophysiological changes and this may explain

the discrepancy in findings. Given the similarities in the pathophysiology of HF and TKI-induced cardiotoxicity, ATPIF1 may also play a role in the cardiotoxic mechanism of TKIs and this should be addressed in future studies.

*4.8 Conclusion:*

The results presented in this chapter investigate the pathophysiological changes that mediate TKI-induced cardiotoxicity in both CFs and PCMs, while exploring whether a role for CaMKII exists in this toxic mechanism. This project was one of just two studies to assess the effect of TKI treatment on CFs and showed that TKI treatment increased intracellular [$Ca^{2+}$] release, Ox-CaMKII expression and mitochondrial superoxide production. These findings are consistent with TKI-induced pathophysiological changes reported in other cardiac cell types reported previously. Furthermore, CaMKII inhibition was found to reduce mitochondrial superoxide production in CFs, though this did not attenuate TKI-induced CF cell death. In contrast to what has been reported previously, the results presented in this chapter show that TKI treatment does not affect intracellular [$Ca^{2+}$] release in PCMs and actually reduced CaMKII phosphorylation; though, as was established in Chapter 3, PCMs lack the protein expression of mature CMs and this may account for difference in findings reported here and in other CM cell models.

# Chapter Five: General Discussion

*5.0. General Discussion:*

This project has evaluated the effects of sunitinib and imatinib on the phenotype and function of both CFs and PCMs to gain insight into possible mechanisms underlying the cardiotoxic profiles of both drugs in each cell type. Effects on cell phenotype, viability, intracellular $Ca^{2+}$ release and mitochondrial superoxide production were assessed and, for the first time, a potential role for CaMKII activation via oxidation as an underlying mechanism of action of sunitinib in CFs was highlighted. This project is also believed to be the first to directly compare the effect of sunitinib or imatinib treatment on both cell types, showing that TKI treatment effects both CFs and PCMs at similar concentrations.

*5.1. Sunitinib displays greater cardiotoxic potential than imatinib:*

Interestingly, but unsurprisingly, sunitinib and imatinib exerted differential effects on both CFs and PCMs and this may provide an indication of the broader cardiotoxic potential of each drug. Sunitinib, a Type I TKI, is known to inhibit upwards of 50 kinases (Cheng and Force, 2010). In comparison, the more selective, Type II TKI imatinib is thought to inhibit approximately 10 kinases. The difference in selectivity is reflected in the associated cardiotoxicity of both drugs (Atallah *et al*., 2007; Burke *et al*., 2019; McMullen *et al*., 2021). The prevalence of sunitinib-induced cardiotoxicity is much higher than that of imatinib. Sunitinib has been reported to exert a wide range of cardiotoxic effects. Reports of hypertension and congestive heart failure in patients receiving sunitinib therapy ranges from 17- 43% and 3-18% respectively (Chen and Ai, 2016). In comparison, the risk of imatinib induced cardiotoxicity is relatively low unless patients already have pre-existing cardiovascular dysfunction (Garcia-Alvarez *et al*., 2010, Ribeiro *et al*., 2008). The incidence of imatinib induced cardiotoxicity is estimated at 0.04-1.8% of patients receiving imatinib therapy and almost exclusively occurs in those with pre-existing cardiac conditions or the

elderly, the majority of whom experience a decline in cardiac function with age (Garcia-Alvarez *et al*., 2010; Atallah *et al*., 2007; Hatfield *et al*., 2007).

In stark contrast to the findings presented in this study, imatinib treatment has been shown to cause cardiac cell death *in vitro*. Burke *et al*. (2019) showed that imatinib treatment significantly reduced CF viability from 10μM Imatinib in a concentration dependent manner. However, the discrepancy in the findings of this study and that of Burke may be explained by the differences in the treatment length and culture conditions between the two studies. For one, CFs were treated with imatinib for a minimum of 24 hours in the study by Burke in comparison to 18 hours in this study. Moreover, the CFs from the study by Burke were maintained in medium containing 10% FBS compared to 20% FBS in this project. This study has already shown that serum offers some protection against drug-induced toxicity (Chapter 3, Figures 3.3.1 and 3.3.2) and this may account for the difference in findings between the two studies. Imatinib has also been reported to cause CM cell death in vitro, with studies from both Kerkela *et al*. (2006) and Barr *et al*. (2014) showing that imatinib treatment significantly reduced NRVM viability at a concentration of 5μM imatinib. Although this study and others have shown that sunitinib is indeed more potent than imatinib (Zamorano *et al*., 2016; Paech *et al*., 2017; Burke *et al*., 2019; McMullen *et al*., 2021), these findings highlight that imatinib still holds cardiotoxic potential.

*5.2. Unravelling the cardiotoxic mechanism of tyrosine kinase inhibitors:*

One of the primary findings of this study is that sunitinib mediates CF toxicity via a mechanism that involves CaMKII activation via oxidation. Furthermore, this study also found evidence that the cardiotoxic mechanism of sunitinib in CFs involves changes in intracellular $Ca^{2+}$ handling and mitochondrial dysfunction. However, this study was not able to replicate these findings in PCMs, despite several studies reporting similar pathophysiological changes

in CMs treated with TKIs. Kerkela *et al*. (2006) reported that imatinib treatment significantly reduced NRVM viability and diminished mitochondrial ATP production, while also showing that drug-induced mitochondrial dysfunction was mediated by changes in intracellular $Ca^{2+}$ in imatinib treated mice. More recently, TKI-induced mitochondrial dysfunction and abnormal $Ca^{2+}$ handling was also reported by Barr *et al*. (2014). Barr showed that imatinib treatment induced hypertrophy and cell death in healthy NRVMs. The study also showed that these pathological changes were caused by impaired $Ca^{2+}$ regulation and activation of the known CaMKII substrates and $Ca^{2+}$ handling proteins PLB (T17) and RyR (S2814). Interestingly, NRVM hypertrophy was ameliorated in the presence of the CaMKII inhibitor AIP and with a dominant negative CaMKIIδc construct, highlighting a possible role for CaMKII in the cardiotoxic mechanism of TKIs in CMs that is similar to the proposed mechanism of TKI-induced cardiotoxicity obtained in CFs in this thesis. Moreover, the findings of Barr et al. may allude as to why this study was not able to replicate the pathophysiological changes induced by TKI treatment that have been reported elsewhere. The NRVMs used by Kerkela *et al*. and Barr *et al*. express the key $Ca^{2+}$ handling proteins, and known CaMKII substrates, RyR2 and PLB that appear to play a role in the pathophysiological changes that underpin TKI-induced cardiotoxicity in CMs (Barr *et al*., 2014). The PCMs used in this project do not express these key $Ca^{2+}$ handling proteins (Chapter 3, Figure 3.6.2) and this may explain why this study did not observe changes in CaMKII expression or activation, $Ca^{2+}$ handling or mitochondrial function reported by others.

The PCMs used in this project were sold as a suitable experimental model that could be maintained in culture and used to examine the effect of chronic drug treatment. However, as the findings of this project demonstrate, the PCMs are not a suitable experimental model to investigate the cardiotoxic mechanism of TKIs. The PCMs display an immature phenotype and do not recapitulate the protein expression or $Ca^{2+}$ handling capabilities of adult CMs. These cells were misrepresented by the supplier and their naïve phenotype must be acknowledged and documented as it will limit their use in cardiovascular research.

*5.3 CaMKII inhibition attenuates cardiovascular pathophysiology:*

CaMKII expression and/or activation is known to be increased in the pathophysiology of several conditions affecting cardiovascular function, including type 2 diabetes (Daniels *et al*., 2018), arrhythmia (Neef *et al*., 2010), myocardial infarction (Luczak *et al*., 2020) and cardiomyopathy (Zhang *et al*., 2003; Beauverger *et al*., 2020). Although the pathology of these conditions differ, CaMKII is known to mediate pathological changes that appear to be common amongst these conditions, including abnormal $Ca^{2+}$ handling, CM hypertrophy and fibrotic remodelling (Zhang *et al*., 2003; Ai *et al*., 2005; Neef *et al*., 2010; Sossalla *et al*., 2010; Zhang *et al*., 2010; Curl *et al*., 2018; Daniels *et al*., 2018; Pyun *et al*., 2018; Beauverger *et al*., 2020). Moreover, inhibition of CaMKII has also been shown to reduce, or in some cases reverse, these pathophysiological changes and significantly improve cardiovascular function as a result (Sossalla *et al*., 2010; Neef *et al*., 2010; Zhang *et al*., 2010; Daniels *et al*., 2018; Suetomi *et al*., 2018; Beauverger *et al*., 2020; Luczak *et al*., 2020). Interestingly, CaMKII activation has also been shown to be increased in anti-cancer drug-induced cardiotoxicity, as has abnormal $Ca^{2+}$ handling and CM hypertrophy (Sag *et al*., 2011; Barr *et al*., 2014).

In terms of anti-cancer drug-induced cardiotoxicity, the anthracycline, doxorubicin, is arguably the best understood, with significant progress having been made in elucidating the cardiotoxic mechanism of doxorubicin (Sag *et al*., 2011; Muppidi *et al*., 2015; Maillet *et al*., 2016). Moreover, CaMKII activation has been shown to be increased following doxorubicin treatment, and this correlated with abnormal $Ca^{2+}$ handling and increased ROS production (Sag *et al*., 2011). The study showed that doxorubicin affected $Ca^{2+}$ mobility, reducing SR $Ca^{2+}$ content via $Ca^{2+}$ leak, inducing diastolic $Ca^{2+}$ overload and, as a result, reducing $Ca^{2+}$ transient amplitude. These pathophysiological changes were attenuated by CaMKII inhibition, reducing SR $Ca^{2+}$ leak which restored SR $Ca^{2+}$ content. This in turn prevented diastolic $Ca^{2+}$ overload while maintaining $Ca^{2+}$ transient amplitude following doxorubicin

treatment. These findings highlight a role for CaMKII in the cardiotoxic mechanism of doxorubicin that can be attenuated by CaMKII inhibition. However, the study also raised a very interesting observation. Doxorubicin treatment significantly increased CaMKII activation via phosphorylation but had no significant effect on CaMKII oxidation despite a significant increase in ROS production. As has been shown in the findings of this project (Chapter 4, Figure 4.3.4), the composition of the sample buffer can mask treatment induced changes in protein oxidation. By excluding the reducing agent DTT from the sample buffer, this study observed an increase in CaMKII oxidation following sunitinib treatment that was suppressed by DTT. The study by Sag *et al*. (2011) does not disclose whether the sample buffer contains a reducing agent. However, given that immunoblot samples typically contain DTT (Zhang *et al*., 2003; Neef *et al*., 2010; Martin *et al*., 2018; Suetomi *et al*., 2018) this may explain why Sag *et al*. (2011) did not see an increase in CaMKII oxidation despite a significant increase in ROS production. This is a very important finding that has been generated by this study and needs to be acknowledged. It also means that the effect of CaMKII oxidation is likely misreported in the literature and may constitute more in terms of mediating cardiovascular pathophysiology than is currently believed.

More recently, Barr *et al*. (2014) showed that imatinib treatment caused abnormal $Ca^{2+}$ handling, hypertrophy and cell death in healthy NRVMs via the phosphorylation of the known CaMKII substrates, PLB and RyR2. However, CaMKII inhibition via both AIP and a dominant negative CaMKII construct attenuated NRVM hypertrophy, indicating a role for CaMKII in the cardiotoxic mechanism of imatinib. These findings are consistent with the findings of this project, which has shown that sunitinib treatment increases CaMKII oxidation, abnormal $Ca^{2+}$ handling and mitochondrial superoxide production in CFs, ultimately causing cell death. However, in this study, CaMKII inhibition via KN-93 did not attenuate TKI-induced cell death. It did significantly reduce mitochondrial superoxide production, however, indicating therapeutic potential in alleviating TKI-induced pathophysiological changes. It may be that the inhibitor of CaMKII used in this study, KN-93, is not as effective as other CaMKII

inhibitors. This is implied in the recent findings of Daniels *et al*. (2018), who showed that the impaired cardiac contractility and relaxation seen in the diabetic heart could be partially restored via CaMKII inhibition using KN-93, yet fully restored by the CaMKII inhibitor AIP. Perhaps then, more efficient CaMKII inhibition using AIP or siRNA for example, could reduce or reverse the cardiotoxic effects of TKIs.

*5.4 Future directions:*

Having shown that CaMKII activation is increased following sunitinib treatment and established a role for CaMKII in mediating the pathophysiology of TKI-induced cardiotoxicity, future work should (i) further investigate the effect of TKI treatment on mitochondrial function and (ii) investigate whether more efficient CaMKII inhibition can reduce or reverse TKI-induced cardiotoxicity. This project has already shown that sunitinib and, to a lesser extent, imatinib significantly increase mitochondrial superoxide production, indicative of mitochondrial dysfunction, and that this can be reduced by CaMKII inhibition. This project also began to optimise conditions to assess the effect of TKI treatment on mitochondrial respiration; however, owing to restrictions implemented due to the COVID-19 pandemic at that time, this work could not be completed. Any future work should begin by completing these experiments. These will provide significant insight into mitochondrial function which, as previous studies have suggested (Kerkela *et al*., 2006; Doherty *et al*., 2013; Paech *et al*., 2017), is likely impacted by TKIs. It would also be prudent to assess how TKI treatment affects ATP production. The outcome of this is two-fold. Firstly, ATP production would reflect mitochondrial function and provide further insight into what effect TKI-treatment has on the mitochondria. Secondly, it may aid in the understanding of how TKI treatment causes abnormal $Ca^{2+}$ handling. Given that one of the main $Ca^{2+}$ transporters in CMs is ATP dependent (SERCA), any change in ATP production may consequently contribute to the $Ca^{2+}$ dysregulation caused by TKI treatment.

Future work should also investigate whether more efficient CaMKII inhibition can attenuate the TKI-induced pathophysiology reported here. This study has already shown that CaMKII inhibition via KN-93 significantly reduced mitochondrial ROS production (Chapter 4, Figure 4.4.7) and had a positive but non-significant effect on Ang II-induced $Ca^{2+}$ mobilisation in CFs (Chapter 4, Figure 4.6.2), but CaMKII inhibition did not reduce TKI-induced cell death (Chapter 4, Figures 4.5.3, 4.5.4, 4.5.5 and 4.5.6). Not surprisingly, studies have shown that inhibitors of CaMKII have different levels of efficacy, and that KN-93 has been shown to be less potent than AIP, for example (Sossalla *et al*., 2010; Daniels *et al*., 2018). It is therefore possible that more efficient inhibitors of CaMKII can reduce or reverse TKI-induced cardiotoxicity and preserve cardiac function. Future work should address this using more potent inhibitors of CaMKII, such as AIP, or suppress CaMKII expression using siRNA to better characterise the role it plays in mediating the cardiotoxic mechanism of TKIs.

# References

Abi-Gerges, N. *et al*. (2013) 'Preservation of cardiomyocytes from the adult heart', *Journal of Molecular and Cellular Cardiology*, **64**: 108–119.

Ai, X. *et al*. (2005) 'Ca2+/Calmodulin–Dependent Protein Kinase Modulates Cardiac Ryanodine Receptor Phosphorylation and Sarcoplasmic Reticulum Ca2+ Leak in Heart Failure', *Circ Res*, **97**: 1314–1322.

Aiello, E. A. and Cingolani, H. E. (2001) 'Angiotensin II stimulates cardiac L-type Ca2+ current by a Ca2+ - and protein kinase C-dependent mechanism', *Am J Physiol Heart Circ Physiol*, **280**: 1528–1536.

Akoglu, H. (2018) 'User's guide to correlation coefficients', *Turkish Journal of Emergency Medicine*, **18**: 91–93.

Akopova, O. V *et al*. (2011) 'The effect of permeability transition pore opening on reactive oxygen species production in rat brain mitochondria', *Ukr Biokhim Zh*, **83**: 46–55.

Al Ghouleh, I. *et al*. (2013) 'Aquaporin 1, Nox1, and Ask1 mediate oxidant-induced smooth muscle cell hypertrophy', *Cardiovascular Research*, **97**: 134–142.

Anderson, M. E. (2015) 'Oxidant stress promotes disease by activating CaMKII', *J Mol Cell Cardiol*., **89**: 160–167.

Anderson, M. E., Brown, J. H. and Bers, D. M. (2011) 'CaMKII in myocardial hypertrophy and heart failure', *J Mol Cell Cardiol*., **51**: 468–473.

Arai, M. *et al*. (1993) ‘Alterations in Sarcoplasmic Reticulum Gene Expression in Human Heart Failure: A Possible Mechanism for Alterations in Systolic and Diastolic Properties of the Failing Myocardium’, *Circulation Research*, **72**: 463–469.

Aronsen, J. M., Swift, F. and Sejersted, O. M. (2013) ‘Cardiac sodium transport and excitation-contraction coupling’, *Journal of Molecular and Cellular Cardiology*, **61**: 11–19.

Atallah, E. *et al*. (2007) ‘Congestive heart failure is a rare event in patients receiving imatinib therapy’, *Blood*. American Society of Hematology, **110**: 1233–1237.

Bae, Y. K. *et al*. (2018) ‘Intracellular Calcium Determines the Adipogenic Differentiation Potential of Human Umbilical Cord Blood-Derived Mesenchymal Stem Cells via the Wnt5a/β-Catenin Signaling Pathway’, *Stem Cells Int*, **2018**.

Bantscheff, M. *et al*. (2007) ‘Quantitative chemical proteomics reveals mechanisms of action of clinical ABL kinase inhibitors’, *Nature Biotechnology*, **25**: 1035–1044.

Bardaweel, S. K. *et al*. (2018) ‘Reactive Oxygen Species: the Dual Role in Physiological and Pathological Conditions of the Human Body’, *The Eurasian Journal of Medicine*, **50**: 193–201.

Barr, L. A. *et al*. (2014) ‘Imatinib Activates Pathological Hypertrophy by Altering Myocyte Calcium Regulation’, *Clin Transl Sci*, **7**: 360–367.

Baudino, T. A. *et al*. (2006) ‘Cardiac fibroblasts: friend or foe?’, *Am J Physiol Heart Circ Physiol*, **291**: 1015–1026.

Beauverger, P. *et al*. (2020) 'Reversion of cardiac dysfunction by a novel orally available calcium/calmodulin-dependent protein kinase II inhibitor, RA306, in a genetic model of dilated cardiomyopathy', *Cardiovascular Research*, **116**: 329–338.

Beckendorf, J., van den Hoogenhof, M. M. G. and Backs, J. (2018) 'Physiological and unappreciated roles of CaMKII in the heart', *Basic Research in Cardiology*, **113**: 1–12.

Bergman, O. and Ben-Shachar, D. (2016) 'Mitochondrial Oxidative Phosphorylation System (OXPHOS) Deficits in Schizophrenia: Possible Interactions with Cellular Processes', *The Canadian Journal of Psychiatry*, **61**: 457–469.

Berk, B. C., Fujiwara, K. and Lehoux, S. (2007) 'ECM remodeling in hypertensive heart disease', *The Journal of Clinical Investigation*, **117**: 568–575.

Bers, D. M. (2002) 'Cardiac excitation–contraction coupling', *Nature*, **415**: 198–205.

Bers, D. M. and Grandi, E. (2009) 'Calcium/calmodulin-dependent kinase II regulation of cardiac ion channels', *Journal of Cardiovascular Pharmacology*, **54**: 180–187.

Beuckelmann, D. J., Nabauer, M. and Erdmann, E. (1992) 'Intracellular Calcium Handling in Isolated Ventricular Myocytes From Patients With Terminal Heart Failure', *Circulation*, **85**: 1046–1055.

Blanca, A. J. *et al*. (2016) 'Inflammatory and fibrotic processes are involved in the cardiotoxic effect of sunitinib: Protective role of L-carnitine', *Toxicology Letters*, **241**: 9–18.

Bolte, S. and Cordelieres, F. P. (2006) 'A guided tour into subcellular colocalization analysis in light microscopy', *Journal of Microscopy*, **224**: 213–232.

Bootman, M. D. *et al*. (2012) 'Calcium Signalling and Regulation of Cell Function', *eLS*. doi: 10.1002/9780470015902.a0001265.pub3.

Bouitbir, J. *et al*. (2020) 'Imatinib and Dasatinib Provoke Mitochondrial Dysfunction Leading to Oxidative Stress in C2C12 Myotubes and Human RD Cells', *Front. Pharmacol*, **11**.

Boveris, A. and Cadenas, E. (1975) 'Mitochondrial Production of Superoxide Anions and its Relationship to the Antimycin Insensitive Respiration', *FEBS Letters*, **54**: 311–314.

Bradham, W. S. *et al*. (2002) 'TNF-alpha and myocardial matrix metalloproteinases in heart failure: relationship to LV remodeling', *Am J Physiol Endocrinol Metab*, **282**: 1288–1295.

Bradley, J. M. *et al*. (2018) 'A novel fibroblast activation inhibitor attenuates left ventricular remodeling and preserves cardiac function in heart failure', *Am J Physiol Heart Circ Physiol*, **315**: 563–570.

Branco, A. F. *et al*. (2015) 'Gene Expression Profiling of H9c2 Myoblast Differentiation towards a Cardiac-Like Phenotype', *Physiological Reports*, **10**: 1–18.

Brand, M. D. and Nicholls, D. G. (2011) 'Assessing mitochondrial dysfunction in cells', *Biochemical Journal*, **435**: 297–312.

Braun, F. *et al*. (2011) 'Serum-Nutrient Starvation Induces Cell Death Mediated by Bax and Puma That Is Counteracted by p21 and Unmasked by Bcl-x L Inhibition', *PLoS ONE*, **6**.

Brown, R. D. *et al*. (2007) ‘Cytokines regulate matrix metalloproteinases and migration in cardiac fibroblasts’, *Biochemical and Biophysical Research Communications*, **362**: 200–205.

Brown, R. D. R. *et al*. (2021) ‘A new model for regulation of sphingosine kinase 1 translocation to the plasma membrane in breast cancer cells’, *Journal of Biological Chemistry*, **296**.

Bujak, M. *et al*. (2008) ‘Interleukin-1 Receptor Type I Signaling Critically Regulates Infarct Healing and Cardiac Remodeling’, *The American Journal of Pathology*, **173**: 57–67.

Burgoyne, J. R. *et al*. (2012) ‘Redox Signaling in Cardiac Physiology and Pathology’, *Circ Res*, **111**: 1091–1106.

Burke, M. J. *et al*. (2019) ‘Receptor tyrosine kinase inhibitors cause dysfunction in adult rat cardiac fibroblasts in vitro’, *Toxicology in Vitro*, **58**: 178–186.

Burridge, P. W. *et al*. (2016) ‘Human Induced Pluripotent Stem Cell–Derived Cardiomyocytes Recapitulate the Predilection of Breast Cancer Patients to Doxorubicin–Induced Cardiotoxicity’, *Nat Med*, **22**: 547–556.

Buse, M. G. *et al*. (2002) ‘Enhanced O -GlcNAc protein modification is associated with insulin resistance in GLUT1-overexpressing muscles’, *Am J Physiol Endocrinol Metab*, **283**: 241–250.

Camelliti, P., Borg, T. K. and Kohl, P. (2005) ‘Structural and functional characterisation of cardiac fibroblasts’, *Cardiovascular Research*, **65**: 40–51.

Campbell, D. L., Stalmer, J. S. and Strauss, H. C. (1996) 'Redox Modulation of L-Type Calcium Channels in Ferret Ventricular Myocytes: Dual Mechanism Regulation by Nitric Oxide and S-Nitrosothiols', *J Gen Physiol*, **108**: 277–293.

Cao, L. *et al*. (2018) 'Angiotensin II upregulates fibroblast-myofibroblast transition through Cx43-dependent CaMKII and TGF-β1 signaling in neonatal rat cardiac fibroblasts', *Acta Biochimica et Biophysica Sinica*, **50**: 843–852.

Cappola, T. P. *et al*. (2001) 'Allopurinol Improves Myocardial Efficiency in Patients With Idiopathic Dilated Cardiomyopathy', *Circulation*, **104**: 2407–2411.

Chaggar, P. S. *et al*. (2009) 'Neuroendocrine Effects on the Heart and Targets for Therapeutic Manipulation in Heart Failure', *Cardiovascular Therapeutics*, **27**.

Chang, Y., Weng, C. and Lin, K. (2020) 'O-GlcNAcylation and its role in the immune system', *Journal of Biomedical Science*, **27**: 1–15.

Chen, Z. I. and Ai, D. I. (2016) 'Cardiotoxicity associated with targeted cancer therapies', *Molecular and Clinical Oncology*, **4**: 675–681.

Cheng, H. and Force, T. (2010) 'Molecular mechanisms of cardiovascular toxicity of targeted cancer therapeutics', *Circulation Research*, **106**: 21–34.

Cheng, T.-H. *et al*. (2003) 'Involvement of Reactive Oxygen Species in Angiotensin II-Induced Endothelin-1 Gene Expression in Rat Cardiac Fibroblasts', *Journal of the American College of Cardiology*. Elsevier Masson SAS, **42**: 1845–1854.

Chu, T. F. *et al*. (2007) 'Cardiotoxicity associated with tyrosine kinase inhibitor sunitinib', *Lancet*, **370**: 2011–2019.

Chung, R., Ghosh, A. K. and Banerjee, A. (2018) 'Cardiotoxicity: precision medicine with imprecise definitions', *Open Heart*, **5**: 2–5.

Clapham, D. E. (2007) 'Calcium Signaling', *Cell*, **131**: 1047–1058.

Cohen, J. D. *et al*. (2011) 'Use of human stem cell derived cardiomyocytes to examine sunitinib mediated cardiotoxicity and electrophysiological alterations', *Toxicology and Applied Pharmacology*, **257**: 74–83.

Curl, C. L. *et al*. (2018) 'Cardiomyocyte Functional Etiology in Heart Failure With Preserved Ejection Fraction Is Distinctive—A New Preclinical Model', *J Am Heart Assoc*, **7**.

Curran, J. *et al*. (2014) 'Nitric Oxide-Dependent Activation of CaMKII Increases Diastolic Sarcoplasmic Reticulum Calcium Release in Cardiac Myocytes in Response to Adrenergic Stimulation', *PLoS ONE*, **9**.

Currie, S. *et al*. (2004) 'Calcium/calmodulin-dependent protein kinase IIδ associates with the ryanodine receptor complex and regulates channel function in rabbit heart', *Biochem. J*, **377**: 357–366.

Currie, S. *et al*. (2016) 'Inositol trisphosphate receptor contribution to ventricular cardiac fibroblast function in healthy and hypertrophied mouse hearts', *FASEB Journal*, **30**(1 Supp).

Daniels, L. J. *et al*. (2015) 'The role of CaMKII in diabetic heart dysfunction', *Heart Failure Reviews*, **20**: 589–600.

Daniels, L. J. *et al*. (2018) 'Inhibition of calcium/calmodulin-dependent kinase II restores contraction and relaxation in isolated cardiac muscle from type 2 diabetic rats', *Cardiovascular Diabetology*, **17**: 1–15.

Dewenter, M. *et al*. (2017) 'Calcium Signaling and Transcriptional Regulation in Cardiomyocytes', *Circ Res*, **121**: 1000–1020.

Diaz-Araya, G. *et al*. (2015) 'Cardiac fibroblasts as sentinel cells in cardiac tissue: Receptors, signaling pathways and cellular functions', *Pharmacological Research*, **101**: 30–40.

Dick, S. A. and Epelman, S. (2016) 'Chronic Heart Failure and Inflammation: What Do We Really Know?', *Circ Res*, **119**: 159–176.

Djafarzadeh, S. and Jakob, S. M. (2017) 'High-resolution Respirometry to Assess Mitochondrial Function in Permeabilized and Intact Cells', *Journal of Visualized Experiments*, **120**.

Dobbin, S. J. H. *et al*. (2018) 'Toxicity of Cancer Therapy: What the Cardiologist Needs to Know about Angiogenesis Inhibitors', *Heart*, **104**: 1995–2002.

Doherty, K. R. *et al*. (2013) 'Multi-parameter in vitro toxicity testing of crizotinib, sunitinib, erlotinib, and nilotinib in human cardiomyocytes', *Toxicology and Applied Pharmacology*, **272**: 245–255.

Doppler, S. A. *et al*. (2017) 'Cardiac fibroblasts: more than mechanical support', *Journal of Thoracic Disease*, **9**: 36–51.

Dunn, K. W., Kamocka, M. M. and Mcdonald, J. H. (2011) 'A practical guide to evaluating colocalization in biological microscopy', *Am J Physiol Cell Physiol*, **300**: 723–742.

Eigel, B. N., Gursahani, H. and Hadley, R. W. (2003) 'Reactive Oxygen Species Are Required for the Rapid Reactivation of the Sodium-Calcium Exchanger in Hypoxic/Reoxygenated Guinea Pig Ventricular Myocytes', *Am J Physiol Heart Circ Physiol*, **286**: 955–963.

Elster, S. K., Braunwald, E., and Wood, H. F. (1956), 'A study of C-reactive protein in the serum of patients with congestive heart failure', *Am Heart J*, **51**: 533-41.

Emadi, E. *et al*. (2019) 'The potential role of mitochondrial impairment in the pathogenesis of imatinib-induced renal injury', *Heliyon*, **5**.

Erickson, J. R. *et al*. (2008) 'A Dynamic Pathway for Calcium-Independent Activation of CaMKII by Methionine Oxidation', *Cell*, **133**: 462–474.

Erickson, J. R. *et al*. (2013) 'Diabetic hyperglycaemia activates CaMKII and arrhythmias by O-linked glycosylation', *Nature*, **502**: 372–376.

Erickson, J. R. *et al*. (2015) 'S-Nitrosylation Induces Both Autonomous Activation and Inhibition of Calcium/Calmodulin-dependent Protein Kinase IIdelta', *Journal of Biological Chemistry*, **290**: 25646–25656.

Esmaeilzadeh, M. and Parsaee, M. (2012) 'The Role of Echocardiography in Coronary Artery Disease and Acute Myocardial Infarction', *J Teh Univ Heart Ctr*, **8**: 1–13.

Fang, L. *et al*. (2010) 'Activation of peripheral blood mononuclear cells and extracellular matrix and inflammatory gene profile in acute myocardial infarction', *Clinical Science*, **119**: 175–183.

Fearon, I. M. *et al*. (1999) 'Modulation of recombinant human cardiac L -type Ca2+ channel alpha1C subunits by redox agents and hypoxia', *Journal of Physiology*, **514**: 629–637.

Finkel, T. *et al*. (2015) 'The Ins and Outs of Mitochondrial Calcium', *Circ Res*, **116**: 1810–1819.

Foley, T. A. *et al*. (2012) 'Imaging Measuring Left Ventricular Ejection Fraction – Techniques and Potential Pitfalls', *European Cardiology*, **8**: 108–114.

Formentini, L. *et al*. (2012) 'Article The Mitochondrial ATPase Inhibitory Factor 1 Triggers a ROS-Mediated Retrograde Prosurvival and Proliferative Response', *Molecular Cell*, **45**: 731–742.

Fujisaki, H. *et al*. (1995) 'Natriuretic Peptides Inhibit Angiotensin II-induced Proliferation of Rat Cardiac Fibroblasts by Blocking Endothelin-1 Gene Expression', *J Clin Invest.*, **96**: 1059–1065.

Fulda, S. and Debatin, K. (2006) 'Extrinsic versus intrinsic apoptosis pathways in anticancer chemotherapy', *Oncogene*, **25**: 4798–4811.

Furtado, M. B. *et al*. (2014) 'Integrative Physiology Cardiogenic Genes Expressed in Cardiac Fibroblasts Contribute to Heart Development and Repair', *Circ Res*, **114**: 1422–1434.

Garcia-Alvarez, A. *et al*. (2010) 'Atypical cardiac manifestation of hypereosinophilic syndrome and reversible cardiotoxicity to imatinib', *International Journal of Cardiology*, **139**.

Gernaat, S. A. M. *et al*. (2017) 'Risk of death from cardiovascular disease following breast cancer : a systematic review', *Breast Cancer Res Treat*, **164**: 537–555.

Goonasekera, S. A. and Molkentin, J. D. (2012) 'Unraveling the secrets of a double life: Contractile versus signaling Ca2+in a cardiac myocyte', *Journal of Molecular and Cellular Cardiology*, **52**: 317–322.

Gotlib, J. *et al*. (2004) 'The FIP1L1-PDGFRα fusion tyrosine kinase in hypereosinophilic syndrome and chronic eosinophilic leukemia: Implications for diagnosis, classification, and management', *Blood*, **103**: 2879–2891.

Green, P. S. and Leeuwenburgh, C. (2002) 'Mitochondrial dysfunction is an early indicator of doxorubicin-induced apoptosis', *Biochimica et Biophysica Acta*, **1588**: 94–101.

Guo, G. *et al*. (2018) 'A modified method for isolation of human cardiomyocytes to model cardiac diseases', *Journal of Translational Medicine*, **16**.

Guo, X. M. *et al*. (2016) 'Knockdown of IRF6 Attenuates Hydrogen Dioxide-Induced Oxidative Stress via Inhibiting Mitochondrial Dysfunction in HT22 Cells' *Cell Mol Neurobiol*, **36**: 1077-86.

Gustafsson, B. and Gottlieb, R. A. (2008) 'Heart mitochondria: Gates of life and death', *Cardiovascular Research*, **77**: 334–343.

Gutierrez-Martin, Y. *et al*. (2004) 'Modulation of sarcoplasmic reticulum Ca2 +-ATPase by chronic and acute exposure to peroxynitrite', *Eur. J. Biochem*, **271**: 2647–2657.

Hall, C. *et al*. (2021) 'Complex Relationship Between Cardiac Fibroblasts and Cardiomyocytes in Health and Disease', *J Am Heart Assoc*, **10**.

Hartupee, J. and Mann, D. L. (2017) 'Neurohormonal activation in heart failure with reduced ejection fraction', *Nat Rev Cardiol.*, **14**.

Hasenfuss, G. *et al*. (1994) 'Relation Between Myocardial Function and Expression of Sarcoplasmic Reticulum Ca2 + -ATPase in Failing and Nonfailing Human Myocardium', *Circ Res*, **75**: 434–442.

Hatfield, A., Owen, S. and Pilot, P. R. (2007) 'In reply to "Cardiotoxicity of the cancer therapeutic agent imatinib mesylate"', *Nat Med*.

Hein, S. *et al*. (2003) 'Progression From Compensated Hypertrophy to Failure in the Pressure-Overloaded Human Heart', *Circulation*, **107**: 984–991.

Hess, D. T. *et al*. (2005) 'Protein S-nitrosylation: purview and parameters', *Nat Rev Mol Cell Bio*l, **6**: 150-66.

Hoelz, A., Nairn, A. C. and Kuriyan, J. (2003) 'Crystal Structure of a Tetradecameric Assembly of the Association Domain of Ca2+/Calmodulin-Dependent Kinase II', *Molecular Cell*, **11**: 1241–1251.

Huang, Y. *et al*. (2018) 'Serum starvation-induces down-regulation of Bcl-2/Bax confers apoptosis in tongue coating-related cells in vitro', *Molecular Medicine Reports*, **17**: 5057–5064.

Hudmon, A. *et al*. (2005) 'CaMKII tethers to L-type Ca2+ channels, establishing a local and dedicated integrator of Ca2+ signals for facilitation', *The Journal of Cell Biology*, **171**: 537–547.

Humeres, C., & Frangogiannis, N. G. (2019) 'Fibroblasts in the Infarcted, Remodeling, and Failing Heart', *JACC*, **4**: 449–467.

Ivey, M. J. and Tallquist, M. D. (2016) 'Defining the Cardiac Fibroblast', *Circulation Journal*, **80**: 2269–2276.

Jaworski, C. *et al*. (2013) 'Cardiac Complications of Thoracic Irradiation', *Journal of the American College of Cardiology*, **61**: 2319–2328.

Jimenez-Tellez, N. and Greenway, S. C. (2019) 'Cellular models for human cardiomyopathy: What is the best option?', *World Journal of Cardiology*, **11**: 221–235.

Joiner, M. A. *et al*. (2012) 'CaMKII determines mitochondrial stress responses in heart', *Nature*, **491**: 269–273.

Jornayvaz, F. R. and Shulman, G. I. (2010) 'Regulation of mitochondrial biogenesis', *Essays Biochem*, **47**.

Kamakura, T. *et al*. (2013) 'Ultrastructural Maturation of Human-Induced Pluripotent Stem Cell-Derived Cardiomyocytes in a Long-Term Culture', *Circ J*, **77**: 1307–1314.

Karaye, K. M. and Sani, M. U. (2008) 'Electrocardiographic abnormalities in patients with heart failure', *Cardiovascular Journal of Africa*, **19**: 22–25.

Kashiwase, K. *et al*. (2005) 'CaMKII activates ASK1 and NF-kB to induce cardiomyocyte hypertrophy', *Biochemical and Biophysical Research Communications*, **327**: 136–142.

Kaur, H. *et al*. (2016) 'Integrative Physiology Targeted Ablation of Periostin-Expressing Activated Fibroblasts Prevents Adverse Cardiac Remodeling in Mice', *Circ Res*, **118**: 1906–1917.

Kawakami, M. and Okabe, E. (1998) 'Superoxide Anion Radical-Triggered Ca2+ Release from Cardiac Sarcoplasmic Reticulum through Ryanodine Receptor Ca2+ Channel', *Mol. Pharmacol.*, **53**: 497–503.

Kerkela, R. *et al*. (2006) 'Cardiotoxicity of the cancer therapeutic agent imatinib mesylate', *Nature Medicine*, **12**: 908–916.

Kerkela, R. *et al*. (2009) 'Sunitinib-induced cardiotoxicity is mediated by off-target inhibition of AMP-activated protein kinase', *Clinical and translational science*, **2**: 15–25.

Khalil, H. *et al*. (2017) 'Fibroblast-specific TGF-β–Smad2/3 signaling underlies cardiac fibrosis', *The Journal of Clinical Investigation*, **127**: 3370–3383.

Kohn, E. C. *et al*. (1995) 'Angiogenesis: Role of calcium-mediated signal transduction', *Proc. Natl. Acad. Sci.*, **92**: 1307–1311.

Konigsberg, W. (1972) Reduction of disulfide bonds in proteins with dithiothreitol, *Methods in Enzymology*.

Krause, D. S., van Etten, R. A. (2005) 'Tyrosine kinases as targets for cancer therapy', *N Engl J Med*, **353**: 172-87.

Kubo, H. *et al*. (2001) 'Patients With End-Stage Congestive Heart Failure Treated With Beta-Adrenergic Receptor Antagonists Have Improved Ventricular Myocyte Calcium Regulatory Protein Abundance', *Circulation*, **104**: 1012–1018.

Kühlbrandt, W. (2015) 'Structure and function of mitochondrial membrane protein complexes', *BMC Biology*, **13**.

Kumar, N. *et al*. (2018) 'Comparison of cell-based assays to quantify treatment effects of anticancer drugs identifies a new application for Bodipy-L-cystine to measure apoptosis', *Scientific Reports*, **8**.

Kwong, J. Q. *et al*. (2014) 'Genetic deletion of the mitochondrial phosphate carrier desensitizes the mitochondrial permeability transition pore and causes cardiomyopathy', *Cell Death and Differentiation*, **21**: 1209–1217.

Lai, Y. *et al*. (1987) 'Ca2+/calmodulin-dependent protein kinase II: Identification of autophosphorylation sites responsible for generation of Ca2+/calmodulin-independence', *Proc Natl Acad Sci U S A*, **84**: 5710–5714.

Larsson, P. *et al*. (2020) 'Optimization of cell viability assays to improve replicability and reproducibility of cancer drug sensitivity screens', *Sci Rep*, **10**.

Lawan, A. *et al*. (2011) 'Deletion of the Dual Specific Phosphatase-4 (DUSP-4) Gene Reveals an Essential Non-redundant Role for MAP Kinase Phosphatase-2 (MKP-2) in Proliferation and Cell Survival', *Journal of Biological Chemistry*, **286**.

Levin, V. A. *et al*. (2010) 'Different Changes in Protein and Phosphoprotein Levels Result from Serum Starvation of High-Grade Glioma and Adenocarcinoma Cell Lines', *J Proteome Res.*, **9**: 179–191.

Levine, B. *et al*. (1990) 'Elevated Circulating Levels of Tumour Necrosis Factor in Severe Chronic Heart Failure', *The New England Journal of Medicine*, **323**: 236–241.

Li, H. *et al*. (2020) 'Optimized Langendorff perfusion system for cardiomyocyte isolation in adult mouse heart', *J Cell Mol Med*, **24**.

Li, X. *et al*. (2018) 'Sulfiredoxin-1 Enhances Cardiac Progenitor Cell Survival against Oxidative Stress via the Upregulation of the ERK/NRF2 Signal Pathway', *Free Radic Biol Med.*, **123**: 8–19.

Lin, C. *et al*. (2012) 'NADPH oxidase 2-derived reactive oxygen species signal contributes to bradykinin-induced matrix metalloproteinase-9 expression and cell migration in brain astrocytes', *Cell Communication and Signalling*, **10**: 1–15.

Liquori, M. E. *et al*. (2014) 'Cardiac biomarkers in heart failure', *Clinical Biochemistry*, **47**: 327–337.

Litviňuková, M. *et al*. (2020) 'Cells of the adult human heart', *Nature*, **588**: 466–472.

Lock, J. T., Parker, I. and Smith, I. F. (2015) 'A comparison of fluorescent Ca2+ indicators for imaging local Ca2+ signals in cultured cells', *Cell Calcium*, **58**: 638–648.

Lu, F.-H. *et al*. (2013) 'Role of the Calcium-Sensing Receptor in Cardiomyocyte Apoptosis via the Sarcoplasmic Reticulum and Mitochondrial Death Pathway in Cardiac Hypertrophy and Heart Failure', *Cellular Physiology and Biochemistry*, **157**: 728–743.

Lu, X. *et al*. (2016) 'Individual Cardiac Mitochondria Undergo Rare Transient Permeability Transition Pore Openings', *Circ Res*, **118**: 834–841.

Luczak, E. D. *et al*. (2020) 'Mitochondrial CaMKII causes adverse metabolic reprogramming and dilated cardiomyopathy', *Nature Communications*, **11**.

Luis, C. *et al*. (2019) 'Avoiding the Interference of Doxorubicin with MTT Measurements on the MCF-7 Breast Cancer Cell Line', *Methods Protoc*, **2**.

Lundy, S. D. *et al*. (2013) 'Structural and Functional Maturation of Cardiomyocytes Derived from Human Pluripotent Stem Cells', *Stem Cells and Development*, **22**: 1991–2002.

Luo M, Anderson ME (2013) 'Mechanisms of altered Ca2+ handling in heart failure', *Circ Res*, **113**: 690-708.

Ma, F. *et al*. (2012) 'Macrophage-Stimulated Cardiac Fibroblast Production of IL-6 Is Essential for TGF b / Smad Activation and Cardiac Fibrosis Induced by Angiotensin II', *PLoS ONE*, **7**: 1–9.

Maillet, A. *et al*. (2016) 'Modeling Doxorubicin-Induced Cardiotoxicity in Human Pluripotent Stem Cell Derived-Cardiomyocytes', *Scientific Reports*, **6**.

Marks, A. R. (2013) ‘Calcium cycling proteins and heart failure: mechanisms and therapeutics’, *J Clin Invest.*, **123**: 46–52.

Martin, T. P. *et al*. (2014) ‘Adult cardiac fibroblast proliferation is modulated by calcium/calmodulin-dependent protein kinase II in normal and hypertrophied hearts’, *Pflügers Archiv - European Journal of Physiology*, **466**: 319–330.

Martin, T. P. *et al*. (2018) ‘CaMKIIδ interacts directly with IKKβ and modulates NF-κB signalling in adult cardiac fibroblasts’, *Cellular Signalling*, **51**: 166–175.

Matsumori, A. *et al*. (1994) ‘Increased circulating cytokines in patients with myocarditis and cardiomyopathy’, *Br Heart J*, **72**: 561–566.

McCluskey, C., Macdonald, M. and Currie, S. (2015) ‘Ageing of the vascular endothelium: a novel role for CaMKIIdelta?’, *Heart*, **101**(Suppl 4).

McMullen, C. J. *et al*. (2021) ‘Sunitinib and Imatinib Display Differential Cardiotoxicity in Adult Rat Cardiac Fibroblasts That Involves a Role for Calcium/Calmodulin Dependent Protein Kinase II’, *Frontiers in Cardiovascular Medicine*, **7**.

Meyer, T. *et al*. (1992) ‘Calmodulin trapping by calcium-calmodulin-dependent protein kinase’, *Science*, **256**: 1199-202.

Micallef, I. and Baron, B. (2020) ‘Annals of Clinical Toxicology Doxorubicin: An Overview of the Anti-Cancer and Chemoresistance Mechanisms’, *Annals of Clinical Toxicology*, **3**.

Milani-Nejad, N. and Janssen, P. M. L. (2014) 'Small and Large Animal Models in Cardiac Contraction Research: Advantages and Disadvantages', *Pharmacol Ther*, **141**: 235–249.

Mitcheson, J. S., Hancox, J. C. and Levi, A. J. (1998) 'Cultured adult cardiac myocytes: Future applications, culture methods, morphological and electrophysiological properties', *Cardiovascular Research*, **39**: 280–300.

Modin, D., Andersen, D. M. and Biering-Sorensen, T. (2018) 'Echo and heart failure: when do people need an echo, and when do they need natriuretic peptides ?', *Echo Research and Practice*, **5**: 65–79.

Mooney, L. *et al*. (2015) 'Effects of acute and chronic sunitinib treatment on cardiac function and calcium/calmodulin-dependent protein kinase II', *British Journal of Pharmacology*, **172**: 4342–4354.

Mori, K. *et al*. (2019) 'A mitochondrial ROS pathway controls matrix metalloproteinase 9 levels and invasive properties in RAS-activated cancer cells', *FEBS J.*, **286**: 459–478.

Moslehi, J. J. and Deininger, M. (2015) 'Tyrosine kinase inhibitor-associated cardiovascular toxicity in chronic myeloid leukemia', *Journal of Clinical Oncology*, **33**: 4210–4218.

Motzer, R. J. *et al*. (2007) 'Sunitinib versus Interferon Alfa in Metastatic Renal-Cell Carcinoma', *New England Journal of Medicine*, **356**: 115–124.

Mukhopadhyay, P. *et al*. (2007) ‘Simple quantitative detection of mitochondrial superoxide production in live cells’, *Biochemical and Biophysical Research Communications*, **358**: 203–208.

Mukhopadhyay, P. *et al*. (2009) ‘Role of superoxide, nitric oxide, and peroxynitrite in doxorubicin-induced cell death in vivo and in vitro’, *Am J Physiol Heart Circ Physiol*, **296**: 1466–1483.

Muppidi, R. *et al*. (2015) ‘Cardiotoxicity of Anticancer Therapies’, *Rev Cardiovasc Med*, **16**: 225–234.

Murtha, L. A. *et al*. (2017) ‘The Processes and Mechanisms of Cardiac and Pulmonary Fibrosis’, *Frontiers in Physiology*, **8**: 1–15.

Musunuru, K. *et al*. (2019) ‘Induced Pluripotent Stem Cells for Cardiovascular Disease Modeling and Precision Medicine: A Scientific Statement From the American Heart Association’, *Circ Genom Precis Med*, **11**: 1–55.

Nag, A. (1980). ‘Study of non-muscle cells of the adult mammalian heart: a fine structural analysis and distribution’, *Cytobios*, **28**: 41-61.

Nagaraju, C. K. *et al*. (2019) ‘Myofibroblast Phenotype and Reversibility of Fibrosis in Patients With End-Stage Heart Failure’, *Journal of the American College of Cardiology*, **73**: 2267–2282.

National Research Council (US) Institute for Laboratory Animal Research. Guide for the Care and Use of Laboratory Animals (1996). Washington (DC): *National Academies Press (US)*. Available from: https://www.ncbi.nlm.nih.gov/books/NBK232589/doi: 10.17226/5140

Neef, S. *et al*. (2010) 'CaMKII-Dependent Diastolic SR Ca2+ Leak and Elevated Diastolic Ca2+ Levels in Right Atrial Myocardium of Patients With Atrial Fibrillation', *Circ Res*, **106**: 1134–1144.

Nerheim, P. *et al*. (2004) 'Heart Failure and Sudden Death in Patients With Tachycardia-Induced Cardiomyopathy and Recurrent Tachycardia', *Circulation*, **110**.

Nickel, A. G. *et al*. (2020) 'CaMKII does not control mitochondrial Ca2+ uptake in cardiac myocytes', *J Physiol*, **598**: 1361–1376.

O'Toole, T. E. *et al*. (2009) 'Acrolein activates matrix metalloproteinases by increasing reactive oxygen species in macrophages', *Toxicology and Applied Pharmacology*, **236**: 194–201.

Ottolia, M. *et al*. (2013) 'Na/Ca exchange and contraction of the heart', *Journal of Molecular and Cellular Cardiology*, **61**: 28–33.

Paech, F., Bouitbir, J. and Krähenbühl, S. (2017) 'Hepatocellular Toxicity Associated with Tyrosine Kinase Inhibitors: Mitochondrial Damage and Inhibition of Glycolysis', *Frontiers in Pharmacology*, **8**.

Palomeque, J. *et al*. (2009) ‘Angiotensin II–Induced Oxidative Stress Resets the Ca2+ Dependence of Ca2+–Calmodulin Protein Kinase II and Promotes a Death Pathway Conserved Across Different Species’, *Circ Res*, **105**: 1204–1212.

Panday, A. *et al*. (2015) ‘NADPH oxidases: an overview from structure to innate immunity-associated pathologies’, *Cellular and Molecular Immunology*, **12**: 5–23.

Pareek, N. *et al*. (2018) ‘Activity and outcomes of a cardio-oncology service in the United Kingdom — a five-year experience’, *European Journal of Heart Failure*, **20**: 1721–1731.

Parikh, S. S. *et al*. (2017) ‘Thyroid and Glucocorticoid Hormones Promote Functional T-Tubule Development in Human-Induced Pluripotent Stem’, *Circ Res*, **121**: 1323–1330.

Parliament, European & Council, European. (2010). DIRECTIVE 2010/63/EU on the protection of animals used for scientific purposes. *EU Official Journal*. L276.

Paul, M. K. and Mukhopadhyay, A. K. (2004) ‘Tyrosine kinase – Role and significance in Cancer’, *Int. J. Med. Sci.*, **1**: 101–115.

Pavez-Giani, M. G. *et al*. (2021) ‘ATPase Inhibitory Factor-1 Disrupts Mitochondrial Ca2+ Handling and Promotes Pathological Cardiac Hypertrophy through CaMKII δ’, *International Journal of Molecular Sciences*, **22**.

Pellicena, P. and Schulman, H. (2014) ‘CaMKII inhibitors: from research tools to therapeutic agents’, *Frontiers in Pharmacology*, **5**.

Pellman, J., Zhang, J. and Sheikh, F. (2016) 'Myocyte-Fibroblast Communication in Cardiac Fibrosis and Arrhythmias: Mechanisms and Model Systems', *J Mol Cell Cardiol*, **94**: 22–31.

Peoples, J. N. *et al*. (2019) 'Mitochondrial dysfunction and oxidative stress in heart disease', *Experimental & Molecular Medicine*, **51**: 1–13.

Peter, A. K., Bjerke, M. A. and Leinwand, L. A. (2016) 'Biology of the cardiac myocyte in heart disease', *Molecular Biology of the Cell*, **27**: 2149–2160.

Piacentino III, V. *et al*. (2003) 'Cellular Basis of Abnormal Calcium Transients of Failing Human Ventricular Myocytes', *Circ Res*, **92**: 651–658.

Pinto, A. R. *et al*. (2016) 'Revisiting Cardiac Cellular Composition', *Circ Res*, **118**: 400–409.

Pirkmajer, S. and Chibalin, A. V. (2011) 'Serum starvation: caveat emptor', *Am J Physiol Cell Physiol*, **301**: C272–C279.

Porter, K. E. and Turner, N. A. (2009) 'Cardiac fibroblasts: At the heart of myocardial remodeling', *Pharmacology and Therapeutics*, **123**: 255–278.

Puls, M. *et al*. (2020) 'Impact of myocardial fibrosis on left ventricular remodelling, recovery, and outcome after transcatheter aortic valve implantation in different haemodynamic subtypes of severe aortic stenosis', *European Heart Journal*, **41**: 1903–1914.

Pyun, J.-H. *et al*. (2018) 'Cardiac specific PRMT1 ablation causes heart failure through CaMKII dysregulation', *Nature Communications*, **9**.

Rajagopalan, S. *et al*. (1996) 'Reactive Oxygen Species Produced by Macrophage-derived Foam Cells Regulate the Activity of Vascular Matrix Metalloproteinases In Vitro Implications for Atherosclerotic Plaque Stability', *J. Clin. Invest.*, **98**: 2572–2579.

Ribeiro, A. L. *et al*. (2008) 'An evaluation of the cardiotoxicity of imatinib mesylate', *Leuk Res*, **32**: 1809-1814.

Roelofs, B. A. *et al*. (2015) 'Low Micromolar Concentrations of the Superoxide Probe MitoSOX Uncouple Neural Mitochondria and Inhibit Complex IV', *Free Radic Biol Med*, **86**: 250–258.

Ruggeri, Z. M. (2007) 'The role of von Willebrand factor in thrombus formation', *Thromb Res*, **120**.

Sag, C. M. *et al*. (2011) 'CaMKII-dependent SR Ca leak contributes to doxorubicin-induced impaired Ca2+ handling in isolated cardiac myocytes', *J Mol Cell Cardiol*., **51**: 749–759.

Sandstedt, J. *et al*. (2019) 'Human cardiac fibroblasts isolated from patients with severe heart failure are immune-competent cells mediating an inflammatory response', *Cytokine*, **113**: 319–325.

Schneider, C. A., Rasband, W. S. and Eliceiri, K. W. (2012) 'NIH Image to ImageJ: 25 years of image analysis', *Nature Methods*, **9**: 671–675.

Seemann, I. *et al*. (2013) 'Radiation- and anthracycline-induced cardiac toxicity and the influence of ErbB2 blocking agents', *Breast Cancer Res Treat*, **141**: 385–395.

Sena, L. A. and Chandel, N. S. (2012) 'Physiological roles of mitochondrial reactive oxygen species', *Mol Cell*, **48**: 158–167.

Shinde, A. V, Humeres, C. and Frangogiannis, N. G. (2017) 'The role of α-smooth muscle actin in fibroblast-mediated matrix contraction and remodeling', *BBA - Molecular Basis of Disease*, **1863**: 298–309.

Sirangelo, I. *et al*. (2020) 'Vanillin Prevents Doxorubicin-Induced Apoptosis and Oxidative Stress in Rat H9c2 Cardiomyocytes', *Nutrients*, **12**.

Siwik, D. A., Pagano, P. J. and Colucci, W. S. (2001) 'Oxidative stress regulates collagen synthesis and matrix metalloproteinase activity in cardiac fibroblasts', *Am J Physiol Cell Physiol*, **280**: 53–60.

Sossalla, S. *et al*. (2010) 'Inhibition of Elevated Ca2+/CalmodulinDependent Protein Kinase II Improves Contractility in Human Failing Myocardium', *Circ Res*, **107**: 1150–1161.

Souders, C. A., Bowers, S. L. K. and Baudino, T. A. (2009) 'Cardiac fibroblast: The renaissance cell', *Circulation Research*, **105**: 1164–1176.

Sourdon, J. *et al*. (2021) 'Sunitinib-induced cardiac hypertrophy and the endothelin axis', *Theranostics*, **11**.

Spinale, F. G. *et al*. (1998) 'Time-Dependent Changes in Matrix Metalloproteinase Activity and Expression During the Progression of Congestive Heart Failure', *Circ Res*, **82**: 482–495.

Squires, C. E. *et al*. (2005) 'Altered fibroblast function following myocardial infarction', *Journal of Molecular and Cellular Cardiology*, **39**: 699–707.

Srivastava, S. *et al*. (2016) 'Cardioprotective effects of Cu(II)ATSM in human vascular smooth muscle cells and cardiomyocytes mediated by Nrf2 and DJ-1', *Scientific Reports*, **6**.

Stolfo, D. *et al*. (2020) 'Association between beta-blocker use and mortality/morbidity in older patients with heart failure with reduced ejection fraction. A propensity score-matched analysis from the Swedish Heart Failure Registry', *European Journal of Heart Failure*, **22**: 103–112.

Strack, S. *et al*. (1997) 'Differential Inactivation of Postsynaptic Density-Associated and Soluble Ca2+/Calmodulin-DependentProtein Kinase II by Protein Phosphatases 1 and 2A', *Journal of Neurochemistry*, **68**: 2119–2128.

Stride, N. *et al*. (2013) 'Decreased mitochondrial oxidative phosphorylation capacity in the human heart with left ventricular systolic dysfunction', *European Journal of Heart Failure*, **15**: 150–157.

Suetomi, T. *et al*. (2018) 'Inflammation and NLRP3 Inflammasome Activation Initiated in Response to Pressure Overload by Ca2+/Calmodulin-Dependent Protein Kinase II δ Signaling in Cardiomyocytes Are Essential for Adverse Cardiac Remodeling', *Circulation*, **138**: 2530–2544.

Swain, S. M., Whaley, F. S. and Ewer, M. S. (2003) 'Congestive Heart Failure in Patients Treated with Doxorubicin. A Retrospective Analysis of Three Trials', *Cancer*, **97**: 2869–2879.

Takeda, N. *et al*. (2010) 'Cardiac fibroblasts are essential for the adaptive response of the murine heart to pressure overload', *The Journal of Clinical Investigation*, **120**: 254–265.

Takimoto, E. and Kass, D. A. (2007) 'Role of Oxidative Stress in Cardiac Hypertrophy and Remodeling', *Hypertension*, **49**: 241–248.

Telli, M. L. *et al*. (2008) 'Cardiotoxicity associated with the cancer therapeutic agent sunitinib malate', *Annals of Oncology*, **19**: 1613–1618.

Testa, M. *et al*. (1996) 'Circulating Levels of Cytokines and Their Endogenous Modulators in Patients With Mild to Severe Congestive Heart Failure Due to Coronary Artery Disease or Hypertension', *Journal of the American College of Cardiology*, **28**: 964–971.

Tham, Y. K. *et al*. (2015) 'Pathophysiology of cardiac hypertrophy and heart failure: signaling pathways and novel therapeutic targets', *Arch Toxicol*, **89**.

Thottakara, T. *et al*. (2020) 'The Cardiac Fibroblast in heart failure – an inflammatory cell', *European Heart Journal*, **41**(Supplement 2).

Torre-Amione, G *et al*. (1996) 'Tumor necrosis factor-alpha and tumor necrosis factor receptors in the failing human heart', *Circulation*, **93**:. 704-11.

Tran, K., Loiselle, D. S. and Crampin, E. J. (2015) 'Regulation of cardiac cellular bioenergetics: mechanisms and consequences', *Physiological Reports*, **3**: 1–16.

Tsiftsoglou, A. S. *et al*. (1986) 'Prevention of Anthracycline-induced Cytotoxicity in Hemopoietic Cells by Hemin1', *Cancer Research*, **46**: 3436–3440.

Tsutsui, H., Kinugawa, S. and Matsushima, S. (2011) 'Oxidative stress and heart failure', *Am J Physiol Heart Circ Physiol*, **301**: 2181–2190.

van der Pol, A. *et al*. (2019) 'Treating oxidative stress in heart failure: past, present and future', *European Journal of Heart Failure*, **21**: 425–435.

Varga, Z. V *et al*. (2015) 'Drug-induced mitochondrial dysfunction and cardiotoxicity', *Am J Physiol Heart Circ Physiol*, **309**: 1453–1467.

Vasquez-Vivar, J. *et al*. (1998) 'Superoxide generation by endothelial nitric oxide synthase: The influence of cofactors', *Proc. Natl. Acad. Sci.*, **95**: 9220–9225.

Vasquez, C., Benamer, N., & Morley, G. E. (2011) 'The cardiac fibroblast: functional and electrophysiological considerations in healthy and diseased hearts', *Journal of cardiovascular pharmacology*, **57**: 380–388.

Villarreal, F. J. and Dillmann, H. (1992) 'Cardiac hypertrophy-induced changes in mRNA for TGF-beta1, fibronectin, and collagen', *Am J Physiol*, **262**: 1861–1866.

Walgren, J. L. E. *et al*. (2002) 'High glucose and insulin promote O-GlcNAc modification of proteins, including alpha-tubulin', *Am J Physiol Endocrinol Metab*, **284**: 424–434.

Wang, X. *et al*. (2010) 'Comparison of MTT assay, flow cytometry, and RT-PCR in the evaluation of cytotoxicity of five prosthodontic materials', *J Biomed Mater Res B Appl Biomater*, **95**: 357–364.

Whorwood, C. B. *et al*. (2001) 'Regulation of Glucocorticoid Receptor alpha and beta Isoforms and Type I 11beta Hydroxysteroid Dehydrogenase Expression in Human Skeletal Muscle Cells: A Key Role in the Pathogenesis of Insulin Resistance?', *The Journal of Clinical Endocrinology & Metabolism*, **86**: 2296–2308.

Will, Y. *et al*. (2008) 'Effect of the Multitargeted Tyrosine Kinase Inhibitors Imatinib, Dasatinib, Sunitinib, and Sorafenib on Mitochondrial Function in Isolated Rat Heart Mitochondria and H9c2 Cells', *Toxocological Sciences*, **106**: 153–161.

Wolf, A. *et al*. (2010) 'Imatinib does not induce cardiotoxicity at clinically relevant concentrations in preclinical studies', *Leukemia Research*, **34**: 1180–1188.

Xu, K. Y., Zweier, J. L. and Becker, L. C. (1997) 'Hydroxyl Radical Inhibits Sarcoplasmic Reticulum Ca2+-ATPase Function by Direct Attack on the ATP Binding Site', *Circ Res*, **80**: 76–81.

Yang, Y. *et al*. (2020) 'Decreased Mortality with Beta-Blocker Therapy in HFpEF Patients Associated with Atrial Fibrillation', *Cardiology Research and Practice*.

Ying, X. *et al*. (2009) 'Characterization of the Inflammatory and Fibrotic Response in a Mouse Model of Cardiac Pressure Overload', *Histochem Cell Biol*, **131**: 471–481.

Yuan, J., Lipinski, M. and Degterev, A. (2003) 'Diversity in the Mechanisms of Neuronal Cell Death', *Neuron*, **40**: 401–413.

Zamorano, J. L. *et al*. (2016) '2016 ESC Position Paper on cancer treatments and cardiovascular toxicity developed under the auspices of the ESC Committee for Practice Guidelines', *European Heart Journal*, **37**: 2768–2801.

Zhang, H. J. *et al*. (2002) 'Activation of Matrix Metalloproteinase-2 by Overexpression of Manganese Superoxide Dismutase in Human Breast Cancer MCF-7 Cells Involves Reactive Oxygen Species *', *Journal of Biological Chemistry*, **277**: 20919–20926.

Zhang, J. *et al*. (2019) 'Functional cardiac fibroblasts derived from human pluripotent stem cells via second heart field progenitors', *Nature Communications*, **10**.

Zhang, P. (2017) 'CaMKII: The molecular villain that aggravates cardiovascular disease', *Experimental and Therapeutic Medicine*, **13**: 815–820.

Zhang, T. *et al*. (2003) 'The deltaC Isoform of CaMKII Is Activated in Cardiac Hypertrophy and Induces Dilated Cardiomyopathy and Heart Failure', *Circ Res*, **92**: 912–919.

Zhang, W. *et al*. (2010) 'Inhibition of Calcium – Calmodulin-Dependent Kinase II Suppresses Cardiac Fibroblast Proliferation and Extracellular Matrix Secretion', *J Cardiovasc Pharmacol*, **55**: 96–105.

Zhang, X. *et al*. (2014) 'Calcium Sensing Receptor Promotes Cardiac Fibroblast Proliferation and Extracellular Matrix Secretion', *Cellular Physiology and Biochemistry*, **33**: 557–568.

Zhao, R.-Z. *et al*. (2019) 'Mitochondrial electron transport chain, ROS generation and uncoupling (Review)', *International Journal of Molecular Medicine*, **44**: 3–15.

Zhou, B. and Tian, R. (2018) ‘Mitochondrial dysfunction in pathophysiology of heart failure’, *The Journal of Clinical Investigation*, **128**: 3716–3726.

Zhuo, J. L. *et al*. (2006) ‘Intracellular ANG II induces cytosolic Ca2+ mobilization by stimulating intracellular AT1 receptors in proximal tubule cells’, *Am J Physiol Renal Physiol.*, **290**: 1–19.